



ulm university universität
uulm

University of Applied Sciences Biberach
Institute of Applied Biotechnology
Prof. Dr. Katharina Zimmermann

Development of models for intranasal drug delivery to identify IgG transport pathways

Cumulative dissertation submitted in partial fulfilment of the requirements for the
degree of “Doctor rerum naturalium” (Dr. rer. nat.) of the Ulm university.

Simone Ladel
Biberach an der Riß

2022

HBC.
HOCHSCHULE
BIBERACH
UNIVERSITY
OF APPLIED SCIENCES

Current dean: Prof. Dr. Thorsten Bernhardt

Thesis advisory committee:

First supervisor: Prof. Dr. Boris Mizaikoff

Second supervisor: Prof. Dr. Katharina Zimmermann

Third supervisor: Prof. Dr. Andrew Chan

Day doctorate awarded: 20/06/2022

The results presented in this thesis have been published previously in the following journals:

Simone Ladel, Johannes Flamm, Arghavan Soleimani Zadeh, Dorothea Filzwieser, Julia Christina Walter, Patrick Schlossbauer, Ralf Kinscherf, Katharina Lischka, Harald Luksch, and Katharina Schindowski. 2018. Allogenic Fc domain-facilitated uptake of IgG in nasal *Lamina propria*: Friend or foe for intranasal CNS delivery? *Pharmaceutics* 10, 3: 1–23. <https://doi.org/10.3390/pharmaceutics10030107> [1]

Simone Ladel, Patrick Schlossbauer, Johannes Flamm, Harald Luksch, Boris Mizaikoff, and Katharina Schindowski. 2019. Improved *In vitro* Model for Intranasal Mucosal Drug Delivery: Primary Olfactory and Respiratory Epithelial Cells Compared with the Permanent Nasal Cell Line RPMI 2650. *Pharmaceutics* 11, 8: 367. <https://doi.org/10.3390/pharmaceutics11080367> [2]

Simone Ladel, Frank Maigler, Johannes Flamm, Patrick Schlossbauer, Alina Handl, Rebecca Hermann, Helena Herzog, Thomas Hummel, Boris Mizaikoff, and Katharina Schindowski. 2020. Impact of Glycosylation and Species Origin on the Uptake and Permeation of IgG's through the Nasal Airway Mucosa. *Pharmaceutics* 12, 11: 1014. <https://doi.org/10.3390/pharmaceutics12111014> [3]

Other original papers co-authored during my doctorate:

Lena Marie Spindler, Andreas Feuerhake, **Simone Ladel**, Cemre Günday, Johannes Flamm, Nazende Günday-Türeli, Emre Türeli, Günter E.M. Tovar, Katharina Schindowski & Carmen Gruber-Traub. (2021). Nano-in-Micro-Particles Consisting of PLGA Nanoparticles Embedded in Chitosan Microparticles via Spray-Drying Enhances Their Uptake in the Olfactory Mucosa. *Frontiers in Pharmacology*, 12. <https://doi.org/10.3389/fphar.2021.732954> [4]

Frank Maigler, **Simone Ladel**, Johannes Flamm, Stella Gänger, Barbara Kurpiers, Stefanie Kiderlen, Ronja Völk, Carmen Hamp, Sunniva Hartung, Sebastian Spiegel, Arghavan Soleimanizadeh, Katharina Eberle, Rebecca Hermann, Lukas Krainer, Claudia Pitzer, Katharina Schindowski. (2021). Selective CNS Targeting and Distribution with a Refined Region-Specific Intranasal Delivery Technique via the Olfactory Mucosa. *Pharmaceutics*, 13(11), 1904. <https://doi.org/10.3390/pharmaceutics13111904> [5]

Detailed declaration of contribution to peer-reviewed original publications

This doctoral thesis is based on three peer-reviewed original publications that have been written by me as first or shared first author.

For the first publication entitled “Allogenic Fc domain-facilitated uptake of IgG in nasal *Lamina propria*: Friend or foe for intranasal CNS delivery?” published in *Pharmaceutics* in 2018 [1], I designed the complete study, performed most and analysed all of the experiments, created the figures and wrote the manuscript.

For the second publication entitled “Improved *In vitro* Model for Intranasal Mucosal Drug Delivery: Primary Olfactory and Respiratory Epithelial Cells Compared with the Permanent Nasal Cell Line RPMI 2650.” published in *Pharmaceutics* in 2019 [2], I was responsible for the study design, the method design and establishment. I further analysed most of the experiments and wrote the manuscript. I share first authorship with MSc. Patrick Schlossbauer.

For the third publication entitled “Impact of Glycosylation and Species Origin on the Uptake and Permeation of IgGs through the Nasal Airway Mucosa.” published in *Pharmaceutics* in 2020 [3], I elaborated the underlying hypothesis, I designed the study, performed and analysed most of the experiments and wrote the manuscript.

For the fourth publication entitled “Nano-in-Micro-Particles Consisting of PLGA Nanoparticles Embedded in Chitosan Microparticles via Spray-Drying Enhances Their Uptake in the Olfactory Mucosa.” Published in *Frontiers in Pharmacology* in 2021 [6], I was involved in the method set-up for *ex vivo* experiments and performed particle permeation through olfactory mucosa.

For the fifth publication entitled “Selective CNS Targeting and Distribution with a Refined Region-Specific Intranasal Delivery Technique via the Olfactory Mucosa.” published in *Pharmaceutics* in 2021 [5], I elaborated parts of the underlying hypothesis, developed the histological protocols for study 3. Further I participated in the design of study 3 and I performed and analysed most of the histological experiments of this study.

The full versions of these publications are provided in the appendix of my doctoral thesis.

Table of Content

1. Summary.....	1
2. Introduction	2
2.1 Nose-to-brain drug delivery	2
2.1.1 The anatomy of the nasal cavity	2
2.1.2 Histological features of the nasal cavity	4
2.1.1 Nose-to brain transport mechanisms – avoiding the barriers	6
2.2 N2B drug delivery of therapeutic antibodies for the therapy of CNS related diseases?	8
2.2.1 IgG structure and function	8
2.2.2 The neonatal Fc receptor – the best known IgG transporter	11
2.2.3 Fc gamma receptors	13
2.3 Ex vivo tissue models of the nasal mucosa	15
2.3.1 The pig as model organism	15
2.3.2 Side-by side cell models.....	16
2.4 In vitro models of the nasal epithelial barrier.....	18
3. Objective of the thesis	20
4. Results and Discussion.....	23
4.1 Development and evaluation of different models to simulate mucosal IgG uptake and permeation	23
4.1.1 The ex vivo model for permeation through the olfactory mucosa– a modified side- by side tissue model using porcine mucosa explants	23
4.1.2 The in vitro model – mimicking the olfactory epithelial barrier using primary cells from the porcine regio olfactoria.....	27
4.2 Evaluation of therapeutic IgGs for N2B dug delivery – Influence of IgG species origin and glycosylation status.....	33
4.2.1 IgG uptake and permeation study – searching for influencing parameters.....	34
4.2.2 Analysis of the molecular mechanism of IgG trafficking	36
5. Conclusion	49
6. References.....	52
7. Appendix.....	80

List of Abbreviations

Abbreviations used in this thesis are listed in alphabetical order.

ALI	air-liquid interface
AP5	aquaporin 5
BBB	blood brain barrier
BC	basal cells
bcsfb	blood cerebrospinal fluid barrier
BNB	blood nerve barrier
CK18	cytokeratin 18
cnd	<i>concha nasalis dorsalis</i>
cnm	<i>concha nasalis media</i>
CNS	central nervous system
CSF	cerebrospinal fluid
ET	ethmoid turbinate
FCGR	Fc gamma receptors
FcRn	neonatal Fc receptor
FITC	Fluorescein isothiocyanate
Fuc	fucose
Gal	galactose
Glc	glucose
GlcNAc	N-acetylglucosamine
IgA	Immunoglobulin A
IgD	Immunoglobulin D
IgE	Immunoglobulin E
IgG	Immunoglobulin G
IgM	Immunoglobulin M
ITAM	immunoreceptor tyrosine-based activation motif
ITIM	immunoreceptor tyrosine-based inhibitory motif
Man	mannose
MUC5AC	mucin type 5AC
N2B	nose-to-brain
NB	neuronal bundles
Neu5Ac	N-acetylneuraminic acid
NF200	neurofilament 200
OEC	olfactory ensheathing cells
OEPC	olfactory epithelial primary cells
OSN	olfactory sensory neurons
PGP9.5	Protein Gene Product 9.5
PNS	peripheral nervous system
REPC	respiratory epithelial primary cells
TEER	transepithelial-electrical resistance
TRIM21	Tripartite motif containing-21
ZO-1	<i>zonula occludens-1</i>

1. Summary

Over the last decades, there is an increasing interest in the intranasal administration of drugs. Especially for high molecular weight proteins such as immunoglobulin G (IgG) the mechanisms and pathways of delivery to the brain remains mainly unclear and studies result in conflicting data. However, the use of therapeutic IgG in neurodegenerative or neuro-oncologic diseases has a high potential for modern therapy but is highly limited due to the poor access of this proteins to the central nervous system. This discrepancy leads to the conclusion that higher effort should be made to understand the molecular background for the use in protein engineering.

In this thesis, two different models were set-up to determine the permeation of IgG through the olfactory mucosa: a mucosa model using porcine olfactory tissue explants and a primary cell epithelial barrier model. In both models, the experiments were done under air-liquid conditions to simulate the environment in the nasal cavity. Hereby, the primary cell model was used to determine the permeation of IgG at the first barrier, the olfactory epithelium, whereas the *ex vivo* model was used to study the more complex permeation through the whole mucosa. To evaluate the pig as model system, the porcine olfactory mucosa was histologically compared to the human counterpart. High similarities were found indicating the pig being a suitable model organism for human olfactory mucosa investigations. To gain as much information as possible from the IgG permeation experiments, several approaches were made investigating the influence of IgG-origin and IgG glycosylation on the transmucosal transport.

In the primary cell epithelial barrier model, no difference in the trans-epithelial transport was detected comparing human and porcine IgGs. However, in the *ex vivo* model porcine IgG seemed not to permeate but remain in the tissue whereas the human IgG was detected in the abluminal compartment. Furthermore, porcine IgG seemed to be cleared from immune sites, so called lymphoid follicles, whereas for human IgG only low co-localization with lymphocytes was found in immunofluorescence studies. In conclusion, there might be an immune system related mechanism in the olfactory *lamina propria* that is species-selective and needs to be further investigated for IgG design.

According to common knowledge, the neonatal Fc receptor (FcRn) is the predominant protein that is involved in IgG transport. Protein expression of FcRn was found in the olfactory primary cells and tissue from the olfactory mucosa concluding that active transport via this receptor would be possible in both models. Further, several studies showed that this receptor binds porcine and human IgG with similar affinities. Thus, the FcRn might not be the only player that is involved in the transport mechanism.

Summary

Another protein family that is known to perform interactions with IgG are Fc gamma receptors (FCGR). Most of these receptors are highly dependent on IgG subclass and Fc-glycosylation. To evaluate the influence of the Fc glycosylation and hereby gaining evidence for a potential involvement of FCGR in IgG trafficking permeation studies were performed using deglycosylated IgGs. In both models, the *ex vivo* and the primary cell *in vitro* model, the deglycosylated IgGs showed higher permeation rate over time. These findings did not fit well to the hypothesis that FCGRs mediate IgG transcytosis in the olfactory epithelium, as the affinity of FCGR for deglycosylated IgG is very low and therefore the permeation should be less compared to the wild-type IgG. Nevertheless, the FCGR subclass FCGR2b was recently connected to IgG transport in the placenta. Therefore, the expression of this receptor was evaluated in both models. Expression or transcription was found in both models hinting again to an involvement of these receptors. Based on the data gained in this thesis a new hypothesis for IgG trafficking in the olfactory mucosa was stated. This hypothesis includes the involvement of FCGR2b in IgG trafficking mechanisms other than transcytosis, meaning recycling and mainly degradation processes, whereas FcRn remains the main mediator of IgG transcytosis. Nevertheless, open questions are still to be addressed in further experiments.

2. Introduction

This thesis deals with the development of animal test replacement methods for the intranasal application of therapeutic antibodies and fills the lack of suitable *in vitro* and *ex vivo* methods to investigate drug transport mechanism at the olfactory mucosa. Furthermore, it provides new insights into the explanation of IgG transport mechanisms and leads to a new hypothesis of IgG transport across the olfactory mucosa.

2.1 Nose-to-brain drug delivery

The administration of drugs through the nose has a long tradition, especially for local diseases such as nasal allergy, congestion and infections. For several decades, there has been a growing interest in using the special features of the nasal mucosa and the nasal neuronal access to the brain at the base of the skull for other therapies as well. At least since the SARS-CoV-2 pandemic in 2020, the intranasal dosage form has been very popular for the treatment of viral respiratory and neuronal diseases [7]. However, there are further additional examples worth to consider. Products already on the market for nasal administration range from anti-migraine drugs such as sumatriptan and butorphanol to smaller peptides such as calcitonin and buserelin [8]. Furthermore, studies have shown that insulin administered intranasally has a positive effect on memory [9–11]. The nose-to brain (N2B) drug delivery systems imply several advantages compared to traditional invasive approaches: The nasal cavity is easily accessible and allows a needle free drug application. Especially lipophilic low molecular weight molecules show a good penetration and a rapid adsorption due to the large surface and high vascularization. Furthermore, the hepatic first pass metabolism as well as the harsh conditions in the gastrointestinal tract are avoided [12].

The most interesting advantage, however, is the direct access to the central nervous system.

2.1.1 The anatomy of the nasal cavity

The human nose extends from the nostrils to the upper part of the throat, called the nasopharynx. It consists of two nasal cavities that are separated by a midline septum. The outer walls of the nasal cavities are folded in three conchae or turbinates, namely the superior, the middle and the inferior turbinate (**Figure 1**). These turbinates function as increased resistance to the airflow and enable a tight contact between the inhaled air and the mucosa. The inferior conchae is the largest of the three and extend the complete length of the outer nasal wall. Above the inferior conchae the middle conchae is located. The superior conchae is the smallest of the three and is located at the upper part of the nasal cavity beneath the ethmoid turbinates and the cribriform plate.

Introduction

The cribriform plate is a porous bone that is spanned by neuronal branches originated in the olfactory epithelium and reaching to the centre of olfaction procession in the brain, the olfactory bulb [8,13–16].

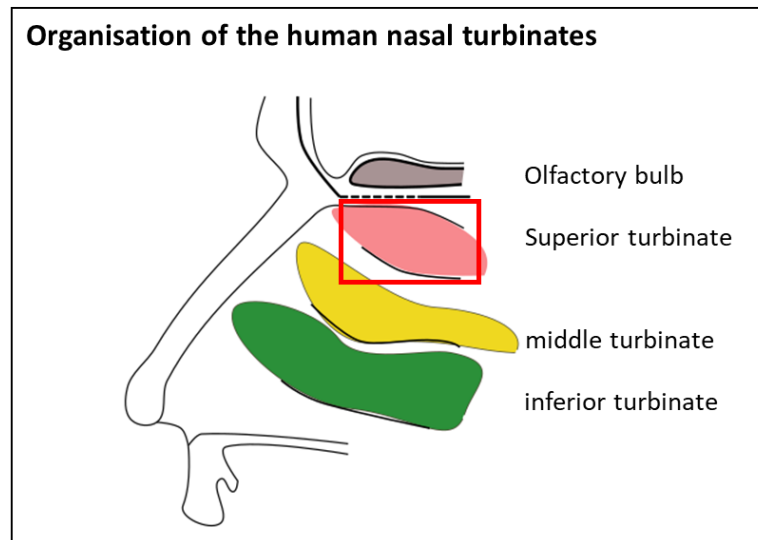


Figure 1: Arrangement of the nasal turbinates in the human nasal cavity. The red box marks the olfactory region as evaluated by Paik *et al.* [17].

Each cavity contains three different regions: the vestibule, the olfactory region and the respiratory region [8,16,18]. The vestibule consists of the area just inside the nostrils at the anterior part of the cavity. It is covered by skin with stiff large hair that protect the entrance of the nasal cavity. The respiratory region covers 77 % of the nasal cavity and is the main location for filtering, warming and humidifying the inhaled air before it reaches the lower airways. The olfactory region is located at the roof of the nasal cavity and covers about 10 % of the total surface area of the nasal mucosa in human. There is a high difference in the percentage coverage of the olfactory epithelium between animal species. For example, around 50 % of the nasal cavity surface in rats is covered with olfactory epithelium and 77 % in dogs [8,19,20]. The total surface area of both nasal cavities in human is about 96.000 cm² if the epithelial microvilli are included [21]. The large absorption capacity of the nasal mucosa is not only due to its large surface area. In addition, the nasal cavity has a complex network of arteries, veins, lymphatic vessels and neurons that enable the rapid dissemination of absorbed substances. As in the intestine, the nasal mucosa contains a large number of glands that produce aqueous secretions in the anterior region, which contain proteins and electrolytes. In the remaining part of the nasal cavity, there are seromucous glands, which produce a region-specific mucus layer. For example, the tubuloalveolar serous Bowman's glands in the olfactory region produce proteinaceous secretions that are important for olfactory action and act as solvents for odoriferous substances [13].

Introduction

For the N2B approach, especially the nerve fibres are of interest as they are possible transport routes for drugs to the brain. The largest cranial nerve is the *nervous trigeminus*, that is mainly a sensory nerve and consists of four subbranches. One subbranch, the nervous maxillaries, spans from the respiratory region to the central nervous system. The most interesting nerves for N2B are the olfactory nerves as they allow direct access to the CNS. Bipolar olfactory neurons are located in the olfactory mucosa and branches out from the nasal cavity through the cribriform plate into the olfactory bulb [13,22].

2.1.2 Histological features of the nasal cavity

In the human nose, four different mucosa types can be roughly classified: the respiratory mucosa, the olfactory mucosa, the squamous mucosa and the transitional mucosa. One third of the anterior part is covered by squamous epithelium. This epithelial type is stratified epithelium that consists of an underlying basal cell layer followed by several layers of squamous cells, which gradually changes into a pseudostratified columnar epithelium that covers the respiratory epithelium. The transition areas between these epithelial types are called transitional epithelium. In all epithelial types, beneath the basal cell layer there is a thick layer of connective tissue with glands, blood vessels and immune cell accumulations called lymphoid follicles. This layer is called the *lamina propria* [13,15,17,23].

The epithelial cells of the respiratory epithelium are covered by microvilli and beating mobile cilia, creating a rapid propelled movement of the mucus layer in direction from the anterior towards the posterior part of the nasal cavity [8]. The respiratory epithelium contains three major cell types: ciliated cells, goblet cells and basal cells. Hereby, the goblet cells are located between the ciliated cells and are packed with mucus vesicle. They function as gland cells in the respiratory epithelium. The basal cells are densely packed in a layer adjacent to the *lamina propria* and have a round appearance with a small cytoplasm. These cells are progenitor cells for all cell types located in the epithelium [13,24].

Introduction

2.1.2.1 The olfactory mucosa

The most interesting epithelium for N2B is the olfactory epithelium (**Figure 2**). It is composed of a pseudostratified epithelium containing microvillar cells, olfactory sensory neurons (OSN), basal cells and supporting cells.

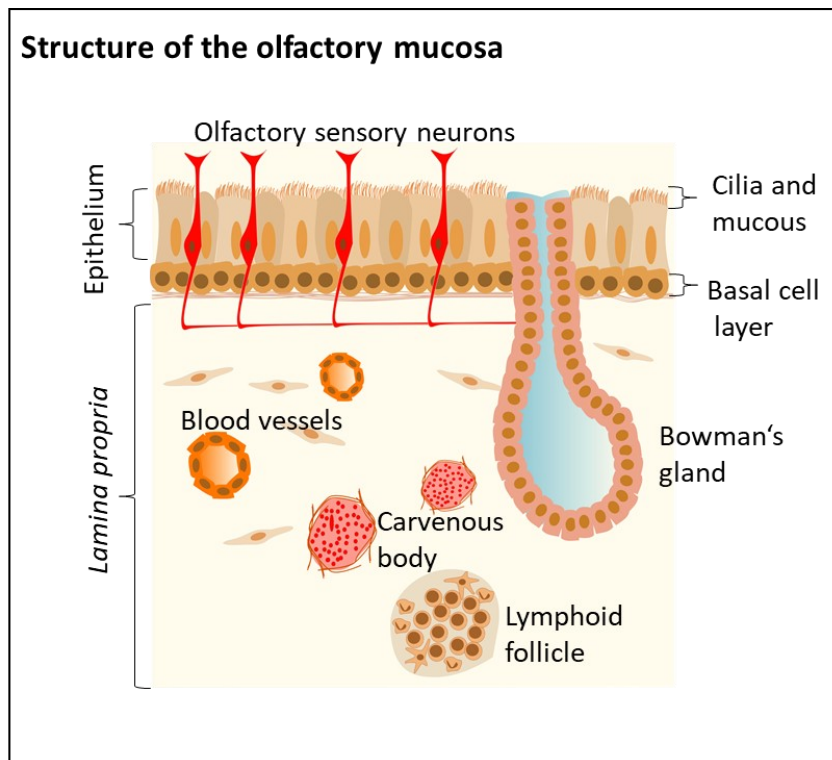


Figure 2: Scheme of the composition of the olfactory mucosa.

The epithelium is composed of the olfactory sensory neurons, microvillar cells and supporting cells. Beneath the epithelium, the basal cell (BC) layer is located. Basal cells are progenitor cells and have the potential to differentiate into the other cell types of the epithelium. Big Bowman's glands span through the epithelial layer and secrete mucus into the lumen. The biggest part of the olfactory mucosa is the underlying connective tissue, the *lamina propria*. In the *lamina propria* blood vessels, cavernous bodies and lymphoid follicles (immune cell agglomerates) are located. The figure is modified from Ladel *et al.* (2018) [1], CC BY 4.0, <http://creativecommons.org/licenses/by/4.0/>.

All cell types except for the basal cells reach the epithelial surface that is covered with a thin mucus layer. In this mucus layer besides the microvilli, long non-motile cilia were found that belong to the OSN. The OSN are bipolar neurons with cell bodies located in the olfactory epithelium. They are structured in the cell body, a dendrite that spans into the nasal lumen expressing olfactory receptor proteins and long axons that cross the *lamina propria* and the cribriform plate to reach their synaptic destination in the olfactory bulb [24]. In the axonal branches of the OSNs are surrounded by specialized cells called olfactory ensheathing cells (OEC). Those cells isolate the olfactory axons from their origin in the epithelial layer to the olfactory bulb glomeruli and form a nerve-blood barrier that limits the uptake of substances and

Introduction

the penetration of e.g. bacteria to the neuronal fibres in the olfactory mucosa [25–28]. The exact location of the olfactory epithelium in human varies in the literature but it usually covers part of the nasal septum, the cribriform plate and the superior turbinate [15,17,22,24]. In comparison to the respiratory epithelium, the olfactory epithelium is much thicker and rests on a highly cellular *lamina propria* without submucosa. The *lamina propria* is a collagenous region of dense, irregular connective tissue that contains agglomerated cells of the immune system (lymphoid follicles), fibroblasts, blood vessels, big Bowman's glands and neuronal fibres that run bundled in the direction of the olfactory bulb. These structures are called neuronal bundles [17,23,24,29].

2.1.1 Nose-to brain transport mechanisms – avoiding the barriers

The low availability of drugs in the brain has been a concern for medicine n issue for therapeutics and development of therapeutics/medicines for decades. The causes of this limitation are specialised borders to the blood that restricts the entry of neurotoxic substances (e.g. toxic substances) and microbial threats into the central nervous system (CNS) and the peripheral nervous system (PNS). Different barriers exist in the surrounding of the nervous system: The blood-brain barrier (BBB) separates the brain interstitial fluid from blood, the blood-cerebrospinal fluid (CSF) barrier (BCSFB) separates the CSF from the choroid plexus interstitial fluid and the blood-nerve barrier (BNB) separates axonal bundles in the periphery of the CNS from blood and the surrounding environment [28,30]. They prevent free paracellular diffusion of polar molecules and high molecular weight molecules by specialised morphological features such as strong tight junctions that cross-link the endothelial and the epithelial cells [31]. The BBB is formed by cerebral vascular endothelial cells that are connected by tight junctions and surrounded by astroglia expressing soluble factors responsible for the formation of tight junctions [32–34]. The BBB functions as a shield of the brain and spinal cord from various substances and pathogens, and however it is also a major hurdle in CNS-drug delivery [35,36]. A large number of invasive strategies such as intraventricular, intraparenchymal and intrathecal delivery as well as non-invasive techniques like chemical modifications and drug conjugations with ligands that can cross the BBB have been developed in the past [30]. One of these strategies is the application of drugs via the intranasal route [8]. In contrast to invasive methods, the non-invasive intranasal approach can be used for e.g. chronically given drugs potentially resulting in a higher patient compliance. Further advantages of the intranasal application are a rapid uptake at the large surface area and the avoidance of the hepatic first-pass elimination. However, there are also disadvantages such as the limitation to potent drugs (only small volumes can be applied intranasally), and the harsh environment on and at the nasal mucosa including the mucociliary clearance and the physico-chemical features of the mucus layer (low pH, enzymatic degradation) [37,38].

Introduction

In the nasal cavity the respiratory and the olfactory epithelium are most likely to be sites of external substance uptake [15]. Substances can enter the epithelial barrier of the respiratory and the olfactory epithelium by two pathways, namely the intracellular and the extracellular pathway: In the olfactory epithelium, intracellularly transported substances can either be endocytosed into olfactory sensory neurons and subsequently be transported to the brain via their axons, or they can be transported via transcytosis across sustentacular cells into the *lamina propria* [39–41]. B. The extracellular pathway means paracellular diffusion into the *lamina propria* through intercellular clefts between the epithelial layer [41].

The drug's pathway through the mucosa mainly depends on its lipophilicity and the molecular weight [42]. The paracellular pathway is mainly reported for small molecules and low molecular weight hydrophilic molecules such as e.g. fluorescein labelled isothiocyanate- dextran (FITC-dextran; 4.4 kD) or sodium fluorescein (0.37 kD) [43–48]. These non-toxic and easily detectable fluorescence labelled chemicals are often used as marker molecules for drug permeation studies [45,46,49]. The feasibility of N2B drug delivery was investigated for sumatriptan, oxytocin and other drugs proving the paracellular pathway is the main route for small molecules [10,50–52]. In contrast, the transcellular transport is described for high molecular weight molecules such as proteins [53].

The precise mechanism underlying N2B drug delivery is still unclear, but several studies connect potential pathways involving neuronal fibres, the vasculature, the CSF and the lymphatic system with the transport of molecules to the CNS [54]. For the olfactory nerve pathway, drugs have to cross the olfactory epithelium to reach the neuronal fibres. There are three possibilities for drugs to transverse this barrier: Firstly, the transcellular crossing of supporting cells by receptor-mediated endocytosis, fluid phase endocytosis or by passive diffusion for lipophilic drugs. Secondly, the paracellular pathway as described before and thirdly the olfactory nerve pathway. Drugs could be taken up into neuronal cells by endocytosis or pinocytosis and transported via intracellular axonal transport to the olfactory bulb [38]. In addition, besides the olfactory nerve pathway there is another nerve-involving pathway for N2B drug delivery: the trigeminal nerve pathway [55]. This nerve connects the respiratory and the olfactory mucosa to the pons in the CNS. It is involved in sensory information communication from the nasal cavity, the oral cavity, eyelids and cornea to the CNS. As an example, 'Thorne *et al.* (2004) demonstrated CNS delivery of insulin-like growth factor-I by the trigeminal nerve branches to the CNS [56].

There are several other studies proving the N2B drug delivery approach is a promising route for protein-based CNS therapy. Insulin is among the most used drugs for intranasal administration studies.

Introduction

Different groups show the uptake and distribution via nerve fibres to the CNS [9,57–61]. For example, intranasally administered insulin was shown to have a positive effect on memory and metabolic effects in human [9,11,57].

The feasibility of N2B drug delivery for high molecular weight proteins such as Immunoglobulin G (IgG) was shown in recent studies in mice that demonstrated the uptake via nervous pathways to different areas of the brain [62].

2.2 N2B drug delivery of therapeutic antibodies for the therapy of CNS related diseases?

During the last decades, the increase of importance of therapeutic IgGs has been exceptional. For antibody-related discoveries, two Nobel prizes have been awarded so far. Furthermore, more than 80 antibodies have entered clinical trials and the approval success rates have been near one in four [63,64]. The areas of application for therapeutic IgGs range from oncology, autoimmune diseases and inflammatory diseases, for the treatment of chronic and acute conditions. However, the use of IgGs for CNS-related diseases is still limited due to the above-described barriers and the low brain permeability in general, since the CNS is an immunological privileged tissue in the mammalian body [8].

2.2.1 IgG structure and function

Immunoglobulin G/antibodies belong to the immunoglobulin superfamily. They are generated via class switching in primary and secondary immune reactions in B cells that are differentiated by secondary signals including cytokines produced by other lymphocytes or antigen presented cells (5,6). Molecules from the immunoglobulin superfamily/antibodies consist of two heavy (H) and two light (L) chains. Each chain contains one NH₂-terminal variable (V) domain and one COOH-terminal constant (C) domain. The heavy chains that are linked via disulphide bond as well as two light chains that are also respectively connected by disulphide bonds to the heavy chain. Each L chains contains one C domain whereas the H chains contains three C domains (CH₁, CH₂, CH₃) in IgGs and more in other members of the immunoglobulin superfamily. The H chains with three C domains include a spacer hinge region between the CH₁ and CH₂ domains [65–67]. By the use of enzymes in earlier studies IgG was digested into two Fab fragments and a Fc fragment. The Fab fragment contains of a variable fragment consisting of VH and VL domains and a constant fragment consisting of the CL and the CH₁ domains [68]. The V domain is functionally divided into three hypervariable regions called complementarity-determining regions that promote specific binding areas to the respective antigens [67].

Introduction

Five classes of immunoglobulins (IgM, IgG, IgE, IgD and IgA) and several subclasses have been described [69]. There are four IgG subclasses in human: IgG1, IgG2, IgG3 and IgG4 [67]. Although their amino acid structure is more than 90 % identical, each subclass shows differences in structure and function that influences the antigen binding, the triggering of effector cells, the serum half-life and placental transport [67]. The subclass depends on the types of antigens that is involved in the antibody response. Antibody responses to soluble protein antigens and membrane proteins primarily induce an IgG1 response, which is also the predominantly subclass of recombinant therapeutic antibodies [69].

One site that shows large differences between the subclasses is the so-called hinge region and the N-terminal CH2 domain. The hinge region forms a flexible linker between the Fab fragments and the Fc domain [69]. Residues most proximal to the hinge region in the CH2 domain of the Fc part are mainly responsible for effector functions of antibodies. The binding sites for C1q (complement system) and the IgG-Fc gamma receptors (FCGR) are located at this site [70–72]. There is a high variability in length and flexibility of the hinge region among the IgG subclasses that affects the confirmations of the Fab fragments relative to the Fc domain. The hinge region of IgG1 is very flexible whereas the hinge region of IgG2 is rigid due to a shorter amino acid chain and extra inter-heavy chain disulphide bridges. Similar to IgG2, also IgG4 has a short hinge region and show less flexibility than IgG1. IgG3 has the longest hinge region that varies between allotypes but ensures the highest flexibility amongst the subclasses. The binding sites for FCGR and C1q are highly affected by the different hinge regions and is due to the flexibility of the Fab-Fc-dynamic. The affinity for these effector molecules in human is as follows: IgG3>IgG1>IgG4>IgG2 [69,73,74].

In contrast, a highly conserved region between the subclasses is the N-linked glycosylation site at the asparagine 297 in the IgG sequence at the interface between the two CH2/CH3 forming the Fc of the IgG molecule (**Figure 3**).

Glycosylation of immunoglobulins play an important role in binding of antigens and especially binding to the respective receptors. Predominantly, human glycoproteins contain seven types of monosaccharides. These are glucose (Glc), galactose (Gal), fucose (Fuc), mannose (Man), N-acetylglucosamine (GlcNAc), and N-acetylneuraminic acid (Neu5Ac) [75]. Besides the N-glycosylation there is an additional glycosylation site in the IgG structure that is rarely present, the O-glycosylation. O-glycans have been found in the hinge region of IgD, IgA and IgG3 [76]. Human IgG contains mainly N-glycans [69]. The heptasaccharide core consist of two GlcNAc residues, three Man residues and two GlcNAc residues. It is called G0 glycosylation. Furthermore, Fuc residue (G0F) branching from the GlcNAc and/or Gal (G1F) and negatively charged sialic acid is detected in some IgGs [77].

Introduction

In 15 – 25 % of IgGs, there is an additional glycosylation site at the Fab fragment containing higher percentage of branching GlcNAc residue and of Gal and sialic acid. Those glycan structures influence the ability to bind antigen, the half-life of the antibody, the aggregation of antibodies and the formation of immune complexes [78–82].

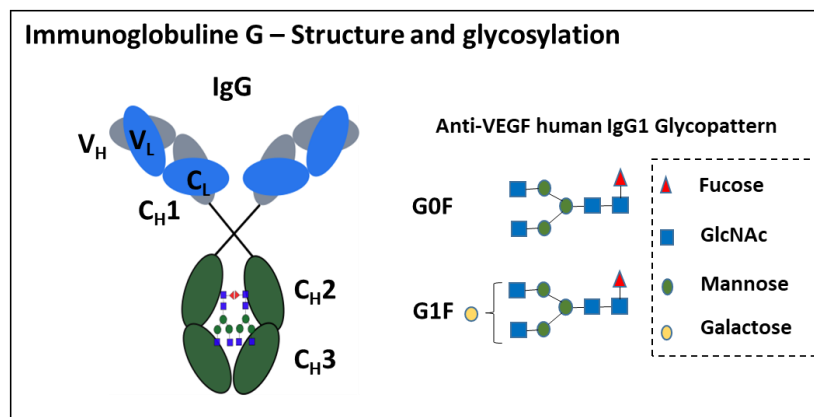


Figure 3: Overview of the IgG structure and the anti-VEGF human IgG1 glycosylation used in this thesis.

The heavy chain is divided into four structural subunits: the constant subunits CH3, CH2, CH1 and the variable subunit VH. The light chain consists of two subunits: the constant subunit CL and the variable subunit VL. The IgG used in this study was an anti-VEGF human IgG1 antibody with a predominantly G0F glycosylation consisting of a heptasaccharide with two GlcNAc, three mannose and two GlcNAc as well as a fucose residue but showed also G1F glycosylation containing an additional galactose residue in a small quantity.

At the Fc-fragment of IgG, the N-linked glycosylation is located in the CH2 domain at position Asn297. The mediation activation of effector functions by FCGR binding and/or C1q binding is highly affected by this glycosylation as it forms a hydrophobic core in the Fc fragment [75]. The glycan structure of the glycosylation is instrumental in maintaining the conformation necessary for binding to this effector protein. In several studies the removal of the N-linked glycan results in a closed formation of the Fc-fragment and prevents the binding of FCGRs [83–85]. Furthermore, it was shown that the presence of fucose in the core glycan reduces the interaction to some FCGR types significantly [84,86–90]. There are other interaction partners to IgG in human. Amongst others the most important are the intracellular TRIM21 that is involved in degradation processes, the neonatal Fc receptor FcRn that will be discussed in the next chapter and the already mentioned complement protein C1q and FCGRs (**Figure 4**).

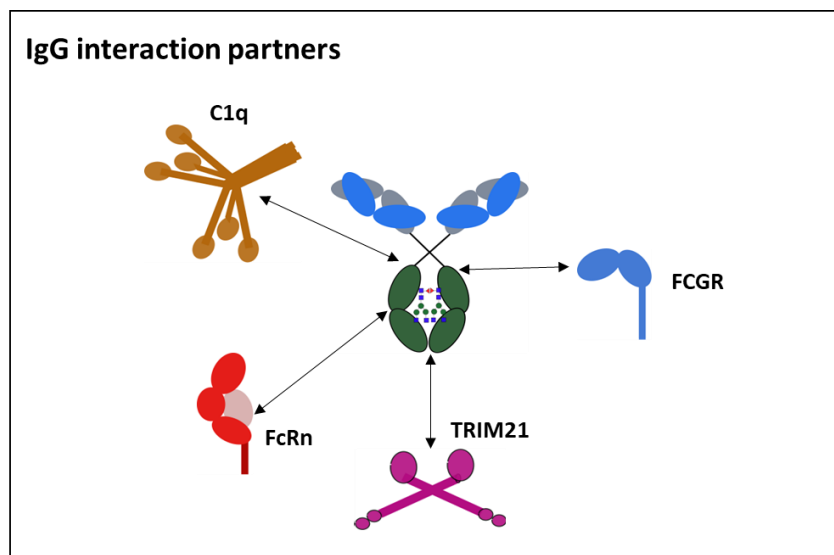


Figure 4: IgG interaction partners and sites of interaction.

Fc engaging molecules that mediates the biological activity of antibodies: Complement component (C1q), Fc gamma receptors (FCGR), the Neonatal Fc receptor (FcRn) and Tripartite motif 21 (Trim21) [72].

The interaction of IgG glycol-variants and subclasses with FCGRs will be discussed in detail in chapter 2.2.3. The IgG used in this study was an anti-VEGF human IgG that belongs to the most common subclass 1. Furthermore, the antibody shows a predominantly G0F glycosylation and a G1F glycosylation in a small quantity (**Figure 3**).

2.2.2 The neonatal Fc receptor – the best-known IgG transporter

The FcRn is a beta-2-microglobulin ($\beta 2m$) associated protein that is structurally related to the major histocompatibility class I family [91]. It consists of a heavy chain that non-covalently associates with the light chain $\beta 2m$. The heavy chain consists of three extracellular domains, a transmembrane domain and a cytoplasmic tail [92–94]. FcRn is ubiquitously expressed in the human body and binds to IgG at a distinct binding site to albumin under acidic pH of 5.0 – 6.5 with the exception of some IgG3 allotypes that bind also at neutral pH [95–97]. The functions of this specialized receptor in the body include increasing the half-life for albumin and IgG through recycling processes and mediating IgG bidirectional transcellular transport in endothelial and epithelial cells (**Figure 5**) [98]. Several studies have also attributed this receptor to have an important role in mediating immunological responses in dendritic cells (DCs) [99,100].

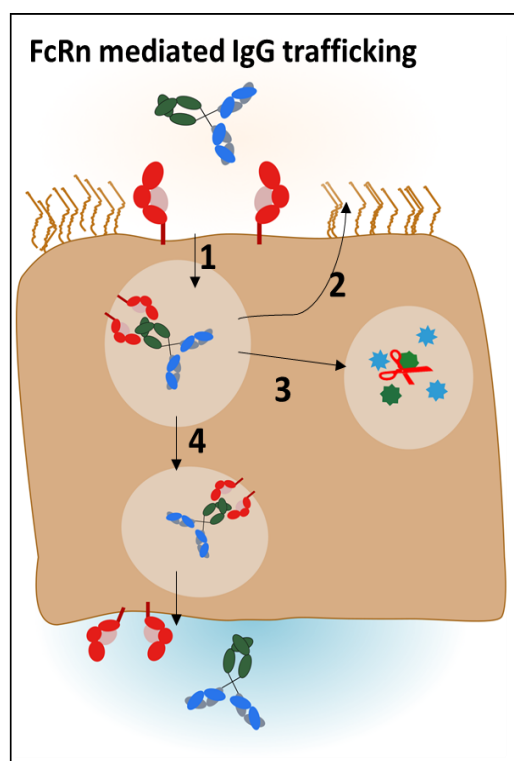


Figure 5: IgG trafficking pathways

IgG uptake in polarized epithelial cells is thought to happen via pinocytosis according to recent literature [[101]]. The FcRn binds to the Fc-domain of the antibody in the slightly acidic environment of the early endosome (1) and mediates recycling of the IgG to the apical side (2), digestion of IgG in the lysosome (3) or transcytosis to the basolateral side (4) [95]. Transcytosis is shown here from apical (nasal cavity) to basolateral, but the reverse direction was also reported [102]. The figure is modified from Ladel *et al.* (2018) [1], CC BY 4.0, <http://creativecommons.org/licenses/by/4.0/>.

The FcRn – IgG Fc interaction takes place at the IgG CH2-CH3 interface. This binding site is distinct of the Fc binding site of FcGRs. Since IgG is a homodimeric molecule, FcRn is thought to bind to the IgG Fc domain with equal affinity in a 2:1 stoichiometry [103]. Other groups have postulated that in addition the Fc binding site also the Fab fragments are involved in FcRn binding [104–106]. Several studies show the involvement of FcRn in IgG transport in different tissues and cell types [72,95,107–109]. Amongst them, the expression of FcRn in the BBB is the most interesting for N2B drug delivery. Here, FcRn is thought to function mainly as efflux transporter [110]. However, there are conflicting studies stating that FcRn may also take part in IgG distribution within the brain [28,111,112]. Recently, Ruano-Salguero and Lee (2020) evaluated the function of FcRn in an *in vitro* BBB model and resulted that antibody transcytosis across brain endothelial-like cells is not dependent on FcRn transport [113]. Despite this finding, they highlighted the lack of knowledge in transcytosis mechanism and the need for further evaluations. In general, the function of FcRn as IgG transporter in mucosal sites was proven in several studies focusing on gut or lung mucosa [108,114].

Introduction

As also for N2B drug delivery, the first the first barrier to overcome is the nasal mucosa, it is of great interest to evaluate if FcRn function at this mucosal site is similar to other reported mucosa or if the function of FcRn in the neuro-epithelium is comparable to sites of neuronal tissue.

2.2.3 Fc gamma receptors

In literature, besides the FcRn other proteins are known to interact with IgG but few are thought to be involved in IgG transport. The other promising protein family that theoretically could act as IgG transporter are other Fc gamma receptors (FCGR, **Figure 6**). These other FCGR are a family of glycoproteins that interact with the IgG Fc domain and trigger a variety of immune related effector functions such as antibody-dependent cellular cytotoxicity, antibody-dependent cellular phagocytosis, antigen internalization and presentation or cytokine release [115]. So far, four different classes of these FGCR have been identified: FCGR1, FCGR2, FCGR3 and FCGR4. Those classes comprise several subclasses such as FCGR2a and b, FCGR3a and b. The best-characterised subclasses are FCGR1, FCGR2a and b and FCGR3a.

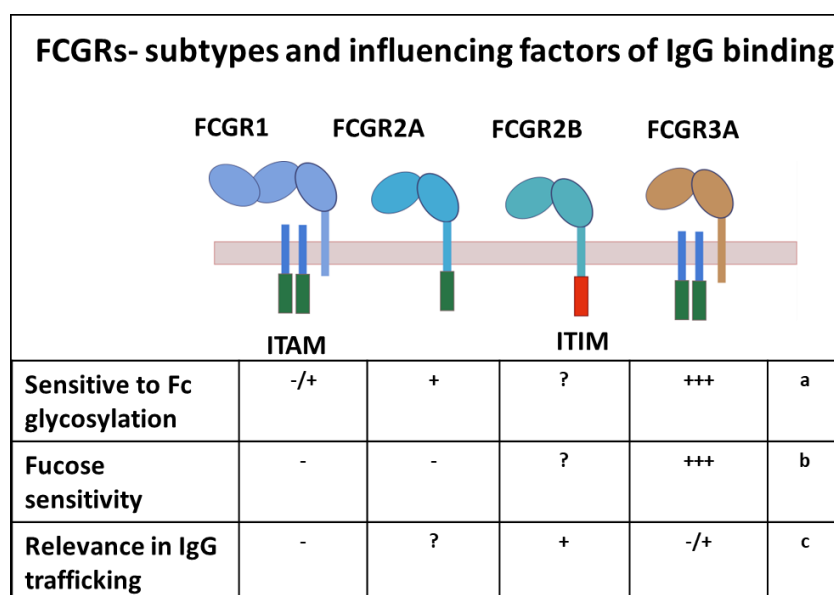


Figure 6: Overview of human FCGR subtypes, their sensitivity to Fc glycosylation, to Fc fucosylation and their involvement in IgG trafficking based on literature data. Ref: a: [88,116,117], b: [87,88,117–119]; c: [88,117,120,121].

Introduction

In contrast to the other classes, FCGR1 has an additional binding domain and show high affinity for the IgG Fc domain as well as restricted IgG isotype specificity. FCGR2 and FCGR3 have low affinity for the IgG Fc part, but a broad isotype binding pattern. FCGR4 is so far least characterized but show an intermediate affinity to IgG Fc and restricted subclass specificity [115,122,123]. These FCGR classes can be divided due to their functional properties: activating and inhibitory receptors. They mediate their function via an intracellular domain called either immunoreceptor tyrosine-based activation (ITAM) or inhibitory motifs (ITAM) [115,124]. The co-expression of activating and inhibitory receptors is one of the key factors in immune system regulation. Besides their expression on different lymphocytes, FCGR have been found to be expressed in other cell types. For example, FCGR1 was found to be expressed in the rat neuronal cells and FCGR3 and FCGR2b expression was detected in epithelial cells of the placenta [118,125,126]. The low affinity FCGRs are highly sensitive to IgG glycosylation pattern as shown by several studies [71,75,88]. In general, deglycosylated Fc does not bind the low affinity FCGRs whereas the binding of the high affinity receptor FCGR1 is preserved. Furthermore, Fc glycan glycosylation pattern/ composition influences the affinity of Fc for FCGRs. Most prominent example is the 10-to-50-fold decrease of affinity of Fc for FCGR3a due to the presence of fucose in the glycostructure whereas a GlcNAC and galactose residue improve affinity for FCGR3a [88]. Subedi *et al.* (2014) revealed that Fc trimmed back to a glycan that consists of a single GlcNAc residue still binds FCGR3a, however the binding is completely inhibited when fucose is still present [71,117]. Due to their expression in the placental barrier, FCGR3a and FCGR2b has been evaluated for their potential to participate in IgG transport with conflicting results. Whereas Ishikawa *et al.* (2015) found evidence that FCGR2b is involved in placental IgG transport, other studies showed that aglycosylated IgGs are still transported to the foetus [118,127].

Taken together, first links of FCGR taking part in IgG trafficking are made, but due to the conflicting results of several studies more effort needs to be done needed to evaluate the diversity of function of these receptors.

2.3 Ex vivo tissue models of the nasal mucosa

2.3.1 *The pig as model organism*

The pig is a well-established model organism for anatomical, genetic and physiological investigation because of its high similarity to humans [128,129]. Both species are omnivorous and their organs share common functional features. In addition, most proteins of the immune system share structural and functional similarities, meaning that more than 80 % of analysed parameters of the immune system resembles the human counterpart whereas in mice less than 10 % are similar to humans [130]. The main differences here are the inversion of lymph nodes, two different types of Peyer's Patches in the intestine and the transfer of passive immunity from the sow to the piglet [131]. Of note, these differences do not interfere with the use of the pig as model organism for the nasal mucosa. Several studies show high similarity between the human and porcine respiratory and olfactory mucosa [132–137]. The structure of the olfactory mucosa in pigs is highly similar including the main features such as the composition of the epithelial layer and the *lamina propria* (Figure 7).

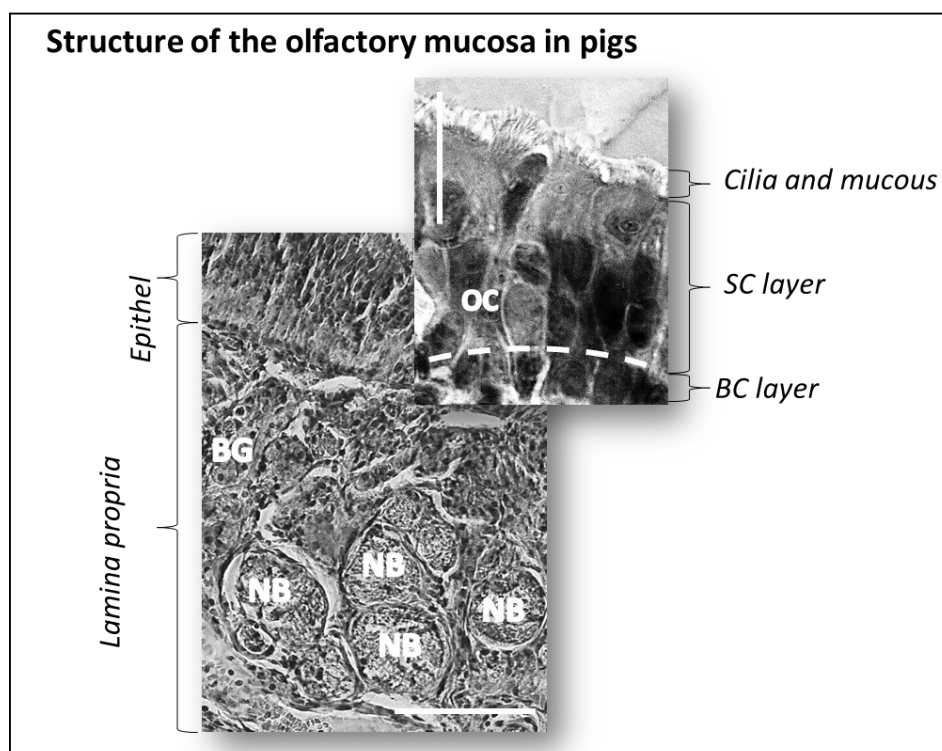


Figure 7: Structure of the olfactory mucosa in pigs.

Like the human counterpart, the olfactory mucosa in pigs is composed of the epithelium with ciliated cells, supporting cells (SC), olfactory sensory neurons (OSN) and basal cell layer (BC layer). In the *lamina propria* Bowman's glands and neuronal bundles analogous to the human olfactory epithelium are visible.

Scale bar mucosa: 200 μm ; scale bar epithelium: 20 μm ; the figure is modified from Ladel *et al.* (2018) [1], CC BY 4.0, <http://creativecommons.org/licenses/by/4.0/>.

Especially the olfactory nerve seems to be functional and structural related to man [138]. The pig is also an interesting model organism regarding the study of the IgG transport mechanism in N2B. Amongst others Ober *et al.* showed cross-species transport of human IgG by the porcine FcRn [139–141] and Egli *et al.* (2019) investigated the cross-species binding of human IgG to porcine FCGRs [142]. Besides its high similarity to human, the pig has several other advantages such as availability (live-stock species, tissues available from slaughterhouses etc), the size of the animal especially the upper respiratory tract, and ethical reasons due to the use of slaughterhouse pigs [131].

2.3.2 Side-by-side cell models

The reproduction of the entire nasal mucosa is highly challenging and has not been achieved by *in vitro* models so far. Therefore, many works have been made to use animal excised nasal mucosa tissue for permeability studies. Several species were used for this purpose, including rabbit, bovine, ovine, porcine, rat and human excised mucosa explants [143]. There are numerous advantages of using excised tissue explants in diffusion chambers such as simple and fast methods compared to *in vivo* however more complex and closer to reality compared to *in vitro* models. Furthermore, continuous validation of the integrity and the viability of the tissue by measuring electro-physical parameters is possible. As an advantage, low donor and receiver volumes are needed to evaluate drug transport. However, the specialised chambers made of glass or Plexiglas® are relatively high in cost compared to other *in vivo* and *in vitro* models and the possibility of substances adsorbing to the material is high [144].

Side-by side cell models rely on the use of chamber systems in which a donor and a receptor medium are separated by a tissue explant. Two standard models have been developed in the past for measuring the transport of mainly small molecular weight drugs across *ex vivo* mucosal explant: The Franz diffusion cell and the Ussing chamber [145–148]. E.g., Mistry (2009) used porcine olfactory epithelium, that was mounted vertically in a Franz diffusion chamber to evaluate the transepithelial passage of nanoparticles.

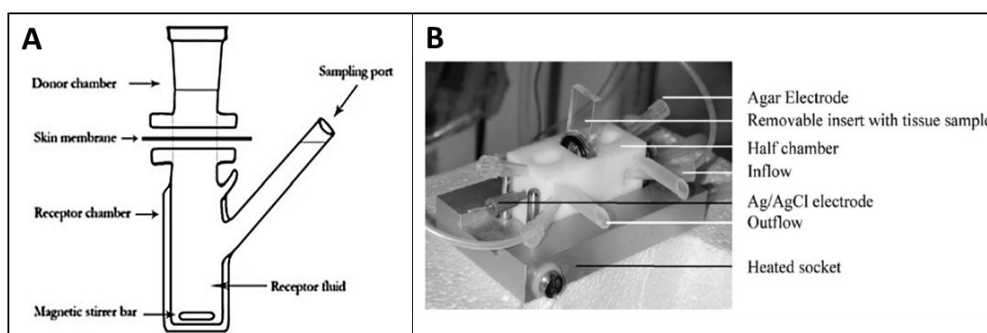


Figure 8: Side by side cell models

A: A Franz static diffusion cell. Figure taken with permission from Seo *et al.* (2017) [148]

B: Continuously perfused Ussing chamber. Figure taken with kind permission from Li *et al.* (2004) [147]

These devices are built of two symmetrical diffusion chambers. The tissue is mounted vertically between the chambers on cork supports. To gain homogeneity in the receiving chamber, magnetic stirrer bars are used [145]. In addition, oxygen supply and temperature control by a water jacket is applicable to both control the system and to keep the tissue viable. Östh *et al.* (2002) published a method for studying drug absorption across pig nasal respiratory mucosa using a horizontal Ussing chamber system. Hereby, the placement of the mucosa is horizontal in contrast to the Franz cell diffusion chamber. This has the advantage to measure the tissue integrity via electro-physical methods and remove the media from the apical mucosa to study permeation under air-liquid interface conditions [144]. However, also for this method the set-up is complex and require many expensive components for the experiments.

In this thesis, another side-by-side set-up was used that is based on the Franz diffusion cell. The basic set-up was developed and described in the thesis of Johannes Flamm in 2021 who used microreaction tubes and simple clamps from construction markets to gain a cheap, but reliable side-by-side model for air-liquid interface permeation experiments [149]. This model was adapted in terms of modification in the tube preparation and media volume. Furthermore, the receiving media was not stirred as there are strong evidence in literature showing that shear stress has a high impact on the tissue and cell integrity [150]. The set-up used in this thesis is displayed in **Figure 13**. Briefly, the excised mucosa is spanned upside down between two microreaction tubes that have small openings for media supply and sampling on the receiving (abluminal) compartment and substance application at the donor (apical) compartment.

Introduction

With these settings, the following advantages are to mention: small, cheap and simple apparatus set-up, incubation in a normal incubator and therefore highly stable temperature control. Furthermore, small tissue explants are needed and therefore a statistically significant amount number of experiments could be performed in parallel with the same donor pig. Last, but not least, very low volumes (<100 µl) are needed for the media supply, which is beneficial an advantage for substances that permeate poorly.

2.4 *In vitro* models of the nasal epithelial barrier

The study of permeation kinetics in an *ex vivo* model has several disadvantages that were mainly due to the short lifespan of the tissue explants and the high variability of the samples resulting in high standard deviations. A promising but less complex alternative are *in vitro* models using epithelial cells that are cultured under highly controlled external conditions. These models allow a simplification of the complex nasal mucosa as they display only the first barrier without considering parameters such as blood stream, immune system and glands. Several primary cell and tumour cell models have been established to perform permeation experiments under mucosal site-like conditions [49,151–156]. Thereby, two approaches are possible for the set-up of *in vitro* barrier models: tumour cell lines and primary cells. Tumour cell lines like the human nasal epithelial cell line RPMI 2650 are a standard tool for modelling mucosal barriers, however they do not display e.g. the heterogeneity of the complex epithelial composition and other features (see below). As a second option primary epithelial cells can be cultivated similarly on cell culture membranes to simulate the epithelial barrier [157,158]. Between these cell models, the lifespan of the cells and differentiation ability differs greatly. Tumour cell lines have a great benefit to be immortal, whereas primary cells are limited to a certain number of cell divisions [159]. On the other hand, the majority of tumour cell lines show a low differentiation status and lack the ability to fully differentiate into e.g. ciliated or mucus producing cells, while primary cell cultures are morphologically and physiologically very close to their native counterpart [49,160]. For N2B drug delivery, factors that influence the clearance and destruction of a drug substance are of high importance, therefore e.g. cilia and mucus formation are important parameters to consider when choosing a cell model. Recently Na *et al.* (2016) built up an *in vitro* model for drug permeation with commercially available human nasal primary cells, however these cells are highly expensive and therefore a poor option for academic research [161].

In the nasal mucosa, epithelial cells show features such as cilia, mucus secretion and the formation of tight junctions that have high impact on the permeation of intranasally applied drugs [38].

Introduction

Therefore, it is preferable to use a heterogenic mixture of different cell types since resembles the mucosal epithelial cell layer more closely and might give better data for the permeation profile of drugs through the cellular barrier [160,162]. Another aspect to consider is the growth behaviour of tumour cells and primary cells. Cultured tumour cells tend to build multilayers because of a lack of contact inhibition after reaching confluency, whereas the growth of primary cells remain in monolayers. Here a clear preference is hard to establish as the olfactory epithelium is composed of at least two cell layers: the basal cell layer and the epithelial cell layer, however due to continuous replacement of cells also more layers are possible. Nevertheless, these cells are highly specialised in their respective layer and cannot be modelled by homogenous cell multilayers. There are several studies supporting the use of the tumour cells line originating from nasal squamous epithelium (septum) like RPMI 2650 as a suitable model for the nasal epithelium [43,44,49,160,163]. The RPMI2650 cell line originate from squamous epithelium of the nasal septum and is closely related to normal human nasal epithelium in terms of its karyotype and the cytokeratin polypeptide pattern as well as the presence of mucus on the cell surface [157,158,164]. Furthermore, several metabolic features were investigated and stated to be similar to the corresponding metabolic features of excised human nasal tissue [165,166].

An important characteristic of nasal epithelial cells is their ability to grow under air-liquid interface (ALI) conditions. The majority of the cellular airway models use the method developed by Tchao *et al.* in 1989 [167]. Briefly, cells are cultivated on porous plastic membrane inserts in multi-well plates with basolateral medium supply, whereas the apical side of the cellular layer is exposed to air. These so-called air-liquid interface (ALI) conditions drive the cells to form strong tight junctions and initiate the differentiation towards e.g. ciliated or mucus producing cells [168–170]. Thereby, as mentioned above, such a differentiation cannot be generalized for tumour cells as they lack the potential to differentiate to a certain extent. Mercier *et al.* (2018) postulated generally accepted key criteria that appropriate *in vitro* barrier cell models should meet when cultivated under ALI conditions [160]: a sufficient high trans-epithelial electrical resistance (TEER), the presence of specific tight junction proteins such as *zonula occludens 1* (ZO-1) and adherents junction proteins such as E-cadherin [171,172]. Furthermore, factors such as the paracellular permeability and the expression of drug transporters for transcellular permeation should be taken into account. Hereby, model substances like e.g. sodium fluorescein or FITC- dextran can be used to study the paracellular permeation.

In this thesis, the criteria set for the validation of the cell models were based on the criteria postulated by Mercier in 2018 and extent to the presence of the mucin MUC5AC and the general morphology of the cells that form the barrier.

3. Objective of the thesis

In the last decades, drug delivery to the brain via the nasal route came more and more into focus. In contrast to other approaches, there is no need for the BBBs to be demolished in order to transport therapeutic molecules to the brain, but rather peripheral nerves such as the olfactory neurons are used as transport channels. However, the exact mechanisms involved have not yet been elucidated [16,30,54].

One of the major problems in N2B investigation is the difficult accessibility of the olfactory epithelium in most mammals, but especially in humans and here particularly for ethical reasons. However, there are big differences in the nasal anatomy and especially the olfactory area between species as summarized by Pabst *et al.* in 2010 [173]. Standard mammal models such as mice and rat are not suitable as the olfactory area is much larger and the local immune system differs essentially [8,19,20,173,174]. However, several attempts were made to test the pig for its suitability as a model for the human nose [138,175,176]. One aim of this thesis was to test the suitability of the pig as a model organism also on the histological level.

As part of the European 3R initiative (Replacement, Reduction, Refinement), the use of animal replacement methods is being increasingly promoted. There are many advantages, such as shorter test durations, higher reproducibility, in some cases easier handling, less need for additional training, and it is also more ethically justifiable [177,178]. However, besides the human tumour cell line RPMI2650 having the typical disadvantages of immortalised cell lines such as low differentiation ability and multi-layer growth there is a lack of good alternative models [160]. Thus, there is a lack of knowledge concerning data of high molecular weight protein transport such as the permeation pathway of therapeutic IgGs. Hereby, also the *lamina propria* beneath the nasal epithelial barrier is of importance as it is a site of bundled neuronal fibres and the local immune system that might interact with therapeutic IgGs and influences the uptake rate to the brain [1,179]. In contrast to systemic or peripheral tissue specific diseases, there are few therapeutic approaches with monoclonal IgGs for CNS-related diseases due to the low bioavailability caused by the restrictive barriers such as the BBB and the BNB [180]. In order to use IgGs in the treatment of CNS diseases successfully, it is necessary to develop reliable models that reflect the *in vivo* situation in humans as closely as possible. Especially the fact that the olfactory region and the mucosa differ between species makes it difficult to project studies in standard laboratory animals like mice or rats correctly to humans. Furthermore, it is important to generate more information on antibody transport across the olfactory mucosa, e.g. the possibility to increase the uptake of therapeutic antibodies by genetic engineering.

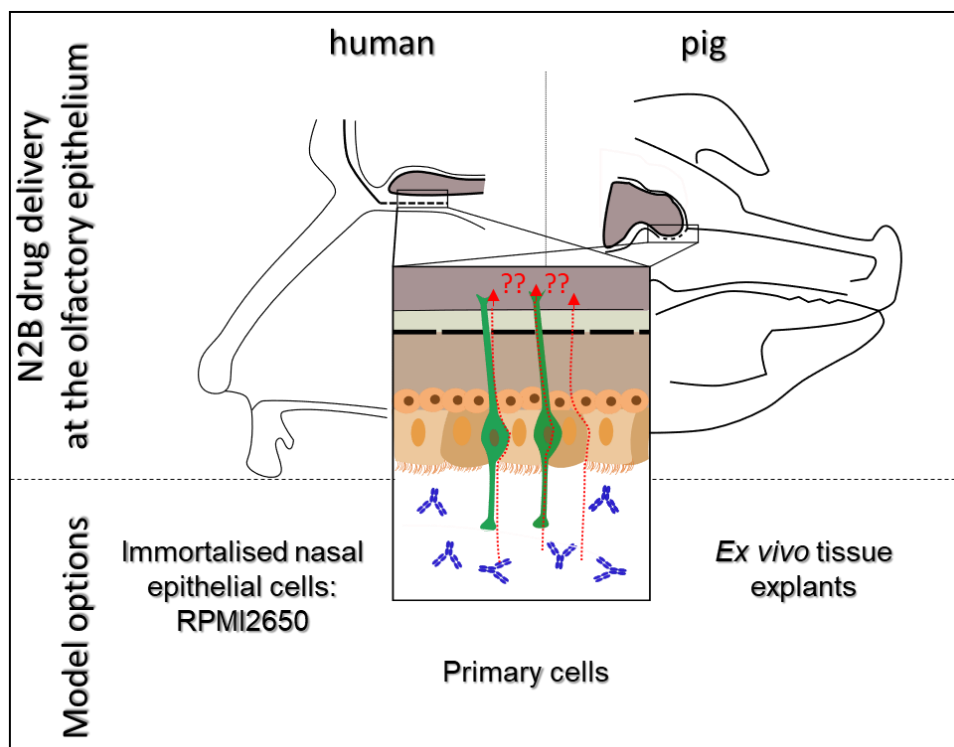


Figure 9: Objective of the thesis: Development of models to simulate N2B drug transport with special focus on IgGs.

The pig as model organism was used by other groups before which strengthens the use of porcine olfactory mucosa for N2B drug delivery investigations [132–136, 181, 182]. Besides *ex vivo* experiments using pig olfactory mucosa and primary cell model using the same area for cell isolation the tumor cell line RPMI2650 is a human alternative that is used as standard model for the human nasal epithelium [2, 43, 44, 160, 162, 165, 183–188]. This thesis aims the development of primary cell models as well as *ex vivo* tissue models and the evaluation of these models compared to the standard RPMI2650. The thesis focused on the N2B drug delivery of IgGs as there are many promising candidates for the treatment of CNS-related diseases. However, due to the low permeability of the BBB and the lack of knowledge concerning IgG transport to the brain, none of the candidates were successfully implemented in therapy so far [120, 180, 189].

Since the transfer of study data of the olfactory mucosa from animal to human is difficult due to the possibly large differences between the species, the olfactory mucosa of the model animal pig was first checked for agreement with the human olfactory mucosa [190].

The main objective of this thesis was the development of suitable animal replacement models considering both the epithelial barrier itself as well as the composite of the epithelial layer and the underlying lamina propria with all its special features, for the future investigation of IgG transport through the nasal olfactory mucosa (**Figure 9**).

Objective of the thesis

During the characterisation of the porcine olfactory mucosa and the development phase of the models several new aspects raised indicating to new insights into IgG trafficking that lead to a previously unplanned objective of this thesis: the investigation of IgG transport. Therefore, further experiments were accomplished to investigate factors influencing the transport of IgGs in the olfactory epithelium and in the nasal mucosa. For this purpose, experiments were performed with human IgGs and porcine IgGs to investigate the dependence of the transport mechanism on the IgG origin. Furthermore, the developed models and additionally the standard model RPMI2650 were compared against each other to be able to determine parallels between the species and to gain new insights into IgG trafficking. Again, as the work progressed, it became clear that interaction with the immune system could play a very important role in N2B drug delivery. Therefore, as a last step the influence of the immune system on the permeation of IgGs through the olfactory mucosa should be investigated using deglycosylated antibodies to reduce the binding to immune-relevant receptors.

In summary, this thesis addresses the following objectives:

- Objective 1: Characterisation of the porcine olfactory mucosa to check its suitability to model the human counterpart
- Objective 2: Development of appropriate models that simulate the human olfactory mucosa for N2B drug delivery investigations
- Objective 3: Investigation of IgG transport mechanism in the olfactory mucosa

4. Results and Discussion

4.1 Development and evaluation of different models to simulate mucosal IgG uptake and permeation

To gain information about the uptake and permeation behaviour of IgGs through the olfactory mucosa, appropriate *ex vivo* and *in vitro* models were developed using porcine olfactory mucosa.

4.1.1 *The ex vivo model for permeation through the olfactory mucosa– a modified side-by side tissue model using porcine mucosa explants*

The pig as model for the human nasal mucosa was used in other studies before [134–138]. However, most of these studies used the respiratory mucosa for the experiments. Therefore, the porcine olfactory mucosa was firstly evaluated for resemblance to the human counterpart. Different parts of the porcine upper nasal mucosa were excised and evaluated for the potential to simulate the human counterpart. Literature-based parameters were considered for this purpose: a. the morphological structure of the epithelial layer, b. the structure of the *lamina propria* and c. the presence of the olfactory marker proteins for nasal mucus (MUC5AC, [191,192]), Bowman's glands (AP5, [193]), microvillar cells (M cells, CK18, [29,194]) and neuronal fibres (PGP 9.5, NF200, [195,196]).

Figure 10 shows the areas of dissection. Samples were taken from the upper part of the concha nasalis dorsalis (cnd), the concha nasalis media (cnm) and the ethmoid turbinates (ET). For simplification, the cnd and cnm will be combined under the term “cnd” in the further course of this work.

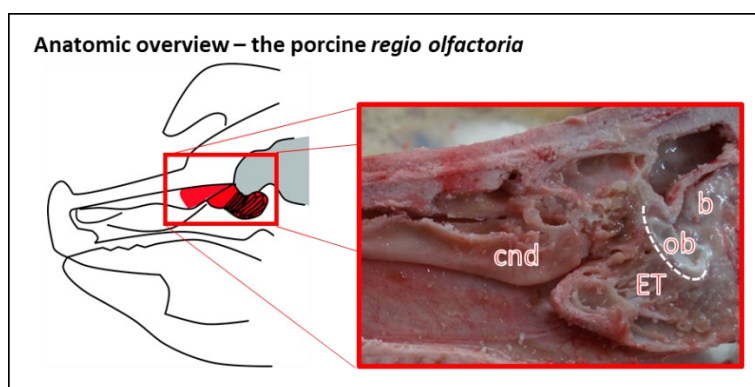


Figure 10: Area of dissection in the porcine nasal cavity: dorsal part of the concha nasalis dorsalis and the concha nasalis media. The concha nasalis dorsalis is the porcine equivalent to the human concha nasalis superior (c.n. superior). To summarize the dissection area will be named concha nasalis dorsalis (cnd). ET: Ethmoid turbinates, ob: olfactory bulb; b: brain. Figure is modified from Ladel *et al.* (2018) [1], CC BY 4.0, <http://creativecommons.org/licenses/by/4.0/>.

For reference, histological examination in literature and mucosa samples from human concha nasalis superior from donor bodies were used (**Figure 11A**) [17,24].

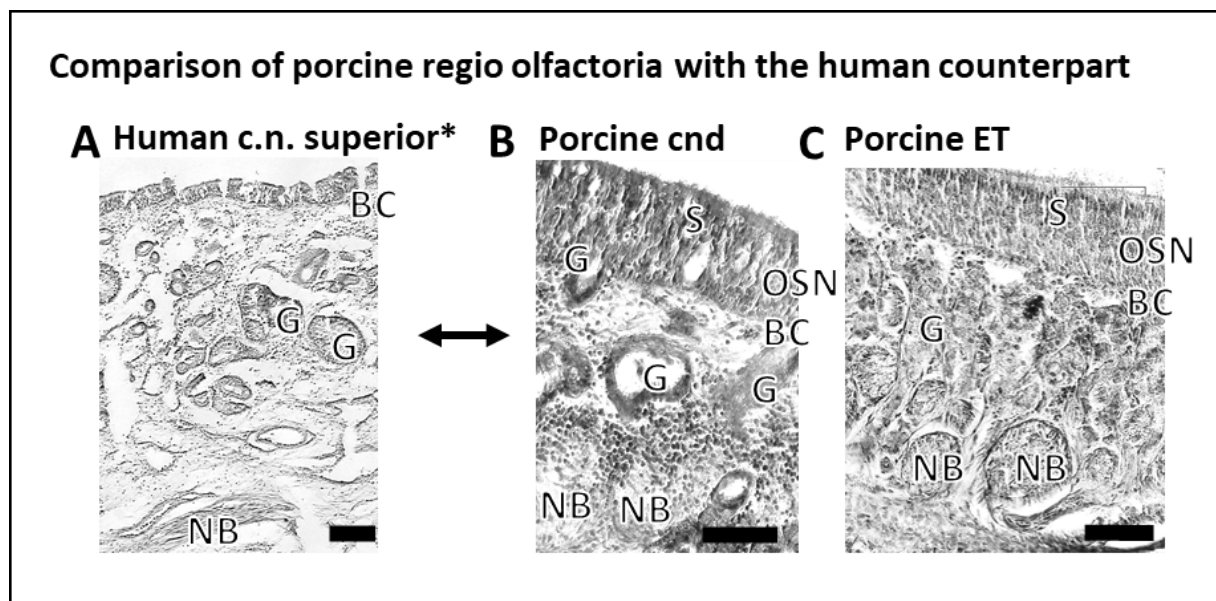


Figure 11: Histological examination of human and porcine olfactory mucosa

A: dissection of human concha nasalis superior from body donation. Due to the incipient decomposition of the body, the tissue and especially the neuronal fibres are not optimally preserved. However, it is ethically unacceptable to take biopsies from the olfactory region in living humans. Scale bar: 100 μ m.

B: Section of porcine cnd stained with Hematoxylin-Eosin (HE) staining. Olfactory epithelium specific structures such as neuronal bundles (NB, Bowman's glands (G) and the typical structure of the epithelial layer with basal cells (BC), olfactory sensory neurons (OSN) and supporting cells are present.

C: Section of porcine ET stained with HE staining. The ET are small folds directly beneath the cribriform plate where the nerve fibres are bundled. Similar to the cnd all feature of the olfactory mucosa are present however less Bowman's glands and bigger NB are visible. Scale bar: 100 μ m.

Figure is modified from Ladel *et al.* (2018) [1], CC BY 4.0, <http://creativecommons.org/licenses/by/4.0/>.

Paik *et al.* (1992) showed that the probability of obtaining intact and functional olfactory tissue in human decreased significantly with increasing age of the subjects. Therefore, literature data were the preferred reference, since as the donor bodies were from people of high age (> 75 years).[17]. In the examination of the porcine nasal mucosa, the upper part of the cnd and cnm were morphologically highly similar. Both showed olfactory mucosa specific features such as Bowman's glands, neuronal fibres formatted in neuronal bundles (NB) and the composition of epithelium with the basal cell layer (BC), olfactory sensory neurons (OSN) and supporting cells (**Figure 11 B**). These finding fits to reported studies of human cnm and concha nasalis superior areas [17].

Results and Discussion

As the ET are the area directly beneath the cribriform plate and the olfactory bulb, it was of interest whether this tissue differs from cnd. In fact, the amount of Bowman's gland and blood vessels was clearly lower in the ET explants whereas the neuronal fibres occur in bigger agglomerates and in higher density compared to the cnd (**Figure 11C**). This again is in alignment with to descriptions of the mucosa beneath the human ethmoid bone [15,17,197,198].

To further strengthen the model and ensure the morphological examination, specific marker proteins were used to further analyse the porcine cnd using immunohistochemistry methods. **Figure 12A** shows a neuronal bundle in the cnd *lamina propria* that is double-stained against the axonal marker NF200 and a marker for sensory neurons, the protein gene product 9.5 (PGP9.5) [199–202]. Furthermore, the presence of Bowman's glands visualised by immunoreactivity against AP5 (**Figure 12B**) and the presence of M cells visualised by immunoreactivity against cytokeratin 18 (CK18) (**Figure 12C**) confirms the findings of high similarity of the human and the porcine olfactory mucosa.

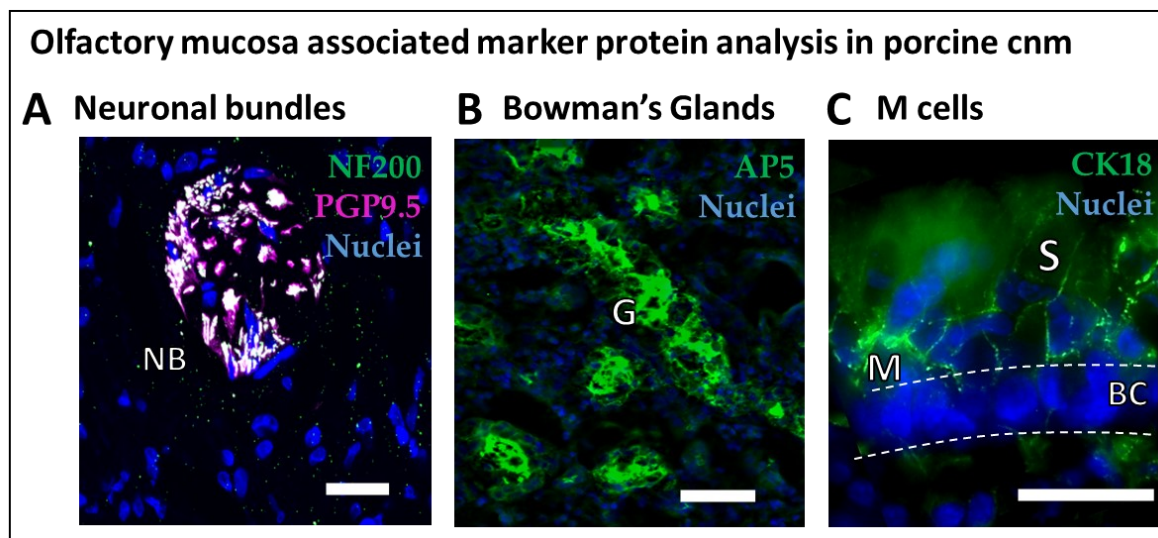


Figure 12: Immunofluorescence study of the porcine olfactory mucosa.

To refine the histological examination, specific markers were stained via specific immunofluorescence against Neurofilament 200 (NF200, green) and Protein Gene Product 9.5 (PGP9.5, pink) as marker for primary neuronal fibres (**A**), against aquaporine 5 (AP5, green) as marker for Bowman's glands (**B**) and cytokeratine 18 (CK18) as marker for microrvillar cells (M cells, **C**). NB: neuronal bundles, G: Bowman's glands; BC: basal cells; S: Supporting cells; M: M cells Scale bars: 50 µm. Figure is modified from Ladel *et al.* (2018) [1], CC BY 4.0, <http://creativecommons.org/licenses/by/4.0/>.

Results and Discussion

Several *ex vivo* mucosa models were set-up in the past decades [203–207]. Here, the developed side-by side chamber model was refined from a model set-up by Johannes Flamm between 2015 and 2019 [149]. The set-up is composed of two 1.5 mL microreaction tubes which have small openings on both tubes and that are immobilised on a hand clamp (**Figure 13**).

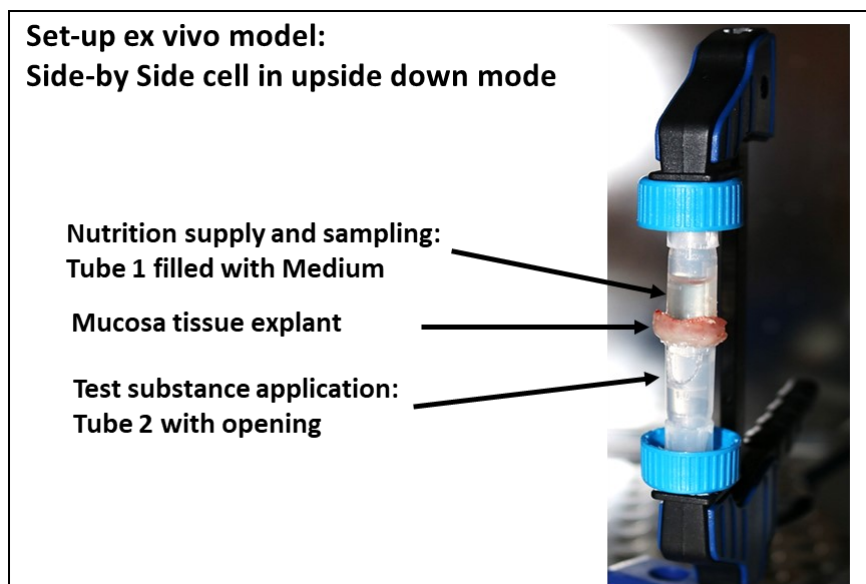


Figure 13: Experimental set-up of the refined ex-vivo model

The mucosa specimens were fixed with a fastening clamp upside down in between two 1.5 mL microreaction tubes. In the upper tube a small opening was introduced into the tube wall for sampling. In the lower tube, a small opening was cut to obtain access to the mucosal surface for antibody or vehicle (PBS) application. Figure is modified from Ladel *et al.* (2018) [1], CC BY 4.0, <http://creativecommons.org/licenses/by/4.0/>.

The mucosa tissue explants are spanned upside-down, meaning the epithelial layer was directed to the lower tube. The reasoning behind this upside-down set-up was to simulate the *in vivo* situation as close as possible. Also *in vivo* in the human nose intranasally applied substances to the olfactory region will permeate against gravity. Furthermore, for practical reasons the medium supply in small volumes to avoid high dilution of the samples was easier to handle if filled into the upper tube. The opening in the upper tube is needed for the addition of medium and for sampling during the permeation experiments. The opening in the lower tube is used for the application of the IgG solution on the epithelial surface. For the preparation, it was essentially to dissect the tissue very carefully to avoid damaging of the neuronal fibres and the epithelial layer. To make sure that the tissues used for the permeation were intact, histological sections were made from each of the explants to test for epithelial integrity and described parameters [1].

4.1.2 The *in vitro* model – mimicking the olfactory epithelial barrier using primary cells from the porcine regio olfactoria

A major disadvantage of using *ex vivo* mucosa explants is the limited lifespan of the tissue. Here, the challenge was to develop models that are as close as possible simulate the *in vivo* situation and with a long lifespan to perform permeation experiments over a certain period.

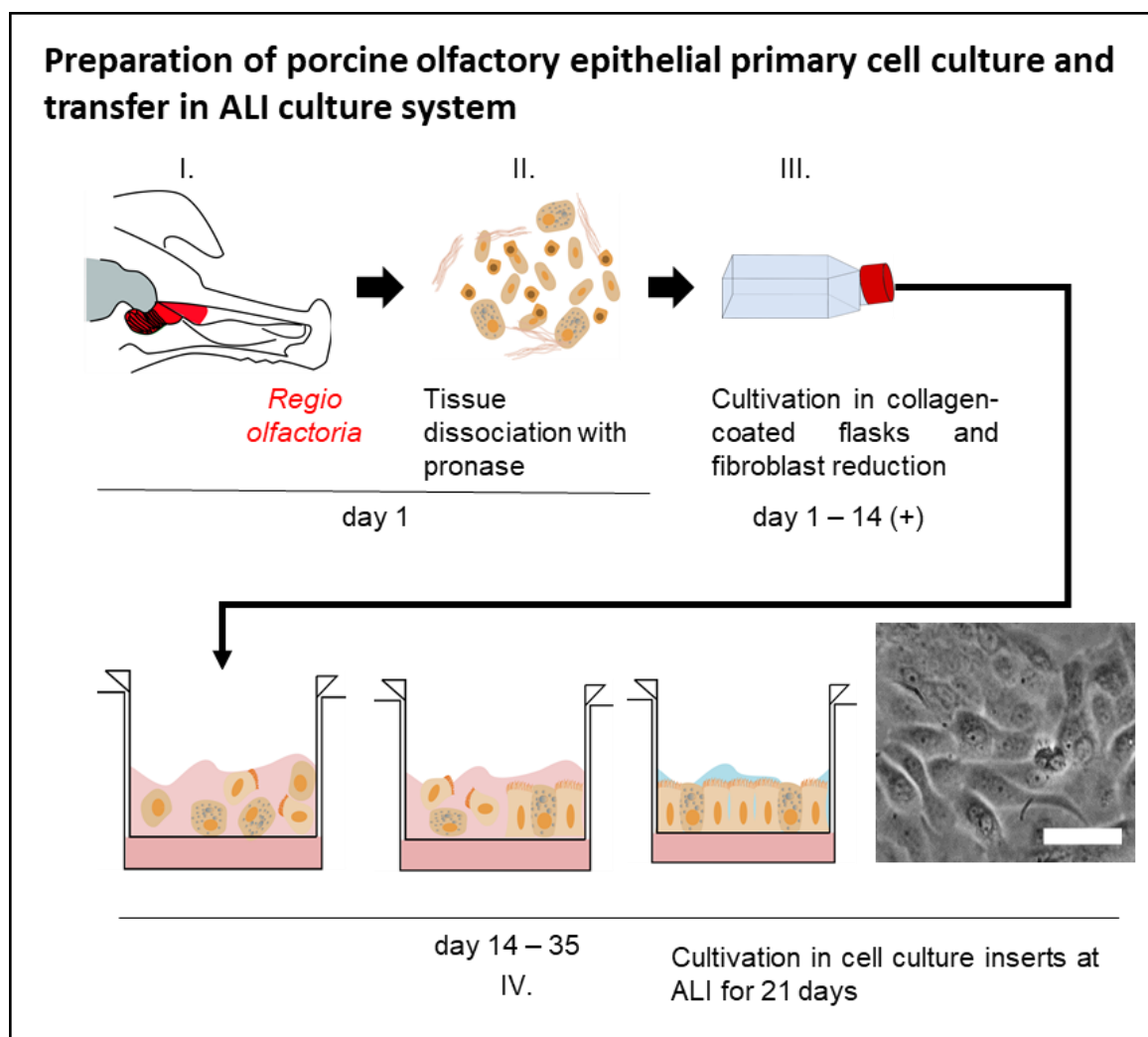


Figure 14: Workflow for porcine olfactory epithelial cell (OEPC) isolation and cultivation under air-liquid interface (ALI) conditions – building up an epithelial barrier for drug permeation studies.

- (I.) The mucosa was dissected from the porcine olfactory region (red).
- (II.) The tissue explant was digested by pronase to obtain single cells.
- (III.) Those were cultivated in collagen coated T75 cell culture flasks.
- (IV.) After cells reached 80 – 90 % confluence in the T75 flasks a transfer into ALI culture system was carried out followed by a cultivation period of 21 days.

Scale bar: 50 µm. Figure is modified from Ladel *et al.* (2019) [2], CC BY 4.0,

<http://creativecommons.org/licenses/by/4.0/>.

Results and Discussion

A promising approach are primary olfactory epithelial cells (OEPC) that are cultured under air-liquid interfaces analogous to the epithelial cells in the nasal cavity [167]. Mercier *et al.* (2018) postulated generally accepted key criteria that appropriate *in vitro* barrier cell models should meet. Those criteria comprise the formation of a barrier with sufficient high trans-epithelial electrical resistance (TEER) and the presence of specific tight junction proteins such as ZO-1 when grown under ALI conditions [171,172]. In this thesis, further criteria were added, that influences the N2B permeation respectively the drug clearance from the mucosal surface: e.g. the formation of cilia and the expression of mucins.

To gain OEPC single cells a pronase enzymatic digest of cnd explants was performed as described by Ladel *et al.* (2019) [2]. Briefly, those cells were cultivated in collagen coated flasks and transferred to a cell insert membrane to grow them under ALI conditions for 21 days (**Figure 14**). The duration of the ALI cultivation was performed analogous to a protocol from Lee *et al.* (2005), who cultured primary nasal epithelial cells from human respiratory mucosa for drug permeation studies [169].

Nevertheless, to evaluate the cultivation time for OEPC the above-mentioned parameters were taken into consideration: the barrier formation (TEER value and tight junction formation), the production of the mucin MUC5AC and the formation of cilia. Each parameter has direct influence on drug permeation through the barrier as described [38]. Besides these parameters the OEPC were compared to primary epithelial cells of the porcine respiratory mucosa (REPC, [2]) to evaluate the necessity of using cells of the olfactory region and not use easier accessible cells from the respiratory region. As this work focuses mainly on the olfactory region the results of the REPC experiments are not displayed here but are included in the original publication that is attached to the appendix of this thesis. Furthermore, the OEPC model was compared to the standard nasal epithelial barrier permeation model RPMI 2650 to evaluate whether the benefits of the primary cell cultivation outweigh the additional expense. Morphologically the OEPC and REPC showed both heterogeneous cell populations and grew as a monolayer on the cell insert membranes (**Figure 15A**). The formation of cilia is shared by REPC and OEPC as seen in the immunoreactivity against acetylated α -tubulin for OEPC (**Figure 15B**). Several studies have validated acetylated α -tubulin as a selective marker for non-motile and motile cilia of polarized cells [208–210]. Interestingly, in contrast to the OEPC the REPC showed a higher number of motile cilia and a high number of cells that contain large vesicles similar to goblet cells [211]. This finding is in line with the literature description of the differences between olfactory and respiratory mucosa. Further on the REPC showed a higher and better-defined signal of the tight junction marker ZO-1 (**Figure 15B**, [212]). This again fits with the literature, as the olfactory epithelium is thought to be less tight connected due to the continuous outgrowth of OSN neurites into the apical space [213].

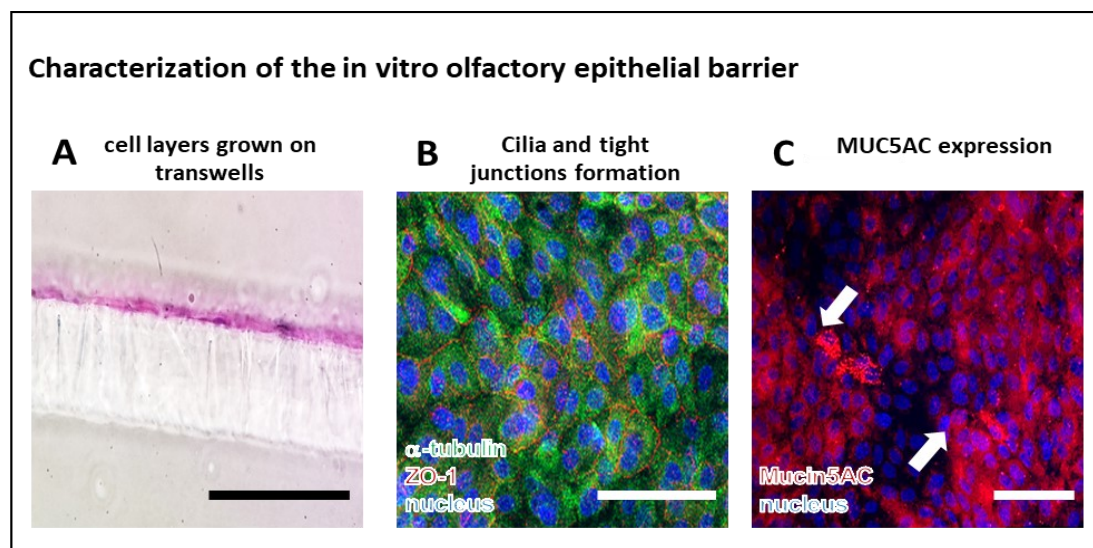


Figure 15: Immunohistological characterization of the OEPC barrier model.

A: To evaluate whether the OEPC grow in a mono- or multilayer, 14 μ m sections of 21 day old ALI cultures including the cell insert membrane were prepared and stained with heamatoxylin and eosin. Thus, the OEPC grew strictly in monolayers with ciliated cell patches distributed throughout the membrane.

B, C: Morphological features including tight junctions and cilia formation are important influencing factors for N2B studies. Double-stainings of acetylated α -tubulin (α -tubulin, green) and the tight junction marker zonula occludens-1 (ZO-1, red) of ALI cultures of OEPC after 21 days of incubation show clear cilia tight junction formation of the OEPCs (**B**). Analogous the immunofluorescence stainings of the olfactory mucus specific protein MUC5AC (red) showed mucus secreting cells in the OEPC ALI culture (**C**). Scale bars: 100 μ m.

Figure is modified from Ladel *et al.* (2019) [2], CC BY 4.0,

<http://creativecommons.org/licenses/by/4.0/>

In contrast to the primary cell models, the RPMI 2650 model after 21 days under ALI cultivation showed only weak expression of ZO-1 and low diffuse signal of acetylated α -tubulin [2]. Furthermore, the cell grew in several layers on the cell insert membrane. All of these features are well known for tumour cell lines. The multilayer growth and a low differentiated status without complete formation of specific characteristics of the original tissue are specific features of most tumour cell lines. The main advantage of using models of immortal cell lines is the homogenous appearance, the easy handling and the infinite growth resulting in generally more homogeneous assays results with lower variability in experiments compared to primary cell models, however with lower correlation to the real *in vivo* situation [143]. Besides the differentiation status of the cell models and the formation of specific features, also the physico-chemical environment plays an important role in N2B drug delivery through the nasal mucosa [37]. Therefore, the expression of the mucin MUC5AC was evaluated in immunofluorescence studies and via transcript analysis. Like other markers, also MUC5AC was expressed and transcribed at higher levels in the primary cell lines. The highest transcription level was detected in the olfactory mucosa followed by the OEPC (**Figure 15C**, **Figure 16**) [2].

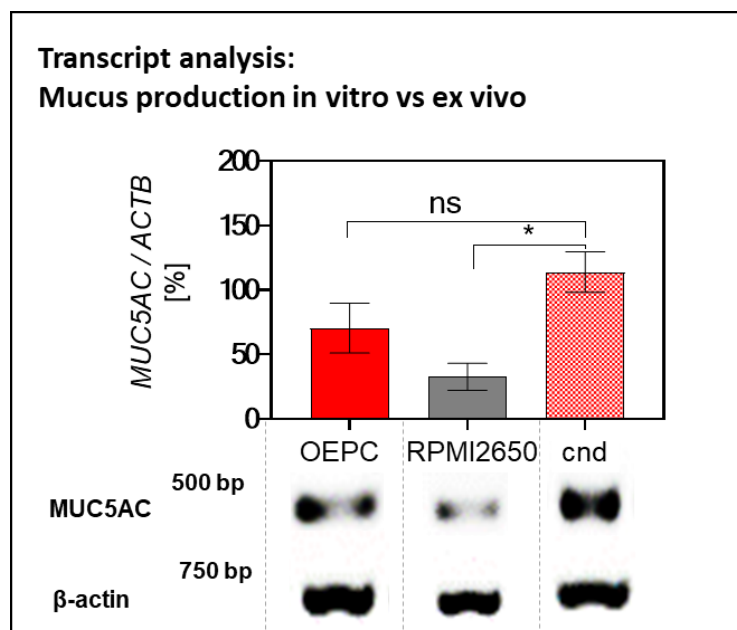


Figure 16: Mucus production in OEPC and RPMI2650 barriers (ALI-cultures) versus mucus production in the porcine cnd.

The tumour cell line RPMI2650 is the standard *in vitro* model for nasal barriers therefore this cell line was cultivated analogous to OPEC and used for cross-evaluation of the primary cell model in addition to the *ex vivo* tissue explant [44,158,160,214]. Transcription analysis (Reverse Transcriptase-Polymerase Chain Reaction, RT-PCR) of *MUC5AC* gene in OEPC, the tumour cell line RPMI 2650 and the *concha nasalis dorsalis* (cnd). The *MUC5AC* transcript signal was normalised to the β-actin gene (ACTB) transcript signal. Statistical analysis was performed using unpaired t-test. *: $p < 0.05$; $n = 4$; error bars represent mean \pm SEM. Figure is modified from Ladel *et al.* (2018) [1], CC BY 4.0, <http://creativecommons.org/licenses/by/4.0/>

As the MUC5AC is known to be mainly expressed in Bowman's glands of the olfactory mucosa, the result of the study is not surprising [16,193,215]. The different MUC5AC expression levels of the individual cell models fit well with the literature description of the mucus secretion of their origin. The REPC originated of the *concha nasalis ventralis*, which is the equivalent to the human concha nasalis inferior. Results from Aust *et al.* (1997) showed MUC5AC expression in few subpopulations of epithelial cells in human inferior turbinate specifying solely the presence of MUC5AC is not a reliable marker for the olfactory region but the level of expression is consistent [216]. In addition, Paik *et al.* (1992) found patches of respiratory epithelium in the olfactory region of humans indicating that the *in vivo* situation knows no explicit boundaries between the olfactory and the respiratory region [17]. In contrast to the primary cell models, the RPMI 2650 cells are not originating from respiratory or olfactory epithelium, but from an anaplastic squamous cell carcinoma of the nasal septum [157,158]. The squamous epithelium does not contain mucus-producing cells such as goblet cells, therefore the low level of MUC5AC production was low [217]. In general, recent studies showed conflicting results in mucin type expression (MUC1, MUC2, MUC5AC, MUC5B) patterns between nasal regions.

Results and Discussion

They were able to assign certain expression patterns to the regions but could not allocate the production of one of the mucin types to specific region [169,191–193,215]. Due to the complexity of the nasal mucosa, it is necessary to evaluate the models multifactorial as it was done in this thesis.

Further experiments were performed to gain better insight into the models. To evaluate the barrier tightness in addition to the ZO-1 expression the TEER values of 21-day ALI cultures of all cell types were determined and compared to literature data of TEER values of the olfactory mucosa (**Figure 17**, [43,160,185,218]). The TEER is influenced by factors such as the thickness of the cell layer and the formation of tight junctions [150].

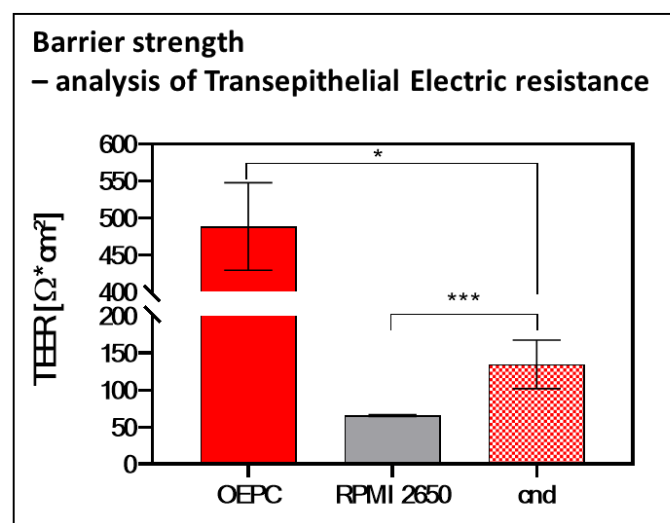


Figure 17: Comparison of barrier tightness of the different models.

A common parameter to determine the barrier tightness is the transepithelial electrical resistance (TEER) value. The OEPC showed the highest TEER value followed by the cnd ([160],) and the RPMI 2650. Statistical analysis was performed using unpaired t-test. *: $p < 0.05$; $n > 5$; error bars represent mean \pm SEM. Figure is modified from Ladel *et al.* (2019) [2], CC BY 4.0, <http://creativecommons.org/licenses/by/4.0/>.

The paracellular permeation of molecules is highly restricted by tight junctions in the epithelial barrier [172]. Therefore, it was not surprising that ZO-1 staining intensity was in accordance with the TEER values of the barriers formed by the different cell types. After 21 days of ALI culture the REPC formed the tightest barrier (TEER value: $850 \Omega \cdot \text{cm}^2$) followed by the OEPC (TEER value: $450 - 550 \Omega \cdot \text{cm}^2$). As both primary cell types formed only monolayers that are comparable in size, but showed differences in ZO-1 expression signal, it was concluded that REPC form a tighter barrier due to a higher formation of tight junctions. These results are supported by literature data *in vivo* olfactory and respiratory epithelium, as the epithelial cells in the respiratory epithelium are strongly connected via tight junctions whereas epithelial cells in the olfactory epithelium are sealed to the OSN neither by tight nor by gap junctions [13,219].

Results and Discussion

Precursor cells in the olfactory epithelium are known to undergo a continuous neurogenesis to replace lost neurons in the epithelial layer, which leaves a gap in the epithelial layer that is replaced by new OSN [220]. The continuous neurogenesis in the origin tissue might be the reason for the lower number of tight junctions and the lower TEER value seen in the OEPC as the formation of strong tight junctions in the olfactory epithelium would be hindering the outgrowth of new ONS. In general, it is rather questionable to compare TEER value of *in vitro* models with TEER values from multi-component systems like excised nasal mucosa, as the latter contains components such as for example glands and neurons that influence TEER values.

Coming back to the model evaluation, very few cellular models exist for comparison of the OEPC. Gouadon *et al.* (2010) developed a protocol for rat olfactory mucosa primary cultures. The morphology of these cultures resembles the OEPC however this thesis focused on the epithelial barrier whereas the study of Gouadon focused on the characterization of neurons in the culture [221]. Nevertheless, regarding the criteria for an *in vitro* olfactory epithelial model the OEPC model met all the specifications that are needed to evaluate the permeation of substances for N2B approaches.

Because of the lack of other *in vitro* olfactory epithelium barrier models the question of the validity of the OEPC model was extended to the question whether cells from the easier accessible respiratory region could also be considered as a model for the olfactory mucosa. For the REPC culture, many references are available. For human nasal epithelial cells TEER values up to 3155 $\Omega\cdot\text{cm}^2$ are reported, which are way higher than the TEER values resulted in the 21-day REPC ALI culture [222,223]. Pezzulo *et al* (2011) described TEER values similar to the values of REPC ranging from 700 to 1200 $\Omega\cdot\text{cm}^2$ for primary cells originated from the tracheal and bronchial tract [170]. Comparing our results of the REPC with publications of the commercially available human nasal primary cell model MucilAir™ similarities in terms of the ZO-1 signal strength and distribution were found [163]. All of these models including OEPC and REPC showed higher TEER values compared to the olfactory mucosa (TEER value: 60 – 180 $\Omega\cdot\text{cm}^2$). In contrast, the RPMI 2650 cells showed a TEER value of around 70 $\Omega\cdot\text{cm}^2$ after 21 days in culture, which is quite similar to the TEER values of the olfactory mucosa. The comparatively low TEER value goes hand in hand with the low and especially the diffuse formation of tight junctions as seen by the ZO-1 staining. The formation of leaky multi-layered barriers is linked to the low TEER values and well known in literature for RPMI 2650 [45,151,162,184,187].

Results and Discussion

Another parameter that is connected to the barrier tightness is the rate of paracellular permeation. Small and low molecular weight hydrophilic molecules such as fluorescein labelled isothiocyanate- dextran (FITC- dextran; 4.4 kDa) or sodium fluorescein (0.37 kDa) cross epithelial barriers mainly by the paracellular pathway [43–48]. The non-toxic and easily detectable fluorescence labelled chemicals are standard model substances for drug permeation studies [45,46,49]. In accordance with the remaining evaluation of the OEPC cell barrier and the knowledge of the respiratory and olfactory mucosal barrier discussed reported above, the REPC showed the least paracellular permeation rate followed by OEPC. The RPMI 2650 model resulted in a significant higher paracellular permeation rate, that again indicates points towards a weaker formation of tight junctions [2].

By the coherence of the results generated by the verification of the initial criteria and the comparisons of the cell models, the OEPC cell model was considered sufficiently characterized to be used as a barrier model for the olfactory mucosa. Furthermore, the comparison of all these nasal barrier models leads to the advanced conclusion that the choice of the cellular model should be based on the site of drug application and the substance of interest. Furthermore, it proves the concept that validation of such models should be on multifactorial basis as performed in this thesis.

4.2 Evaluation of therapeutic IgGs for N2B drug delivery – Influence of IgG species origin and glycosylation status

Therapeutic IgGs are amongst the most promising inventions of the last decades. They are broadly used in cancer therapy, autoimmune and inflammatory diseases. However, in the field of CNS related diseases therapeutic IgGs are almost completely banned due to the low penetration rate through the blood brain barrier. Many efforts have been made to overcome non-invasively this barrier but so far with little success [180]. One idea is the reduction of size as it is known that the molecular weight is one limiting parameter in N2B drug delivery [12].

Röhm *et al.* compared in 2017 the permeation of a 4000 kDa FITC-dextran with a Fab-fragment (25 kDa) and a full IgG1 (150 kDa) through a RPMI2650 barrier model. It clearly resulted in a size dependent permeation rate whereas IgG1 showed the poorest and FITC-dextran the highest transport rate [224]. This could indicate IgG1 being not an ideal molecule for the treatment of CNS related diseases due to its large molecular weight. In contrast, full IgGs have several advantages compared to other molecules such as a long half-life in blood compared due to their Fc domain and the interaction with the FcRn which is of high interest for therapeutic applications. Furthermore, several studies indicate that there is active transport through epithelial barriers mediated by receptor interactions with the Fc-domain of IgGs [113,120,189].

To get more insights in the permeation of IgGs through the olfactory epithelial barrier, several experiments were performed and described in this chapter in different barrier models, with IgGs of different origin and glycosylation status.

4.2.1 IgG uptake and permeation study – searching for influencing parameters

The overall purpose of the development of the barrier model in this thesis was the evaluation of the porcine mucosa as a model for of IgG transport through the human olfactory mucosa and the underlying mechanisms for further use in therapy of CNS-related diseases. For the nasal absorption of high molecular weight molecules, the low epithelial membrane permeability and the mucociliary clearance are important limiting factors [12]. Furthermore, also immune cells, gland cells and blood vessels might limit the permeation of especially IgGs as specific IgG binding receptors are expressed on those cells that mediate uptake and influence distribution of the IgG proteins. As the OEPC *in vitro* model displays only the epithelial layer of the olfactory mucosa also the *ex vivo* model was used to study further the influence of the *lamina propria* on IgG permeation. Firstly, differences in permeation rates of IgGs of different origin (porcine IgG, pIgG and human IgG, hIgG) were examined *ex vivo* and *in vitro*. Secondly, to gain further insights into the molecular mechanisms concerning the transport mediated by known Fc receptors, the influence of IgG glycosylation on permeation was investigated by comparing the wild-type glycosylated (WT) IgG and enzymatically deglycosylated (DG) IgG.

4.2.1.1 New insights in the mechanism: species specificity of IgG transport

To exclude artefacts of IgG permeation through the olfactory mucosa due to species related differences in IgG structure, both WT hIgG and WT pIgG were used for the experiments. The OEPC model was used to simplify the complex mucosa with the highly heterogeneous epithelial layer and the underlying *lamina propria* including blood vessels, glands and the local immune system and to display the permeation in the first barrier of the mucosa. Here, the great difference between the permeation through OEPC barriers and the mucosa explant in the *ex vivo* model was striking (**Figure 18**). In the OEPC ALI cultures the permeation of hIgG was significantly faster in the first four hours but assimilates to pIgG after 12 h (**Figure 18A**). However, in the *ex vivo* model the hIgG permeation was 12 times higher and no assimilation was detectable (**Figure 18B**). This finding could be related to different binding affinities to IgG transport-related receptors or differences in intracellular trafficking pathways depending on the IgG origin. Interestingly in the *ex vivo* model, pIgG level in the abluminal compartment (compartment beneath the *lamina propria*) was close to detection limit of the ELISA throughout the experiment duration. Again, this could indicate to IgG origin-dependent differences in IgG trafficking in the olfactory epithelium but without major impact on the overall permeation capacity of the IgG through the epithelial barrier as shown in the OEPC permeation data.

Results and Discussion

This hypothesis will be addressed later in this thesis on a molecular basis. As mentioned before, comparing the IgG permeation through OEPC barriers directly with the permeation through the *cnd* explant, a significantly lower permeation in the *ex vivo* model was detected after 2 h (**Figure 18C**). To get further information of the distribution of IgG in the porcine mucosa, histological sections were analysed using fluorescence immunoreactivity against pIgG and hIgG (**Figure 18D**, [1]). The results showed that pIgG gave a strong signal in the tissue even after 8 h, whereas hIgG was almost completely cleared. Furthermore, especially for pIgG circular structures in the *lamina propria* were spared from IgG signal, which might indicate a degradation of the pIgG in the tissue. In contrast to the permeation through the OEPC model, the species origin of the IgG seemed to have a high influence on transport and clearance in the nasal olfactory mucosa.

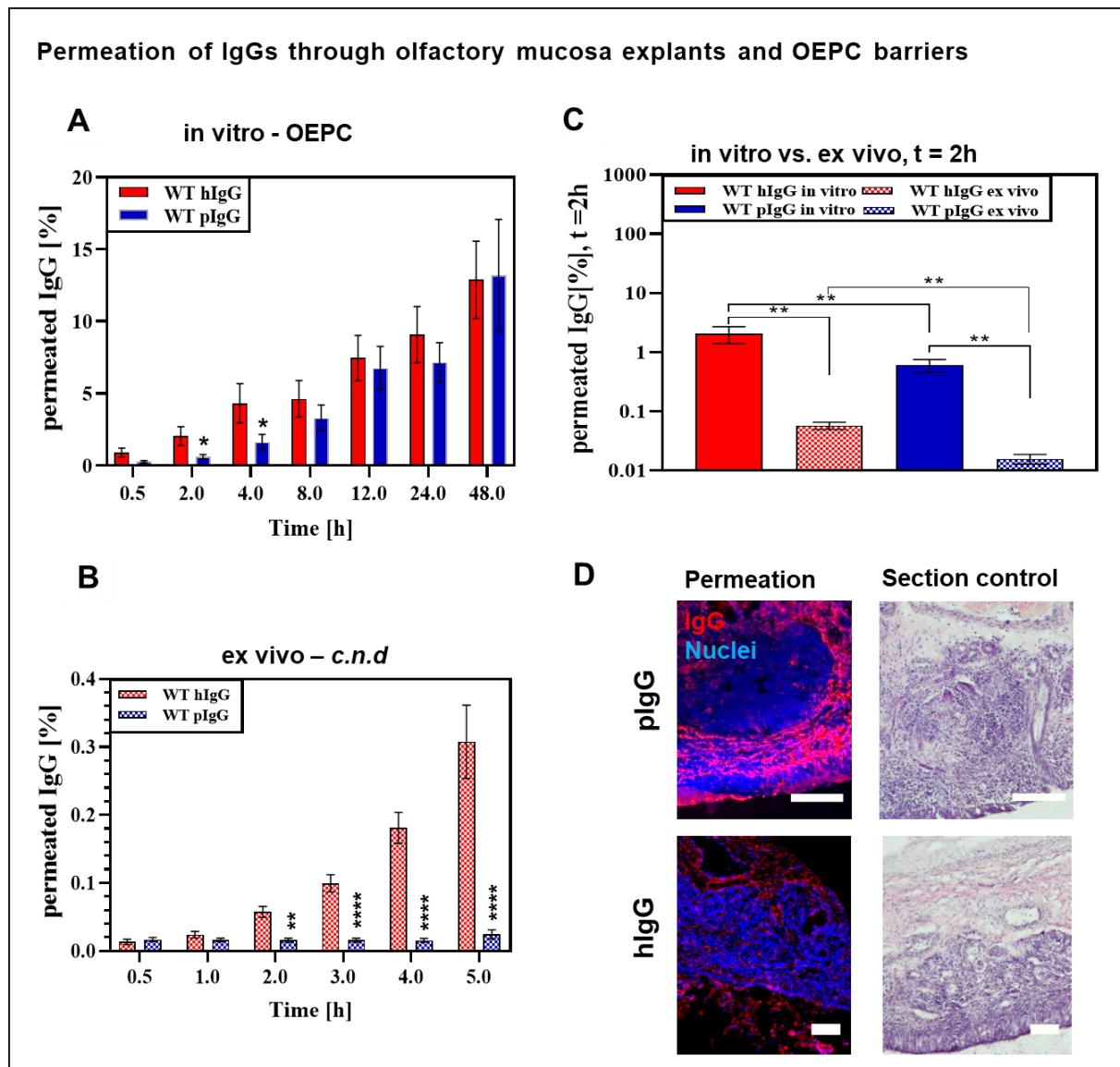


Figure 18: Investigation of human and porcine IgG permeation through excised porcine nasal mucosa and OEPC barriers.

A: Percentage permeation of wild-type hIgG (WT hIgG) and porcine serum IgG (WT pIgG) through OEPC over 48 h. Error bars represent mean \pm SEM. N = 4, n = 21.

B: Percentage permeation of WT hIgG and WT pIgG through excised nasal mucosa tissue explants (cnd) over 5 h. Error bars represent mean \pm SEM. WT hIgG: N = 4, n = 29, WT pIgG: N = 4, n = 12.

C: Comparison of percentage permeated IgG through the OEPC in vitro model and the ex vivo model after 2 h. The significance was analysed by unpaired t-test. * p < 0.05, ** p < 0.001, *** p < 0.0001; **** p < 0.00001, error bars represent mean \pm SEM.

D: Comparison of distribution of pIgG and hIgG through porcine olfactory mucosa. Immunoreactivity against porcine IgG (pIgG) and human IgG (hIgG) after 8 hr incubation (intrinsic IgG signal was subtracted for all data presented). Section controls were prepared by hematoxylin and eosin stain for the verification of the intact section. N = 4, n = 4; Scale bar: 200 μ m.

Figure is modified from Ladel *et al.* (2018) and Ladel *et al.* (2019) [1,2], CC BY 4.0, <http://creativecommons.org/licenses/by/4.0/>

4.2.2 Analysis of the molecular mechanism of IgG trafficking

The permeation through the OEPC model and the *ex vivo* model resulted in conflicting data concerning the dependency on IgG species origin. Therefore, attempts were made to further analyse the IgG trafficking through the olfactory mucosa. In general, it is known that high molecular weight proteins permeate via the transcellular transport pathway through mucosal barriers [53]. As summarised in **Figure 4** IgGs have several known interaction partners that could potentially be involved in IgG trafficking in the olfactory mucosa. Amongst them, the best characterised protein that is connected to IgG transport is the FcRn [28,53,72,111,127,225]. Other promising receptors are FCGRs, especially FCGR2b, that were recently associated with IgG transport through the placenta by Ishikawa *et al.* (2015) [118].

4.2.2.1 The FcRn – the major player in IgG trafficking?

Until today, the FcRn is the best described protein that is involved in IgG transport. Several studies using Fc engineering has shown enhanced transport via FcRn through increased binding [101,108]. In their study of the porcine FcRn, Ober *et al.* (2001) and Stirling *et al.* (2005) showed cross-species binding of human IgG to porcine FcRn [139,140]. In a first attempt, immunofluorescence co-localisation assays were used to identify sites of IgG localisation after *ex vivo* permeation experiments described above in Chapter 4.2.1 [1]. According to earlier studies, IgG uptake occurs via pinocytosis at the apical epithelial side followed by fusion of the pinocytotic endosomes with FcRn containing acidic endosomes. Under acidic conditions, FcRn binds to IgG and either recycles the IgG's back to the apical surface or transfer them to the lysosome or the basolateral side of the cell [55,226]. In the cnd explants, co-localisation of

Results and Discussion

FcRn and IgG occurred in the epithelial layer as well as in the basal cell layer in short time (**Figure 19A**).

Cianga *et al.* (2011) investigated the FcRn expression in several tissues in the human body and amongst others found FcRn expression in peripheral neurons [227]. Due to the fact that Broadwell and Balin published in 1985 the N2B transport of the high molecular weight protein horseradish peroxidase in mice [41,228], co-localisation experiments of IgG and neuronal fibers were performed to evaluate the potential IgG localization in ONS fibers. Immunofluorescence double staining of the axonal marker NF200 ([196]) and IgG showed co-localisation alongside neuronal fibres throughout the *lamina propria* (**Figure 19B**). There are conflicting data from the literature regarding the role of FcRn in the brain. FcRn was found to be expressed at the BBB and hypothesized to function as an efflux transporter of IgG from the brain tissue in studies where proteins were fused to IgG or the Fc part [110,229–231]. However, in experiments with knockout mice, Garg and Balthasar (2009) found the ratio of brain and plasma IgG exposure was nearly identical to the wild-type mice. They concluded, that FcRn might not play a significant role in limiting or facilitating IgG distribution to the brain [112]. This report was supported by other experiments [232]. Ruano-Salguero and Lee (2020) recently stated, that IgG transcytosis across brain endothelial-like cells occurs independently of FcRn after performing *in vitro* experiments with IgGs that lack FcRn recognition. However, they found evidence that FcRn is involved in IgG recycling in these cells [113]. An explanatory hypothesis that explains the conflicting studies involves a so far unknown factor X [112].

Another inconsistency that occurred during the IgG *ex vivo* permeation experiments were circular structures in the *lamina propria* circular that seemed to be spared from IgG as described in Chapter 4.2.1. Debertin *et al.* (2003) postulated those so-called lymphoid follicles are morphologically similar to Peyer's patches in the nasal cavity of infants [23]. Analogous to the findings in the porcine nasal mucosa, they discovered described those structures mainly in the upper nasal cavity. The morphological resemblance and the location of these lymphoid follicles in children and pigs further confirms the findings described herein, that the pig is a good model for the olfactory mucosa also for immunological investigations.

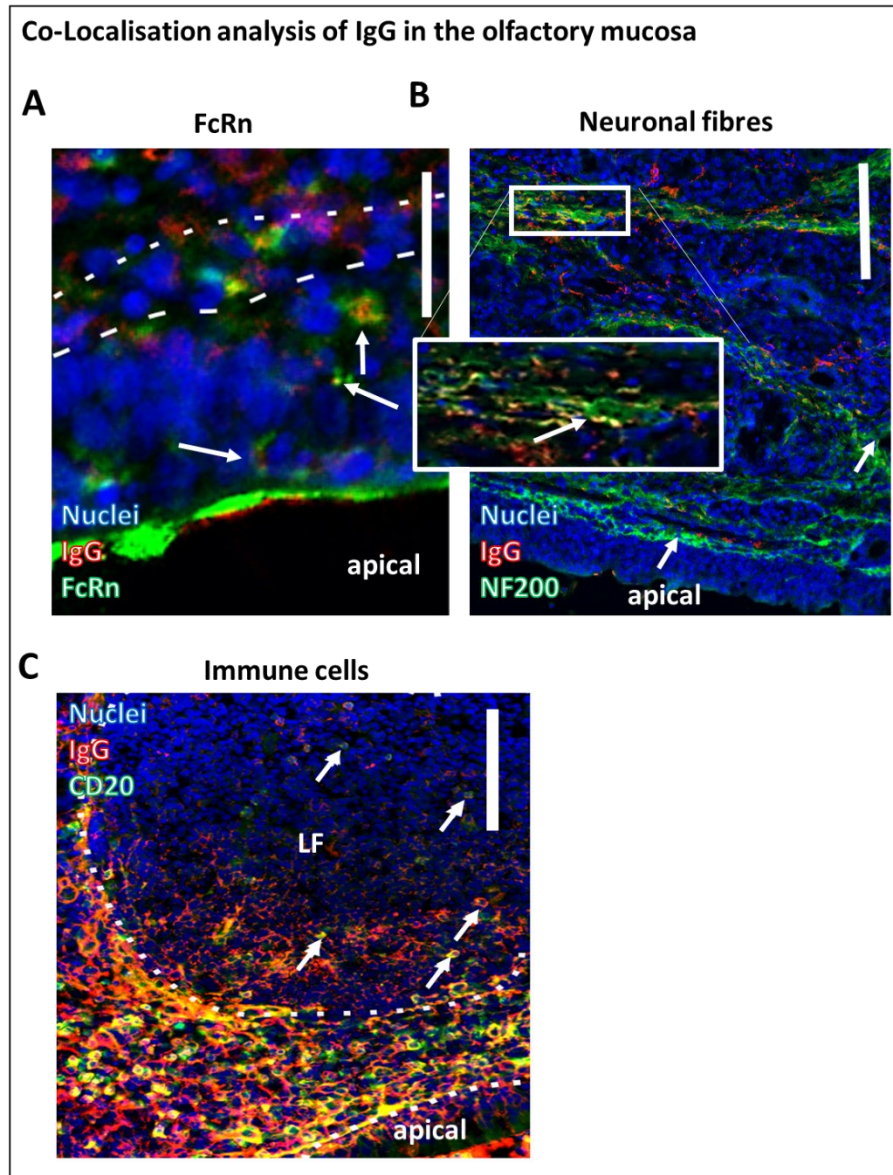


Figure 19: Co-localisation analysis of IgG with different marker proteins for IgG transport, neuronal fibers and immune cells

A: WT plgG (red) and FcRn (green) co-localisation (yellow) in the epithelial layer after 8 h of incubation. Scale bar: 50 μ m.

B: Co-localisation (yellow) of neuronal marker NF200 (green) with WT plgG (red) after 30 min of permeation. Scale bar: 200 μ m.

C: Co-localizing (yellow) of WT plgG (red) with CD20 positive cells (green) of the lymphoid follicle after 8 hr of incubation. Nuclei are stained with DAPI (blue); Scale bar: 200 μ m.

Figure is modified from Ladel *et al.* (2018) [1], CC BY 4.0,
<http://creativecommons.org/licenses/by/4.0/>

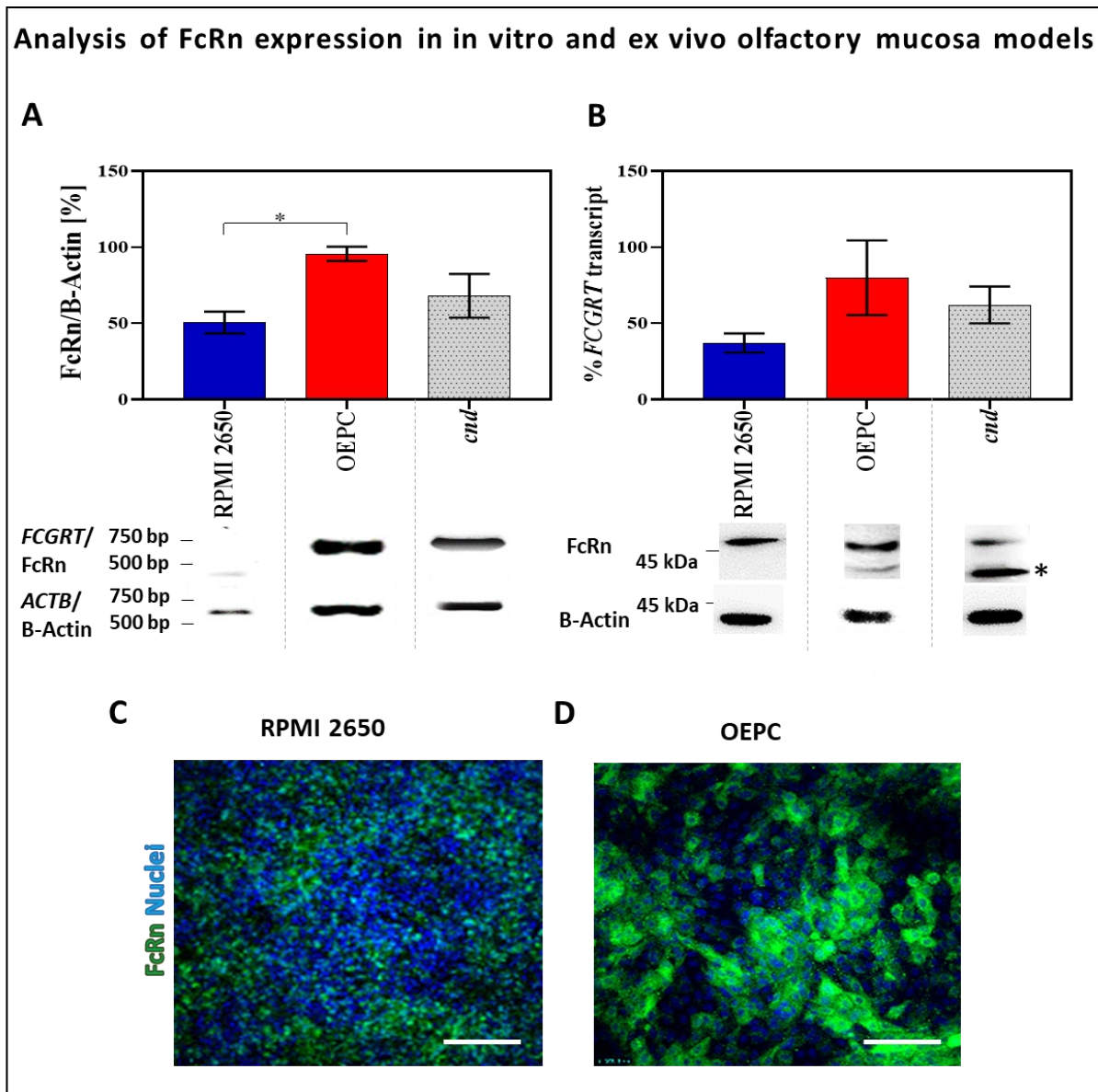
According to literature data, the lymphoid follicles and the cellular immune system therein consists mainly of monocytes, dendritic cells, B and T lymphocytes, described in the mucosa of the gut, the lung and the nose [233]. To verify the spared spots as lymphoid follicles and to gain further information about the fate of IgGs in the *lamina propria*, double staining of IgG with

Results and Discussion

either CD20 (B cells, **Figure 19C**), CD14 (data not shown) or CD3 (data not shown, [1]) were performed.

All cell types were present in the investigated structure. Co-localisation with pIgG was mainly found at the border of the lymphoid follicle. However, for hIgG almost no co-localisation was found indicating again a species-dependency for IgG trafficking. In earlier studies endocytic uptake of IgG by dendritic cells and macrophages was suggested at immune relevant sites [99,100,234]. The logic behind the uptake of IgGs in the *lamina propria* could be a monitoring of the apical environment as known for other sides in the body [235]. Infiltrated IgGs from the mucosa may bind important antigens at the apical nasal cavity and transport them to the *lamina propria*. In the *lamina propria*, those IgG-antigen complexes are recognised by specific receptors on the surface of antigen presenting cells, the FCGRs. After uptake and proteolytically digestion the IgG-antigen complex is subsequently presented to the cellular immune system [236,237]. There are several studies that show FcRn expression on immune cells such as dendritic cells and B cells, that further strengthens the theory of FcRn being a major player in olfactory mucosal IgG trafficking [100,238]. Therefore, the digestion of pIgG at lymphoid follicles could be the reason for the lack of IgG signal in the mucosa explants.

To generate other lines of evidence, transcript and protein expression analysis of the FcRn gene respectively its gene FCGRT were performed in all models used in this thesis. Hereby In addition, the *in vitro* models OEPC and RPMI 2650 were compared to the olfactory mucosa explant (cnd) (**Figure 20**). The differences in transcript level of the *in vitro* models compared to the *ex vivo* model were not significant, but there was a tendency observable for a lower FcRn transcript level in RPMI 2650 in comparison to cnd (**Figure 20A**). OPEC cells showed the highest transcript level of the FCGRT gene.



Results and Discussion

Also, at the protein level the RPMI 2650 cells produced lower amounts of FcRn compared to OEPC and cnd (**Figure 20A, B**). The difference in FcRn protein expression was confirmed in immunofluorescence stainings of RPMI 2650 and OEPC (**Figure 20C, D**).

Several studies investigated the FcRn expression on mucosal epithelial cells confirming the ability to perform transcytosis to underlying tissue [95,240]. Thereby, as already mentioned above, the binding of IgGs to FcRn showed high cross-species reactivity with species-dependent differing in the binding affinities [139,241,242]. Studies further show that the binding affinity and the FcRn-related transport is fairly similar for hIgG and pIgG in porcine epithelial cells, but the uptake of hIgGs is mediated more rapidly by porcine FcRn compared to pIgG uptake [239]. Considering now the permeation rate of human and porcine antibodies through OEPC shown in **Figure 18A**, this finding of the uptake dynamics of FcRn could explain the faster uptake of human IgG at early time points.

What remains still unclear concerning the results of the IgG permeation in this thesis is the huge difference in permeation of hIgG and pIgG through the *ex vivo* tissue explant. Thus, also in literature, there are still open questions concerning IgG trafficking, especially from the nasal mucosa to the brain [113,232,243]. Among them there is the open question of the intracellular sorting mechanism for IgGs and the distinguishing between IgGs and immune complexes comprising IgG [120]. Furthermore, the uptake theory by pinocytosis is not completely proven, especially binding of surface located FcRn to IgG in the olfactory mucosa could be possible as its binding affinity for IgG is highest around pH 6 – 6.5 which matches the acidic environment in the nasal cavity [244]. Hornby *et al.* (2014) showed binding of FcRn to IgG at the surface of Caco-2 cells that was inconsequential for overall transcytosis [245]. Furthermore, there is evidence for a bidirectional transport of IgG mediated by FcRn in the MDCK cell line expressing human FcRn [246]. This does not match the common knowledge of acidic binding of IgG and FcRn as the pH at the basolateral side is considered as physiologic (pH 7 to 7.4). Sockolosky and Szoka have already addressed these questions in 2016 and concluded, that FcRn cannot act as the sole mediator in IgG trafficking [189]. They assumed an unknown factor X being involved in IgG trafficking in addition to FcRn.

The results from this thesis support their hypothesis as the data indicate species-dependent IgG trafficking—however, not in the epithelial layer but in cellular structures of the underlying *lamina propria*. As the expression of FcRn was proven in OEPC, RPMI 2650 and cnd the influence of this receptor in terms of hIgG and pIgG permeation should be consequently considered throughout all models. Therefore, an involvement of an unknown factor X that influences IgG trafficking depending on the species origin is conceivable.

4.2.2.2 Investigation IgG glycosylation-dependence of the transport mechanism in ex vivo and in vitro models – FCGR as co-receptors for IgG trafficking?

To get further information of the involvement of a factor X, an extended literature search was performed to identify other IgG associated proteins that might have to the potential to be involved in IgG trafficking. In the literature several links from IgG trafficking to FCGR were made in the past [118,125,126,232]. However, the influence of FCGR on IgG trafficking at mucosal sites has not been clarified yet. There are several studies investigating the influence of different FCGR's on transplacental IgG transfer with conflicting outcomes. Whereas some of these studies confirmed the involvement of FCGR's, especially FCGR2, others could not find evidence for this hypothesis [127,247,248]. An indication that FCGR's may indeed be involved in IgG trafficking is the fact that the IgG subclasses are differentially transported across the placenta [249,250]. Since FcRn-mediated transport is known to be mainly subclass independent, it is possible that this peculiarity is caused by FCGRs, which are known to be highly IgG subclass dependent in their binding affinities [226,251]. According to literature, the FCGR's are largely involved in mediating immunological effector functions and are highly dependent on IgG Fc glycosylation [71,252]. Several studies investigated the interaction of FCGR's with wild type (WT) and deglycosylated (DG) IgGs and show altered interaction of low affinity FCGR's like (FCGR2 and FCGR3) with DG IgG. The exception is the high affinity Fc receptor FCGR1, which has an additional domain that acts with the upper hinge region of the IgG and is largely glycosylation independent [88,242]. Interestingly, this receptor was already described to be expressed in sensory neurons and be involved in pain signalling [253]. Thus, if FCGR1 is involved in IgG trafficking a removal of the glycan structure should not lead to a high difference in permeation behaviour between WT IgG and DG IgG. In contrast to FCGR1, the Fc glycosylation has the highest impact to FCGR3a. Several studies investigated the binding affinity of different glycosylated and deglycosylated IgGs to FCGR3. They found strong and consistent evidence that deglycosylation of IgG strongly decreases the binding to FCGR3aA and inhibits its effector functions such as ADCC [71,254,255]. Another important parameter that influences the IgG- FCGR3a binding is the core-fucosylation of the Fc glycan. Cambay *et al.* (2020) showed that reduced fucosylation leads to an increased FCGR3a binding, whereas even Fc glycan cleaved to GlcNac and fucose reduces the binding affinity significantly [84,87,117]. As the FCGR3a was found on human nasal epithelial cells by Golebski *et al.* in 2019 it might be a candidate for the unknown factor X. They investigated the involvement of FCGR3 and the Toll Like Receptor 4 in discrimination between commensal and invading bacteria in human nasal epithelial cells linking the expression of FCGR in the nasal epithelium with the hypothesis of crosstalk between FCGR and FcRn [121].

Results and Discussion

However, the most interesting candidate is FCGR2b as it was already connected described to IgG transcytosis in the placenta. Ishikawa *et al.* (2015) further suggested that IgG internalization and transcytosis is mediated rather by FCGR2b than FcRn in the placental endothelium [118]. This could be an explanation why serum albumin is not transcytosed across the placental barrier despite being recycled by FcRn [256]. Also, for FCGR2b the binding to DG IgGs is known to be highly reduced compared to the binding to WT IgGs [71,87].

In general, an involvement of low affinity FCGR's in IgG trafficking could be influenced by the glycosylation status of the IgG. In contrast, the FcRn binding should not be affected by the Fc glycosylation according to the common scientific opinion [257]. Therefore, permeation experiments were performed *ex vivo* and *in vitro* with WT and DG hIgG to evaluate the effect of the presence of Fc glycan to the permeation behaviour (**Figure 21**).

The bacterial enzyme EndoS hydrolyses the asparagine-linked glycan on IgG and has been used in several preclinical studies for the treatment of autoimmune diseases [85,87,258,259]. Allhorn *et al.* (2008) published data that show a significant decrease in FCGR2a/b and FCGR3a binding to IgGs that are deglycosylated by EndoS [87]. To simplify the linking of the permeation data to a specific FCGR subtype, a fucosylated human monoclonal IgG1 was used that show a defined G1F glycopattern [85,258]. This Endo S digestion leaves a glycan residue of GlcNac and fucose at asparagine 297 (**Figure 21A**) [87]. A well-defined and characterized human IgG was used in this study due to the lack of commercially available monomeric porcine IgGs with a defined glycopattern. It was recently shown by Egli *et al.* (2019) that the binding of human and porcine IgG to the porcine FCGR1, FCGR2a and FCGR2b is comparable however no interaction of hIgG with the porcine FCGR3a was detected [142]. As FCGR3a is mainly expressed by immune cells, this is highly interesting and can be linked to the rare co-localisation events in the immunofluorescence study of hIgG and the immune cell marker CD14, CD20 and CD3 (**Figure 19**). The fact that human IgG does not bind to porcine FCGR3a together with the fucose-containing glycosylation-pattern of the used hIgG, an interaction between this hIgG and FCGR3a is rather unlikely [88]. Thus, if FCGR3a is involved in IgG trafficking there should be differences in permeation rate of hIgG and pIgG also in the epithelial layer due to the non-binding of the hIgG to porcine FCGR3a. As this was not the case in the OEPC barrier model, FCGR3a was not further considered as potential factor X.

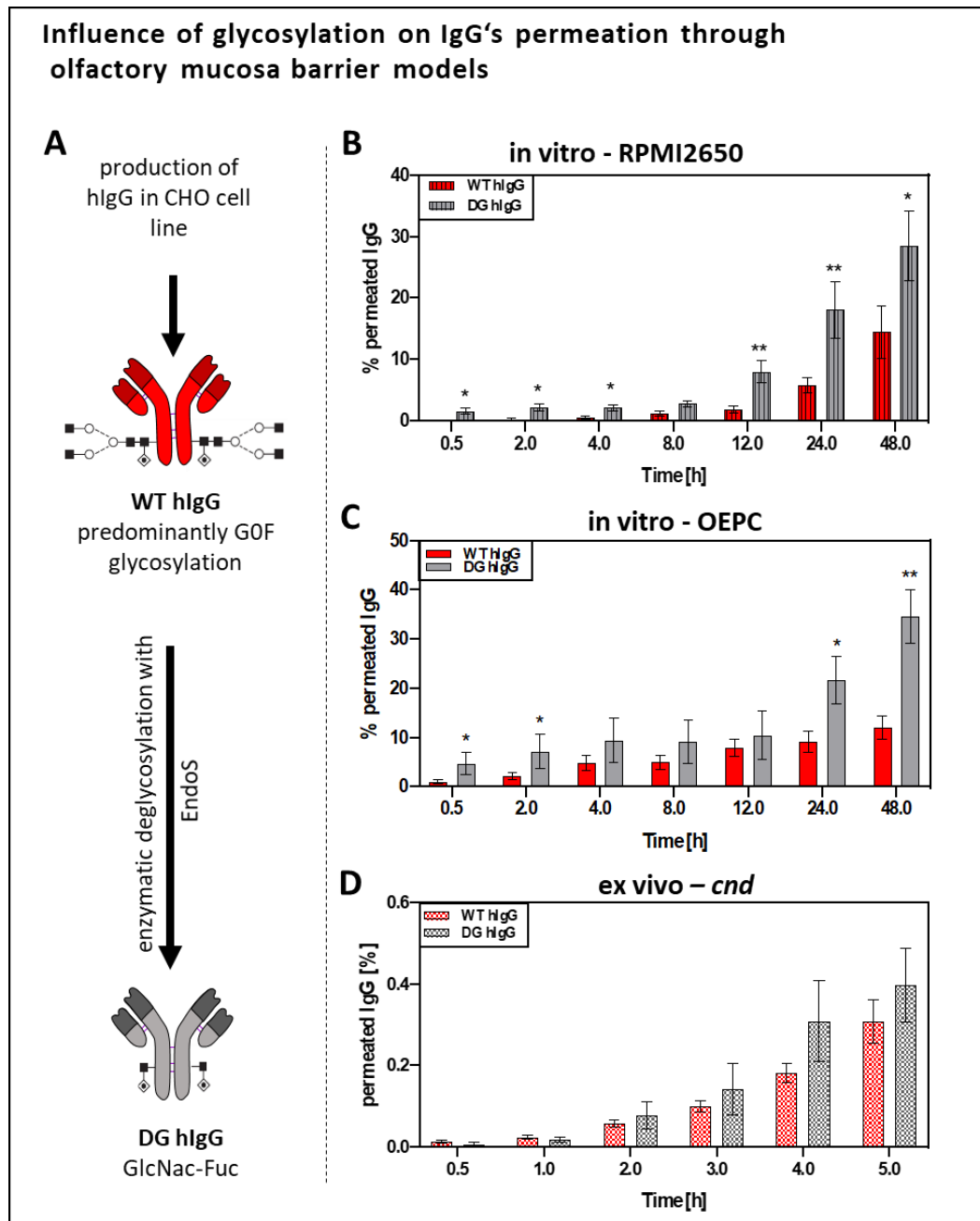


Figure 21: Investigation of IgG glycosylation dependency of IgG permeation processes. Permeation of WT hlgG and deglycosylated hlgG (DG hlgG) through RPMI 2650, OEPC and porcine olfactory mucosa (cnd).

A: schematic description of the deglycosylation procedure by Endo S digestion.

B: Percentage permeation of WT hlgG and DG hlgG through RPMI 2650 cells over 48 h. Error bars represent mean \pm SEM. N = 3, n = 11.

C: Percentage permeation of WT hlgG and DG hlgG through OEPC barrier model over 48 h. Error bars represent mean \pm SEM. WT hlgG: N = 4, n = 21, DG hlgG: N = 3, n = 10.

D: Percentage permeation of WT hlgG and DG hlgG through excised nasal mucosa tissue explants (ex vivo) over 5 h. Error bars represent mean \pm SEM. WT hlgG: N = 4, n = 29, DG hlgG: N = 3, n = 10.

Statistical analysis was performed using an unpaired t-test. * $p < 0.05$, ** $p < 0.001$

Figure was modified from Ladel *et al.* (2020) [3], CC BY 4.0,

<http://creativecommons.org/licenses/by/4.0/>

Results and Discussion

It was necessary to also consider species-related specials, because of conflicting literature data, for example even though FcRn is expressed in the porcine placenta maternal IgGs do not cross the barrier to reach the foetus [260]. Therefore, to exclude experimental bias due to species-specific properties of the IgG trafficking pathways, again the human tumour cell line RPMI 2650 was used for the permeation experiments in addition to OEPC and cnd explants.

The permeation of WT and DG IgG showed comparable profiles for the RPMI 2650 (**Figure 21B**) and OEPC (**Figure 21C**) barrier model. The permeation rate of DG hIgG was significantly higher compared to the WT hIgG. Interestingly, the permeation rate of DG IgG was higher in the OEPC barrier model which was quite surprising as the barrier tightness of RPMI 2650 model (transepithelial resistance: 50–70 Ωcm^2) is much lower than OEPC (transepithelial resistance: 450–550 Ωcm^2) and therefore the RPMI 2650 model was suspected to show higher IgG permeation rate due to paracellular transport [2]. This result fits to the analysis of FcRn expression in the two cell models and gives further evidence that a. mainly active transport is involved in IgG trafficking and b. primary cell models might be preferable to tumour cell models, at least for the investigation of molecular interaction. By contrast, the permeation rate of DG hIgG and WT hIgG did not show significant differences in the *ex vivo* model, but a weak low tendency of DG IgG showing for higher permeation was observed (**Figure 21D**). In conclusion, the overall permeation profile was similar between the RPMI 2650 and the OEPC model. Therefore, a consequence of the DG IgG showing a higher permeation in all models, a potential factor X must have cross-species and Fc glycosylation sensitive binding properties to IgG. As FcRn is known to be insensitive to Fc glycosylation, these findings exclude again the FCGR3a as no cross-species binding was detected in surface plasmon resonance studies and gives further hints to FCGR2 being involved in the IgG trafficking [142,257]. Furthermore, in immunofluorescence co-localisation studies signal overlapping areas were found for WT pIgG and WT hIgG with FcRn and FCGR2 in OEPC barriers (**Figure 22**) giving further evidence for the involvement of this receptor. However, due to the lack of porcine FCGR2b specific antibodies the presence and involvement of FCGR2a cannot be excluded. Thus, the significantly higher permeation of DG hIgG excludes the mediation of active transcytosis by FCGRs but could imply an involvement of FCGR2 either in IgG recycling or degradation or both.

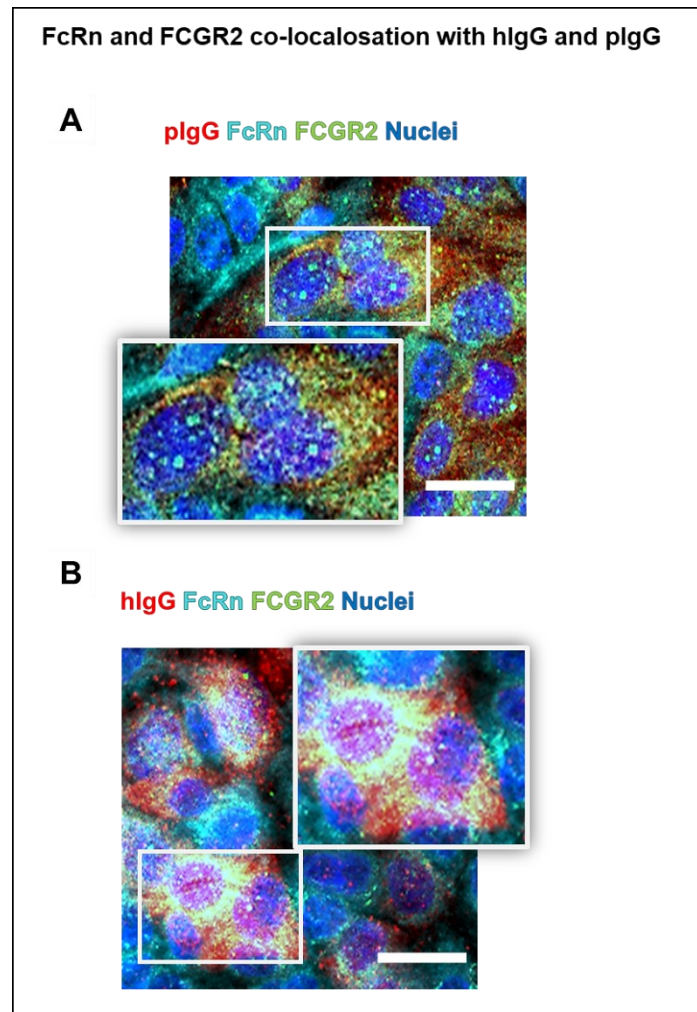


Figure 22: Co-localisation of FcRn and FCGR2 with allogenic and xenogenic IgGs in OEPC.

A: Co-localization of FCGR2 (green), FcRn (cyan) and plgG (red).

B: Co-localization of FCGR2 (green), FcRn (cyan) and hlgG (red). Scale bar: 20 μ m, sites of co-localization are yellowish to white coloured.

Figure was modified from Ladel *et al.* (2020) [3], CC BY 4.0,

<http://creativecommons.org/licenses/by/4.0/>

The slightly higher permeation rate of DG IgG in the cnd explants may indicate further that FCGR's (other than FCGR3) are also involved in crosstalk to cells of the *lamina propria*. Beneath the epithelial layer, DCs and macrophages are known to be involved in immune surveillance at the mucosal barrier [29,236,261]. In earlier studies evidence was shown for a direct or indirect interaction of FcRn with FCGRs due to the FcRn-mediated intracellular routing to cross-presentation compartments in DCs but leaving the intracellular mechanism mostly unclear [120].

Results and Discussion

In interaction studies via immunoprecipitation, the FcRn-IgG interaction was confirmed for WT and DG hIgG and pIgG in OEPC cells (signal strength variation was due to high standard variations of the lysed tissue and was not significant, **Figure 23A**). This is in accordance with the literature opinion of FcRn being largely independent of Fc glycosylation and show cross-species binding [140,257]. The intent to find FCGR2 – IgG interaction in immunoprecipitation studies of OEPC lysates failed most probably because of the lower limit of detection limit (**Figure 23B**). The immunoprecipitation studies of IgG-FCGR2 interaction in olfactory mucosa lysates resulted in very weak signals indicating that this receptor might be low only expressed at low levels. Unfortunately, the expression strength of FCGR2 was not investigated so far. Transcript analysis of OEPC done by other members of the group (Helena Herzog; Hochschule Biberach, group of Prof. Katharina Zimmermann) showed low level of FCGR2b mRNA supporting both the hypothesis of low expression and the presence of FCGR2b in OEPC (**Figure 23C**).

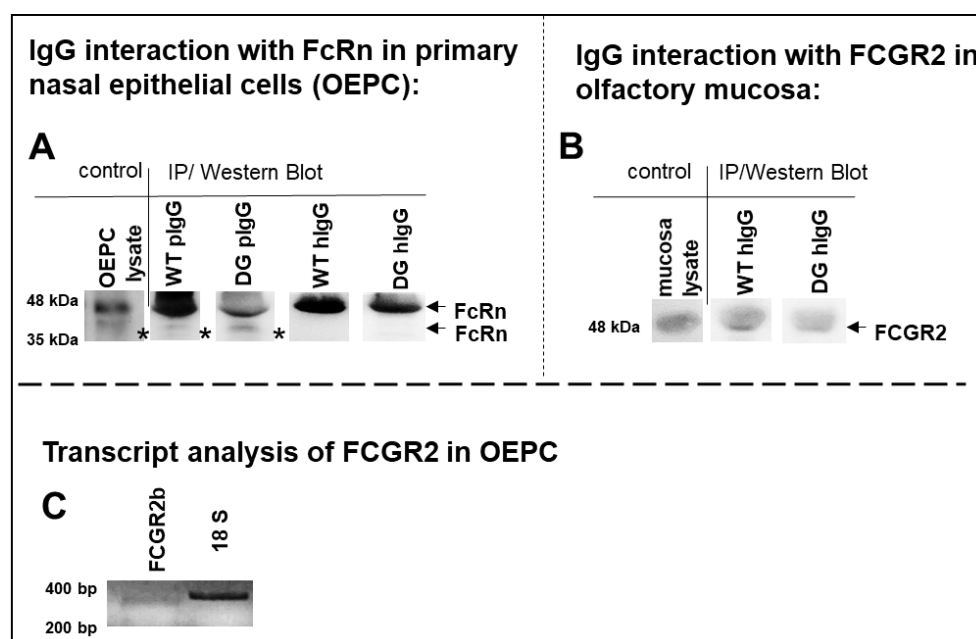


Figure 23: Immunoprecipitation and Western Blot for the investigation of IgG interaction in OEPC and cnd.

A: Interaction study via immunoprecipitation analysis of WT pIgG, DG IgG, WT hIgG and DG hIgG and Western Blot against FcRn in OEPC (N = 3; * glycovariants [140]). IgGs were incubated with OEPC cell lysate and captured using Protein A agarose beads. The resulting bands could not be quantified due to high batch-to-batch variations in the cell lysates.

B: Interaction study (immunoprecipitation) of WT hIgG and DG hIgG with FCGR2 using whole olfactory mucosa lysates.

C: Transcript analysis (reverse transcription PCR) of FCGR2b in OEPC (FCGR2B: 245 bp; housekeeping gene 18S: 313 bp).

Figure was modified from Ladel *et al.* (2020) [3], CC BY 4.0,

<http://creativecommons.org/licenses/by/4.0/>

Results and Discussion

In this thesis, several lines of evidence were brought out that favours the hypothesis of FCGR2b involvement in IgG trafficking, which still is somehow conflicting with other studies. In general, a conflicting fact is the low binding of FCGR2b to monomeric IgG postulated by several groups in *in vitro* and kinetic experiments [123,262]. Mathiesen *et al.* (2013) published an IgG3 variant with disrupted binding to FCGRs was still transported across human placenta explants. However, on the other hand they found evidence that the underlying transport mechanism is sensitive to alterations of the hinge region of IgG3 which again indicates to an additional mechanism to FcRn [127]. Stapleton *et al.* (2018) compared the glycosylation patterns of fetal and maternal IgG and concluded that IgG transport is not glycosylation selective [263]. This finding is not completely contraire to the results gained in this thesis as the FCGR2b is known to be less sensitive to specific glycosylation pattern compared to FCGR3a [117]. In other studies, deglycosylated IgG lacking effector functions *in vivo* but were transported to the brain in mouse models nevertheless [264].

Critical appraisal of results obtained:

The results of this thesis together with the mentioned partly controversial studies and the fact that transport mechanism at mucosal sites is IgG subclass dependent leaves no other explanation than the involvement of an unknown factor X as concluded earlier also by Sockolosky and Szoka in 2016 [189,249,265,266]. Furthermore, an involvement of FCGR2b in IgG recycling and/or degradation, but not in transcytosis, could be a promising hypothesis, which unites all previous seemingly contradictory studies with the herein presented data.

5. Conclusion

The aim of the presented thesis was to evaluate the porcine olfactory mucosa as valid model for the human counterpart and to investigate the permeation of human and porcine IgG through this mucosal site including molecular mechanisms for the use of therapeutic IgGs for intranasal drug delivery.

Using different experimental approaches, the validity of porcine olfactory mucosa as a model for the human counterpart was shown for *in vitro* primary cell barrier models as well for *ex vivo* model by using the TEER value, the tight junction formation, the expression of mucus and the expression of IgG receptors FcRn and FCGR2 as validation parameters. Furthermore, for the first time it was shown that the location of the mucosa used for *in vitro* and *ex vivo* models influence the experimental results and is an important factor to consider. We found evidence that there are species-dependent IgG permeation and trafficking mechanisms in the *lamina propria*, especially alongside neuronal fibres and in lymphoid follicles. In contrast, no species-dependent permeation was detected in the epithelial barrier of OEPC models.

To get further insights into the molecular mechanisms we investigated the role of FcRn and FCGR2b in IgG trafficking and found strong evidence of the involvement of a Fc glycosylation-dependent factor X in addition to the well-characterized IgG transporter FcRn. In permeation experiments using WT and DG hIgGs we found significantly higher permeation rates of DG hIgG in the epithelial barrier models. As a result, in **Figure 24**, the cross-binding hypothesis is displayed. It implies the hypothesis that immune complexes are transported from the apical space to immune competent cells in the *lamina propria* to monitor the environment at the mucosal surface and prevent potential threats. This hypothesis further implies that suggested factor X is expressed in a substantially lower amount compared to FcRn and therefore a binding of Fc by FcRn with a stoichiometry of 1:2 is engaged if a high amount of IgG is present on the apical side of the epithelial cell. The additional factor X might be involved in the recognition of immune complexes. It is known that smaller immune complexes are rather recycled, whereas large immune complexes are degraded [267]. Furthermore, for mucosal sites there are several studies showing that monomeric IgGs and multimeric immune complexes are transcytosed through the epithelial cell layer to dendritic cells in the *lamina propria* by FcRn [235,268]. In the cross-binding hypothesis the factor X binds to the glycosylated hinge region of IgG in addition to FcRn to mediate either lysosomal IgG degradation or recycling back to the apical surface (**Figure 24 I.**). As for FCGR the hinge region is described as critical for the binding it could be that in immune complexes of a specific size, the hinge region might not be freely accessible and may not bind to factor X due to steric problems [127].

Conclusion

Again, double binding of Fc by FcRn could be a possible approach, giving the signal for transcytosis and the basolateral exocytosed immune complex could consequently be taken up by DCs via FCGRs (**Figure 24 II.**). There might be additional mechanisms involved such as phosphorylation of FcRn after double binding to Fc or different glyco- or isoforms of FcRn with altered function as hypothesised by other groups [226,246,269–273].

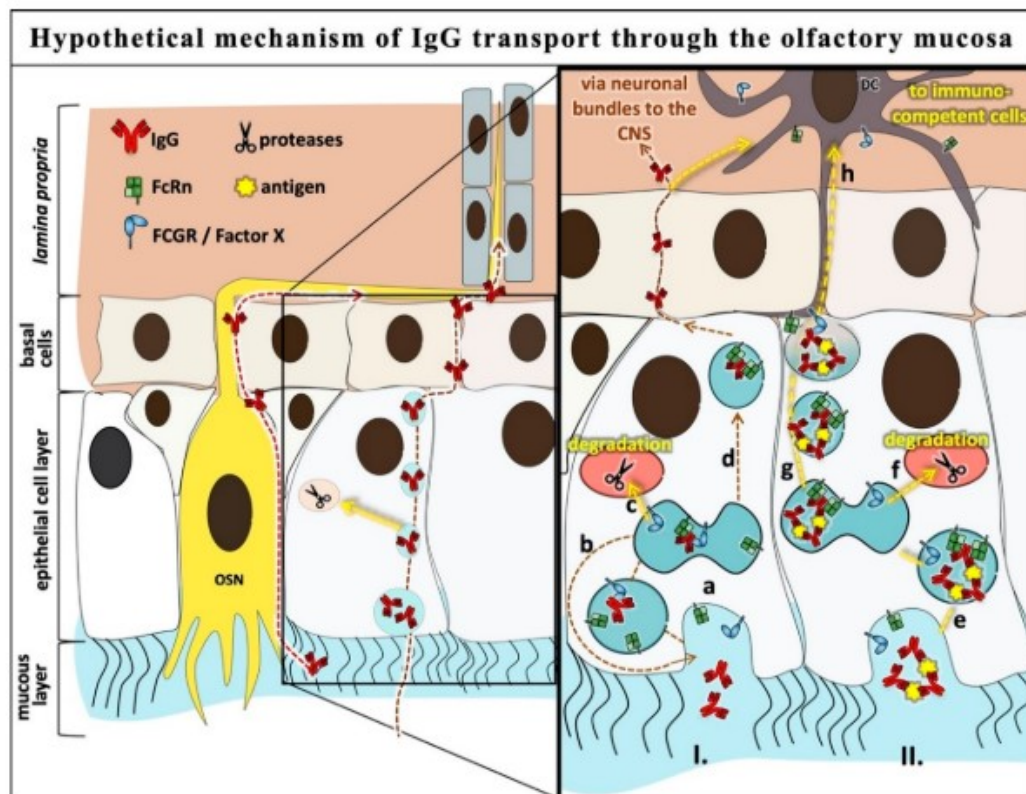


Figure 24: Cross-binding hypothesis: hypothetical mechanism of IgG transport through the olfactory mucosa.

I. monomeric IgG transport

- (a) Uptake of monomeric IgGs was presumably via pinocytosis, but FcRn was also found at the apical surface [1] and vesicle transport to the sorting compartment.
- (b) Cross-binding of IgG with FcRn and a second Fc receptor such as FCGR2, which might be factor X as suggested [189]; recycling back to the apical surface or
- (c) lysosomal degradation. Alternatively, a second FcRn replaces FCGR2/factor X and (d) the monomeric IgG is transcytosed to the *lamina propria*/basolateral side.

II. transport of immune complexes

- (e) Uptake of immune complexes similar to monomeric IgG and vesicle transport to the sorting compartment. Binding to FCGR2/factor X is not possible due to steric hindrance; therefore, double binding of FcRn to one Fc part is possible. The complex can either
- (f) be degraded in the lysosome or
- (g) transcytosed to the *lamina propria* and
- (h) taken up by dendritic cells (DC) via different FCGRs or FcRn. Further studies are needed to confirm the role of FCGR2 in IgG trafficking in the airway epithelia. Due to limitations of the commercially available anti-porcine FCGR2 antibodies, we could not distinguish between FCGR2a and FCGR2b. Nevertheless, other studies and the transcript analysis suggest FCGR2b to be expressed in olfactory epithelial cells.

Figure and hypothesis were published by Ladel *et al.* (2020) [3], CC BY 4.0, <http://creativecommons.org/licenses/by/4.0/>.

Conclusion

The exact mechanism for transcytosis remains still unclear and needs to be deeply investigated in future work. However, we found several evidences of FCGR2b being involved in IgG trafficking others than transcytosis at the mucosa epithelium.

As for N2B drug delivery the transcytosis is of main importance it is highly interesting that the use of deglycosylated IgG enhances the permeation through the olfactory epithelial barrier. In addition, concerning FCGR interaction, the interaction of the IgGs with the local immune system in lymphoid follicle should be taken into account when designing therapeutic IgG against CNS-related diseases. A depletion of the binding site for FCGRs could also here be advantageous for the bioavailability in the brain as higher levels of DG IgG crossed the olfactory epithelial barrier and the *lamina propria* in the *in vitro* and *ex vivo* experiments. On the other hand, potentially the immunogenicity of intranasally applied vaccines could be increase by the fusion of an Fc part. Here in both cases, confirmation of the hypothesis needs to be done *in vivo* in suitable animal models such as the Göttingen Minipig [142].

6. References

1. Ladel, S.; Flamm, J.; Zadeh, A.S.; Filzwieser, D.; Walter, J.C.; Schlossbauer, P.; Kinscherf, R.; Lischka, K.; Luksch, H.; Schindowski, K. Allogenic Fc Domain-Facilitated Uptake of IgG in Nasal Lamina Propria: Friend or Foe for Intranasal CNS Delivery? *Pharmaceutics* **2018**, *10*, 1–23, doi:10.3390/pharmaceutics10030107.
2. Ladel, S.; Schlossbauer, P.; Flamm, J.; Luksch, H.; Mizaikoff, B.; Schindowski, K. Improved In Vitro Model for Intranasal Mucosal Drug Delivery: Primary Olfactory and Respiratory Epithelial Cells Compared with the Permanent Nasal Cell Line RPMI 2650. *Pharmaceutics* **2019**, *11*, 367, doi:10.3390/pharmaceutics11080367.
3. Ladel, S.; Maigler, F.; Flamm, J.; Schlossbauer, P.; Handl, A.; Hermann, R.; Herzog, H.; Hummel, T.; Mizaikoff, B.; Schindowski, K. Impact of Glycosylation and Species Origin on the Uptake and Permeation of IgGs through the Nasal Airway Mucosa. *Pharmaceutics* **2020**, *12*, 1014, doi:10.3390/pharmaceutics12111014.
4. Spindler, L.M.; Feuerhake, A.; Ladel, S.; Günday, C.; Flamm, J.; Günday-Türeli, N.; Türeli, E.; Tovar, G.E.M.; Schindowski, K.; Gruber-Traub, C. Nano-in-Micro-Particles Consisting of PLGA Nanoparticles Embedded in Chitosan Microparticles via Spray-Drying Enhances Their Uptake in the Olfactory Mucosa. *Frontiers in Pharmacology* **2021**, *12*, doi:10.3389/fphar.2021.732954.
5. Maigler, F.; Ladel, S.; Flamm, J.; Gänger, S.; Kurpiers, B.; Kiderlen, S.; Völk, R.; Hamp, C.; Hartung, S.; Spiegel, S.; et al. Selective CNS Targeting and Distribution with a Refined Region-Specific Intranasal Delivery Technique via the Olfactory Mucosa. *Pharmaceutics* **2021**, *13*, 1904, doi:10.3390/pharmaceutics13111904.
6. Spindler, L.M.; Feuerhake, A.; Ladel, S.; Günday, C.; Flamm, J.; Günday-Türeli, N.; Türeli, E.; Tovar, G.E.M.; Schindowski, K.; Gruber-Traub, C. Nano-in-Micro-Particles Consisting of PLGA Nanoparticles Embedded in Chitosan Microparticles via Spray-Drying Enhances Their Uptake in the Olfactory Mucosa. *Frontiers in Pharmacology* **2021**, *12*, doi:10.3389/fphar.2021.732954.
7. Higgins, T.S.; Wu, A.W.; Illing, E.A.; Sokoloski, K.J.; Weaver, B.A.; Anthony, B.P.; Hughes, N.; Ting, J.Y. Intranasal Antiviral Drug Delivery and Coronavirus Disease 2019 (COVID-19): A State of the Art Review. *Otolaryngology - Head and Neck Surgery (United States)* **2020**, *163*, 682–694, doi:10.1177/0194599820933170.
8. Illum, L. Nasal Drug Delivery - Possibilities, Problems and Solutions. *Journal of Controlled Release* **2003**, *87*, 187–198, doi:10.1016/S0168-3659(02)00363-2.

References

9. Benedict, C.; Hallschmid, M.; Hatke, A.; Schultes, B.; Fehm, H.L.; Born, J.; Kern, W. Intranasal Insulin Improves Memory in Humans. *Psychoneuroendocrinology* **2004**, *29*, 1326–1334, doi:10.1016/j.psyneuen.2004.04.003.
10. Hallschmid, M.; Schmitz, K.; Kern, W.; Fehm, H.L.; Ratter, F.; Benedict, C.; Schultes, B.; Born, J. Intranasal Insulin Improves Memory in Humans: Superiority of Insulin Aspart. *Neuropsychopharmacology* **2006**, *32*, 239–243, doi:10.1038/sj.npp.1301193.
11. Benedict, C.; Frey, W.H.; Schioth, H.B.; Schultes, B.; Born, J.; Hallschmid, M. Intranasal Insulin as a Therapeutic Option in the Treatment of Cognitive Impairments. *Experimental Gerontology* **2011**, *46*, 112–115, doi:10.1016/j.exger.2010.08.026.
12. Jadhav, K.; Gambhire, M.; Shaikh, I.; Kadam, V.; Pisal, S. Nasal Drug Delivery System-Factors Affecting and Applications. *Current Drug Therapy* **2008**, *2*, 27–38, doi:10.2174/157488507779422374.
13. Gizurarson, S. Anatomical and Histological Factors Affecting Intranasal Drug and Vaccine Delivery. *Current Drug Delivery* **2012**, *9*, 566–582, doi:10.2174/156720112803529828.
14. Pardeshi, C.V.; Belgamwar, V.S. Direct Nose to Brain Drug Delivery via Integrated Nerve Pathways Bypassing the Blood–Brain Barrier: An Excellent Platform for Brain Targeting. *Expert Opinion on Drug Delivery* **2013**, *10*, 957–972, doi:10.1517/17425247.2013.790887.
15. Harkema, J.R.; Carey, S.A.; Wagner, J.G. The Nose Revisited: A Brief Review of the Comparative Structure, Function, and Toxicologic Pathology of the Nasal Epithelium. *Toxicologic Pathology* **2006**, *34*, 252–269, doi:10.1080/01926230600713475.
16. Gänger, S.; Schindowski, K. Tailoring Formulations for Intranasal Nose-to-Brain Delivery : A Review on Architecture , Physico- Chemical Characteristics and Mucociliary Clearance of the Nasal Olfactory Mucosa. *Pharmaceutics* **2018**, *116*, 1–28, doi:10.3390/pharmaceutics10030116.
17. Paik, S.; Lehman, M.; Seiden, A.M.; Duncan, H.J. Olfactory Biopsy. *Arch Otolaryngol Head Neck Surg* **1992**, *118*, 731–738.
18. Gizurarson, S. Anatomical and Histological Factors Affecting Intranasal Drug and Vaccine Delivery. *Current drug delivery* **2012**, *9*, 566–582, doi:10.2174/156720112803529828.
19. Gross, E.A.; Swenberg, J.A.; Fields, S.; Popp, J.A. Comparative Morphometry of the Nasal Cavity in Rats and Mice. *Journal of anatomy* **1982**, *135*, 83–88.

References

20. Charles G., P.; Jack R., H. The Respiratory System and Its Use in Research. *The Laboratory Primate* **2005**, 503–526, doi:10.1016/B978-012080261-6/50030-1.
21. Gizurarson, S. The Relevance of Nasal Physiology to the Design of Drug Absorption Studies. *Advanced Drug Delivery Reviews* **1993**, 11, 329–347, doi:10.1016/0169-409X(93)90015-V.
22. Getchell, M.L.; Getchell, T. v. Fine Structural Aspects of Secretion and Extrinsic Innervation in the Olfactory Mucosa. *Microscopy Research and Technique* **1992**, 23, 111–127, doi:10.1002/jemt.1070230203.
23. Debertin, A.S.; Tschernig, T.; Tönjes, H.; Kleemann, W.J.; Tröger, H.D.; Pabst, R. Nasal-Associated Lymphoid Tissue (NALT): Frequency and Localization in Young Children. *Clinical and Experimental Immunology* **2003**, 134, 503–507, doi:10.1111/j.1365-2249.2003.02311.x.
24. Moran, D.T.; Rowley, C.; Jafek, B.W.; Levell, M.A. The Fine Structure of the Olfactory Mucosa in Man. *Journal of Neurocytology* **1982**, 11, 721–746.
25. Au, E.; Roskams, A.J. Olfactory Ensheathing Cells of the Lamina Propria in Vivo and in Vitro. *Glia* **2003**, 41, 224–236, doi:10.1002/glia.10160.
26. Honoré, A.; le Corre, S.; Derambure, C.; Normand, R.; Duclos, C.; Boyer, O.; Marie, J.-P.; Guérout, N. Isolation, Characterization, and Genetic Profiling of Subpopulations of Olfactory Ensheathing Cells from the Olfactory Bulb. *Glia* **2012**, 60, 404–413, doi:10.1002/glia.22274.
27. Harris, J.A. *Anti-Bacterial Properties of Olfactory Ensheathing Cells and the Primary Olfactory Pathway* By; 2013; ISBN 1742209491.
28. Iwasaki, A. Immune Regulation of Antibody Access to Neuronal Tissues. *Trends in Molecular Medicine* **2017**, 23, 227–245, doi:10.1016/j.molmed.2017.01.004.
29. Brandtzaeg, P.; Pabst, R. Let's Go Mucosal: Communication on Slippery Ground. *Trends in Immunology* **2004**, 25, 570–577, doi:10.1016/j.it.2004.09.005.
30. Mittal, D.; Ali, A.; Md, S.; Baboota, S.; Sahni, J.K.; Ali, J. Insights into Direct Nose to Brain Delivery: Current Status and Future Perspective. *Drug Deliv* **2014**, 21, 75–86, doi:10.3109/10717544.2013.838713.
31. Redzic, Z. Molecular Biology of the Blood-Brain and the Blood-Cerebrospinal Fluid Barriers: Similarities and Differences. *Fluids and Barriers of the CNS* **2011**, 8, 3, doi:10.1186/2045-8118-8-3.

References

32. Neuhaus, J.; Risau, W.; Wolburg, H. Induction of Blood–Brain Barrier Characteristics in Bovine Brain Endothelial Cells by Rat Astroglial Cells in Transfilter Coculture. *Annals of the New York Academy of Sciences* **1991**, *633*, 578–580.
33. Ballabh, P.; Braun, A.; Nedergaard, M. The Blood-Brain Barrier: An Overview: Structure, Regulation, and Clinical Implications. *Neurobiology of Disease* **2004**, *16*, 1–13, doi:10.1016/j.nbd.2003.12.016.
34. Reese, T.S.; Karnovsky, M.J. Fine Structural Localization of a Blood-Brain Barrier to Exogenous Peroxidase. *The Journal of Cell Biology* **1967**, *34*, 207–217.
35. Neuwelt, E.; Abbott, N.J.; Abrey, L.; Banks, W.A.; Blakley, B.; Engelhardt, B.; Grammas, P.; Nedergaard, M.; Nutt, J.; Pardridge, W.; et al. Strategies to Advance Translational Research into Brain Barriers. *The Lancet Neurology* **2008**, *7*, 84–96, doi:10.1016/s1474-4422(07)70326-5.
36. Gao, H. Progress and Perspectives on Targeting Nanoparticles for Brain Drug Delivery. *Acta Pharmaceutica Sinica B* **2016**, *6*, 268–286, doi:10.1016/j.apsb.2016.05.013.
37. Costantino, H.R.; Illum, L.; Brandt, G.; Johnson, P.H.; Quay, S.C. Intranasal Delivery: Physicochemical and Therapeutic Aspects. *International Journal of Pharmaceutics* **2007**, *337*, 1–24, doi:10.1016/j.ijpharm.2007.03.025.
38. Lochhead, J.J.; Thorne, R.G. Intranasal Delivery of Biologics to the Central Nervous System. *Advanced Drug Delivery Reviews* **2012**, *64*, 614–628, doi:10.1016/j.addr.2011.11.002.
39. Anton, F.; Peppel, P. Central Projections of Trigeminal Primary Afferents Innervating the Nasal Mucosa: A Horseradish Peroxidase Study in the Rat. *Neuroscience* **1991**, *41*, 617–628, doi:10.1016/0306-4522(91)90354-Q.
40. Deatly, A.M.; Haase, A.T.; Fewster, P.H.; Lewis, E.; Ball, M.J. Human Herpes Virus Infections and Alzheimer's Disease. *Neuropathology and Applied Neurobiology* **1990**, *16*, 213–223, doi:10.1111/j.1365-2990.1990.tb01158.x.
41. Balin, B.J.; Broadwell, R.D.; Salcmant, M.; El-Kalliny, M. Avenues for Entry of Peripherally Administered Protein to the Central Nervous System in Mouse, Rat and Squirrel Monkey. *The Journal of Comparative Neurology* **1986**, *251*, 260–280.
42. Bahadur, S.; Pathak, K. Physicochemical and Physiological Considerations for Efficient Nose-to-Brain Targeting. *Expert Opinion on Drug Delivery* **2011**, *9*, 19–31, doi:10.1517/17425247.2012.636801.

References

43. Wengst, A.; Reichl, S. RPMI 2650 Epithelial Model and Three-Dimensional Reconstructed Human Nasal Mucosa as in Vitro Models for Nasal Permeation Studies. *European Journal of Pharmaceutics and Biopharmaceutics* **2010**, *74*, 290–297, doi:10.1016/j.ejpb.2009.08.008.
44. Gonçalves, V.S.S.; Matias, A.A.; Poejo, J.; Serra, A.T.; Duarte, C.M.M. Application of RPMI 2650 as a Cell Model to Evaluate Solid Formulations for Intranasal Delivery of Drugs. *International Journal of Pharmaceutics* **2016**, *515*, 1–10, doi:10.1016/j.ijpharm.2016.09.086.
45. Kürti, L.; Veszélka, S.; Bocsik, A.; Dung, N.T.K.; Ózsvári, B.; Puskás, L.G.; Kittel, Á.; Szabó-Révész, P.; Deli, M.A. The Effect of Sucrose Esters on a Culture Model of the Nasal Barrier. *Toxicology in Vitro* **2012**, *26*, 445–454, doi:10.1016/j.tiv.2012.01.015.
46. Nakamura, K.; Maitani, Y.; Takayama, K. The Enhancing Effect of Nasal Absorption of FITC-Dextran 4,400 by β -Sitosterol β -D-Glucoside in Rabbits. *Journal of Controlled Release* **2002**, *79*, 147–155, doi:10.1016/S0168-3659(01)00540-5.
47. Grainger, C.I.; Greenwell, L.L.; Martin, G.P.; Forbes, B. The Permeability of Large Molecular Weight Solutes Following Particle Delivery to Air-Interfaced Cells That Model the Respiratory Mucosa. *European Journal of Pharmaceutics and Biopharmaceutics* **2009**, *71*, 318–324, doi:10.1016/j.ejpb.2008.09.006.
48. Nicolazzo, J.A.; Reed, B.L.; Finnin, B.C. The Effect of Various in Vitro Conditions on the Permeability Characteristics of the Buccal Mucosa. *Journal of Pharmaceutical Sciences* **2003**, *92*, 2399–2410, doi:10.1002/jps.10505.
49. Schmidt, M.C.; Peter, H.; Lang, S.R.; Ditzinger, G.; Merkle, H.P. In Vitro Cell Models to Study Nasal Mucosal Permeability and Metabolism. *Advanced Drug Delivery Reviews* **1998**, *29*, 51–79.
50. Born, J.; Lange, T.; Kern, W.; McGregor, G.P.; Bickel, U.; Fehm, H.L. Sniffing Neuropeptides: A Transnasal Approach to the Human Brain. *Nature Neuroscience* **2002**, *5*, 514–516, doi:10.1038/nn0602-849.
51. Brambilla, M.; Manenti, R.; de Girolamo, G.; Adenzato, M.; Bocchio-Chiavetto, L.; Cotelli, M. Effects of Intranasal Oxytocin on Long-Term Memory in Healthy Humans: A Systematic Review. *Drug Development Research* **2016**, *77*, 479–488.
52. Winner, P.; Rothner, A.D.; Saper, J.; Nett, R.; Asgharnejad, M.; Laurenza, A.; Austin, R.; Peykamian, M. A Randomized, Double-Blind, Placebo-Controlled Study of Sumatriptan Nasal Spray in the Treatment of Acute Migraine in Adolescents. *Pediatrics* **2000**, *106*, 989–997.

References

53. Kim, K.-J.; Malik, A.B. Protein Transport across the Lung Epithelial Barrier. *American Journal of Physiology-Lung Cellular and Molecular Physiology* **2015**, *284*, L247–L259, doi:10.1152/ajplung.00235.2002.
54. Pardeshi, C.V.; Belgamwar, V.S. Direct Nose to Brain Drug Delivery via Integrated Nerve Pathways Bypassing the Blood-Brain Barrier: An Excellent Platform for Brain Targeting. *Expert opinion on drug delivery* **2013**, *10*, 957–972, doi:10.1517/17425247.2013.790887.
55. Crowe, T.P.; Greenlee, M.H.W.; Kanthasamy, A.G.; Hsu, W.H. Mechanism of Intranasal Drug Delivery Directly to the Brain. *Life Sciences* **2018**, *195*, 44–52, doi:10.1016/j.lfs.2017.12.025.
56. Thorne, R.G.; Pronk, G.J.; Padmanabhan, V.; Frey, W.H. Delivery of Insulin-like Growth Factor-I to the Rat Brain and Spinal Cord along Olfactory and Trigeminal Pathways Following Intranasal Administration. *Neuroscience* **2004**, *127*, 481–496, doi:10.1016/j.neuroscience.2004.05.029.
57. Reger, M.A.; Watson, G.S.; Frey, W.H.; Baker, L.D.; Cholerton, B.; Keeling, M.L.; Belongia, D.A.; Fishel, M.A.; Plymate, S.R.; Schellenberg, G.D.; et al. Effects of Intranasal Insulin on Cognition in Memory-Impaired Older Adults: Modulation by APOE Genotype. *Neurobiology of Aging* **2006**, *27*, 451–458, doi:10.1016/j.neurobiolaging.2005.03.016.
58. Heni, M.; Kullmann, S.; Ketterer, C.; Guthoff, M.; Linder, K.; Wagner, R.; Stingl, K.T.; Veit, R.; Staiger, H.; Häring, H.-U.; et al. Nasal Insulin Changes Peripheral Insulin Sensitivity Simultaneously with Altered Activity in Homeostatic and Reward-Related Human Brain Regions. *Diabetologia* **2012**, *55*, 1773–1782, doi:10.1007/s00125-012-2528-y.
59. Sintov, A.C.; Levy, H. v.; Botner, S. Systemic Delivery of Insulin via the Nasal Route Using a New Microemulsion System: In Vitro and in Vivo Studies. *Journal of Controlled Release* **2010**, *148*, 168–176, doi:10.1016/j.jconrel.2010.08.004.
60. Lochhead, J.J.; Kellohen, K.L.; Ronaldson, P.T.; Davis, T.P. Distribution of Insulin in Trigeminal Nerve and Brain after Intranasal Administration. *Scientific Reports* **2019**, *9*, 1–9, doi:10.1038/s41598-019-39191-5.
61. Kullmann, S.; Frank, S.; Heni, M.; Ketterer, C.; Veit, R.; Häring, H.U.; Fritsche, A.; Preissl, H. Intranasal Insulin Modulates Intrinsic Reward and Prefrontal Circuitry of the Human Brain in Lean Women. *Neuroendocrinology* **2013**, *97*, 176–182, doi:10.1159/000341406.

References

62. Kumar, N.N.; Lochhead, J.J.; Pizzo, M.E.; Nehra, G.; Boroumand, S.; Greene, G.; Thorne, R.G. Delivery of Immunoglobulin G Antibodies to the Rat Nervous System Following Intranasal Administration: Distribution, Dose-Response, and Mechanisms of Delivery. *Journal of Controlled Release* **2018**, *286*, 467–484, doi:10.1016/j.jconrel.2018.08.006.
63. Kaplon, H.; Reichert, J.M. Antibodies to Watch in 2019. *mAbs* **2019**, *11*, 219–238, doi:10.1080/19420862.2018.1556465.
64. Hay, M.; Thomas, D.W.; Craighead, J.L.; Economides, C.; Rosenthal, J. Clinical Development Success Rates for Investigational Drugs. *Nature Biotechnology* **2014**, *32*, 40–51, doi:10.1038/nbt.2786.
65. Murphy, K.; with acknowledgement:; Janeway, C.A.J.; Travers P, W.M. The Structure of a Typical Antibody Molecule. In *Immunobiology: The Immune System in Health and Disease. 8th edition.*; New York: Garland Science, 2012; pp. 128–133 ISBN 9780815342434.
66. Edelman, G.M. Antibody Structure and Molecular Immunology. *Science* **1973**, *180*, 830–840.
67. Schroeder, H.W.; Cavacini, L. Structure and Function of Immunoglobulins. *Journal of Allergy and Clinical Immunology* **2010**, *125*, 41–52, doi:10.1016/j.jaci.2009.09.046.
68. Mage, M.G. Preparation of Fab Fragments from IgGs of Different Animal Species. In; 1980; pp. 142–150.
69. Vidarsson, G.; Dekkers, G.; Rispens, T. IgG Subclasses and Allotypes: From Structure to Effector Functions. *Frontiers in Immunology* **2014**, *5*, 1–17, doi:10.3389/fimmu.2014.00520.
70. Wang, X.; Mathieu, M.; Brezski, R.J. IgG Fc Engineering to Modulate Antibody Effector Functions. *Protein and Cell* **2018**, *9*, 63–73, doi:10.1007/s13238-017-0473-8.
71. Subedi, G.P.; Barb, A.W. The Immunoglobulin G1 N-Glycan Composition Affects Binding to Each Low Affinity Fc γ Receptor. *mAbs* **2016**, *8*, 1512–1524, doi:10.1080/19420862.2016.1218586.
72. de Taeye, S.W.; Rispens, T.; Vidarsson, G. The Ligands for Human IgG and Their Effector Functions. *Antibodies* **2019**, *8*, 30, doi:10.3390/antib8020030.
73. Roux, K.H.; Strelets, L.; Michaelsen, T.E. Flexibility of Human IgG Subclasses. *Journal of immunology (Baltimore, Md. : 1950)* **1997**, *159*, 3372–3382.

References

74. Michaelsen, T.E.; Naess, L.M.; Aase, A. Human IgG3 Is Decreased and IgG1, IgG2 and IgG4 Are Unchanged in Molecular Size by Mild Reduction and Reoxidation without Any Major Change in Effector Functions. *Molecular immunology* **1993**, *30*, 35–45, doi:10.1016/0161-5890(93)90424-a.
75. Dorokhov, Y.L.; Sheshukova, E. v.; Kosobokova, E.N.; Shindyapina, A. v.; Kosorukov, V.S.; Komarova, T. v. Functional Role of Carbohydrate Residues in Human Immunoglobulin G and Therapeutic Monoclonal Antibodies. *Biochemistry (Moscow)* **2016**, *81*, 835–857, doi:10.1134/S0006297916080058.
76. Plomp, R.; Dekkers, G.; Rombouts, Y.; Visser, R.; Koeleman, C.A.M.; Kammeijer, G.S.M.; Jansen, B.C.; Rispen, T.; Hensbergen, P.J.; Vidarsson, G.; et al. Hinge-Region O-Glycosylation of Human Immunoglobulin G3 (IgG3). *Molecular & Cellular Proteomics* **2015**, *14*, 1373–1384, doi:10.1074/mcp.M114.047381.
77. Hamm, M.; Wang, Y.; Rustandi, R.R. Characterization of N-Linked Glycosylation in a Monoclonal Antibody Produced in NS0 Cells Using Capillary Electrophoresis with Laser-Induced Fluorescence Detection. *Pharmaceuticals* **2013**, *6*, 393–406, doi:10.3390/ph6030393.
78. Alessandri, L.; Ouellette, D.; Acquah, A.; Rieser, M.; LeBlond, D.; Saltarelli, M.; Radziejewski, C.; Fujimori, T.; Correia, I. Increased Serum Clearance of Oligomannose Species Present on a Human IgG1 Molecule. *mAbs* **2012**, *4*, 509–520, doi:10.4161/mabs.20450.
79. Bork, K.; Horstkorte, R.; Weidemann, W. Increasing the Sialylation of Therapeutic Glycoproteins: The Potential of the Sialic Acid Biosynthetic Pathway. *Journal of Pharmaceutical Sciences* **2009**, *98*, 3499–3508, doi:10.1002/jps.21684.
80. Naso, M.F.; Tam, S.H.; Scallon, B.J.; Raju, T.S. Engineering Host Cell Lines to Reduce Terminal Sialylation of Secreted Antibodies. *mAbs* **2010**, *2*, 519–527, doi:10.4161/mabs.2.5.13078.
81. Courtois, F.; Agrawal, N.J.; Lauer, T.M.; Trout, B.L. Rational Design of Therapeutic MAbs against Aggregation through Protein Engineering and Incorporation of Glycosylation Motifs Applied to Bevacizumab. *mAbs* **2016**, *8*, 99–112, doi:10.1080/19420862.2015.1112477.
82. Retamozo, S.; Brito-Zerón, P.; Bosch, X.; Stone, J.H.; Ramos-Casals, M. Cryoglobulinemic Disease. *Oncology (Williston Park, N. Y.)* **2013**, *27*, 1098–1105, 1110–1116.

References

83. Schlothauer, T.; Herter, S.; Koller, C.F.; Grau-Richards, S.; Steinhart, V.; Spick, C.; Kubbies, M.; Klein, C.; Umaña, P.; Mössner, E. Novel Human IgG1 and IgG4 Fc-Engineered Antibodies with Completely Abolished Immune Effector Functions. *Protein engineering, design & selection: PEDS* **2016**, 29, 457–466, doi:10.1093/protein/gzw040.
84. Yamaguchi, Y.; Nishimura, M.; Nagano, M.; Yagi, H.; Sasakawa, H.; Uchida, K.; Shitara, K.; Kato, K. Glycoform-Dependent Conformational Alteration of the Fc Region of Human Immunoglobulin G1 as Revealed by NMR Spectroscopy. *Biochimica et Biophysica Acta - General Subjects* **2006**, 1760, 693–700, doi:10.1016/j.bbagen.2005.10.002.
85. Collin, M.; Shannon, O.; Björck, L. IgG Glycan Hydrolysis by a Bacterial Enzyme as a Therapy against Autoimmune Conditions. *Proceedings of the National Academy of Sciences of the United States of America* **2008**, 105, 4265–4270, doi:10.1073/pnas.0711271105.
86. Li, B.; Lai, J.; Meng, Y.G.; Fox, J.A.; Shields, R.L.; Namenuk, A.K.; Briggs, J.; Stadlen, A.; Presta, L.G.; Rae, J.; et al. High Resolution Mapping of the Binding Site on Human IgG1 for FcγRI, FcγRII, FcγRIII, and FcRn and Design of IgG1 Variants with Improved Binding to the FcγR. *Journal of Biological Chemistry* **2002**, 276, 6591–6604, doi:10.1074/jbc.m009483200.
87. Allhorn, M.; Olin, A.I.; Nimmerjahn, F.; Colin, M. Human IgG/FcγR Interactions Are Modulated by Streptococcal IgG Glycan Hydrolysis. *PLoS ONE* **2008**, 3, doi:10.1371/journal.pone.0001413.
88. Hanson, Q.M.; Barb, A.W. A Perspective on the Structure and Receptor Binding Properties of Immunoglobulin G Fc. *Biochemistry* **2015**, 54, 2931–2942, doi:10.1021/acs.biochem.5b00299.
89. Wada, R.; Matsui, M.; Kawasaki, N. Influence of N-Glycosylation on Effector Functions and Thermal Stability of Glycoengineered IgG1 Monoclonal Antibody with Homogeneous Glycoforms. *mAbs* **2019**, 11, 350–372, doi:10.1080/19420862.2018.1551044.
90. O'Connell, L.Y.; Lai, J.; Presta, L.G.; Keck, R.; Meng, Y.G.; Hong, K.; Weikert, S.H.A.; Shields, R.L. Lack of Fucose on Human IgG1 N -Linked Oligosaccharide Improves Binding to Human FcγRIII and Antibody-Dependent Cellular Toxicity . *Journal of Biological Chemistry* **2002**, 277, 26733–26740, doi:10.1074/jbc.m202069200.

References

91. Raghavan, M.; Bjorkman, P.J. Fc Receptors and Their Interactions with Immunoglobulins. *Annual Review of Cell and Developmental Biology* **1996**, *12*, 181–220, doi:10.1146/annurev.cellbio.12.1.181.
92. Burmeister, W.P.; Gastinel, L.N.; Simister, N.E.; Blum, M.L.; Bjorkman, P.J. Crystal Structure at 2.2 Å Resolution of the MHC-Related Neonatal Fc Receptor. *Nature* **1994**, *372*, 336–343, doi:10.1038/372336a0.
93. Simister, N.E.; Mostov, K.E. An Fc Receptor Structurally Related to MHC Class I Antigens. *Nature* **1989**, *337*, 184–187, doi:10.1038/337184a0.
94. Story, C.M.; Mikulska, J.E.; Simister, N.E. A Major Histocompatibility Complex Class I-like Fc Receptor Cloned from Human Placenta: Possible Role in Transfer of Immunoglobulin G from Mother to Fetus. *Journal of Experimental Medicine* **1994**, *180*, 2377–2381, doi:10.1084/jem.180.6.2377.
95. Roopenian, D.C.; Akilesh, S. FcRn: The Neonatal Fc Receptor Comes of Age. *Nature Reviews Immunology* **2007**, *7*, 715–725, doi:10.1038/nri2155.
96. Terje Andersen, J.; Bekele Daba, M.; Berntzen, G.; Michaelsen, T.E.; Sandlie, I. Cross-Species Binding Analyses of Mouse and Human Neonatal Fc Receptor Show Dramatic Differences in Immunoglobulin G and Albumin Binding. *Journal of Biological Chemistry* **2010**, *285*, 4826–4836, doi:10.1074/jbc.M109.081828.
97. Raghavan, M.; Gastinel, L.N.; Bjorkman, P.J. The Class I Major Histocompatibility Complex Related Fc Receptor Shows PH-Dependent Stability Differences Correlating with Immunoglobulin Binding and Release. *Biochemistry* **1993**, *32*, 8654–8660, doi:10.1021/bi00084a037.
98. Lencer, W.I.; Blumberg, R.S. A Passionate Kiss , Then Run : Exocytosis and Recycling of IgG by FcRn. **2005**, *15*, 5–9, doi:10.1016/j.tcb.2004.11.005.
99. Liu, X.; Lu, L.; Yang, Z.; Palaniyandi, S.; Zeng, R.; Gao, L.-Y.; Mosser, D.M.; Roopenian, D.C.; Zhu, X. The Neonatal FcR-Mediated Presentation of Immune-Complexed Antigen Is Associated with Endosomal and Phagosomal PH and Antigen Stability in Macrophages and Dendritic Cells. *The Journal of Immunology* **2011**, *186*, 4674–4686, doi:10.4049/jimmunol.1003584.
100. Baker, K.; Qiao, S.-W.; Kuo, T.T.; Aveson, V.G.; Platzer, B.; Andersen, J.-T.; Sandlie, I.; Chen, Z.; de Haar, C.; Lencer, W.I.; et al. Neonatal Fc Receptor for IgG (FcRn) Regulates Cross-Presentation of IgG Immune Complexes by CD8-CD11b+ Dendritic Cells. *Proceedings of the National Academy of Sciences* **2011**, *108*, 9927–9932, doi:10.1073/pnas.1019037108.

References

101. Foss, S.; Grevys, A.; Sand, K.M.K.; Bern, M.; Blundell, P.; Michaelsen, T.E.; Pleass, R.J.; Sandlie, I.; Andersen, J.T. Enhanced FcRn-Dependent Transepithelial Delivery of IgG by Fc-Engineering and Polymerization. *Journal of Controlled Release* **2016**, *223*, 42–52, doi:10.1016/j.jconrel.2015.12.033.
102. Dickinson, B.L.; Badizadegan, K.; Wu, Z.; Ahouse, J.C.; Zhu, X.; Simister, N.E.; Blumberg, R.S.; Lencer, W.I. Bidirectional FcRn-Dependent IgG Transport in a Polarized Human Intestinal Epithelial Cell Line. *Journal of Clinical Investigation* **1999**, *104*, 903–911, doi:10.1172/JCI6968.
103. Abdiche, Y.N.; Yeung, Y.A.; Chaparro-Riggers, J.; Barman, I.; Strop, P.; Chin, S.M.; Pham, A.; Bolton, G.; McDonough, D.; Lindquist, K.; et al. The Neonatal Fc Receptor (FcRn) Binds Independently to Both Sites of the IgG Homodimer with Identical Affinity. *mAbs* **2015**, *7*, 331–343, doi:10.1080/19420862.2015.1008353.
104. Schlothauer, T.; Rueger, P.; Stracke, J.O.; Hertenberger, H.; Fingas, F.; Kling, L.; Emrich, T.; Drabner, G.; Seeber, S.; Auer, J.; et al. Analytical FcRn Affinity Chromatography for Functional Characterization of Monoclonal Antibodies. *mAbs* **2013**, *5*, 576–586, doi:10.4161/mabs.24981.
105. Piche-Nicholas, N.M.; Avery, L.B.; King, A.C.; Kavosi, M.; Wang, M.; O'Hara, D.M.; Tchistiakova, L.; Katragadda, M. Changes in Complementarity-Determining Regions Significantly Alter IgG Binding to the Neonatal Fc Receptor (FcRn) and Pharmacokinetics. *mAbs* **2018**, *10*, 81–94, doi:10.1080/19420862.2017.1389355.
106. Jensen, P.F.; Larraillet, V.; Schlothauer, T.; Kettenberger, H.; Hilger, M.; Rand, K.D. Investigating the Interaction between the Neonatal Fc Receptor and Monoclonal Antibody Variants by Hydrogen/Deuterium Exchange Mass Spectrometry. *Molecular & Cellular Proteomics* **2015**, *14*, 148–161, doi:10.1074/mcp.M114.042044.
107. Spiekermann, G.M.; Finn, P.W.; Ward, E.S.; Dumont, J.; Dickinson, B.L.; Blumberg, R.S.; Lencer, W.I. Receptor-Mediated Immunoglobulin G Transport Across Mucosal Barriers in Adult Life. *The Journal of Experimental Medicine* **2002**, *196*, 303–310, doi:10.1084/jem.20020400.
108. Yoshida, M.; Masuda, A.; Kuo, T.T.; Kobayashi, K.; Claypool, S.M.; Takagawa, T.; Kutsumi, H.; Azuma, T.; Lencer, W.I.; Blumberg, R.S. IgG Transport across Mucosal Barriers by Neonatal Fc Receptor for IgG and Mucosal Immunity. *Springer Seminars in Immunopathology* **2006**, *28*, 397–403, doi:10.1007/s00281-006-0054-z.
109. Zhang, W.; Wang, W.; Li, S.; Jia, S.; Zhang, X.; Cao, T. Localization of Neonatal Fc Receptor for IgG in Aggregated Lymphoid Nodules Area in Abomasum of Bactrian

References

- Camels (*Camelus Bactrianus*) of Different Ages. *BMC Veterinary Research* **2016**, 1–9, doi:10.1186/s12917-016-0847-9.
110. Schlachetzki, F.; Zhu, C.; Pardridge, W.M. Expression of the Neonatal Fc Receptor (FcRn) at the Blood-Brain Barrier. *Journal of Neurochemistry* **2002**, 81, 203–206, doi:10.1046/j.1471-4159.2002.00840.x.
111. Xiao, G.; Gan, L.-S. Receptor-Mediated Endocytosis and Brain Delivery of Therapeutic Biologics. *International journal of cell biology* **2013**, 2013, 703545, doi:10.1155/2013/703545.
112. Garg, A.; Balthasar, J.P. Investigation of the Influence of FcRn on the Distribution of IgG to the Brain. *The AAPS Journal* **2009**, 11, 553–557, doi:10.1208/s12248-009-9129-9.
113. Ruano-Salguero, J.S.; Lee, K.H. Antibody Transcytosis across Brain Endothelial-like Cells Occurs Nonspecifically and Independent of FcRn. *Scientific Reports* **2020**, 10, 1–10, doi:10.1038/s41598-020-60438-z.
114. Guillemineault, L.; Azzopardi, N.; Arnoult, C.; Sobilo, J.; Herve, V.; Montharu, J.; Diot, P. Fate of Inhaled Monoclonal Antibodies after the Deposition of Aerosolized Particles in the Respiratory System. *Journal of Controlled Release* **2014**, 196, 344–354.
115. Nimmerjahn, F.; Ravetch, J. v. Fcγ Receptors as Regulators of Immune Responses. *Nature Reviews Immunology* **2008**, 8, 34–47, doi:10.1038/nri2206.
116. Hayes, J.M.; Wormald, M.R.; Rudd, P.M.; Davey, G.P. Fc Gamma Receptors: Glycobiology and Therapeutic Prospects. *Journal of Inflammation Research* **2016**, 9, 209–219, doi:10.2147/JIR.S121233.
117. Cambay, F.; Raymond, C.; Brochu, D.; Gilbert, M.; Tu, T.M.; Cantin, C.; Lenferink, A.; Grail, M.; Henry, O.; de Crescenzo, G.; et al. Impact of IgG1 N-Glycosylation on Their Interaction with Fc Gamma Receptors. *Current Research in Immunology* **2020**, 1, 23–37, doi:10.1016/j.crimmu.2020.06.001.
118. Ishikawa, T.; Takizawa, T.; Iwaki, J.; Mishima, T.; Ui-Tei, K.; Takeshita, T.; Matsubara, S.; Takizawa, T. Fc Gamma Receptor IIb Participates in Maternal IgG Trafficking of Human Placental Endothelial Cells. *International Journal of Molecular Medicine* **2015**, 35, 1273–1289, doi:10.3892/ijmm.2015.2141.
119. Hayes, J.M.; Cosgrave, E.F.J.; Struwe, W.B.; Wormald, M.; Davey, G.P.; Jefferis, R.; Rudd, P.M. Fc Receptors: Humanized Mice to Study FcγR Function. *Current Topics in Microbiology and Immunology* **2014**, 382, 237–248, doi:10.1007/978-3-319-07911-0.

References

120. Pyzik, M.; Sand, K.M.K.; Hubbard, J.J.; Andersen, J.T.; Sandlie, I.; Blumberg, R.S. The Neonatal Fc Receptor (FcRn): A Misnomer? *Frontiers in Immunology* **2019**, *10*, doi:10.3389/fimmu.2019.01540.
121. Golebski, K.; Hoepel, W.; van Egmond, D.; de Groot, E.J.; Amatngalim, G.D.; Beekman, J.M.; Fokkens, W.J.; van Drunen, C.M.; den Dunnen, J. FcγRIII Stimulation Breaks the Tolerance of Human Nasal Epithelial Cells to Bacteria through Cross-Talk with TLR4. *Mucosal Immunology* **2019**, *12*, 425–433, doi:10.1038/s41385-018-0129-x.
122. Davis, R.S.; Wang, Y.H.; Kubagawa, H.; Cooper, M.D. Identification of a Family of Fc Receptor Homologs with Preferential B Cell Expression. *Proceedings of the National Academy of Sciences of the United States of America* **2001**, *98*, 9772–9777, doi:10.1073/pnas.171308498.
123. Nimmerjahn, F.; Ravetch, J. v. Fcγ Receptors: Old Friends and New Family Members. *Immunity* **2006**, *24*, 19–28, doi:10.1016/j.immuni.2005.11.010.
124. Ravetch, J. V. Immune Inhibitory Receptors. *Science* **2000**, *290*, 84–89, doi:10.1126/science.290.5489.84.
125. Jennewein, M.F.; Goldfarb, I.; Dolatshahi, S.; Cosgrove, C.; Noelette, F.J.; Krykbaeva, M.; Das, J.; Sarkar, A.; Gorman, M.J.; Fischinger, S.; et al. Fc Glycan-Mediated Regulation of Placental Antibody Transfer. *Cell* **2019**, *178*, doi:10.1016/j.cell.2019.05.044.
126. Stamou, M.; Grodzki, A.C.; van Oostrum, M.; Wollscheid, B.; Lein, P.J. Fc Gamma Receptors Are Expressed in the Developing Rat Brain and Activate Downstream Signaling Molecules upon Cross-Linking with Immune Complex. *Journal of Neuroinflammation* **2018**, *15*, 1–23, doi:10.1186/s12974-017-1050-z.
127. Mathiesen, L.; Nielsen, L.K.; Andersen, J.T.; Grevys, A.; Sandlie, I.; Michaelsen, T.E.; Hedegaard, M.; Knudsen, L.E.; Dziegiel, M.H. Maternofetal Transplacental Transport of Recombinant IgG Antibodies Lacking Effector Functions. *Blood* **2013**, *122*, 1174–1181, doi:10.1182/blood-2012-12-473843.
128. Hart, E.A.; Caccamo, M.; Harrow, J.L.; Humphray, S.J.; Gilbert, J.G.; Trevanion, S.; Hubbard, T.; Rogers, J.; Rothschild, M.F. Lessons Learned from the Initial Sequencing of the Pig Genome: Comparative Analysis of an 8 Mb Region of Pig Chromosome 17. *Genome Biology* **2007**, *8*, R168, doi:10.1186/gb-2007-8-8-r168.
129. Swindle, M.M.; Makin, A.; Herron, A.J.; Clubb, F.J.; Frazier, K.S. Swine as Models in Biomedical Research and Toxicology Testing. *Veterinary Pathology* **2012**, *49*, 344–356, doi:10.1177/0300985811402846.

References

130. Blanco-Arias, P.; Sargent, C.A.; Affara, N.A. A Comparative Analysis of the Pig, Mouse, and Human PCDHX Genes. *Mammalian Genome* **2004**, *15*, 296–306, doi:10.1007/s00335-003-3034-9.
131. Meurens, F.; Summerfield, A.; Nauwynck, H.; Saif, L.; Gerdts, V. The Pig: A Model for Human Infectious Diseases. *Trends in Microbiology* **2012**, *20*, 50–57, doi:10.1016/j.tim.2011.11.002.
132. Wadell, C.; Björk, E.; Camber, O. Nasal Drug Delivery--Evaluation of an in Vitro Model Using Porcine Nasal Mucosa. *European journal of pharmaceutical sciences* **1999**, *7*, 197–206, doi:S0928-0987(98)00023-2 [pii].
133. Wadell, C.; Björk, E.; Camber, O. Permeability of Porcine Nasal Mucosa Correlated with Human Nasal Absorption. *European Journal of Pharmaceutical Sciences* **2003**, *18*, 47–53, doi:10.1016/S0928-0987(02)00240-3.
134. Samson, G.; García De La Calera, A.; Dupuis-Girod, S.; Faure, F.; Decullier, E.; Paintaud, G.; Vignault, C.; Scoazec, J.Y.; Pivot, C.; Plauchu, H.; et al. Ex Vivo Study of Bevacizumab Transport through Porcine Nasal Mucosa. *European Journal of Pharmaceutics and Biopharmaceutics* **2012**, *80*, 465–469, doi:10.1016/j.ejpb.2011.11.004.
135. Tulinski, P.; Fluit, A.C.; van Putten, J.P.M.; de Bruin, A.; Glorieux, S.; Wagenaar, J.A.; Duim, B. An Ex Vivo Porcine Nasal Mucosa Explants Model to Study MRSA Colonization. *PLoS ONE* **2013**, *8*, doi:10.1371/journal.pone.0053783.
136. Glorieux, S.; van den Broeck, W.; van der Meulen, K.M.; van Reeth, K.; Favoreel, H.W.; Nauwynck, H.J. In Vitro Culture of Porcine Respiratory Nasal Mucosa Explants for Studying the Interaction of Porcine Viruses with the Respiratory Tract. *Journal of Virological Methods* **2007**, *142*, 105–112, doi:10.1016/j.jviromet.2007.01.018.
137. Lobasso, S.; Lopalco, P.; Angelini, R.; Baronio, M.; Fanizzi, F.P.; Babudri, F.; Corcelli, A. Lipidomic Analysis of Porcine Olfactory Epithelial Membranes and Cilia. *Lipids* **2010**, *45*, 593–602, doi:10.1007/s11745-010-3432-1.
138. Pabst, R. The Pig as a Model for Immunology Research. *Cell and Tissue Research* **2020**, *380*, 287–304, doi:10.1007/s00441-020-03206-9.
139. Ober, R.J.; Radu, C.G.; Ghetie, V.; Ward, E.S. Differences in Promiscuity for Antibody–FcRn Interactions across Species: Implications for Therapeutic Antibodies. *International Immunology* **2001**, *13*, 1551–1559.

References

140. Stirling, C.M.A.; Charleston, B.; Takamatsu, H.; Claypool, S.; Lencer, W.; Blumberg, R.S.; Wileman, T.E. Characterization of the Porcine Neonatal Fc Receptor - Potential Use for Trans-Epithelial Protein Delivery. *Immunology* **2005**, *114*, 542–553, doi:10.1111/j.1365-2567.2004.02121.x.
141. Baker, K.; Qiao, S.-W.; Kuo, T.; Kobayashi, K.; Yoshida, M.; Lencer, W.I.; Blumberg, R.S. Immune and Non-Immune Functions of the (Not so) Neonatal Fc Receptor, FcRn. **2009**, *31*, 223–236, doi:10.1007/s00281-009-0160-9.Immune.
142. Egli, J.; Schlothauer, T.; Spick, C.; Seeber, S.; Singer, T.; Odermatt, A.; Iglesias, A. The Binding of Human IgG to Minipig FcγRs – Implications for Preclinical Assessment of Therapeutic Antibodies. *Pharmaceutical Research* **2019**, *36*, doi:10.1007/s11095-019-2574-y.
143. Sosnik, A. Tissue-Based in Vitro and Ex Vivo Models for Nasal Permeability Studies. In *Concepts and Models for Drug Permeability Studies*; Elsevier, 2016; pp. 237–254.
144. Östh, K.; Grasjö, J.; Björk, E. A New Method for Drug Transport Studies on Pig Nasal Mucosa Using a Horizontal Ussing Chamber. *Journal of Pharmaceutical Sciences* **2002**, *91*, 1259–1273, doi:10.1002/jps.10123.
145. Mistry, A. The Development and Application of Biological Models for Evaluation of Direct Nose-to-Brain Drug Delivery Systems., 2009.
146. Khanvilkar, K. Drug Transfer through Mucus. *Advanced Drug Delivery Reviews* **2001**, *48*, 173–193, doi:10.1016/S0169-409X(01)00115-6.
147. Li, H.; Sheppard, D.N.; Hug, M.J. Transepithelial Electrical Measurements with the Ussing Chamber. *Journal of Cystic Fibrosis* **2004**, *3*, 123–126, doi:10.1016/j.jcf.2004.05.026.
148. Seo, J.E.; Kim, S.; Kim, B.H. In Vitro Skin Absorption Tests of Three Types of Parabens Using a Franz Diffusion Cell. *Journal of Exposure Science and Environmental Epidemiology* **2017**, *27*, 320–325, doi:10.1038/jes.2016.33.
149. Flamm, J.E. Intranasal Application of CNS-Active Drugs, Ulm, 2021.
150. Srinivasan, B.; Kolli, A.R.; Esch, M.B.; Abaci, H.E.; Shuler, L.; Hickman, J.J.; Srinivasan, B.; Kolli, A.R.; Esch, M.B.; Abaci, H.E.; Shuler, M.L.; Hickman, J.J. *TEER Measurement Techniques for in Vitro Barrier Model Systems*; 2016; Vol. 20; ISBN 4078822819.
151. Mercier, C.; Perek, N.; Delavenne, X. Is RPMI 2650 a Suitable In Vitro Nasal Model for Drug Transport Studies? *European Journal of Drug Metabolism and Pharmacokinetics* **2018**, *43*, 13–24, doi:10.1007/s13318-017-0426-x.

References

152. Imagawa, W.; Yang, J.; Richards, J.; Guzman, R.; Nandi, S. Sustained Growth in Primary Culture of Normal Mammary Epithelial Cells Embedded in Collagen Gels. *Proceedings of the National Academy of Sciences* **2006**, *77*, 2088–2092, doi:10.1073/pnas.77.4.2088.
153. Werner, U.; Kissel, T. Development of a Human Nasal Epithelial Cell Culture Model and Its Suitability for Transport and Metabolism Studies Under in Vitro Conditions. *Pharmaceutical Research: An Official Journal of the American Association of Pharmaceutical Scientists* 1995, *12*, 565–571.
154. Li, Z.; Palaniyandi, S.; Zeng, R.; Tuo, W.; Roopenian, Derry.C.; Zhu, X. Transfer of IgG in the Female Genital Tract by MHC Class I-Related Neonatal Fc Receptor (FcRn) Confers Protective Immunity to Vaginal Infection. *Proceedings of the National Academy of Sciences* **2011**, *108*, 4388–4393, doi:10.1073/pnas.1012861108.
155. Bruijn, M.; Lutter, R.; Eldering, E.; Bos, A.P.; van Woensel, J.B.M. Effect of Oxidative Stress on Respiratory Epithelium from Children with Down Syndrome. *Eur Respir J* **2013**, *42*, 1037–1045, doi:10.1183/09031936.00122812.
156. Zabner, J.; Starner, T.D.; Traver, G.L.; McCray, P.B.; Crystal, R.G.; Tilley, A.E.; Pezzulo, A.A.; Scheetz, T.E.; Harvey, B.-G. The Air-Liquid Interface and Use of Primary Cell Cultures Are Important to Recapitulate the Transcriptional Profile of in Vivo Airway Epithelia. *American Journal of Physiology-Lung Cellular and Molecular Physiology* **2010**, *300*, L25–L31, doi:10.1152/ajplung.00256.2010.
157. Moore, G.E.; Sandberg, A.A. Studies of a Human Tumor Cell Line with a Diploid Karyotype. *Cancer* **1964**, *17*, 170–175.
158. Moorhead, P.S. Human Tumor Cell Line with a Quasi-Diploid Karyotype (RPMI 2650). *Experimental cell research* **1965**, *39*, 190–196.
159. Hayflick, L.; Moorhead, P.S. The Serial Cultivation of Human Cell Strains'. *Experimental Cell Research* **1961**, *621*, 585–621.
160. Mercier, C.; Perek, N.; Delavenne, X. Is RPMI 2650 a Suitable In Vitro Nasal Model for Drug Transport Studies? *European Journal of Drug Metabolism and Pharmacokinetics* **2018**, *43*, 13–24, doi:10.1007/s13318-017-0426-x.
161. Na, K.; Lee, M.; Shin, H.; Chung, S. In Vitro Nasal Mucosa Gland-like Structure Formation on a Chip†. *Lab on a Chip* **2017**, doi:10.1039/C6LC01564F.
162. Mercier, C.; Hodin, S.; He, Z.; Perek, N.; Delavenne, X. Pharmacological Characterization of the RPMI 2650 Model as a Relevant Tool for Assessing the

References

- Permeability of Intranasal Drugs. *Molecular Pharmaceutics* **2018**, *15*, 2246–2256, doi:10.1021/acs.molpharmaceut.8b00087.
163. Mercier, C.; Jacqueroux, E.; He, Z.; Hodin, S.; Perek, N.; Boudard, D.; Delavenne, X.; Constant, S. European Journal of Pharmaceutics and Biopharmaceutics Pharmacological Characterization of the 3D MucilAir™ Nasal Model. **2019**, *139*, 186–196, doi:10.1016/j.ejpb.2019.04.002.
 164. Moll, R.; Krepler, R.; Franke, W.W. Complex Cytokeratin Polypeptide Patterns Observed in Certain Human Carcinomas. *Differentiation* **1982**, *23*, 256–269, doi:10.1111/j.1432-0436.1982.tb01291.x.
 165. Peter, H.G. Cell Culture Sheets to Study Nasal Peptide Metabolism the Human Nasal RPMI 2650 Cell Line Model, Zürich, Switzerland, 1996.
 166. Stratford, R.E.; Lee, V.H.L. Aminopeptidase Activity in Homogenates of Various Absorptive Mucosae in the Albino Rabbit: Implications in Peptide Delivery. *International Journal of Pharmaceutics* **1986**, *30*, 73–82, doi:10.1016/0378-5173(86)90137-7.
 167. Tchao, R. Epithelial Cell Interaction in Air-Liquid Interface Culture. *In vitro cellular & developmental biology : journal of the Tissue Culture Association* **1989**, *25*, 460–465.
 168. de Jong, P.M.; van Sterkenburg, M.A.; Hesseling, S.C.; Kempenaar, J.A.; Mulder, A.A.; Mommaas, A.M.; Dijkman, J.H.; Ponc, M. Ciliogenesis in Human Bronchial Epithelial Cells Cultured at the Air-Liquid Interface. *American journal of respiratory cell and molecular biology* **1994**, *10*, 271–277, doi:10.1165/ajrcmb.10.3.8117445.
 169. Lee, M.K.; Yoo, J.W.; Lin, H.; Kim, Y.S.; Kim, D.D.; Choi, Y.M.; Park, S.K.; Lee, C.H.; Roh, H.J. Air-Liquid Interface Culture of Serially Passaged Human Nasal Epithelial Cell Monolayer for in Vitro Drug Transport Studies. *Drug Delivery: Journal of Delivery and Targeting of Therapeutic Agents* **2005**, *12*, 305–311, doi:10.1080/10717540500177009.
 170. Pezzulo, A.A.; Starner, T.D.; Scheetz, T.E.; Traver, G.L.; Tilley, A.E.; Harvey, B.-G.; Crystal, R.G.; McCray, P.B.; Zabner, J. The Air-Liquid Interface and Use of Primary Cell Cultures Are Important to Recapitulate the Transcriptional Profile of in Vivo Airway Epithelia. *American Journal of Physiology-Lung Cellular and Molecular Physiology* **2010**, *300*, L25–L31, doi:10.1152/ajplung.00256.2010.
 171. Chen, S.; Einspanier, R.; Schoen, J. Transepithelial Electrical Resistance (TEER): A Functional Parameter to Monitor the Quality of Oviduct Epithelial Cells Cultured on Filter Supports. *Histochemistry and Cell Biology* **2015**, *144*, 509–515, doi:10.1007/s00418-015-1351-1.

References

172. van Itallie, C.M.; Anderson, J.M. Claudins and Epithelial Paracellular Transport. *Annual Review of Physiology* **2005**, *68*, 403–429, doi:10.1146/annurev.physiol.68.040104.131404.
173. Reinhold, P.; Grützenmacher, S.; Pabst, R.; Koch, R.; Schulz, R.; Kirschvink, N.; Oechtering, G.U.; Lippert, J.P.; Fey, K.; Rosenbruch, M. Die Oberen Atemwege Im Spezies Vergleich Betrachtungen Zur Anatomie Und Physiologie von Säugetiernasen. *Pneumologie* **2010**, *64*, 442–455.
174. Pabst, R. Mucosal Vaccination by the Intranasal Route. Nose-Associated Lymphoid Tissue (NALT)-Structure, Function and Species Differences. *Vaccine* **2015**, *33*, 4406–4413, doi:10.1016/j.vaccine.2015.07.022.
175. Bradley, P.; Bourne, F.J.; Brown, P.J. The Respiratory Tract Immune System in the Pig. *Vet. Pathol* **1976**, *13*, 90–97.
176. Krejci, J.; Nechvatalova, K.; Blahutkova, M.; Faldyna, M. The Respiratory Tract in Pigs and Its Immune System: A Review. *Veterinarni Medicina* **2013**, *58*, 206–220.
177. Erkekoglu, P.; Kocer Giray, B.; Başaran, N. *3R Principle and Alternative Toxicity Testing Methods*; 2011; Vol. 36;.
178. Würbel, H. More than 3Rs: The Importance of Scientific Validity for Harm-Benefit Analysis of Animal Research. *Lab Animal* **2017**, *46*, 164–166.
179. Au, E.; Roskams, A.J. Olfactory Ensheathing Cells of the Lamina Propria in Vivo and in Vitro. *Glia* **2003**, *41*, 224–236, doi:10.1002/glia.10160.
180. Freskgård, P.O.; Urich, E. Antibody Therapies in CNS Diseases. *Neuropharmacology* **2017**, *120*, 38–55, doi:10.1016/j.neuropharm.2016.03.014.
181. Horter, D.C.; Yoon, K.-J.; Zimmerman, J.J. A Review of Porcine Tonsils in Immunity and Disease. *Animal Health Research Reviews* **2003**, *4*, 143–155, doi:10.1079/AHRR200358.
182. Jeliaskova-Mecheva, V. v.; Bobilya, D.J. A Porcine Astrocyte/Endothelial Cell Co-Culture Model of the Blood-Brain Barrier. *Brain Research Protocols* **2003**, *12*, 91–98, doi:10.1016/j.brainresprot.2003.08.004.
183. Pozzoli, M.; Sonvico, F.; Ong, H.X.; Traini, D.; Bebawy, M.; Young, P.M. Optimization of RPMI 2650 Cells as a Model for Nasal Mucosa. **2014**, *2*, 739–742.
184. de Fraissinette, A.; Brun, R.; Felix, H.; Vonderscher, J.; Rummelt, A. Evaluation of the Human Cell Line RPMI 2650 as an in Vitro Nasal Model. *Rhinology* **1995**, *33*, 194–198.

References

185. Dolberg, A.M.; Reichl, S. Expression of P-Glycoprotein in Excised Human Nasal Mucosa and Optimized Models of RPMI 2650 Cells. *International Journal of Pharmaceutics* **2016**, *508*, 22–33, doi:10.1016/j.ijpharm.2016.05.010.
186. Kittel, Á.; Szabó-Révész, P.; Bocsik, A.; Deli, M.A.; Veszélka, S.; Puskás, L.G.; Kürti, L.; Ózsvári, B. Retinoic Acid and Hydrocortisone Strengthen the Barrier Function of Human RPMI 2650 Cells, a Model for Nasal Epithelial Permeability. *Cytotechnology* **2012**, *65*, 395–406, doi:10.1007/s10616-012-9493-7.
187. Reichl, S.; Becker, K. Cultivation of RPMI 2650 Cells as an In-Vitro Model for Human Transmucosal Nasal Drug Absorption Studies: Optimization of Selected Culture Conditions. *Journal of Pharmacy and Pharmacology* **2012**, *64*, 1621–1630, doi:10.1111/j.2042-7158.2012.01540.x.
188. Kreft, M.E.; Lasi, E.; Kristan, K. The Characterization of the Human Nasal Epithelial Cell Line RPMI 2650 Under Different Culture Conditions and Their Optimization for an Appropriate in Vitro Nasal Model. **2015**, 665–679, doi:10.1007/s11095-014-1494-0.
189. Sockolosky, J.T.; Szoka, F.C. The Neonatal Fc Receptor, FcRn, as a Target for Drug Delivery and Therapy. *Advanced Drug Delivery Reviews* **2016**, *91*, 109–124, doi:10.1016/j.addr.2015.02.005.
190. Uraih, L.C.; Maronpot, R.R. Normal Histology of the Nasal Cavity and Application of Special Techniques. *Environmental Health Perspectives* **1990**, *85*, 187–208, doi:10.2307/3430683.
191. Berger, J.T.; Voynow, J.A.; Peters, K.W.; Rose, M.C. Respiratory Carcinoma Cell Lines MUC Genes and Glycoconjugates. *American Journal of Respiratory Cell and Molecular Biology* **1999**, *20*, 500–510, doi:10.1165/ajrcmb.20.3.3383.
192. Kennel, C.; Gould, E.A.; Larson, E.D.; Salcedo, E.; Vickery, T.W.; Restrepo, D.; Ramakrishnan, V.R. Differential Expression of Mucins in Murine Olfactory Versus Respiratory Epithelium. *bioRxiv* **2019**, 1–32, doi:https://doi.org/10.1101/620757.
193. Solbu, T.T.; Holen, T. Aquaporin Pathways and Mucin Secretion of Bowman's Glands Might Protect the Olfactory Mucosa. *Chemical Senses* **2012**, *37*, 35–46, doi:10.1093/chemse/bjr063.
194. Hondo, T.; Kanaya, T.; Takakura, I.; Watanabe, H.; Takahashi, Y.; Nagasawa, Y.; Terada, S.; Ohwada, S.; Watanabe, K.; Kitazawa, H.; et al. Cytokeratin 18 Is a Specific Marker of Bovine Intestinal M Cell. *AJP: Gastrointestinal and Liver Physiology* **2011**, *300*, G442–G453, doi:10.1152/ajpgi.00345.2010.

References

195. Day, I.N.M.; Thompson, R.J. UCHL1 (PGP 9.5): Neuronal Biomarker and Ubiquitin System Protein. *Progress in Neurobiology* **2010**, *90*, 327–362, doi:10.1016/j.pneurobio.2009.10.020.
196. Lischka, K.; Ladel, S.; Luksch, H.; Weigel, S. Expression Patterns of Ion Channels and Structural Proteins in a Multimodal Cell Type of the Avian Optic Tectum. *Journal of Comparative Neurology* **2018**, *526*, 412–424, doi:10.1002/cne.24340.
197. Ding, X.; Xie, F. Olfactory Mucosa: Composition, Enzymatic Localization, and Metabolism. In *Handbook of Olfaction and Gustation*; Doty, R.L., Ed.; CRC Press: Boca Raton, 2003; pp. 63–91 ISBN 9780203911457.
198. Epithelium, O. Olfactory Epithelium. *Journal of Comparative Neurology* 2009, 113–118.
199. Genç, B.; Lagrimas, A.K.B.; Kuru, P.; Hess, R.; Tu, M.W.; Menichella, D.M.; Miller, R.J.; Paller, A.S.; Özdinler, P.H. Visualization of Sensory Neurons and Their Projections in an Upper Motor Neuron Reporter Line. *PLoS ONE* **2015**, *10*, 1–20, doi:10.1371/journal.pone.0132815.
200. Witt, M.; Bormann, K.; Gudziol, V.; Pehlke, K.; Barth, K.; Minovi, A.; H??hner, A.; Reichmann, H.; Hummel, T. Biopsies of Olfactory Epithelium in Patients with Parkinson's Disease. *Movement Disorders* **2009**, *24*, 906–914, doi:10.1002/mds.22464.
201. Wilson, P.O.; Barber, P.C.; Hamid, Q.A.; Power, B.F.; Dhillon, A.P.; Rode, J.; Day, I.N.; Thompson, R.J.; Polak, J.M. The Immunolocalization of Protein Gene Product 9.5 Using Rabbit Polyclonal and Mouse Monoclonal Antibodies. *British journal of experimental pathology* **1988**, *69*, 91–104.
202. Jimenez-Andrade, J.M.; Peters, C.M.; Mejia, N.A.; Ghilardi, J.R.; Kuskowski, M.A.; Mantyh, P.W. Sensory Neurons and Their Supporting Cells Located in the Trigeminal, Thoracic and Lumbar Ganglia Differentially Express Markers of Injury Following Intravenous Administration of Paclitaxel in the Rat. *Neuroscience Letters* **2006**, *405*, 62–67, doi:10.1016/j.neulet.2006.06.043.
203. Addicks, W.J.; Flynn, G.L.; Weiner, N. Validation of a Flow-through Diffusion Cell for Use in Transdermal Research. *Pharmaceutical research* **1987**, *4*, 337–341, doi:10.1023/a:1016405506028.
204. Lampen, A.; Christians, U.; Gonschior, A.K.; Bader, A.; Hackbarth, I.; von Engelhardt, W.; Sewing, K.F. Metabolism of the Macrolide Immunosuppressant, Tacrolimus, by the Pig Gut Mucosa in the Ussing Chamber. *British Journal of Pharmacology* **1996**, *117*, 1730–1734, doi:10.1111/j.1476-5381.1996.tb15346.x.

References

205. Bonferoni, M.C.; Rossi, S.; Ferrari, F.; Caramella, C. A Modified Franz Diffusion Cell for Simultaneous Assessment of Drug Release and Washability of Mucoadhesive Gels. *Pharmaceutical Development and Technology* **1999**, *4*, 45–53, doi:10.1080/10837459908984223.
206. Bechgaard, E.; Gizurarson, S.; Jørgensen, L.; Larsen, R. The Viability of Isolated Rabbit Nasal Mucosa in the Ussing Chamber, and the Permeability of Insulin across the Membrane. *International Journal of Pharmaceutics* **1992**, *87*, 125–132, doi:10.1016/0378-5173(92)90235-T.
207. Venter, J.P.; Muller, D.G.; du Plessis, J.; Goosen, C. A Comparative Study of an in Situ Adapted Diffusion Cell and an in Vitro Franz Diffusion Cell Method for Transdermal Absorption of Doxylamine. *European Journal of Pharmaceutical Sciences* **2001**, *13*, 169–177, doi:10.1016/S0928-0987(01)00110-5.
208. Piperno, G.; Fuller, M.T. Monoclonal Antibodies Specific for an Acetylated Form of Alpha-Tubulin Recognize the Antigen in Cilia and Flagella from a Variety of Organisms. *The Journal of cell biology* **1985**, *101*, 2085–2094.
209. Quinones, G.B.; Danowski, B.A.; Devaraj, A.; Singh, V.; Ligon, L.A. The Posttranslational Modification of Tubulin Undergoes a Switch from Detyrosination to Acetylation as Epithelial Cells Become Polarized. *Molecular biology of the cell* **2011**, *22*, 1045–1057, doi:10.1091/mbc.E10-06-0519.
210. Zholos, A. v.; Atherton-Watson, H.; Elborn, J.S.; Ennis, M.; de Courcey, F.; Danahay, H.L.; Canning, P.; Williams, M.T.S. Development of Primary Human Nasal Epithelial Cell Cultures for the Study of Cystic Fibrosis Pathophysiology. *American Journal of Physiology-Cell Physiology* **2012**, *303*, C1173–C1179, doi:10.1152/ajpcell.00384.2011.
211. Shatos, M.A.; Ríos, J.D.; Horikawa, Y.; Hodges, R.R.; Chang, E.L.; Bernardino, C.R.; Rubin, P.A.D.; Dartt, D.A. Isolation and Characterization of Cultured Human Conjunctival Goblet Cells. *Investigative Ophthalmology and Visual Science* **2003**, *44*, 2477–2486, doi:10.1167/iovs.02-0550.
212. Heijink, I.H.; Brandenburg, S.M.; Noordhoek, J.A.; Postma, D.S.; Slebos, D.J.; van Oosterhout, A.J.M. Characterisation of Cell Adhesion in Airway Epithelial Cell Types Using Electric Cell-Substrate Impedance Sensing. *European Respiratory Journal* **2010**, *35*, 894–903, doi:10.1183/09031936.00065809.
213. Graziadei, P.P.; Graziadei, G. a Neurogenesis and Neuron Regeneration in the Olfactory System of Mammals. I. Morphological Aspects of Differentiation and Structural

References

- Organization of the Olfactory Sensory Neurons. *J Neurocytol* **1979**, *8*, 1–18, doi:10.1007/BF01206454.
214. Werner, U.; Kissel, T. In-Vitro Cell Culture Models of the Nasal Epithelium: A Comparative Histochemical Investigation of Their Suitability for Drug Transport Studies. *Pharmaceutical Research* 1996, *13*, 978–988.
215. Kim, C.-H.; Song, K.S.; Kim, S.-S.; Kim, H.-U.; Seong, J.-K.; Yoon, J.-H. Expression of MUC5AC mRNA in the Goblet Cells of Human Nasal Mucosa. *The Laryngoscope* **2000**, *110*, 2110–2113, doi:10.1097/00005537-200012000-00026.
216. Aust, M.R.; Madsen, C.S.; Jennings, A.; Kasperbauer, J.L.; Gendler, S.J.; Ph, D. Mucin mRNA Expression in Normal and Vasomotor Inferior Turbinates. *American Journal of Rhinology II*, **1997**, *11*, 293–302, doi:https://doi.org/10.2500/105065897781446685.
217. Larochelle, R.; Martineau-doize, B. Distribution and Histochemical Characterization of Goblet Cells in the Nasal Cavity of Piglets. **1991**, *111*, 103–111.
218. Boucher, R.C.; Yankaskas, J.R.; Cotton, C.U.; Knowles, M.R.; Stutts, M.J. Cell Culture Approaches to the Investigation of Human Airway Ion Transport. *European journal of respiratory diseases. Supplement* **1987**, *153*, 59–67.
219. Engström, B.; Ekblom, A.; Hansson, P. The Olfactory and Respiratory Epithelium in Rhesus and Squirrel Monkeys Studied with Freeze- Fracture Technique The Olfactory and Respiratory Epithelium in Rhesus and Squirrel. **2009**, *6489*, doi:10.3109/00016488909125526.
220. Holcomb, J.D.; Graham, S.; Calof, A.L. Neuronal Homeostasis in Mammalian Olfactory Epithelium: A Review. *American Journal of Rhinology* **1996**, *10*, 125–134.
221. Gouadon, E.; Meunier, N.; Grebert, D.; Durieux, D.; Baly, C.; Salesse, R.; Caillol, M.; Congar, P. Endothelin Evokes Distinct Calcium Transients in Neuronal and Non-Neuronal Cells of Rat Olfactory Mucosa Primary Cultures. *Neuroscience* **2010**, *165*, 584–600, doi:10.1016/j.neuroscience.2009.10.046.
222. Yoo, J.-W.; Kim, Y.-S.; Lee, S.-H.; Lee, M.-K.; Roh, H.-J.; Jhun, B.-H.; Lee, C.-H.; Kim, D.-D. Serially Passaged Human Nasal Epithelial Cell Monolayer for in Vitro Drug Transport Studies. *Pharmaceutical research* **2003**, *20*, 1690–1696.
223. Kim, N.; Hee, D.; Suh, M.; Ho, J.; Oh, S.; Kyun, M. Effect of Lipopolysaccharide on Diesel Exhaust Particle-Induced Junctional Dysfunction in Primary Human Nasal Epithelial Cells *. **2019**, *248*, 736–742, doi:10.1016/j.envpol.2019.02.082.

References

224. Röhm, M.; Carle, S.; Maigler, F.; Flamm, J.; Kramer, V.; Mavoungou, C.; Schmid, O.; Schindowski, K. A Comprehensive Screening Platform for Aerosolizable Protein Formulations for Intranasal and Pulmonary Drug Delivery. *International Journal of Pharmaceutics* **2017**, *49*, 1–42, doi:10.1016/j.ijpharm.2017.09.027.
225. Spiekermann, G.M.; Finn, P.W.; Ward, E.S.; Dumont, J.; Dickinson, B.L.; Blumberg, R.S.; Lencer, W.I. Receptor-Mediated Immunoglobulin G Transport Across Mucosal Barriers in Adult Life. *The Journal of Experimental Medicine* **2002**, *196*, 303–310, doi:10.1084/jem.20020400.
226. Pyzik, M.; Rath, T.; Lencer, W.I.; Baker, K.; Blumberg, R.S. FcRn: The Architect Behind the Immune and Nonimmune Functions of IgG and Albumin. *The Journal of Immunology* **2015**, *194*, 4595–4603.
227. Cianga, C.; Cianga, P.; Plamadeala, P.; Amalinei, C. Nonclassical Major Histocompatibility Complex I-like Fc Neonatal Receptor (FcRn) Expression in Neonatal Human Tissues. *Human Immunology* **2011**, *72*, 1176–1187, doi:10.1016/j.humimm.2011.08.020.
228. Broadwell, R.D.; Balin, B.J. Endocytic and Exocytic Pathways of the Neuronal Secretory Process and Trans Synaptic Transfer of Wheat Germ Agglutinin-Horseradish Peroxidase in Vivo. *The Journal of Comparative Neurology* **1985**, *242*, 632–650, doi:10.1002/cne.902420410.
229. Zhang, Y.; Pardridge, W.M. Mediated Efflux of IgG Molecules from Brain to Blood across the Blood-Brain Barrier. *Journal of neuroimmunology* **2001**, *114*, 168–172, doi:10.1016/s0165-5728(01)00242-9.
230. Deane, R.; Sagare, A.; Hamm, K.; Parisi, M.; LaRue, B.; Guo, H.; Wu, Z.; Holtzman, D.M.; Zlovic, B. v. IgG-Assisted Age-Dependent Clearance of Alzheimer's Amyloid Peptide by the Blood-Brain Barrier Neonatal Fc Receptor. *Journal of Neuroscience* **2005**, *25*, 11495–11503, doi:10.1523/JNEUROSCI.3697-05.2005.
231. Zlokovic, B. v.; Skundric, D.S.; Segal, M.B.; Lipovac, M.N.; Mackic, J.B.; Davson, H. A Saturable Mechanism for Transport of Immunoglobulin G across the Blood-Brain Barrier of the Guinea Pig. *Experimental neurology* **1990**, *107*, 263–270, doi:10.1016/0014-4886(90)90144-h.
232. Abuqayyas, L.; Balthasar, J.P. Investigation of the Role of FcγR and FcRn in MAb Distribution to the Brain. *Molecular Pharmaceutics* **2013**, *10*, 1505–1513, doi:10.1021/mp300214k.

References

233. Brandtzaeg, P.; Baekkevold, E.S.; Farstad, I.N.; Jahnsen, F.L.; Johansen, F.-E.; Nilsen, E.M.; Yamanaka, T. Regional Specialization in the Mucosal Immune System: What Happens in the Microcompartments? *Immunology Today* **1999**, *20*, 141–151.
234. Jahnsen, F.L.; Gran, E.; Haye, R.; Brandtzaeg, P. Human Nasal Mucosa Contains Antigen-Presenting Cells of Strikingly Different Functional Phenotypes. *American Journal of Respiratory Cell and Molecular Biology* **2004**, *30*, 31–37, doi:10.1165/rcmb.2002-0230OC.
235. Yoshida, M.; Kobayashi, K.; Kuo, T.T.; Bry, L.; Glickman, J.N.; Claypool, S.M.; Kaser, A.; Nagaishi, T.; Higgins, D.E.; Mizoguchi, E.; et al. Neonatal Fc Receptor for IgG Regulates Mucosal Immune Responses to Luminal Bacteria. *Journal of Clinical Investigation* **2006**, *116*, 2142–2151, doi:10.1172/JCI27821.
236. Iwasaki, A. Mucosal Dendritic Cells. *Annual Review of Immunology* **2007**, *25*, 381–418, doi:10.1146/annurev.immunol.25.022106.141634.
237. Lugton, I. Mucosa-Associated Lymphoid Tissues as Sites for Uptake, Carriage and Excretion of Tubercle Bacilli and Other Pathogenic Mycobacteria. *Immunology and cell biology* **1999**, *77*, 364–372, doi:10.1046/j.1440-1711.1999.00836.x.
238. Akilesh, S.; Christianson, G.J.; Roopenian, Derry.C.; Shaw, A.S. Neonatal FcR Expression in Bone Marrow-Derived Cells Functions to Protect Serum IgG from Catabolism. *The Journal of Immunology* **2007**, *179*, 4580–4588, doi:10.4049/jimmunol.179.7.4580.
239. Stirling, C.M.A.; Charleston, B.; Takamatsu, H.; Claypool, S.; Lencer, W.; Blumberg, R.S.; Wileman, T.E. Characterization of the Porcine Neonatal Fc Receptor - Potential Use for Trans-Epithelial Protein Delivery. *Immunology* **2005**, *114*, 542–553, doi:10.1111/j.1365-2567.2004.02121.x.
240. Dickinson, B.L.; Blumberg, R.S.; Wayne, I.; Invest, J.C.; Dickinson, B.L.; Badizadegan, K.; Wu, Z.; Ahouse, J.C.; Zhu, X.; Simister, N.E.; et al. Bidirectional FcRn-Dependent IgG Transport in a Polarized Human Intestinal Epithelial Cell Line Find the Latest Version : Bidirectional FcRn-Dependent IgG Transport in a Polarized Human Intestinal Epithelial Cell Line. **1999**, *104*, 903–911.
241. Neuber, T.; Frese, K.; Jaehrling, J.; Jäger, S.; Daubert, D.; Felderer, K.; Linnemann, M.; Höhne, A.; Kaden, S.; Kölln, J.; et al. Characterization and Screening of IgG Binding to the Neonatal Fc Receptor. *mAbs* **2014**, *6*, 928–942, doi:10.4161/mabs.28744.
242. Kacskovics, I. Fc Receptors in Livestock Species. *Veterinary Immunology and Immunopathology* **2004**, *102*, 351–362, doi:10.1016/j.vetimm.2004.06.008.

References

243. Zhang, Y.; Pardridge, W.M. Mediated Efflux of IgG Molecules from Brain to Blood across the Blood–Brain Barrier. *Journal of Neuroimmunology* **2001**, *114*, 168–172, doi:10.1016/S0165-5728(01)00242-9.
244. England, R.J.; Homer, J.J.; Knight, L.C.; Ell, S.R. Nasal PH Measurement: A Reliable and Repeatable Parameter. *Clinical otolaryngology and allied sciences* **1999**, *24*, 67–68, doi:10.1046/j.1365-2273.1999.00223.x.
245. Hornby, P.J.; Cooper, P.R.; Kliwinski, C.; Ragwan, E.; Mabus, J.R.; Harman, B.; Thompson, S.; Kauffman, A.L.; Yan, Z.; Tam, S.H.; et al. Human and Non-Human Primate Intestinal FcRn Expression and Immunoglobulin G Transcytosis. *Pharmaceutical Research* **2014**, *31*, 908–922, doi:10.1007/s11095-013-1212-3.
246. Claypool, S.M.; Dickinson, B.L.; Wagner, J.S.; Johansen, F.; Venu, N.; Borawski, J.A.; Lencer, W.I.; Blumberg, R.S. Bidirectional Transepithelial IgG Transport by a Strongly Polarized Basolateral Membrane Fc γ -Receptor α . **2004**, *15*, 1746–1759, doi:10.1091/mbc.E03.
247. Saji, F. Dynamics of Immunoglobulins at the Feto-Maternal Interface. *Reviews of Reproduction* **2004**, *4*, 81–89, doi:10.1530/revreprod/4.2.81.
248. Mohanty, S.; Kim, J.; Ganesan, L.P.; Phillips, G.S.; Hua, K.; Jarjoura, D.; Hayton, W.L.; Robinson, J.M.; Anderson, C.L. IgG Is Transported across the Mouse Yolk Sac Independently of Fc γ R1b. *Journal of Reproductive Immunology* **2010**, *84*, 133–144, doi:10.1016/j.jri.2009.10.008.
249. Stapleton, N.M.; Andersen, J.T.; Stemerding, A.M.; Bjarnarson, S.P.; Verheul, R.C.; Gerritsen, J.; Zhao, Y.; Kleijer, M.; Sandlie, I.; de Haas, M.; et al. Competition for FcRn-Mediated Transport Gives Rise to Short Half-Life of Human IgG3 and Offers Therapeutic Potential. *Nature Communications* **2011**, *2*, 599, doi:10.1038/ncomms1608.
250. Malek, A.; Sager, R.; Zakher, A.; Schneider, H. Transport of Immunoglobulin G and Its Subclasses across the in Vitro-Perfused Human Placenta. *American Journal of Obstetrics and Gynecology* **1995**, *173*, 760–767, doi:10.1016/0002-9378(95)90336-4.
251. Bruhns, P.; Iannascoli, B.; England, P.; Mancardi, D.A.; Fernandez, N.; Jorieux, S.; Daéron, M. Specificity and Affinity of Human Fc γ Receptors and Their Polymorphic Variants for Human IgG Subclasses. *Blood* **2009**, *113*, 3716–3725, doi:10.1182/blood-2008-09-179754.
252. Stewart, R.; Hammond, S.A.; Oberst, M.; Wilkinson, R.W. The Role of Fc Gamma Receptors in the Activity of Immunomodulatory Antibodies for Cancer. *Journal for ImmunoTherapy of Cancer* **2014**, *2*, doi:10.1186/s40425-014-0029-x.

References

253. Andoh, T.; Kuraishi, Y. Direct Action of Immunoglobulin G on Primary Sensory Neurons through Fc Gamma Receptor I. *The FASEB journal : official publication of the Federation of American Societies for Experimental Biology* **2004**, *18*, 182–184, doi:10.1096/fj.02-1169fje.
254. Ferrara, C.; Stuart, F.; Sondermann, P.; Brünker, P.; Umaña, P. The Carbohydrate at FcγRIIIa Asn-162: An Element Required for High Affinity Binding to Non-Fucosylated IgG Glycoforms. *Journal of Biological Chemistry* **2006**, *281*, 5032–5036, doi:10.1074/jbc.M510171200.
255. Sazinsky, S.L.; Ott, R.G.; Silver, N.W.; Tidor, B.; Ravetch, J. v; Dane Wittrup, K. *Aglycosylated Immunoglobulin G 1 Variants Productively Engage Activating Fc Receptors*; 2008;
256. Gitlin, D.; Koch, C. On the Mechanisms of Maternofetal Transfer of Human Albumin and Gamma-G Globulin in the Mouse. *The Journal of clinical investigation* **1968**, *47*, 1204–1209, doi:10.1172/JCI105809.
257. Mackness, B.C.; Jaworski, J.A.; Boudanova, E.; Park, A.; Valente, D.; Mauriac, C.; Pasquier, O.; Schmidt, T.; Kabiri, M.; Kandira, A.; et al. Antibody Fc Engineering for Enhanced Neonatal Fc Receptor Binding and Prolonged Circulation Half-Life. *mAbs* **2019**, *11*, 1276–1288, doi:10.1080/19420862.2019.1633883.
258. Collin, M.; Björck, L. Toward Clinical Use of the IgG Specific Enzymes IdeS and EndoS against Antibody-Mediated Diseases. *Methods in Molecular Biology* **2017**, *1535*, 357 pp., doi:10.1007/978-1-4939-6673-8_23.
259. Collin, M.; Olsén, A. Effect of SpeB and EndoS from Streptococcus Pyogenes on Human Immunoglobulins. *Infection and Immunity* **2001**, *69*, 7187–7189, doi:10.1128/IAI.69.11.7187-7189.2001.
260. Jacobsen, B.; Hill, M.; Reynaud, L.; Hey, A.; Barrow, P. FcRn Expression on Placenta and Fetal Jejunum during Early, Mid-, and Late Gestation in Minipigs. *Toxicologic Pathology* **2016**, *44*, 486–491, doi:10.1177/0192623315610821.
261. Kang, H.; Yan, M.; Yu, Q.; Yang, Q. Characteristics of Nasal-Associated Lymphoid Tissue (NALT) and Nasal Absorption Capacity in Chicken. *PLoS ONE* **2013**, *8*, doi:10.1371/journal.pone.0084097.
262. Lux, A.; Yu, X.; Scanlan, C.N.; Nimmerjahn, F. Impact of Immune Complex Size and Glycosylation on IgG Binding to Human FcγRs. *The Journal of Immunology* **2013**, *190*, 4315–4323, doi:10.4049/jimmunol.1200501.

References

263. Stapleton, N.M.; Armstrong-Fisher, S.S.; Andersen, J.T.; van der Schoot, C.E.; Porter, C.; Page, K.R.; Falconer, D.; de Haas, M.; Williamson, L.M.; Clark, M.R.; et al. Human IgG Lacking Effector Functions Demonstrate Lower FcRn-Binding and Reduced Transplacental Transport. *Molecular Immunology* **2018**, *95*, 1–9, doi:10.1016/j.molimm.2018.01.006.
264. Bakchoul, T.; Walek, K.; Krautwurst, A.; Rummel, M.; Bein, G.; Santoso, S.; Sachs, U.J. Glycosylation of Autoantibodies: Insights into the Mechanisms of Immune Thrombocytopenia. *Thrombosis and Haemostasis* **2013**, *110*, 1259–1266, doi:10.1160/TH13-04-0294.
265. Malek, A. Ex Vivo Human Placenta Models: Transport of Immunoglobulin G and Its Subclasses. **2003**, *21*, 3362–3364, doi:10.1016/S0264-410X(03)00333-5.
266. Stapleton, N.M.; Brinkhaus, M.; Armour, K.L.; Bentlage, A.E.H.; de Taeye, S.W.; Temming, A.R.; Mok, J.Y.; Brasser, G.; Maas, M.; van Esch, W.J.E.; et al. Reduced FcRn-Mediated Transcytosis of IgG2 Due to a Missing Glycine in Its Lower Hinge. *Scientific Reports* **2019**, *9*, 1–10, doi:10.1038/s41598-019-40731-2.
267. Weflen, A.W.; Baier, N.; Tang, Q.J.; van den Hof, M.; Blumberg, R.S.; Lencer, W.I.; Massol, R.H. Multivalent Immune Complexes Divert FcRn to Lysosomes by Exclusion from Recycling Sorting Tubules. *Molecular Biology of the Cell* **2013**, *24*, 2398–2405, doi:10.1091/mbc.E13-04-0174.
268. Yoshida, M.; Claypool, S.M.; Wagner, J.S.; Mizoguchi, E.; Mizoguchi, A.; Roopenian, D.C.; Lencer, W.I.; Blumberg, R.S. Human Neonatal Fc Receptor Mediates Transport of IgG into Luminal Secretions for Delivery of Antigens to Mucosal Dendritic Cells. *Immunity* **2004**, *20*, 769–783, doi:10.1016/j.immuni.2004.05.007.
269. Newton, E.E. Characterization of Basolateral-Targeting Signals in the Neonatal Fc Receptor. *Journal of Cell Science* **2005**, *118*, 2461–2469, doi:10.1242/jcs.02367.
270. McCarthy, K.M.; Lam, M.; Subramanian, L.; Shakya, R.; Wu, Z.; Newton, E.E.; Simister, N.E. Effects of Mutations in Potential Phosphorylation Sites on Transcytosis of FcRn. *Journal of Cell Science* **2001**, *114*, 1591–1598.
271. He, W.; Ladinsky, M.S.; Huey-tubman, K.E.; Jensen, G.J.; McIntosh, R.; Björkman, P.J. NIH Public Access. **2009**, *455*, 542–546, doi:10.1038/nature07255.FcRn-mediated.
272. Kuo, T.T.; de Muinck, E.J.; Claypool, S.M.; Yoshida, M.; Nagaishi, T.; Aveson, V.G.; Lencer, W.I.; Blumberg, R.S. N-Glycan Moieties in Neonatal Fc Receptor Determine Steady-State Membrane Distribution and Directional Transport of IgG. *Journal of Biological Chemistry* **2009**, *284*, 8292–8300, doi:10.1074/jbc.M805877200.

References

273. Wu, Z.; Simister, N.E. Tryptophan- and Dileucine-Based Endocytosis Signals in the Neonatal Fc Receptor. *Journal of Biological Chemistry* **2001**, *276*, 5240–5247, doi:10.1074/jbc.M006684200.

7. Appendix

7.1 Publications

Simone Ladel, Johannes Flamm, Arghavan Soleimani Zadeh, Dorothea Filzwieser, Julia Christina Walter, Patrick Schlossbauer, Ralf Kinscherf, Katharina Lischka, Harald Luksch, and Katharina Schindowski. 2018. Allogenic Fc domain-facilitated uptake of IgG in nasal *Lamina propria*: Friend or foe for intranasal CNS delivery? *Pharmaceutics* 10, 3: 1–23. <https://doi.org/10.3390/pharmaceutics10030107>

© 2018 by the authors. Licensee MDPI, Basel, Switzerland. This article is an open access article distributed under the terms and conditions of the Creative Commons Attribution 4.0 International (CC BY 4.0) license (<http://creativecommons.org/licenses/by/4.0/>).



Article

Allogenic Fc Domain-Facilitated Uptake of IgG in Nasal *Lamina Propria*: Friend or Foe for Intranasal CNS Delivery?

Simone Ladel ^{1,2}, Johannes Flamm ^{1,2}, Arghavan Soleimani Zadeh ^{1,2,3}, Dorothea Filzwieser ¹, Julia-Christina Walter ^{1,2}, Patrick Schlossbauer ¹, Ralf Kinscherf ⁴, Katharina Lischka ⁵ , Harald Luksch ⁵ and Katharina Schindowski ^{1,*}

¹ Institute of Applied Biotechnology, University of Applied Science Biberach, 88400 Biberach, Germany; ladel@hochschule-bc.de (S.L.); flamm@hochschule-bc.de (J.F.); soleimanizadeh@hochschule-bc.de or arghavan.soleimani@uni-ulm.de (A.S.Z.); dorothea.filzwieser@hochschule-bc.de (D.F.); juliawalter1993@yahoo.de or julia-christina.walter@uni-ulm.de (J.-C.W.); patrick.schlossbauer@hochschule-bc.de (P.S.)

² Faculty for Natural Sciences, University of Ulm, 89081 Ulm, Germany

³ Faculty of Medicine, Graduate School 'Molecular Medicine', University of Ulm, 89081 Ulm, Germany

⁴ Department of Medical Cell Biology, Institute for Anatomy and Cell Biology, Philipps-University Marburg, 35032 Marburg, Germany; Ralf.Kinscherf@uni-marburg.de

⁵ Chair of Zoology, Technical University of Munich, 85354 Freising-Weihenstephan, Germany; katharina.lischka@tum.de (K.L.); harald.luksch@wzw.tum.de (H.L.)

* Correspondence: zimmermann@hochschule-bc.de; Tel.: +49-7351-582-498

Received: 24 June 2018; Accepted: 20 July 2018; Published: 26 July 2018



Abstract: Background: The use of therapeutic antibodies for the treatment of neurological diseases is of increasing interest. Nose-to-brain drug delivery is one strategy to bypass the blood brain barrier. The neonatal Fc receptor (FcRn) plays an important role in transepithelial transcytosis of immunoglobulin G (IgG). Recently, the presence of the FcRn was observed in nasal respiratory mucosa. The aim of the present study was to determine the presence of functional FcRn in olfactory mucosa and to evaluate its role in drug delivery. Methods: Immunoreactivity and messenger RNA (mRNA) expression of FcRn was determined in ex vivo porcine olfactory mucosa. Uptake of IgG was performed in a side-by-side cell and analysed by immunofluorescence. Results: FcRn was found in epithelial and basal cells of the olfactory epithelium as well as in glands, cavernous bodies and blood vessels. Allogenic porcine IgGs were found time-dependently in the *lamina propria* and along axonal bundles, while only small amounts of xenogenic human IgGs were detected. Interestingly, lymphoid follicles were spared from allogenic IgGs. Conclusion: Fc-mediated transport of IgG across the nasal epithelial barrier may have significant potential for intranasal delivery, but the relevance of immune interaction in lymphoid follicles must be clarified to avoid immunogenicity.

Keywords: olfactory epithelium; respiratory epithelium; nasal mucosa; NALT; lymphoid follicles; neuronal bundles; antibody; permeation; nose to brain; drug delivery

1. Introduction

Biopharmaceuticals are of increasing importance in the therapy of various diseases. Since the development of the hybridoma technology by Köhler and Milstein, some of the most important biopharmaceutical molecules are antibodies, in particular immunoglobulin G (IgGs) [1,2].

Despite their great therapeutic potential, the tissue penetration of large molecules like IgGs is a critical aspect for the development of therapies and administration routes, in particular for

neurological disorders. The blood-brain barrier (BBB) is a highly selective barrier and severely limits the use of antibodies for the therapy of diseases of the central nervous system (CNS). The BBB consists of cerebral vascular endothelial cells that are firmly connected by tight junctions and surrounded by astroglia expressing soluble factors responsible for the formation of tight junctions [3–5].

One strategy to bypass the BBB is to deliver drugs to the CNS by intranasal drug delivery. In humans intranasally administered insulin was already shown to have a positive effect on memory and metabolic effects via the hypothalamic-pituitary-axis [6–11]. Advantages of the intranasal route are the minimally-invasive administration, reduced systemic side effects due to direct CNS targeting, and improved patient compliance compared to intrathecal delivery [6,7]. As the feasibility of nose to brain (N2B) drug delivery was already shown for sumatriptan, oxytocin, insulin, and some other drugs, it is of particular interest to investigate whether the N2B route is also suitable for proteins with a higher molecular weight such as antibodies [7,12–14].

IgG antibodies contain two different kinds of polypeptide chains: the heavy chain and light chain. Each IgG is composed of two heavy chains that are linked via disulfide bond as well as two light chains that are respectively connected by disulfide bonds. The light chain consists of one variable domain (V_L) and one constant domain (C_L). The heavy chain is structured into four domains: three constant domains (C_H1 , C_H2 , C_H3) and one variable domain (V_H) [15,16].

In endothelial cells and monocytes but also in epithelial cells, a specialized IgG transporter, the neonatal Fc receptor (FcRn) binds specifically to the C_H3 and parts of the C_H2 regions of IgGs (Figure 1C). The FcRn is composed of a heterodimer of major immunohistocompatibility (MHC) class I-like heavy chain and a microglobulin β light chain. It binds the Fc γ domain preferentially at pH < 6.5 but hardly at physiological pH [17–19]. FcRn immunoreactivity was previously demonstrated by Heidl et al. in the human nasal respiratory mucosa of the inferior turbinate, in particular in epithelial, basal, endothelial and gland cells. However, the presence of FcRn in the *regio olfactoria* of higher mammals, a region that is highly implicated in N2B drug delivery, has yet not been described [19–21].

As demonstrated for lung and gut, FcRn can facilitate IgG transport from the apical to the basolateral side in polarized cells and vice versa [22,23]. As indicated in Figure 1B,C, IgGs are taken up by pinocytosis, but also specific uptake via FcRn is discussed [24–26]. In the acidic environment of the early endosome, the Fc γ domain binds to the FcRn. During exocytosis, after recycling or transcytosis, the pH shift at the extracellular environment to physiological pH (pH 7.4) causes a release of the IgG molecule [27].

Ober et al. showed cross-species transport of human IgG by the porcine FcRn, making porcine tissue a promising model organism to test ex vivo epithelial transport of IgGs [28]. In addition to the molecular similarities, the cellular composition of the respiratory mucosa was also shown to be comparable between humans and pigs [29,30]. Thus, it is reasonable to assume that there are strong similarities between human and porcine olfactory mucosa. The olfactory mucosa in general is composed of a pseudostratified epithelium containing polarized epithelial cells, olfactory neurons, basal cells (progenitor cells), and supporting cells. Beneath the basal cell layer, there is a thick layer of connective tissue with neuronal bundles, Bowman's glands, cavernous bodies and smaller blood capillaries (Figure 1A) [31–33]. This layer is called the *lamina propria*. In addition, Debertin and colleagues investigated the nasal immune system in newborn children. They found B and T lymphocytes arranged in so-called lymphoid follicles similar to the Peyer's patches in the gut [34].

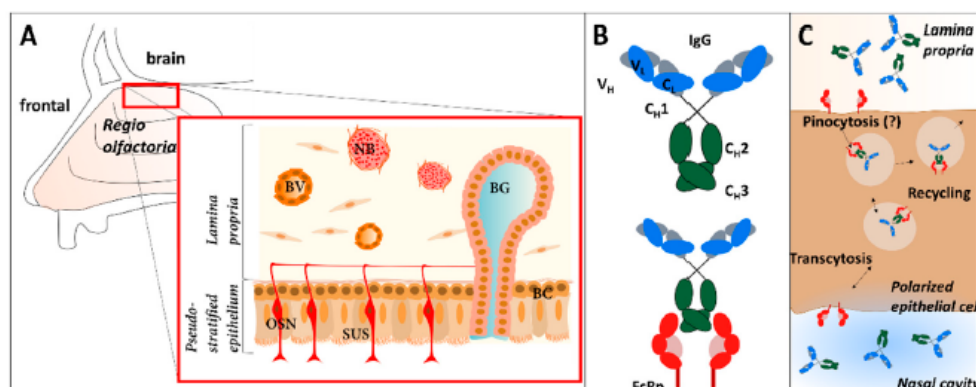


Figure 1. Transcytosis and recycling of IgGs in the nasal mucosa mediated by the neonatal Fc receptor (FcRn) and structural overview of the mucosa composition. (A) The olfactory mucosa in mammals is composed of a pseudostratified epithelium that contains olfactory sensory neurons (OSN), supporting cells (SUS) and basal cells. The olfactory epithelium is lined by a thick connective tissue, called the *lamina propria*, containing Bowman's gland (BG), blood vessels (BV), and neuronal bundles (NB). (B) Structure of immunoglobulin G (IgG) and binding to FcRn. (C) Immunoglobulin G (IgG) is incorporated into polarized cells of the epithelium via pinocytosis. The FcRn binds to the Fc-domain of the antibody in the slightly acidic environment of the early endosome and mediates transcytosis to the basolateral side or recycling of the IgG to the apical side. Transcytosis is shown here from apical (nasal cavity) to basolateral, but the reverse direction was also reported.

The neuronal bundles are accumulated axons of the olfactory receptor neurons projecting to the olfactory bulb, a brain region specialized for olfaction [35]. Balin et al. demonstrated that horseradish peroxidase (HRP), administered to the olfactory mucosa, was detectable in the olfactory bulb of rodents and monkeys within 45 to 90 min [36]. Therefore, it could be assumed that axons of the olfactory neurons present a pathway into the brain for therapeutic protein drugs such as antibodies [37].

In a previous study, the permeation of the human therapeutic IgG Avastin® (bevacizumab) through two subtypes of porcine mucosa from the septum and the snout cavity was shown, and a link between FcRn and the IgG's pathway through the epithelium was suspected [38].

The aim of the present *ex vivo* study was to evaluate the presence of FcRn in porcine olfactory mucosa. Nasal porcine mucosa explants were excised from the dorsal part of the *concha nasalis dorsalis* (superior turbinate in humans) covered with olfactory mucosa and from the *concha nasalis ventralis* (inferior turbinate in humans) that is covered with respiratory mucosa. Furthermore, the function of FcRn was evaluated by determining the qualitative transport of allogenic porcine IgGs in comparison to a xenogenic human IgG (a biosimilar of bevacizumab). These experiments should also clarify whether xenogenic human IgGs are transported via the porcine FcRn. Using immunofluorescence, qualitative uptake and the fate of IgGs in the *lamina propria* was investigated, in particular in neuronal bundles and in lymphoid follicles.

2. Material and Methods

2.1. Antibodies

According to Table 1 the following antibodies were used for uptake and distribution studies as well as for immunofluorescence and Western blotting.

Table 1. List of antibodies used in this study.

Antibody	Antigen	Immunogen	Host	Source, Cat. #
IgG from porcine serum	-	-	pig	Sigma-Aldrich, Germany, Cat.#I4381
bevacizumab biosimilar	VEGF	VEGF-165 isoform	humanized antibody	In-house
Anti-porcine FcRn	cytoplasmic tail of the porcine FcRn	Peptide: CPWISFHGDDVGGALLP TPDLDTTMLNLRI	rabbit	Pirbright Institute, UK [17]
Anti-Neurofilament 200	neurofilament heavy polypeptide	IgG fraction of antiserum	rabbit	Sigma-Aldrich, Germany, Cat. # N4142
Anti-CD3 (SP7)	intracytoplasmic portion of the CD3 antigen	synthetic peptide: KAKAKPVTRGAGA	rabbit	NovusBio, Germany, Cat.# NB600-1441
Anti-MS4A1/CD20 (MEM-97)	CD20 (Bp35)	Raji human Burkitt's lymphoma cell line (NM_021950.3)	mouse	NovusBio, Germany, Cat.# NBP1-44634
Anti-CD14 Monoclonal (TüK4)	CD14	not specified	mouse	Thermo Fisher Scientific, Germany, Cat.# MA5-16956
Anti-β Actin (AC-15)	β Actin	not specified	mouse	Sigma Aldrich, Germany, Cat.# A5441
Anti-murine IgG-Alexa Fluor®488	whole molecule mouse IgG	not specified	goat	Jackson Immuno Research Europe Ltd., UK; Cat.#115-545-003
Anti-rabbit IgG-Rhodamine Red™-X	whole molecule rabbit IgG	not specified	donkey	Jackson Immuno Research Europe Ltd., UK, Cat.#711-295-152
Anti-swine IgG-Rhodamine Red™-X	whole molecule porcine IgG	not specified	goat	Jackson Immuno Research Europe Ltd., UK, Cat.#114-295-003
Anti-human IgG-FITC (Fluorescein isothiocyanat)	whole molecule human IgG	not specified	goat	Sigma-Aldrich, Germany, Cat.# F3512
Anti-rabbit IgG-HRP	whole molecule rabbit IgG	not specified	goat	Jackson Immuno Research Europe Ltd., UK, Cat.#111-035-003
Anti-murine IgG-HRP	whole molecule mouse IgG	not specified	goat	Sigma Aldrich, Germany, Cat.# AP5278

2.2. Tissue Preparation

The mucosa explants were collected from the nasal cavity of slaughterhouse pigs aged 4 to 6 months old from a local butcher. The tissue specimens were excised from the dorsal part of the *concha nasalis dorsalis* (olfactory epithelium) and the middle part of the *concha nasalis ventralis* (respiratory epithelium) according to [39]. In detail, approximately 2 cm² of the mucosa were dissected with a scalpel and removed gently from the cartilage using a blunt spatula to avoid damage to the mucosa explants. The post mortem delay of the porcine tissue was below 2 h. For morphological comparison human *regio olfactoria* was excised from anatomical donations fixed in 4% paraformaldehyde/96% ethanol for anatomical teaching courses. The human specimens were used including cartilages as the tissue was too fragile to remove the mucosa without damage. The different qualities observed in the sections from human and porcine tissue are due to these different tissue processing procedures.

2.3. Reverse Transcription and Polymerase Chain Reaction (PCR)

To isolate total RNA from the specimens, TRIzol (Thermo Fisher Scientific, Dreieich, Germany) was used according to the manufacturer's instructions. Tissue sections of 200 mg were used per library and the RNA was stored at -80°C . For reverse transcription to complementary DNA (cDNA), 1 μg of total RNA was mixed with 2U RNase inhibitor (InvitrogenTM, USA) and added up to 10 μL with ultra-pure distilled RNase-free water (InvitrogenTM, USA). The RNA secondary structure was denatured by heating to 65°C for 15 min. Per reaction, 100 pM oligo-dT₁₅ primer, 20 mM deoxynucleotides (dNTPs), and 400 U murine leukemia virus (MLV) reverse transcriptase were diluted in M-MLV buffer containing ultra-pure distilled RNase-free water and were added to the denatured RNA. The mix was incubated at 37°C for 1 h and then inactivated for 10 min at 65°C . The cDNA templates were stored at -20°C until use.

2 μg cDNA, 1 μM of the appropriate primer pairs (see Table 2; Thermo Fisher Scientific, Dreieich, Germany), 25 mM MgCl_2 (Thermo Fisher Scientific, Dreieich, Germany), 2.5 mM dNTP Mix (Thermo Fisher Scientific, Dreieich, Germany), and 0.5 U/ μL Taq polymerase (InvitrogenTM, USA) were diluted in Taq-PCR buffer (Thermo Fisher Scientific, Dreieich, Germany) containing RNase-free water (InvitrogenTM, USA) to amplify the DNA target sequences by PCR.

Table 2. Sequences of forward and reverse primer for reverse transcriptase-PCR (RT-PCR) of the targets FcRn und β -actin.

Targets	Forward Primer (5'-3')	Reverse Primer (5'-3')
FcRn	CTAACAGTCAAGAGCGGCGA	AGATTCCACCATGCCAGCAA
β -actin	GACACCAGGGCGTGATGG	GCAGCTCGTAGCTCTTCTCC

The PCR was performed with initial denaturation for 30 s at 95°C , 40 cycles with denaturation at 95°C for 30 s, annealing at 60°C for 30 s, elongation at 72°C for 60 s, and a final elongation at 72°C for 10 min. The amplicons were analysed by agarose gel electrophoresis.

2.4. Western Blot

The tissue explants were homogenized, chilled RIPA (radioimmunoprecipitation) cell lysis buffer (10 mM Tris-Cl, pH8.0; 1 mM EDTA, 0.5 mM EGTA, 1% Triton X-100, 0.1% sodium deoxycholate, 0.1% SDS (sodium dodecyl sulfate), 140 mM NaCl, and protease inhibitor mix (Thermo Fisher Scientific, Dreieich, Germany)) were added, and the samples were agitated for complete cell lysis.

Equal volumes of homogenized tissue were loaded, separated in a 12.5% SDS PAGE, and blotted onto a nitrocellulose membrane (Carl Roth, Karlsruhe, Germany). The membrane was blocked (5% skimmed milk powder in PBS/0.1% Tween20, pH 7.4). Primary antibodies (details see Table 1) were diluted by 1:5000 and incubated overnight at 4°C . The secondary antibodies were used at 1:100,000 (Anti-rabbit IgG-HRP) and 1:4000 (Anti-murine IgG-HRP), and the membrane developed with the chemoluminescence substrate Immobilon[®] (Merck Millipore, Darmstadt, Germany) according to the manufacturer's instructions. Image acquisition and quantitation of band intensity were performed using Fusion FX Imaging systems (VILBER Lourmat, Collégien, France) and Image J (java.version: 1.8.0_171).

2.5. Uptake and Distribution Studies

To simulate the upside-down conditions at the olfactory region, a 2 cm^2 mucosa specimen was placed in a modified side-by-side cell consisting of two microreaction tubes (1.5 mL) to avoid leakages (Figure 2B). 1 mL of simulated nasal solution (SNS, 1.5 mM NaH_2PO_4 , 0.83 mM NaHPO_4 , 1.67 mM Mg_2Cl_2 , 4.56 mM KCl, 119.78 mM NaCl, 10 mM D-glucose, 15 mM NaHCO_3 , 1.2 mM CaCl_2 , osmolarity: 300 ± 10 mol/kg; pH 7.4; buffer was oxygenated for 10 min before use [40]) was filled in the upper tube prior to sealing with the mucosa. The assay set-up was developed to display conditions as similar as possible to in vivo conditions. Therefore, the mucosa explants were not washed before placing them

in the side-by-side cell, and the mucus layer was not removed to keep the system as close as possible to the native situation in intranasal drug application (mucus, upside-down, temperature: 35 °C).

A volume of 10 µL containing 8 mg/mL (54 µM) porcine serum IgGs in 0.1 M phosphate-buffered saline (PBS, Sigma Aldrich, Taufkirchen, Germany) or the same concentration of the humanized antibody bevacizumab biosimilar (in-house production) were pipetted carefully onto the epithelial layer. The mucosa was incubated at 35 °C and >90% humidity for either 30 min, 2 h, 4 h, or 8 h. The negative/vehicle control (buffer without antibody) was incubated for 8 h in parallel. At least four independent experiments were performed, and representative data are shown. Samples without an intact epithelial layer (see below) were excluded, and the experiment was repeated to obtain the necessary number of intact samples.

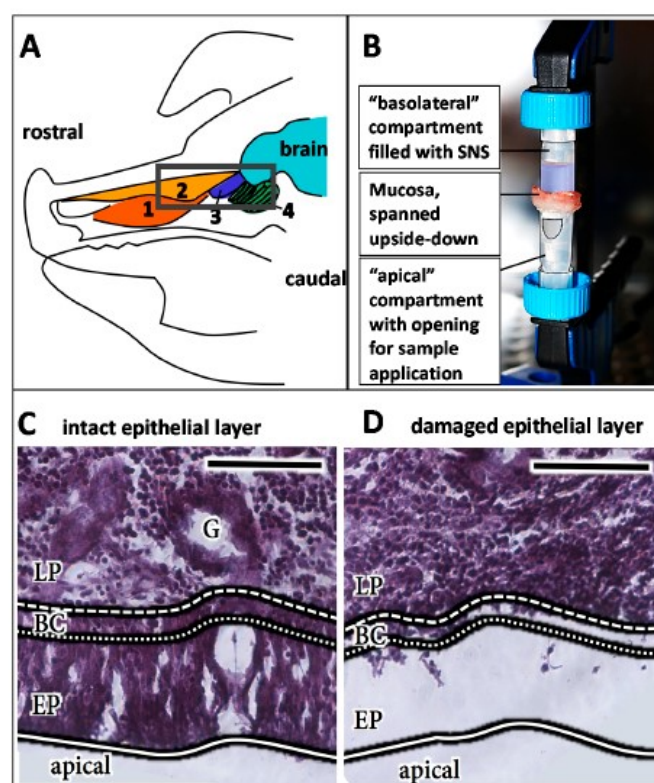


Figure 2. Experimental set-up of the uptake and distribution studies. Anatomical sketch of the sagittal section of a pig head according to [39], (A) 1: *concha nasalis ventralis*; 2: *concha nasalis dorsalis*; 3: *concha nasalis media*; 4: ethmoidal turbinates; Black box: *regio olfactoria*, from which tissue specimens were taken. (B) Experimental set-up: The mucosa specimen was fixed with a fastening clamp upside down in between two microreaction tubes. In the lower tube, a small opening was cut into the tube wall to obtain access to the mucosal surface for antibody or vehicle (PBS) application. (C) HE staining of an intact epithelial layer. (D) HE staining of a damaged epithelial layer. Detachment and damage of the epithelial layer leads to loss of its barrier function and, hence, has an important influence on the experimental read-out (see also Supplementary Materials). Therefore, all samples were analysed for the integrity of their epithelial layer by HE staining, and damaged samples as shown here were excluded from the analysis. LP: *lamina propria*; BC: basal cells; EP: epithelial layer. Scale bar: 100 µm.

After the respective incubation time, the mucosa explants were directly fixed in 4% paraformaldehyde for 2 h, cryoconserved in 30% sucrose overnight, and stored at 4 °C until sectioning. The tissue was cut in 14 µm slices in a cryostat at −25 °C (HM525 NX, Thermo Fisher Scientific,

Dreieich, Germany) and mounted on Superfrost® Plus Micro slides (VWR International GmbH, Darmstadt, Germany).

2.6. Immunohistochemistry and Histological Staining

Slides were washed three times for 5 min with PBS (Roti® PBS 7.2, Carl Roth, Karlsruhe, Germany; pH 7.4) followed by blocking with 4% BSA, 0.5% Saponin and 10% NGS solution in PBS for 1 h. The primary antibodies (Table 1) were diluted 1:100 in PBS containing 4% BSA/0.5% Saponin and incubated on the tissue sections for 2 days at 4 °C. The slices were washed again (5 min, 10 min, and 15 min), and incubated with the corresponding secondary antibodies (Table 1, 1:500 diluted in PBS containing 4% BSA/1% Saponin) for 2 h. After another three washing steps as described before, slides were mounted with Fluoroshield™ mounting medium containing DAPI (4',6-diamidin-2-phenylindol; Sigma-Aldrich, Taufkirchen, Germany).

To verify tissue integrity, adjacent or following slides from each sample were stained with hematoxylin-eosin (HE; Gil III, Merck Millipore, Germany). Briefly, the slides were washed with distilled water for 1 min, followed by staining in hematoxylin solution for 2 min, destained under running tap water for 12 min, and counterstained with Eosin-0.5% acidic acid (Sigma-Aldrich, Taufkirchen, Germany) for 3 min. Slides were additionally destained under running tap water for 1 min. Subsequently, the slides were dehydrated and mounted in Eukitt Quick hardening mounting medium (Sigma-Aldrich, Taufkirchen, Germany). The human tissue sections were only HE-stained similar to the porcine sections.

2.7. Analysis

The samples were analysed either by phase-contrast microscopy (Nikon Eclipse 80 I; Nikon Instruments Europe B.V., Duesseldorf, Germany) and epi-fluorescence microscopy (Olympus BX63, Olympus Europa SE & Co. KG, Hamburg, Germany) or by confocal microscopy (Zeiss LSM 7MP, Carl Zeiss AG, Jena, Germany). To blank the signal of endogenous porcine IgGs from the exogenously administered allogenic porcine serum IgGs (Sigma-Aldrich, Taufkirchen, Germany), the Image J (java.version: 1.8.0_171) macro "Image Calculator" was used. With this tool, the fluorescence intensity of the negative/vehicle control stained with anti-swine-RhodamineRed secondary antibody was subtracted from the respective sample tif data files. For comparability, the FITC signal of hIgG was converted to a red colour in Image J.

3. Results

The bioavailability in the CNS of intravenously administrated antibodies is limited and N2B drug delivery is discussed as an attractive alternative, in particular for higher molecular weight biopharmaceuticals. In this context, the antibody transporter FcRn is implicated in transport and distribution of IgGs from mucosal surfaces. Thus, the aim of the present study was to evaluate the presence and the function of FcRn in porcine olfactory mucosa explants and finally the fate of transported IgGs in the nasal *lamina propria*. The presence of FcRn could facilitate IgG intracellular uptake from endosomes and tissue distribution, but FcRn is also associated in mucosal immune defence and, thus, FcRn interaction with biopharmaceuticals could result in undesired immunogenicity.

The use of appropriate human nasal tissue is ethically challenging and mostly limited to specimens from nasal surgery, which are predominantly from polyps or lower parts of the nasal turbinates that are covered with respiratory mucosa only. Therefore, fresh porcine nasal tissue from the roof of the nasal cavity containing predominantly olfactory mucosa was used here. Comparison of the morphology of the *regio olfactoria* from humans and pigs showed a high similarity (Figure 3A), and these findings are supported by published data [41–43]. The use of porcine tissue as a model to determine the penetration and distribution of antibodies, both allogenic and xenogenic, i.e., porcine (pIgG) and human IgGs (hIgG) was investigated in this study.

3.1. Presence and Localisation of FcRn in the Porcine Regio Olfactoria

The key histological features of the olfactory mucosa include an epithelium with basal cells, olfactory sensory neurons, and sustentacular cells, as well as axonal bundles and glands with epithelial openings (Bowman's glands) in the *lamina propria* [44]. All these characteristics were found in the porcine *regio olfactoria*, especially in the dorsal part of the *concha nasalis media* (not shown), the dorsal part of the *concha nasalis dorsalis*, and the *ethmoidal turbinates* (Figure 3A–C).

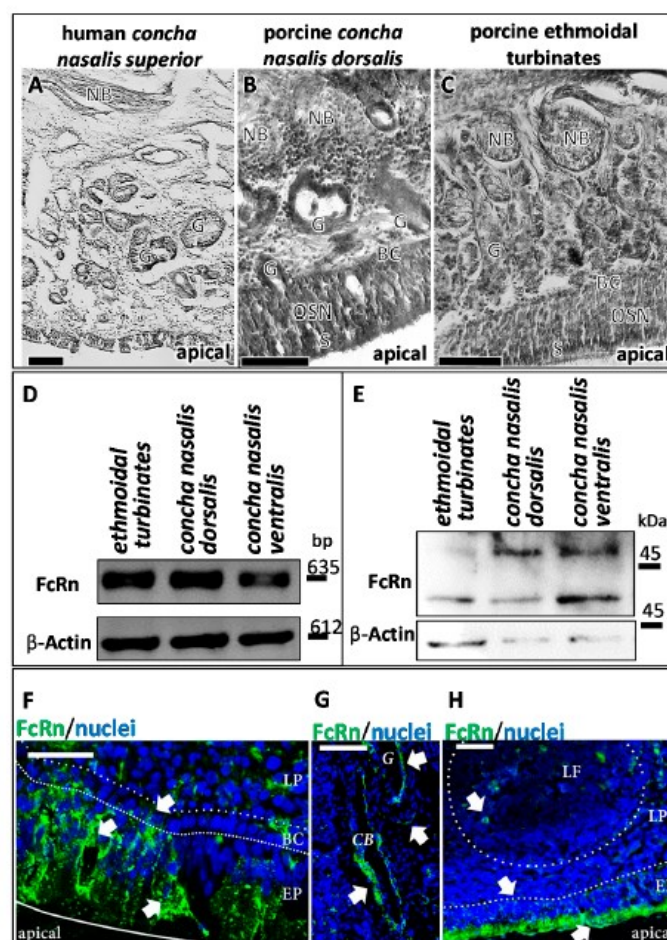


Figure 3. FcRn in porcine olfactory mucosa. (A–C) Porcine olfactory mucosa shows a similar architecture as observed in humans [44]. Comparable to human tissue (A); neuronal bundles, Bowman's glands and a pseudostratified epithelium are found in the porcine *concha nasalis dorsalis* (B); and in the porcine ethmoidal turbinates (C); Scale bar: 200 μ m. FcRn expression and immunoreactivity were evaluated in the *regio olfactoria* by reverse transcriptase-PCR (RT-PCR) (D) and Western Blot (E). Protein (E) and mRNA (D) of FcRn were observed in all investigated olfactory regions: Ethmoidal turbinates (*regio olfactoria*), *concha nasalis ventralis* (respiratory region), *concha nasalis media* (*regio olfactoria*, not shown), and *concha nasalis dorsalis*. PCR fragment sizes: FcRn:635 bp; Beta Actin: 612 bp (loading control). Molecular Weight: FcRn:40 kDa; higher molecular weight band FcRn: different glycosylation patterns according to [17]; Beta Actin: 42 kDa (loading control). FcRn immunoreactivity was observed throughout the porcine olfactory mucosa: (F) FcRn is detected in epithelial cells, cells of the basal membrane and in blood vessels. In epithelial cells, FcRn is observed in vesicles, but apparently also at the apical side; Scale bar: 50 μ m. (G): FcRn expression in cavernous bodies and glands in the *lamina propria*; Scale bar: 50 μ m. (H): vesicular transport of FcRn in the epithelial layer and FcRn expression in lymphoid follicles; Scale bar: 200 μ m; DAPI stained nuclei. BC: basal cells; CB: cavernous body; G: glands; LF: lymphoid follicle; LP: *lamina propria*; NB: neuronal bundles; OSN: olfactory sensory neurons; SUS: sustentacular cells.

In humans, Heidl et al. demonstrated immunoreactivity against FcRn in epithelial cells, basal cells, gland cells, and endothelial cells of the nasal mucosa [19]. In line with these findings, FcRn expression was confirmed by RT-PCR and Western Blot in different parts of the porcine *regio olfactoria* (*concha nasalis dorsalis*, *concha nasalis media*, *ethmoidal turbinates*) as well as in the porcine respiratory epithelium (*concha nasalis ventralis*; Figure 3D,E).

Immunoreactivity against FcRn was observed in the porcine *regio olfactoria*, in particular in the epithelial cells, mainly at the apical sides, but also inside their cell bodies. Furthermore, immunoreactivity was revealed at both, the apical and basolateral sides of cavernous bodies and at the apical side of gland cells as wells, as at the apical side of endothelial cells forming blood vessels (Figure 3F–H).

3.2. IgG Uptake and Distribution in Porcine Olfactory Mucosa Explants

The findings of an earlier study suggested the feasibility of porcine tissue for studying FcRn-mediated transport processes of human antibodies [28]. To investigate this assumption, allogenic porcine IgGs (pIgG) and xenogenic human monoclonal IgGs (hIgG) were applied to the apical side of olfactory mucosa in a side-by-side cell setup. The mucosa explants were collected after different incubation periods, fixed immediately, and processed for the immunofluorescent detection of IgG and FcRn. The mucosa received nutrients and oxygen via an oxygenated buffer at the basolateral side. In addition, it was observed by histology during the establishment of the method that even the smallest damages and injuries resulted in a loss of the epithelial layer. Any disruption of the epithelial layer during the preparation procedure destroyed its barrier function and resulted in complete penetration of the lamina propria by the applied IgGs after only 30 min (see Supplementary Figure S1). Therefore, the presence of an intact epithelial layer was confirmed as a quality control parameter for a successful experiment. Adjacent or following sections of all processed samples were used for HE staining to confirm that the epithelium was present and intact during the experiment (epithelial control, Figure 4).

To reduce the background caused by the basal endogenous levels of pIgG, vehicle-treated samples were processed identically and their detected fluorescence was subtracted from the IgG-treated samples. Both pIgGs as well as hIgGs penetrated the *lamina propria*, but with different kinetics and at significantly different levels. An obvious immunoreactivity against pIgG was observed after 8 h (Figure 4A–C) while the detected fluorescence indicative for immunoreactivity against hIgG was considerably lower (Figure 4E–G) after 8 h, but detectable in epithelial and basal cells. These data clearly implicate species-specific dependency of the transport. Interestingly, hIgG was also observed in cavernous bodies and blood vessels with a more diffuse pattern. In particular, the selective presence of bevacizumab at structures formed from endothelial cells may result from binding to its antigen vascular endothelial growth factor (VEGF). An alignment of human (UniProt ID P15692) and porcine (UniProt ID 49151) VEGFA revealed a 100% homology in the bevacizumab epitope from amino acid (aa)79 to aa94 [45]. Hence, it can be assumed that the localization of bevacizumab at blood vessels and cavernous bodies is related to binding of its antigen VEGF, which is secreted from endothelial cells.

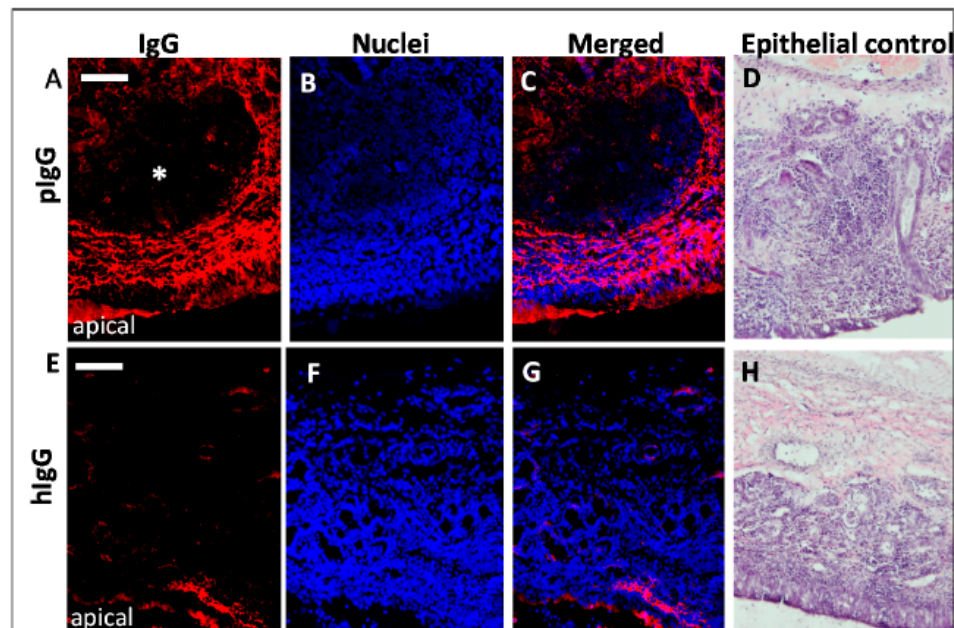


Figure 4. Comparison of uptake and distribution of porcine vs. human IgG through porcine olfactory mucosa. (A,C) immunoreactivity against porcine IgG (pIgG) after 8 h incubation and (E,G) immunoreactivity against human IgG (hIgG; bevacizumab biosimilar) after 8 h incubation (intrinsic porcine IgG signal was subtracted for all data presented). (B,F): nuclei counterstain; (C): Image of pIgG staining and nuclei overlay after 8 h incubation. (D,H) HE staining of the mucosa explants as quality control for an intact epithelial barrier. Moreover, round subepithelial structures were observed (*) that seem to be spared from IgG immunoreactivity. Nuclei are stained with DAPI; Scale bar: 200 μ m.

3.3. Fc-Mediated Transport of Allogenic IgGs, but also Potential Fc-Mediated Clearance Pathways

Earlier studies imply pinocytosis as an uptake mechanism of IgGs from the apical epithelial side, followed from fusion of early pinocytotic endosomes with FcRn-containing acidic endosomes. FcRn binds to IgGs and directs them to the basolateral side of the epithelium facing the *lamina propria*. Some other studies describe apical uptake via FcRn at low pH and transcytosis through the epithelial cells [24,25]. Regardless of the mechanism involved here, an indication for IgG-FcRn interactions should be observable by co-localisation studies. Thus, samples of pIgG, hIgG and vehicle experiments were stained for FcRn and pIgG, hIgG, respectively. The representative data in Figure 5 show co-localisation of FcRn and pIgG after 30 min of incubation, but hardly any co-localisation of FcRn and hIgG after the same incubation time. A weak co-localisation of hIgG with basal and epithelial cells was found at later incubation intervals. After 8 h, the above-mentioned diffuse signal was observed in blood vessels and cavernous bodies of the *lamina propria*. For pIgGs, clear co-localisation was found in blood vessels, cavernous bodies, glands, and the epithelial cells, including the basal cells (Figure 5B,C). Most probably due to fixation at the end of each experiment, the exogenously applied proteins could not be washed away and were still detectable (Figure 5C,D). Interestingly, only traces of pIgG were detected at the apical side, implying higher absorption. In contrast, large amounts of hIgG were apparently not taken up and remained at the apical side (see * in Figure 5D). The potential FcRn-mediated transport of epithelial and basal cells towards the *lamina propria* facilitated the apical uptake of allogenic, and in lesser amounts, xenogenic IgG. However, drainage to blood vessels could result in distribution to different compartments such as blood, and result in a reduction of the drug that is transported to the brain. Similarly, uptake of IgG by acinar cells of glands may lead to excretion of these IgGs with nasal mucus.

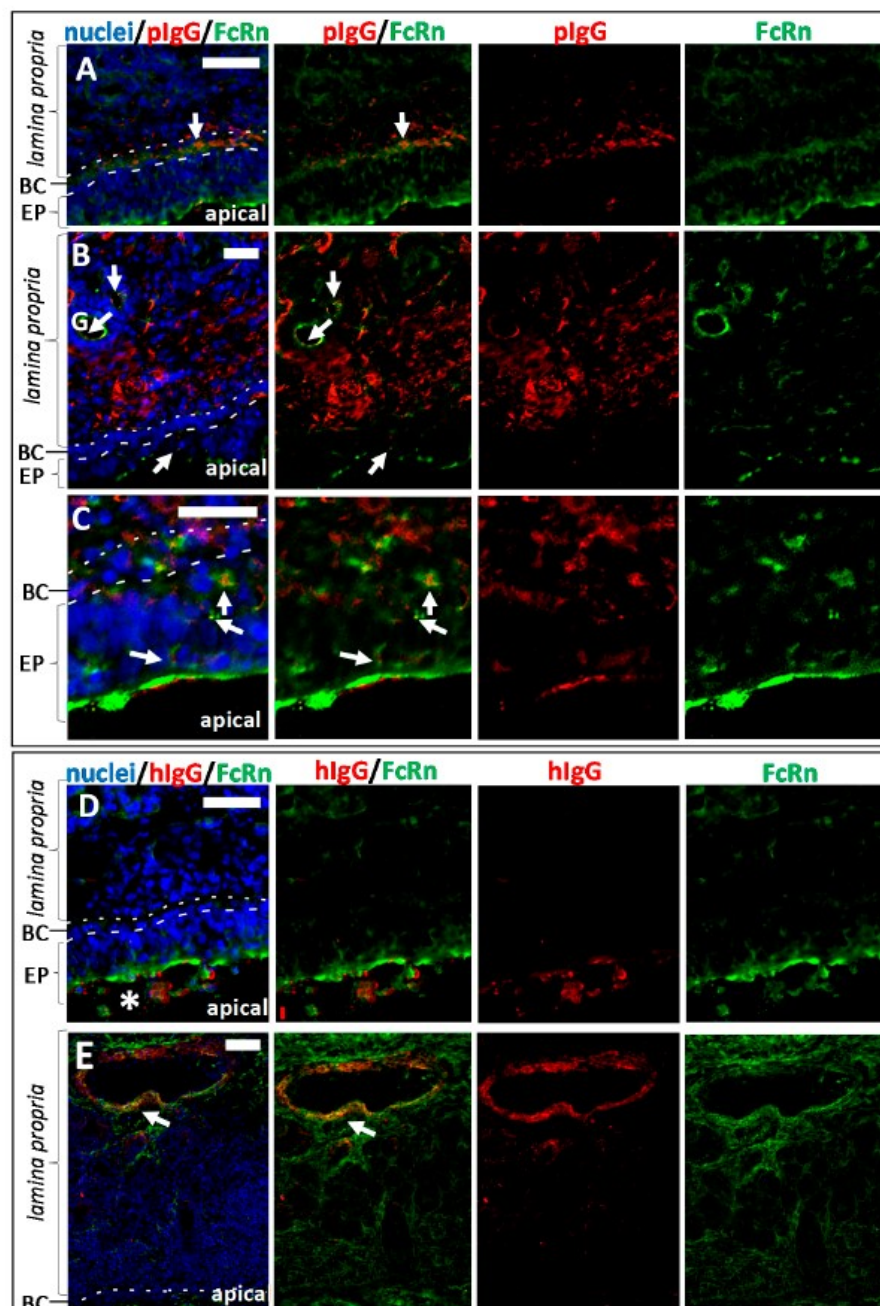


Figure 5. Co-localisation study of immunoreactivity against FcRn and IgG in the porcine *regio olfactoria*. (A) pIgG and FcRn localisation in the olfactory mucosa after 30 min of incubation. Co-localisation could already be detected in basal cells of the epithelial layer. (B) pIgG and FcRn localisation in the olfactory mucosa after 8 h of incubation. Double staining of FcRn and pIgG revealed co-localisation in glands (identified according to their morphology with an accumulation of round vessel-like structures), basal cells and polarized epithelial cells. (C) pIgG and FcRn co-localisation in the epithelial layer after 8 h of incubation. (D) Co-localisation of FcRn and hIgG (bevacizumab) after 0.5 h of incubation. The hIgG remains mainly at the apical surface (*). Diffusion through the epithelial layer was not detected after this incubation time. (E) After 8 h of hIgG incubation, co-localisation of FcRn and hIgG was mainly found in blood vessels and cavernous bodies, presumably caused by the presence of VEGF -the antigen of bevacizumab. Thus, in general the hIgG penetration into the tissue was weaker compared to pIgG. Arrows indicate sites of co-localisation. BC: basal cells; EP: epithelial layer; G: gland; Scale bar: 50 µm.

3.4. Kinetics of Allogenic IgG Uptake and Distribution into Olfactory Mucosa Lamina Propria

A kinetic study of pIgG uptake in olfactory mucosa showed a time-dependent increase of IgG-immunoreactivity. While after 30 min only traces of pIgG were detectable within the epithelial cell layer (Figure 6), 2 h of incubation were sufficient to transport the pIgG to the *lamina propria* (data not shown). After 4 h of incubation, a clear strong immunofluorescent signal was detected throughout the whole *lamina propria*. This signal was only slightly amplified after 4 additional hours (8 h in total). As a concentration of 54 μ M pIgG was used, it was assumed that all FcRn-dependent transport was saturated, thereby subsequently limiting the IgG's transport velocity.

After 4 h and later, an interesting observation was obvious in most samples: large structures were spared more and more from pIgG immunoreactivity (*, Figure 4A–C; Figure 6). HE stain revealed these structures to be lymphoid follicles—nasal mucosa immune structures, which are similarly organized as intestinal Peyer's patches [33,43,46].

As indicated above, the integrity of the epithelial layer was evaluated for all samples (Figure 6 last column). The result of an experiment with a damaged epithelium is shown in Supplementary Figure S1. Here, even at the earliest time investigated (30 min of incubation), a complete coverage of the *lamina propria* with the apically applied IgGs was observed.

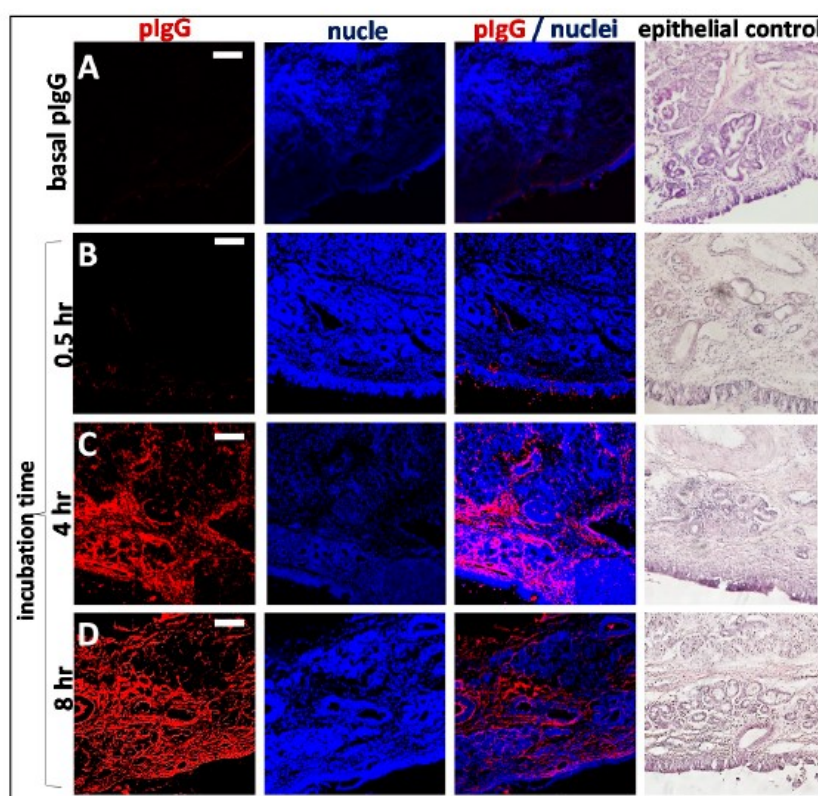


Figure 6. Time dependent penetration of pIgG through olfactory mucosa (*concha nasalis dorsalis*). (A) Basal levels of endogenous pIgG were detected with a low signal at the apical side, in the basal cell layer, glands, cavernous bodies, and blood vessels. This signal served as a blank and was subtracted from the photos showing the penetration of exogenous pIgG. (B) After 30 min, only the areas close to the apical side show immunoreactivity for pIgG, but some signal was detected in the *lamina propria*. (C) After 4 h, the pIgGs obviously distributed into the *lamina propria*. * indicate round structure filled with cells and mostly spared from IgG (D) After 8 h, pIgG were detected throughout the whole *lamina propria*. Nuclei stained with DAPI; epithelial control: quality control for tissue integrity, stained with HE. Scale bar: 100 μ m.

3.5. The Fate of Allogenic IgG in the Lamina Propria and Potential Drug Routes to the Brain

In N2B drug delivery, the neuronal fibres of the olfactory sensory neurons, but also the trigeminal nerve endings are of high interest as a potential transport route to the CNS [25]. The neuronal bundles travel through the cribriform plate to the olfactory bulb. Beneath the basal cell layer, olfactory ensheathing cells enwrap neuronal bundles and are involved in neurogenesis of olfactory sensory neurons [47]. During tissue preparation, these projections have to be carefully disconnected with a blunt scalpel to excise the mucosa. Therefore, the whole potential route cannot be evaluated in this ex vivo model. Nevertheless, to elucidate uptake of pIgG either into olfactory axons or among the axons and the olfactory ensheathing cells, double staining of the axonal marker neurofilament 200 (NF200, [48]) with pIgG and hIgG was performed. Thirty minutes of incubation were sufficient to detect co-localisation of pIgGs along axonal fibre tracts. It should be noted that even in axonal bundles rather far from the epithelial layer, immunoreactivity against pIgG was observed. This observation is in accordance with the rather fast kinetics of intranasally applied drugs that are reported from clinical and in vivo studies (for summary see [49]). By contrast, co-localisation of hIgGs and NF200 was found only after 8 h, and here the concerned neuronal bundles were rather close to the epithelial cell layer (Figure 7A–C). Our data may indicate that an increased uptake into the *lamina propria* could be associated with an increased uptake into neuronal bundles. Thus, even if FcRn is apparently not relevant for direct uptake into neuronal fibres, an indirect connection could be plausible. However, the IgG signal observed was rather weak, which could indicate a limitation of this neuronal pathway. It should be noted however, that the immunofluorescent signal was generally weak for pIgG after 30 min, and for hIgG even after 8 h of incubation.

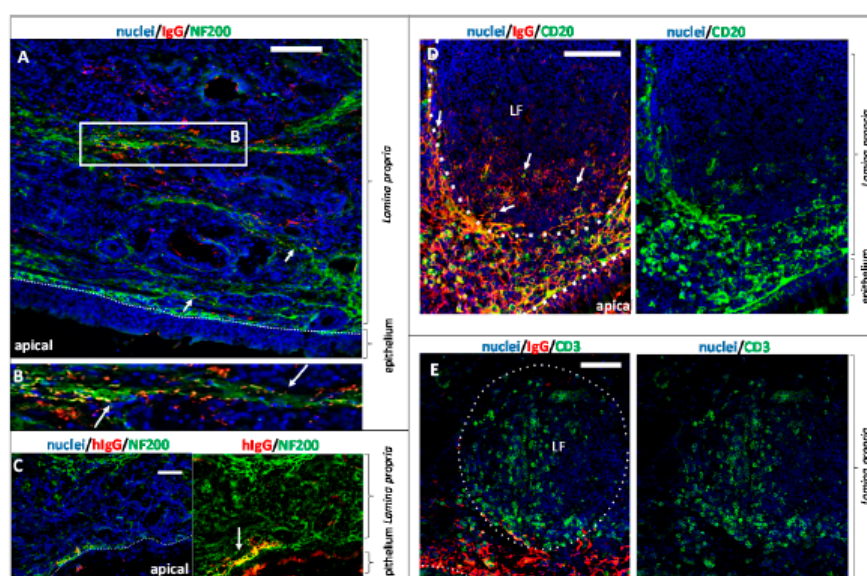


Figure 7. Exogenous IgG distribution in lymphoid follicles and potential interaction with neuronal fibres and the local immune system in the *regio olfactoria*. (A) 30 min of pIgG permeation: investigation of neuronal transport routes. The axonal marker Neurofilament 200 (NF200) was stained in green. pIgGs are stained in red. Arrowheads indicate pIgGs in close vicinity or co-localizing with neuronal fibres. pIgG in or along neuronal fibres were observed throughout the whole *lamina propria*, even in regions rather far away from the apical side. (B) Close-up of framed region in A. Co-localisation of NF200 and pIgG; Arrows indicate sites of co-localisation. (C) 8 h after apical hIgG application: co-localisation of hIgG and NF200 indicating a transport along the neuronal fibres. Note that hIgG was found in fibres, which are close to the apical site (D) Investigation of pIgG co-localizing with B cells of the lymphoid follicle after 8 h of incubation. B lymphocytes (antigen CD20) are stained in green. pIgGs are stained in red. (E) Lymphoid follicle in the *lamina propria* of the olfactory mucosa. Left: pIgG after 8 h of incubation (red), T lymphocytes (green), nuclei (DAPI, blue). LF: lymphoid follicle; Scale bar: 100 μ m.

As described above, structures which apparently were lymphoid follicles were time-dependently spared from allogenic IgG signal. Brandtzaeg et al. described lymphoid follicles in the mucosa of the gut, the lung and the nose, consisting amongst others of B and T lymphocytes [50]. To verify that such structures were lymphoid follicles, a double staining of pIgG with either CD20 (to detect B cells, Figure 7D) or CD3 (to detect T cells, Figure 7E) was performed. In contrast to the latter study, CD20 immunoreactivity was mainly located at borders of the lymphoid follicles. For CD14 (monocytes/macrophages) the location was similar as for CD20 (data not shown). As the borders of the lymphoid follicles were not spared from pIgG signal, a strong co-localisation was observed (Figure 7D). It should be noted that the goat-anti-swine IgG secondary antibody used throughout this study does not show cross-reactivity or unspecific binding to the B cell receptor. Therefore, co-localisation of pIgG and B cells is unlikely to be caused by staining of B cells via CD20 and Fc domains of their B cell receptors. T cells were found inside the follicles; thus, no co-localisation was evident. Earlier reports suggested an endocytic uptake of IgG from dendritic cells and macrophages. Infiltrated IgGs from the mucosa may bind important antigens from the apical nasal cavity. The IgGs are proteolytically digested, including the antigen, which is subsequently presented on the cell surface to the cellular immune system. Preliminary data showed that macrophages could be detected in relatively high amounts in the subepithelial dome underneath the basal cell layer, as well as occasionally inside the follicles (data not shown). Like other antigen-presenting cells, macrophages could have engulfed and digested the pIgGs, so that they were not detectable anymore. The above described effects were not observed for xenogenic hIgG. Based on these results, an interaction of the mucosal immune system with the externally applied pIgGs could be concluded.

4. Discussion

N2B drug delivery is of increasing interest since it was demonstrated that tracers like wheat-germ agglutinin-HRP conjugates could be found in the axonal projections of olfactory sensory neurons and in the olfactory bulb [36]. As clinical studies with intranasally delivered CNS-active peptides and small proteins are ongoing, the delivery of larger proteins via the nasal pathway as an alternative to bypass the BBB becomes more and more attractive [13,51–53].

Recently, it was shown in human nasal tissue that the IgG specific transporter FcRn is expressed in the respiratory regions of the nose [19]. Here, we demonstrated that FcRn is also widely expressed in the porcine nasal mucosa, which makes the pig an interesting model for receptor-mediated uptake and transport of IgGs. We found FcRn expression in all regions of the porcine nasal mucosa, also in the *regio olfactoria*. The *regio olfactoria* is the region of interest with regard to N2B drug delivery, as the epithelium is widely spanned with olfactory sensory neurons that are projecting into the brain, but it is also innervated by the trigeminal branches that connect to the brain stem [33]. We demonstrated that in epithelial cells of the olfactory epithelium, the FcRn is strongly expressed on the apical side, whereas in blood vessels and glands a weaker basolateral expression was found. We could additionally demonstrate intracellular localisation of FcRn in the epithelial layer that hint to a possible FcRn-mediated transport mechanism. Such FcRn-mediated transcytosis has hitherto mostly been analysed in other mucosa sites in the body such as lung and gut [18,23,54,55].

The results of the IgG transport and distribution studies, double staining of IgG and FcRn together with the mentioned literature data, give strong indications for an involvement of FcRn in IgG transport through the olfactory mucosa. However, a direct FcRn-IgG interaction cannot be concluded from our co-localisation data. Further experiments using FcRn knock-out or similar models are needed to confirm the involvement of FcRn in this process. Nevertheless, our results indicate a species-preference of IgG transport mechanisms, since our data show significant differences in uptake kinetics of allogenic porcine IgGs vs. xenogenic human IgG. An alignment of human (UniProt ID P01860) and porcine (UniProt ID L8AXL3) immunoglobulin heavy constant chains and, in particular, the C_H3 domain hosting the binding site of FcRn revealed identities of less than 50%. This is supported by Ober et al. which showed species-specific preferences by the human FcRn in vitro [28]. Their kinetic

data suggested a very low affinity of human FcRn to murine IgGs, but a higher affinity to rabbit IgG. In contrast, Stirling et al. showed in vitro that hIgG yields a higher porcine FcRn-mediated uptake [17]. These results are further supported by kinetic investigations of the rabbit FcRn that showed binding to human IgG with higher affinity than rabbit IgG in surface plasmon resonance experiments [56]. Similarly, it was reported that the serum half-life of human IgGs administered to mice is significantly lower than the half-life of murine antibodies. Ober et al. (2001) showed that the recycling mechanism of FcRn was not functional with xenogenic IgGs [28]. Our data support the hypothesis of species-dependent IgG transport, as we did not observe significant hIgG levels in the *lamina propria* after 8 h of permeation. There are studies showing efficient FcRn-mediated transport of xenogenic IgGs in cell culture models that may not reflect the same conditions as under ex vivo and in vivo conditions [17,56]. However, we cannot exclude that other transport mechanisms than FcRn are responsible for our observations. For example, Ishikawa et al. found evidences that Fc gamma receptor IIb is involved in IgG transcytosis in the placental endothelium [57]. Other Fc receptors are mainly known for effector function in immune surveillance and response [58–61].

Further on, we cannot rule out the influence of the apical pH on the antibodies directly in the tissue. As it is described to be a sour environment at the apical surface aggregation of the hIgG is possible [62,63]. As we used the natural mucus layer located on the tissue explant, we do not know the pH exactly. Another possibility would be to wash the specimen and to use artificial mucus with a defined pH as described by Rinaldi et al. [63].

In this study, we were also interested in the involvement of neuronal fibres in N2B transport. Our results show co-localisation of neuronal fibres and pIgG after only 30 min, even in the deeper *lamina propria*. In contrast to allogenic pIgG, co-localisation of xenogenic hIgG with NF200 was only detectable after 8 h, and only close to the basal cell layer. As we did not find significant levels of hIgG in general in the *lamina propria*, this finding might be due to the concentrations used, and could be investigated in future experiments with higher concentrations for bevacizumab. But according to the most common hypothesis, intranasal applied drugs are taken up by apical dendrites of olfactory neurons and are transported inside or along the axons to the brain [21,64]. This mechanism was discussed as unspecific, and a species-dependency has not been described before. Therefore, the observation that xenogenic IgG was rarely found in or along neuronal bundles was rather unexpected. However, the olfactory ensheathing cells surrounding the neuronal fibres can be detected in the basal cell layer and in the *lamina propria* [21]. Thus, the olfactory axons are unshielded from the epithelial layer down to the basal cell layer and an uptake of molecules into the unwrapped fibre tracts starting from the basal cell layer could explain these observations (Figure 8). Finally, it can be speculated that endocytosis and allogenic FcRn-mediated transcytosis facilitate the uptake over the epithelial layer, leading to an increased absorption in neuronal bundles at the stage of the basal cells.

In general, barriers like the BBB and the blood nerve barrier protect neuronal tissues from entry of antibodies, T cells, and toxic components of the blood [65]. Previous studies revealed that the perineural route is faster than intracellular axonal transport [25]. FcRn was found to be expressed in peripheral nerves, and was further described as a transporter at the blood nerve barrier [66,67]. An uptake of IgG into neuronal bundles would indeed be surprising, as in the BBB, the FcRn is known to act as an efflux transporter, but we cannot exclude this possibility [68,69]. Another explanation may be that the uptake of IgGs into neurons occurs at the basolateral side of the epithelial cell layer or in the *lamina propria* and not by apical dendrites of the olfactory sensory neurons. Thus, the FcRn-mediated transport of allogenic IgG at the epithelial barrier could explain our observations as we demonstrated poor uptake of hIgG into the epithelial layer. In upcoming in vivo experiments, it will be of interest whether allogenic IgG can be transported into the olfactory bulb as shown for other proteins. Furthermore, the fate of the hIgG in the *lamina propria* remains to be elucidated. We observed predominantly that hIgG was co-localised with endothelial cells of cavernous bodies and blood vessels, but also in glands, although no general tissue distribution was observed in the *lamina propria*.

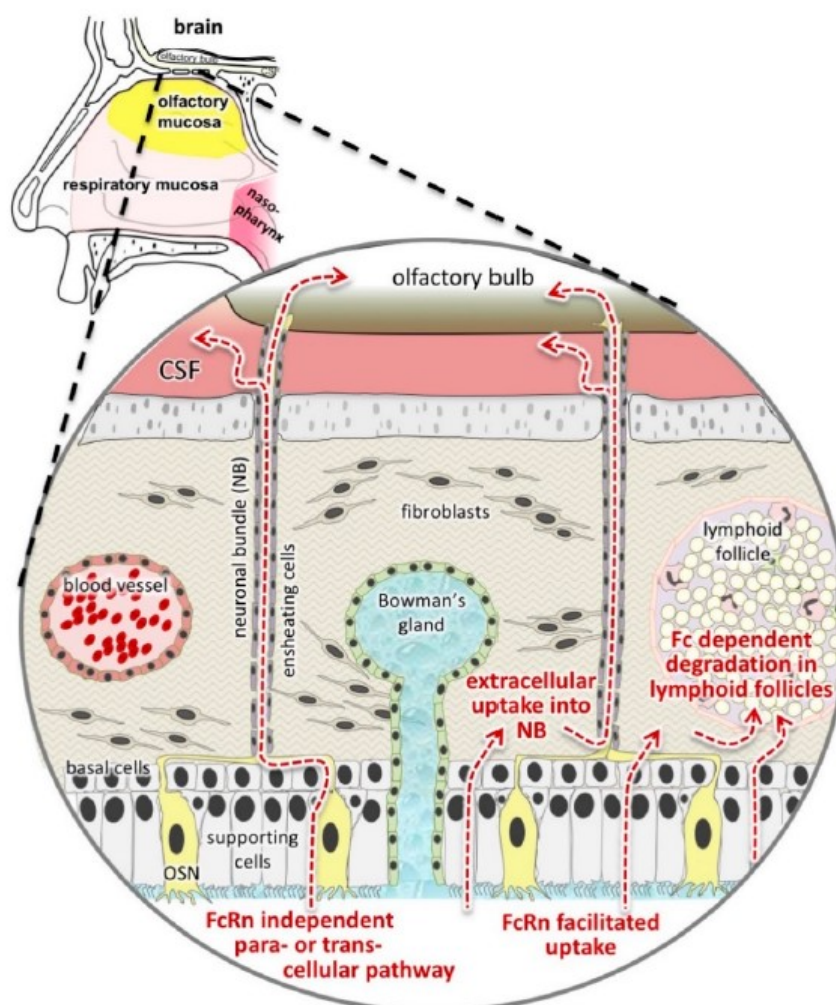


Figure 8. Hypotheses based on our study results: We presented evidences implying an FcRn-mediated transport in the porcine *regio olfactoria* and we have observed three different destinations of the absorbed IgGs: uptake into or along neuronal fibres (final destination: central nervous system (CNS)), uptake into blood vessels or in glands (final destination: blood and mucus), or potential degradation in lymphoid follicles (final destination: presented as antigen with a potential to cause immunogenicity). In this sketch, the uptake into blood vessels was neglected as compared to the respiratory mucosa, as the olfactory mucosa harbours only small and rare blood vessels. In upcoming studies, the potential of Fc-bearing molecules such as IgGs and Fc fusion proteins to target lymphoid follicles will be determined. In parallel, the levels of Fc-deleted proteins such as scFv or domain antibodies that reach the brain will be studied. The aim is to resolve if those pathways can be targeted separately or if intranasal N2B delivery will always be a mixture of CNS, blood, and immune system targeting. CSF: cerebrospinal fluid; Fc: Fc domain; FcRn: neonatal Fc receptor; NB: neuronal bundle; OSN: olfactory sensory neuron.

During the IgG distribution experiments, we found circular structures in the *lamina propria* that were almost completely spared from permeating IgG. As their morphology resembles Peyer's patches in the gut, we started to investigate the local immune system in the *regio olfactoria*. The architecture of Peyer's Patches in the intestine is separated into three main domains: the follicular area, the interfollicular area, and the follicle-associated epithelium [70]. Around the follicle B cells, T cells, macrophages, and dendritic cells are located in the subepithelial dome [71]. Debertin et al. found lymphoid follicles morphologically similar to Peyer's patches in the nasal cavity of infants [34]. Similar to our findings, they discovered that lymphoid follicles are mainly located in the upper nasal cavity. Thus, morphologically the lymphoid follicles show the same features in young children and pigs.

In summary, little is known about the development and the exact function of the immune system in the upper part of the nose in mammals. Concerning the distribution of immune cells in the local lymphoid follicles, we found partially CD3⁺ cells in the germinal centre of the lymphoid follicle whereas in the subepithelial dome CD3⁺, CD20⁺, and CD14⁺ (data not shown) cells were located in high amounts. These findings are in accordance with Peyer's patches in men and sheep [46,72–75]. Our data are somewhat in conflict with data of Brandtzaeg et al. who found mainly CD20⁺ cells inside and CD3⁺ cells outside the lymphoid follicles in human Peyer's patches. The exact cellular composition is up to now a controversial topic. Studies show an age-related change in B- and T-cell localisation in and around lymphoid follicles [74,75].

In our uptake and distribution experiments we observed very few antibodies inside the lymphoid follicles whereas the pIgGs were concentrated in the subepithelial dome. In double staining, we saw co-localisation of CD20⁺ and pIgGs that hints to a molecular interaction. Akilesh et al. observed FcRn expression on B cells, which further strengthens our results of an interaction between permeated pIgGs with CD20⁺ cells [76]. Our results show no co-localisation of CD3⁺ cells and pIgGs. Baker et al. showed that cross-presentation of IgG immune complexes by dendritic cells is mediated by FcRn and controls cross-priming of CD8⁺ T cells in mice [77]. It is commonly known that diverse types of dendritic cells reside in the lymphoid follicle, the subepithelial dome and the surrounding epithelium in the intestine [71,72]. It is likely that the nasal lymphoid follicles show a similar distribution of dendritic cells. Double staining with CD20 and CD3 specific antibodies did not completely reveal the cellular composition in the lymphoid follicles, as most of the follicle was still unstained. Dendritic cells could be one cell type to fill the gaps.

Referring to N2B drug delivery, again the risk of undesired immunogenicity could be significant, especially when FcRn mediated processes like IgG transport are involved. Certainly, there are several links between FcRn and immune response in mucosal sites. For example, the ability of FcRn to direct antigens to inductive sites of the mucosal immune system was demonstrated to play an important role in immune surveillance [78]. It was further observed that bidirectional IgG transport retrieved luminal antigens into the mucosa, where they can be captured by dendritic cells for CD4⁺ T cell presentation [79]. An FcRn-targeted mucosal delivery of a herpes simplex virus type-2 glycoprotein fused to an Fcγ domain resulted in an effective memory immune response in mice [80].

A huge challenge and problem in investigating the clinical potential of intranasal N2B delivery of biopharmaceuticals is the choice of model organisms. Species-specific effects can be only overcome by using allogenic/surrogate proteins of the respective model species, and using the clinical candidates are of limited value. Furthermore, to elucidate potential risks of immune interactions, the differences in the organisation and morphology of nasal immune systems between species is of great importance. Rodents lack the typical nasopharynx- and nose-associated lymphoid tissue (NALT) described in human, sheep or other farm animals, but they possess locally organized lymphoid tissue at the bottom of their nasal passages [81].

Transmucosal permeation was used in several studies as a model to predict bioavailability as is well established for intestinal cellular models such as Caco-2 [82]. Also, permeation was presented in studies focusing on N2B delivery [38,40,83]. However, the data presented here raise the question about the suitability of using permeation experiments to extrapolate or conclude from these data the clinical feasibility of N2B drug delivery. Most in vitro models for permeation consist of epithelial carcinoma cells, but only some express functional FcRn [84]. The use of primary cultures seems to overcome this lack of FcRn, but here the neuronal bundles and axons as well as lymphoid structures are still missing [19,85]. As we presented in this work for olfactory mucosa, absorbed IgGs were drained either by neuronal bundles, by blood or lymphatic vessels, or by lymphoid follicles. Hence, a permeation through an in vitro model is limited in comparison with in vivo models concerning multifactorial drug pathways in vivo. Remarkably, the use of ex vivo tissue combined with histological techniques, appears to be rather close to in vivo models, but lacking of course, blood circulation and intact axonal projections. Consequently, the ex vivo nasal mucosa model complemented our test and

screening battery consisting of an in vitro cellular model (RPMI 2650; [83]) and a refined intranasal administration technique in mice as in vivo model [86].

5. Conclusions

The present study demonstrated that functional FcRn expression in the olfactory mucosa seems to be both friend and foe for intranasal drug delivery. Our results indicate transport of allogenic IgGs across the epithelial barrier and along neuronal bundles of the olfactory sensory neurons. Whether this transport actually results in increased concentration of IgGs in the olfactory bulb and other brain regions needs to be explored in future in vivo studies.

On the other hand, our data indicate an interaction of the applied pIgGs with the local immune system, possibly a first step in a cascade causing immunogenicity against the applied drug. In further studies we will investigate the fate of proteins with and without the Fc domain when applied intranasally (see Figure 8). Probably, the immunogenicity of vaccines can be improved by fusion to Fc, while Fc-deleted antibody fragments with a lower molecular weight are better suited to reach the brain via axonal projections. In conclusion, profound investigations of transport pathways are required to develop valid pharmacokinetic models for a predictive clinical translation, but the intra-mucosal activities of drugs should not be neglected.

Supplementary Materials: The following are available online at <http://www.mdpi.com/1999-4923/10/3/107/s1>, Figure S1: Influence of damaged epithelial layer on the experimental readout.

Author Contributions: S.L.: established the histological methods and designed and performed most experiments, participated in the study design and prepared the manuscript; J.F.: established absorption experiments and experimental set-up; A.S.Z.: performed bioinformatic analysis and designed RT-PCR experiments; D.F.: participated in the histological experiments and analysis; J.-C.W.: participated in the histological analysis; P.S.: participated in the absorption experiments and analysis; R.K.: conceived and advised the analysis of human olfactory mucosa and provided the human samples; K.L.: participated in establishment of histological methods and in the image analysis; H.L.: conceived and advised image capture techniques and analysis of these; K.S.: conceived of the study, participated in its design and coordination and prepared the manuscript.

Funding: This study was supported by a funding from the European Union's Horizon 2020 research and innovation programme to the project N2B-patch (grant 721098, www.n2b-patch.eu). SL and JF received Klaus Murmann fellowships from Stiftung der Deutschen Wirtschaft and AS received a fellowship from Ulm and Biberach joint graduate school in pharmaceutical biotechnology funded by the Baden-Württemberg State Ministry of Science, Research and Arts.

Acknowledgments: We thank Chris Netherton and his colleagues from the Pirbright Institute (Pirbright, Surrey) for providing us with the FcRn antiserum. A special thanks to Reinhard Pabst from the MHH Hannover for his advice, input and fruitful discussions about immune follicles and the mucosal immune system. A particular thanks to the N2B-patch team for their critical but fruitful discussion and their ambitious efforts and high motivation. Finally, the authors like to thank Jens Cordes from Marburg University for ingenious and perfect technical assistance to dissect the human material from the olfactory cleft, Jürgen Zimmermann and Christoph Ladel for brilliant support with the manuscript and Rene Handrick from Biberach University for excellent advisory and technical support whenever needed.

Conflicts of Interest: The authors declare no conflicts of interest.

References

1. Köhler, G.; Milstein, C. Continuous cultures of fused cells secreting antibody of predefined specificity. 1975. *Biotechnology* **1992**, *24*, 524–526. [PubMed]
2. Brekke, O.H.; Sandlie, I. Therapeutic antibodies for human diseases at the dawn of the twenty-first century. *Nat. Rev. Drug Discov.* **2003**, *2*, 52–62. [CrossRef] [PubMed]
3. Neuhaus, J.; Risau, W.; Wolburg, H. Induction of blood–brain barrier characteristics in bovine brain endothelial cells by rat astroglial cells in transfilter coculture. *Ann. N. Y. Acad. Sci.* **1991**, *633*, 578–580. [CrossRef] [PubMed]
4. Ballabh, P.; Braun, A.; Nedergaard, M. The blood–brain barrier: An overview: Structure, regulation, and clinical implications. *Neurobiol. Dis.* **2004**, *16*, 1–13. [CrossRef] [PubMed]

5. Reese, T.S.; Karnovsky, M.J. Fine structural localization of a blood-brain barrier to exogenous peroxidase. *J. Cell Biol.* **1967**, *34*, 207–217. [[CrossRef](#)] [[PubMed](#)]
6. Benedict, C.; Hallschmid, M.; Hatke, A.; Schultes, B.; Fehm, H.L.; Born, J.; Kern, W. Intranasal insulin improves memory in humans. *Psychoneuroendocrinology* **2004**, *29*, 1326–1334. [[CrossRef](#)] [[PubMed](#)]
7. Benedict, C.; Hallschmid, M.; Schmitz, K.; Schultes, B.; Ratter, F.; Fehm, H.L.; Born, J.; Kern, W. Intranasal insulin improves memory in humans: Superiority of insulin aspart. *Neuropsychopharmacology* **2007**, *32*, 239–243. [[CrossRef](#)] [[PubMed](#)]
8. Benedict, C.; Frey, W.H.; Schiöth, H.B.; Schultes, B.; Born, J.; Hallschmid, M. Intranasal insulin as a therapeutic option in the treatment of cognitive impairments. *Exp. Gerontol.* **2011**, *46*, 112–115. [[CrossRef](#)] [[PubMed](#)]
9. Heni, M.; Wagner, R.; Kullmann, S.; Veit, R.; Mat Husin, H.; Linder, K.; Benkendorff, C.; Peter, A.; Stefan, N.; Häring, H.U.; et al. Central insulin administration improves whole-body insulin sensitivity via hypothalamus and parasympathetic outputs in men. *Diabetes* **2014**, *63*, 4083–4088. [[CrossRef](#)] [[PubMed](#)]
10. Heni, M.; Kullmann, S.; Ketterer, C.; Guthoff, M.; Linder, K.; Wagner, R.; Stingl, K.T.; Veit, R.; Staiger, H.; Häring, H.-U.; et al. Nasal insulin changes peripheral insulin sensitivity simultaneously with altered activity in homeostatic and reward-related human brain regions. *Diabetologia* **2012**, *55*, 1773–1782. [[CrossRef](#)] [[PubMed](#)]
11. Kullmann, S.; Frank, S.; Heni, M.; Ketterer, C.; Veit, R.; Häring, H.-U.; Fritsche, A.; Preissl, H. Intranasal insulin modulates intrinsic reward and prefrontal circuitry of the human brain in lean women. *Neuroendocrinology* **2013**, *97*, 176–182. [[CrossRef](#)] [[PubMed](#)]
12. Born, J.; Lange, T.; Kern, W.; McGregor, G.P.; Bickel, U.; Fehm, H.L. Sniffing neuropeptides: A transnasal approach to the human brain. *Nat. Neurosci.* **2002**, *5*, 514–516. [[CrossRef](#)] [[PubMed](#)]
13. Brambilla, M.; Manenti, R.; de Girolamo, G.; Adenzato, M.; Bocchio-Chiavetto, L.; Cotelli, M. Effects of Intranasal Oxytocin on Long-Term Memory in Healthy Humans: A Systematic Review. *Drug Dev. Res.* **2016**, *77*, 479–488. [[CrossRef](#)] [[PubMed](#)]
14. Winner, P.; Rothner, A.D.; Saper, J.; Nett, R.; Asgharnejad, M.; Laurenza, A.; Austin, R.; Peykamian, M. A randomized, double-blind, placebo-controlled study of sumatriptan nasal spray in the treatment of acute migraine in adolescents. *Pediatrics* **2000**, *106*, 989–997. [[CrossRef](#)] [[PubMed](#)]
15. Murphy, K.; Janeway, C.A.J.; Travers, P.W.M. The structure of a typical antibody molecule. In *Immunobiology: The Immune System in Health and Disease*, 8th ed.; Garland Science: New York, NY, USA, 2012; pp. 128–133. ISBN 9780815342434.
16. Edelman, G.M. Antibody Structure and Molecular Immunology. *Science* **1973**, *180*, 830–840. [[CrossRef](#)] [[PubMed](#)]
17. Stirling, C.M.A.; Charleston, B.; Takamatsu, H.; Claypool, S.; Lencer, W.; Blumberg, R.S.; Wileman, T.E. Characterization of the porcine neonatal Fc receptor—Potential use for trans-epithelial protein delivery. *Immunology* **2005**, *114*, 542–553. [[CrossRef](#)] [[PubMed](#)]
18. Roopenian, D.C.; Akilesh, S. FcRn: The neonatal Fc receptor comes of age. *Nat. Rev. Immunol.* **2007**, *7*, 715–725. [[CrossRef](#)] [[PubMed](#)]
19. Heidl, S.; Ellinger, I.; Niederberger, V.; Walzl, E.E.; Fuchs, R. Localization of the human neonatal Fc receptor (FcRn) in human nasal epithelium. *Protoplasma* **2016**, *253*, 1557–1564. [[CrossRef](#)] [[PubMed](#)]
20. Scheibe, M.; Bethge, C.; Witt, M.; Hummel, T.; Article, O. Intranasal administration of drugs. *Arch. Otolaryngol. Head. Neck Surg.* **2008**, *134*, 643–646. [[CrossRef](#)] [[PubMed](#)]
21. Lochhead, J.J.; Thorne, R.G. Intranasal delivery of biologics to the central nervous system. *Adv. Drug Deliv. Rev.* **2012**, *64*, 614–628. [[CrossRef](#)] [[PubMed](#)]
22. Guilleminault, L.; Azzopardi, N.; Arnoult, C.; Sobilo, J.; Herve, V.; Montharu, J.; Diot, P. Fate of inhaled monoclonal antibodies after the deposition of aerosolized particles in the respiratory system. *J. Control. Release* **2014**, *196*, 344–354. [[CrossRef](#)] [[PubMed](#)]
23. Yoshida, M.; Masuda, A.; Kuo, T.T.; Kobayashi, K.; Claypool, S.M.; Takagawa, T.; Kutsumi, H.; Azuma, T.; Lencer, W.I.; Blumberg, R.S. IgG transport across mucosal barriers by neonatal Fc receptor for IgG and mucosal immunity. *Springer Semin. Immunopathol.* **2006**, *28*, 397–403. [[CrossRef](#)] [[PubMed](#)]
24. Pyzik, M.; Rath, T.; Lencer, W.I.; Baker, K.; Blumberg, R.S. FcRn: The Architect Behind the Immune and Nonimmune Functions of IgG and Albumin. *J. Immunol.* **2015**, *194*, 4595–4603. [[CrossRef](#)] [[PubMed](#)]
25. Crowe, T.P.; Greenlee, M.H.W.; Kanthasamy, A.G.; Hsu, W.H. Mechanism of intranasal drug delivery directly to the brain. *Life Sci.* **2018**, *195*, 44–52. [[CrossRef](#)] [[PubMed](#)]

26. Junghans, R.P.; Anderson, C.L. The protection receptor for IgG catabolism is the beta2-microglobulin-containing neonatal intestinal transport receptor. *Proc. Natl. Acad. Sci. USA* **1996**, *93*, 5512–5516. [[CrossRef](#)] [[PubMed](#)]
27. Tzaban, S.; Massol, R.H.; Yen, E.; Hamman, W.; Frank, S.R.; Lapierre, L.A.; Hansen, S.H.; Goldenring, J.R.; Blumberg, R.S.; Lencer, W.I. The recycling and transcytotic pathways for IgG transport by FcRn are distinct and display an inherent polarity. *J. Cell Biol.* **2009**, *185*, 673–684. [[CrossRef](#)] [[PubMed](#)]
28. Ober, R.J.; Radu, C.G.; Ghetie, V.; Ward, E.S. Differences in promiscuity for antibody–FcRn interactions across species: Implications for therapeutic antibodies. *Int. Immunol.* **2001**, *13*, 1551–1559. [[CrossRef](#)] [[PubMed](#)]
29. Lobasso, S.; Lopalco, P.; Angelini, R.; Baronio, M.; Fanizzi, F.P.; Babudri, F.; Corcelli, A. Lipidomic analysis of porcine olfactory epithelial membranes and cilia. *Lipids* **2010**, *45*, 593–602. [[CrossRef](#)] [[PubMed](#)]
30. Glorieux, S.; Van den Broeck, W.; van der Meulen, K.M.; Van Reeth, K.; Favoreel, H.W.; Nauwynck, H.J. In vitro culture of porcine respiratory nasal mucosa explants for studying the interaction of porcine viruses with the respiratory tract. *J. Virol. Methods* **2007**, *142*, 105–112. [[CrossRef](#)] [[PubMed](#)]
31. Paik, S.; Lehman, M.; Seiden, A.M.; Duncan, H.J. Olfactory Biopsy. *Arch. Otolaryngol. Head Neck Surg.* **1992**, *118*, 731–738. [[CrossRef](#)] [[PubMed](#)]
32. Holbrook, E.H.; Wu, E.; Curry, W.T.; Lin, D.T.; Schwob, J.E. Immunohistochemical characterization of human olfactory tissue. *Laryngoscope* **2011**, *121*, 1687–1701. [[CrossRef](#)] [[PubMed](#)]
33. Ding, X.; Xie, F. Olfactory Mucosa: Composition, Enzymatic Localization, and Metabolism. In *Handbook of Olfaction and Gustation*; Doty, R.L., Ed.; CRC Press: Boca Raton, FL, USA, 2003; pp. 63–91. ISBN 9780203911457.
34. Debertin, A.S.; Tschernig, T.; Tönjes, H.; Kleemann, W.J.; Tröger, H.D.; Pabst, R. Nasal-associated lymphoid tissue (NALT): Frequency and localization in young children. *Clin. Exp. Immunol.* **2003**, *134*, 503–507. [[CrossRef](#)] [[PubMed](#)]
35. Graziadei, P.P.; Graziadei, G.M. Neurogenesis and neuron regeneration in the olfactory system of mammals. I. Morphological aspects of differentiation and structural organization of the olfactory sensory neurons. *J. Neurocytol.* **1979**, *8*, 1–18. [[CrossRef](#)] [[PubMed](#)]
36. Balin, B.J.; Broadwell, R.D.; Salcmant, M.; El-Kalliny, M. Entry of peripherally administered protein to the CNS in mouse, rat and squirrel monkey. *J. Comp. Neurol.* **1986**, *251*, 260–280. [[CrossRef](#)] [[PubMed](#)]
37. Warnken, Z.N.; Smyth, H.D.C.; Watts, A.B.; Weitman, S.; Kuhn, J.G.; Williams, R.O., III. Formulation and device design to increase nose to brain drug delivery. *J. Drug Deliv. Sci. Technol.* **2016**, *35*, 213–222. [[CrossRef](#)]
38. Samson, G.; García De La Calera, A.; Dupuis-Girod, S.; Faure, F.; Decullier, E.; Paintaud, G.; Vignault, C.; Scoazec, J.Y.; Pivot, C.; Plauchu, H.; et al. Ex vivo study of bevacizumab transport through porcine nasal mucosa. *Eur. J. Pharm. Biopharm.* **2012**, *80*, 465–469. [[CrossRef](#)] [[PubMed](#)]
39. Kyllar, M.; Štembírek, J.; Putnová, I.; Stehlik, L.; Odehnalová, S.; Buchtová, M. Radiography, computed tomography and magnetic resonance imaging of craniofacial structures in pig. *J. Vet. Med. Ser. C Anat. Histol. Embryol.* **2014**, *43*, 435–452. [[CrossRef](#)] [[PubMed](#)]
40. Illum, L.; Mistry, A.; Stolnik, S. Nose-to-Brain Delivery: Investigation of the Transport of Nanoparticles with Different Surface Characteristics and Sizes in Excised Porcine Olfactory Epithelium. *Mol. Pharm.* **2015**, *12*, 2755–2766. [[CrossRef](#)]
41. Morrison, E.E.; Costanzo, R.M. Morphology of the Human Olfactory Epithelium. *J. Comp. Neurol.* **1990**, *297*, 1–13. [[CrossRef](#)] [[PubMed](#)]
42. Moran, D.T.; Rowley, C.; Jafek, B.W.; Levell, M.A. The fine structure of the olfactory mucosa in man. *J. Neurocytol.* **1982**, *11*, 721–746. [[CrossRef](#)] [[PubMed](#)]
43. Wadell, C.; Björk, E.; Camber, O. Nasal drug delivery—Evaluation of an in vitro model using porcine nasal mucosa. *Eur. J. Pharm. Sci.* **1999**, *7*, 197–206. [[CrossRef](#)]
44. Morrison, E.E.; Costanzo, R.M. Morphology of olfactory epithelium in humans and other vertebrates. *Microsc. Res. Tech.* **1992**, *23*, 49–61. [[CrossRef](#)] [[PubMed](#)]
45. Muller, Y.A.; Chen, Y.; Christinger, H.W.; Li, B.; Cunningham, B.C.; Lowman, H.B.; de Vos, A.M. VEGF and the Fab fragment of a humanized neutralizing antibody: Crystal structure of the complex at 2.4 Å resolution and mutational analysis of the interface. *Structure* **1998**, *6*, 1153–1167. [[CrossRef](#)]
46. Farstad, I.N.; Halstensen, T.S.; Fausa, O.; Brandtzaeg, P. Heterogeneity of M-cell-associated B and T cells in human Peyer's patches. *Immunology* **1994**, *83*, 457–464. [[PubMed](#)]
47. Honoré, A.; Le Corre, S.; Derambure, C.; Normand, R.; Duclos, C.; Boyer, O.; Marie, J.-P.; Guérout, N. Isolation, characterization, and genetic profiling of subpopulations of olfactory ensheathing cells from the olfactory bulb. *Glia* **2012**, *60*, 404–413. [[CrossRef](#)] [[PubMed](#)]

48. Lischka, K.; Ladel, S.; Luksch, H.; Weigel, S. Expression patterns of ion channels and structural proteins in a multimodal cell type of the avian optic tectum. *J. Comp. Neurol.* **2018**, *526*, 412–424. [[CrossRef](#)] [[PubMed](#)]
49. Stützle, M.; Flamm, J.; Carle, S.; Schindowski, K. Nose-to-Brain delivery of insulin for Alzheimer's disease. *Admet Dmpk* **2015**, *3*, 190–202. [[CrossRef](#)]
50. Brandtzaeg, P.; Baekkevold, E.S.; Farstad, I.N.; Jahnsen, F.L.; Johansen, F.-E.; Nilsen, E.M.; Yamanaka, T. Regional specialization in the mucosal immune system: What happens in the microcompartments? *Immunol. Today* **1999**, *20*, 141–151. [[CrossRef](#)]
51. Reger, M.A.; Watson, G.S.; Frey, W.H.; Baker, L.D.; Cholerton, B.; Keeling, M.L.; Belongia, D.A.; Fishel, M.A.; Plymate, S.R.; Schellenberg, G.D.; et al. Effects of intranasal insulin on cognition in memory-impaired older adults: Modulation by APOE genotype. *Neurobiol. Aging* **2006**, *27*, 451–458. [[CrossRef](#)] [[PubMed](#)]
52. Reger, M.A.; Watson, G.S.; Green, P.S.; Baker, L.D.; Cholerton, B.; Fishel, M.A.; Plymate, S.R.; Cherrier, M.M.; Schellenberg, G.D.; Frey, W.H., II; et al. Intranasal Insulin Administration Dose-Dependently Modulates Verbal Memory and Plasma Amyloid- β in Memory-Impaired Older Adults. *J. Alzheimer's Dis.* **2008**, *13*, 323–331. [[CrossRef](#)]
53. Bourganis, V.; Kammona, O.; Alexopoulos, A.; Kiparissides, C. Recent advances in carrier mediated nose-to-brain delivery of pharmaceuticals. *Eur. J. Pharm. Biopharm.* **2018**, *128*, 337–362. [[CrossRef](#)] [[PubMed](#)]
54. Li, Z.; Palaniyandi, S.; Zeng, R.; Tuo, W.; Roopenian, D.C.; Zhu, X. Transfer of IgG in the female genital tract by MHC class I-related neonatal Fc receptor (FcRn) confers protective immunity to vaginal infection. *Proc. Natl. Acad. Sci. USA* **2011**, *108*, 4388–4393. [[CrossRef](#)] [[PubMed](#)]
55. Vogelzang, A.; Lozza, L.; Reece, S.T.; Perdomo, C.; Zedler, U.; Hahnke, K.; Oberbeck-Mueller, D.; Dorhoi, A.; Kaufmann, S.H.E. Neonatal Fc Receptor Regulation of Lung Immunoglobulin and CD103⁺ Dendritic Cells Confers Transient Susceptibility to Tuberculosis. *Infect. Immun.* **2016**, *84*, 2914–2921. [[CrossRef](#)] [[PubMed](#)]
56. Szikora, B.; Hiripi, L.; Bender, B.; Kacsokovics, I.; Iliás, A. Characterization of the interactions of rabbit neonatal Fc receptor (FcRn) with rabbit and human IgG isotypes. *PLoS ONE* **2017**, *12*, e0185662. [[CrossRef](#)] [[PubMed](#)]
57. Ishikawa, T.; Takizawa, T.; Iwaki, J.; Mishima, T.; Ui-Tei, K.; Takeshita, T.; Matsubara, S.; Takizawa, T. Fc gamma receptor IIb participates in maternal IgG trafficking of human placental endothelial cells. *Int. J. Mol. Med.* **2015**, *35*, 1273–1289. [[CrossRef](#)] [[PubMed](#)]
58. Rath, T.; Kuo, T.T.; Baker, K.; Qiao, S.W.; Kobayashi, K.; Yoshida, M.; Roopenian, D.; Fiebig, E.; Lencer, W.I.; Blumberg, R.S. The immunologic functions of the neonatal FC receptor for IGG. *J. Clin. Immunol.* **2013**, *33*, 9–17. [[CrossRef](#)] [[PubMed](#)]
59. Kempers, A.C.; Reza Nejadnik, M.; Rombouts, Y.; Ioan-Facsinay, A.; van Oosterhout, M.; Jiskoot, W.; Huizinga, T.W.J.; Toes, R.E.M.; Scherer, H.U. Fc gamma receptor binding profile of anti-citrullinated protein antibodies in immune complexes suggests a role for Fc γ RI in the pathogenesis of synovial inflammation. *Clin. Exp. Rheumatol.* **2018**, *36*, 284–293. [[PubMed](#)]
60. Stamou, M.; Grodzki, A.C.; van Oostrum, M.; Wollscheid, B.; Lein, P.J. Fc gamma receptors are expressed in the developing rat brain and activate downstream signaling molecules upon cross-linking with immune complex. *J. Neuroinflamm.* **2018**, *15*, 1–23. [[CrossRef](#)] [[PubMed](#)]
61. Thulin, N.; Wang, T. The Role of Fc Gamma Receptors in Broad Protection against Influenza Viruses. *Vaccines* **2018**, *6*, 36. [[CrossRef](#)] [[PubMed](#)]
62. Patel, M.R.; Hirani, S.N.; Patel, R.B. Microemulsion for nasal delivery of Asenapine maleate in treatment of schizophrenia: Formulation considerations. *J. Pharm. Investig.* **2018**, *48*, 301–312. [[CrossRef](#)]
63. Rinaldi, F.; Hanieh, P.N.; Chan, L.K.N.; Angeloni, L.; Passeri, D.; Rossi, M.; Wang, J.T.W.; Imbriano, A.; Carafa, M.; Marianecchi, C. Chitosan glutamate-coated niosomes: A proposal for nose-to-brain delivery. *Pharmaceutics* **2018**, *10*, 38. [[CrossRef](#)] [[PubMed](#)]
64. Kristensson, K.; Olsson, Y. Diffusion pathways and retrograde axonal transport of protein tracers in peripheral nerves. *Prog. Neurobiol.* **1973**, *1*, 85–109. [[CrossRef](#)]
65. Zhao, Z.; Nelson, A.R.; Betsholtz, C.; Zlokovic, B.V. Perspective Establishment and Dysfunction of the Blood-Brain Barrier. *Cell* **2015**, *163*, 1064–1078. [[CrossRef](#)] [[PubMed](#)]

66. Schlachetzki, F.; Zhu, C.; Pardridge, W.M. Expression of the neonatal Fc receptor (FcRn) at the blood-brain barrier. *J. Neurochem.* **2002**, *81*, 203–206. [[CrossRef](#)] [[PubMed](#)]
67. Garg, A.; Balthasar, J.P. Investigation of the Influence of FcRn on the Distribution of IgG to the Brain. *AAPS J.* **2009**, *11*, 553–557. [[CrossRef](#)] [[PubMed](#)]
68. Deane, R.; Sagare, A.; Hamm, K.; Parisi, M.; LaRue, B.; Guo, H.; Wu, Z.; Holtzman, D.M.; Zlovic, B.V. IgG-Assisted Age-Dependent Clearance of Alzheimer's Amyloid Peptide by the Blood-Brain Barrier Neonatal Fc Receptor. *J. Neurosci.* **2005**, *25*, 11495–11503. [[CrossRef](#)] [[PubMed](#)]
69. Zhang, Y.; Pardridge, W.M. Mediated efflux of IgG molecules from brain to blood across the blood-brain barrier. *J. Neuroimmunol.* **2001**, *114*, 168–172. [[CrossRef](#)]
70. Neutra, M.R.; Mantis, N.J.; Kraehenbuhl, J.P. Collaboration of epithelial cells with organized mucosal lymphoid tissues. *Nat. Immunol.* **2001**, *2*, 1004–1009. [[CrossRef](#)] [[PubMed](#)]
71. Jung, C.; Hugot, J.-P.; Barreau, F. Peyer's Patches: The Immune Sensors of the Intestine. *Int. J. Inflam.* **2010**, *2010*, 1–12. [[CrossRef](#)] [[PubMed](#)]
72. Owen, R.L.; Jones, A.L. Epithelial Cell Specialization within Human Peyer's Patches: An Ultrastructural Study of Intestinal Lymphoid Follicles. *Gastroenterology* **1974**, *66*, 189–203. [[CrossRef](#)] [[PubMed](#)]
73. Owen, R.L. Uptake and transport of intestinal macromolecules and microorganisms by M cells in Peyer's patches—A personal and historical perspective. *Semin. Immunol.* **1999**, *11*, 157–163. [[CrossRef](#)] [[PubMed](#)]
74. Griebel, P.J.; Kennedy, L.; Graham, T.; Davis, W.C.; Reynolds, J.D. Characterization of B-cell phenotypic changes during ileal and jejunal Peyer's patch development in sheep. *Immunology* **1992**, *77*, 564–570. [[PubMed](#)]
75. Yasuda, M.; Jenne, C.N.; Kennedy, L.J.; Reynolds, J.D. The sheep and cattle Peyer's patch as a site of B-cell development. *Vet. Res.* **2006**, *37*, 401–415. [[CrossRef](#)] [[PubMed](#)]
76. Akilesh, S.; Christianson, G.J.; Roopenian, D.C.; Shaw, A.S. Neonatal FcR Expression in Bone Marrow-Derived Cells Functions to Protect Serum IgG from Catabolism. *J. Immunol.* **2007**, *179*, 4580–4588. [[CrossRef](#)] [[PubMed](#)]
77. Baker, K.; Qiao, S.-W.; Kuo, T.T.; Aveson, V.G.; Platzer, B.; Andersen, J.-T.; Sandlie, I.; Chen, Z.; de Haar, C.; Lencer, W.I.; et al. Neonatal Fc receptor for IgG (FcRn) regulates cross-presentation of IgG immune complexes by CD8-CD11b+ dendritic cells. *Proc. Natl. Acad. Sci. USA* **2011**, *108*, 9927–9932. [[CrossRef](#)] [[PubMed](#)]
78. Yoshida, M.; Kobayashi, K.; Kuo, T.T.; Bry, L.; Glickman, J.N.; Claypool, S.M.; Kaser, A.; Nagaishi, T.; Higgins, D.E.; Mizoguchi, E.; et al. Neonatal Fc receptor for IgG regulates mucosal immune responses to luminal bacteria. *J. Clin. Investig.* **2006**, *116*, 2142–2151. [[CrossRef](#)] [[PubMed](#)]
79. Yoshida, M.; Claypool, S.M.; Wagner, J.S.; Mizoguchi, E.; Mizoguchi, A.; Roopenian, D.C.; Lencer, W.I.; Blumberg, R.S. Human neonatal Fc receptor mediates transport of IgG into luminal secretions for delivery of antigens to mucosal dendritic cells. *Immunity* **2004**, *20*, 769–783. [[CrossRef](#)] [[PubMed](#)]
80. Ye, L.; Zeng, R.; Bai, Y.; Roopenian, D.C.; Zhu, X. Efficient mucosal vaccination mediated by the neonatal Fc receptor. *Nat. Biotechnol.* **2011**, *29*, 158–165. [[CrossRef](#)] [[PubMed](#)]
81. Pabst, R. Mucosal vaccination by the intranasal route. Nose-associated lymphoid tissue (NALT)-Structure, function and species differences. *Vaccine* **2015**, *33*, 4406–4413. [[CrossRef](#)] [[PubMed](#)]
82. Sambuy, Y.; De Angelis, I.; Ranaldi, G.; Scarino, M.L.; Stamatii, A.; Zucco, F. The Caco-2 cell line as a model of the intestinal barrier: Influence of cell and culture-related factors on Caco-2 cell functional characteristics. *Cell Biol. Toxicol.* **2005**, *21*, 1–26. [[CrossRef](#)] [[PubMed](#)]
83. Röhm, M.; Carle, S.; Maigler, F.; Flamm, J.; Kramer, V.; Mavoungou, C.; Schmid, O.; Schindowski, K. A comprehensive screening platform for aerosolizable protein formulations for intranasal and pulmonary drug delivery. *Int. J. Pharm.* **2017**, *49*, 1–42. [[CrossRef](#)] [[PubMed](#)]
84. Dickinson, B.L.; Badizadegan, K.; Wu, Z.; Ahouse, J.C.; Zhu, X.; Simister, N.E.; Blumberg, R.S.; Lencer, W.I. Bidirectional FcRn-dependent IgG transport in a polarized human intestinal epithelial cell line. *J. Clin. Investig.* **1999**, *104*, 903–911. [[CrossRef](#)] [[PubMed](#)]

85. Gartzandia, O.; Egusquiaguirre, S.P.; Bianco, J.; Pedraz, J.L.; Igartua, M.; Hernandez, R.M.; Pr  at, V.; Belouqui, A. Nanoparticle transport across in vitro olfactory cell monolayers. *Int. J. Pharm.* **2016**, *499*, 81–89. [CrossRef] [PubMed]
86. Flamm, J.; Boscher, M.; Maigler, F.; Akana, C.; Lindemann, J.; Kleiner, S.; Sommer, F.; Schindowski, K. Standardized Refined Intranasal Administration for Region-Specific Intranasal Drug Deposition in Mice Established with 3D Rapid Prototypes under 3R Criteria. *Berl. Munch. Tierarztl. Wochenschr.* **2018**. Available online: <https://vetline.de/standardized-refined-intranasal-administration-for-region-specific-intranasal-drug-deposition-in-mice-established-with-3d-rapid-prototypes-under-3r-criteria/150/3130/108530> (accessed on 26 July 2018).



   2018 by the authors. Licensee MDPI, Basel, Switzerland. This article is an open access article distributed under the terms and conditions of the Creative Commons Attribution (CC BY) license (<http://creativecommons.org/licenses/by/4.0/>).

Simone Ladel, Patrick Schlossbauer, Johannes Flamm, Harald Luksch, Boris Mizaikoff, and Katharina Schindowski. 2019. Improved *In vitro* Model for Intranasal Mucosal Drug Delivery: Primary Olfactory and Respiratory Epithelial Cells Compared with the Permanent Nasal Cell Line RPMI 2650. *Pharmaceutics* 11, 8: 367. <https://doi.org/10.3390/pharmaceutics11080367>

© 2019 by the authors. Licensee MDPI, Basel, Switzerland. This article is an open access article distributed under the terms and conditions of the Creative Commons Attribution 4.0 International (CC BY 4.0) license (<http://creativecommons.org/licenses/by/4.0/>).



Article

Improved In Vitro Model for Intranasal Mucosal Drug Delivery: Primary Olfactory and Respiratory Epithelial Cells Compared with the Permanent Nasal Cell Line RPMI 2650

Simone Ladel ^{1,2,†}, Patrick Schlossbauer ^{1,†}, Johannes Flamm ¹, Harald Luksch ³ , Boris Mizaikoff ² and Katharina Schindowski ^{1,*}

¹ Institute of Applied Biotechnology, University of Applied Science Biberach, Hubertus-Liebrecht Straße 35, 88400 Biberach, Germany

² Institute of Analytical and Bioanalytical Chemistry, University of Ulm, Albert-Einstein-Allee 11, 89081 Ulm, Germany

³ School of Life Sciences, Technical University of Munich, Liesel-Beckmann-Straße 4, 85354 Freising-Weißenstephan, Germany

* Correspondence: schindowski@hochschule-bc.de; Tel.: +49-7351-582-498

† These authors contributed equally to this work.

Received: 24 June 2019; Accepted: 20 July 2019; Published: 1 August 2019



Abstract: Background: The epithelial layer of the nasal mucosa is the first barrier for drug permeation during intranasal drug delivery. With increasing interest for intranasal pathways, adequate in vitro models are required. Here, porcine olfactory (OEPC) and respiratory (REPC) primary cells were characterised against the nasal tumour cell line RPMI 2650. Methods: Culture conditions for primary cells from porcine nasal mucosa were optimized and the cells characterised via light microscope, RT-PCR and immunofluorescence. Epithelial barrier function was analysed via transepithelial electrical resistance (TEER), and FITC-dextran was used as model substance for transepithelial permeation. Beating cilia necessary for mucociliary clearance were studied by immunoreactivity against acetylated tubulin. Results: OEPC and REPC barrier models differ in TEER, transepithelial permeation and MUC5AC levels. In contrast, RPMI 2650 displayed lower levels of MUC5AC, cilia markers and TEER, and higher FITC-dextran flux rates. Conclusion: To screen pharmaceutical formulations for intranasal delivery in vitro, translational mucosal models are needed. Here, a novel and comprehensive characterisation of OEPC and REPC against RPMI 2650 is presented. The established primary models display an appropriate model for nasal mucosa with secreted MUC5AC, beating cilia and a functional epithelial barrier, which is suitable for long-term evaluation of sustained release dosage forms.

Keywords: barrier model; nose-to-brain; primary cells; RPMI 2650; olfactory epithelium; respiratory epithelium

1. Introduction

Drug delivery to the brain for the treatment of central nervous system (CNS)-related diseases became of great interest and one of the most challenging research areas in the last decade [1,2]. The brain has a unique barrier to restrict the entry of neurotoxic substances into the CNS: the blood–brain barrier (BBB). This endothelial barrier, with a low rate of pinocytosis and strong tight junctions, is a major hurdle in CNS drug delivery. Over the last years, the need for alternative drug delivery strategies became more and more obvious [3,4]. One of these strategies is the application of drugs via the intranasal route [5]. In contrast to invasive methods like intraparenchymal, intracerebroventricular, or intrathecal

injections/infusions, the noninvasive intranasal approach can be used for chronically given drugs potentially resulting in a higher patient compliance. Further advantages of the intranasal application are the large surface area for absorption, rapid uptake and the avoidance of the hepatic first-pass elimination. Disadvantages of this form of application are the limitation to potent drugs (only small volumes can be applied), the mucociliary clearance, and the physico-chemical features of the mucus layer (low pH, enzymatic degradation) [6,7]. In general, there are three relevant consecutive steps for nose-to-brain drug delivery (N2B): The first step is overcoming the epithelial barrier, the second step is the transport from the mucosa to sites of brain entry and the last step is the transport to other sites in the CNS [7]. In this work, for simplification only the first step is modelled. The nasal mucosa can be divided into four epithelial types: the squamous epithelium, the respiratory epithelium, the transitional epithelium and the olfactory epithelium. Of these epithelial types, the respiratory and the olfactory epithelium are most likely to be sites of substance uptake [8]. The detailed composition of those epithelial types have been extensively studied [9–12]. Briefly, the olfactory mucosa covers ~10% of the nasal cavity surface in man. It is characterised by a pseudostratified columnar epithelium that is located in the upper dorsal part of the nasal cavity. Olfactory sensory neurons are located in the epithelial layer, with neurites spanning from the nasal cavity into the olfactory bulb in the brain. In addition to these neurons, three further cell types are part of the olfactory epithelial layer: structuring sustentacular cells that function as epithelial supporting cells, tubular type duct cells from Bowman's glands and basal cells (progenitor cells) [13,14]. Approximately 90% of the human nasal mucosa is covered with the respiratory epithelium. This pseudostratified columnar secretory epithelium consist of goblet cells, ciliated cells, intermediate cells and basal cells [15].

There are two pathways to overcome the epithelial barrier of the respiratory and the olfactory epithelium: the intracellular pathway and the extracellular pathway. Intracellularly transported substances can either be endocytosed into olfactory sensory neurons and subsequently be transported to the brain via their axons, or they can be transported via transcytosis across sustentacular cells into the underlying connective tissue (*lamina propria*) [16–18]. The extracellular pathway comprises paracellular diffusion into the *lamina propria* through intercellular clefts [18]. The drug's pathway through the mucosa mainly depends on its lipophilicity and the molecular weight [19]. For small and low molecular weight hydrophilic molecules, such as fluorescein-labelled isothiocyanate-dextran (FITC-dextran; 4.4 kD) or sodium fluorescein (0.37 kD), mainly the paracellular pathway is reported [20–25]. These nontoxic and easily detectable fluorescence labelled chemicals are widely used model substances for drug permeation studies [22,23,26]. In contrast, the transcellular transport is described for large molecules such as proteins [27].

To sum up, the nasal mucosa has become a focus of interest for drug application, to overcome the BBB issue. However, for research the olfactory mucosa as well as the dorsal part of the respiratory mucosa is rather difficult to access [28]. A feasible and simple solution may be the use of *post-mortem* porcine mucosa. The pig's nasal mucosa resembles well the human nasal histology and physiology [29]. The approach to use pigs as model organism for ex vivo mucosa-related experiments is well established [29–33]. The major problem using ex vivo mucosa explants is the limited lifespan of the tissue even under nutritional support. A promising alternative are in vitro models, using epithelial cells under controlled external experimental conditions, allowing a simplification to display only the first barrier without considering blood flow, systemic distribution and other *lamina propria*-related effects [26]. There are two different approaches available for the establishment of in vitro epithelial barrier models. First, there are standard tumour cell lines like the human nasal epithelial cell line RPMI 2650, and primary epithelial cell models can be cultivated as second option [34,35]. These two cell types vary greatly in their lifespan and their differentiation ability. In theory, tumour cell lines are immortal, whereas primary cells are limited to a certain number of cell divisions [36]. However, most tumour cells lack the ability to fully differentiate into, e.g., ciliated or mucus producing cells, while primary cell cultures are morphologically and physiologically very close to their native state [26,37]. As factors such as cilia and mucus can possibly influence the drug uptake time and the bioavailability

due to, e.g., enzymes even in stagnant cell culture, these are important parameters to consider for drug permeation evaluations. This is especially important to evaluate drug potential in vitro for simulations of the whole nasal mucosa as it was recently built up by Na et al. (2017) with commercially available human nasal primary cells [38].

Epithelial cell features such as the presence of cilia, mucus secretion and tight junction formation are important factors that influence the bioavailability of nasally applied drugs [7]. Generally, a heterogenic mixture of different cell types is preferred for a valid model, since this better represents the mucosal epithelial assembly in respect to the permeation profile of drugs through the cellular barrier [37,39]. Furthermore, cultured tumour cells tend to build multilayers, as their growth is mostly not limited by contact inhibition after reaching confluency, whereas primary cells remain in monolayers. For epithelial barrier models, monolayers should be preferred as these resemble the natural epithelial structure more closely. Nevertheless, there are several studies proving the tumour cells line originating from nasal squamous epithelium (septum) RPMI 2650 is a suitable model for the nasal epithelium [20,21,26,37,40]. This cell line is closely related to normal human nasal epithelium in terms of its karyotype and the cytokeratin polypeptide pattern as well as the presence of mucus on the cell surface [34,35,41]. Also the metabolic features of the cellular barrier were shown to be vaguely similar to the one of excised human nasal tissue [42,43]. A special characteristic of nasal epithelial cells is their ability to adapt to growth under air–liquid interface (ALI) conditions. The vast majority of recently developed cellular airway models use this method developed by Tchao et al. (1989) [44]. Hereby, cells are grown on porous plastic membrane inserts in multiwell plates with basolateral medium supply whereas the apical side of the cellular layer is exposed to air. These ALI conditions naturally drive cells to form strong tight junctions and to start differentiating towards, e.g., ciliated or mucus producing cells [45–47]. Hereby, the lack of differentiation of tumour cells can be a major problem to mimic epithelial barriers. In an attempt to validate these different approaches, Mercier et al. (2018) postulated generally accepted key criteria that appropriate in vitro barrier cell models should meet [37]. These key criteria comprise a sufficient high transepithelial electrical resistance (TEER) coupled with the presence of specific tight junction proteins such as *zonula occludens* 1 (ZO-1) and adherents junction proteins such as E-cadherin when grown under ALI conditions [48,49]. Furthermore, cellular models must allow a measurement of paracellular permeability and ideally express drug transporters for transcellular permeation. The ability to measure paracellular permeation of small to medium sized model substances like sodium fluorescein or FITC-dextran and the screen for cilia and marker proteins such as ZO-1 and mucins allows a comparison of different models.

In our research group, we focus on region-specific model development and application methods for the olfactory mucosa and for nose-to-brain drug delivery. Flamm et al. recently published a method to deliver drugs directly to the olfactory region in mice [50]. Furthermore, Röhm et al. established a screening platform for aerosolizable protein formulations for intranasal drug delivery [51].

In accordance to former investigations, in this study an epithelial barrier model for intranasal delivery was established and characterised that used olfactory and respiratory primary cells. We considered criteria that strongly affect intranasal delivery such as mucin production and cilia formation important for mucociliary clearance. First, the differences between respiratory and olfactory primary cells were investigated. Second, the primary cell barrier models were evaluated and compared against the well-established tumour cell line RPMI 2650. The suitability and feasibility of primary cells as nasal epithelial barrier models for intranasal delivery studies was determined by immunofluorescence, molecular and biochemical investigations of marker proteins, TEER value determination and FITC-dextran permeation.

2. Materials and Methods

2.1. Cell Culture

2.1.1. Primary Cells

Primary cells were harvested from mucosal explants from the respiratory and olfactory region of 4–6-month-old slaughterhouse pigs. Respiratory tissue was dissected with a short *post-mortem* delay of below 1.5 h from the *concha nasalis ventralis* (*c.n. ventralis*) and olfactory tissue from the dorsal part of the *concha nasalis dorsalis* (*c.n. dorsalis*) and the *concha nasalis media* (*c.n. media*) (see Figure 1). The dissected mucosa explants were disinfected using Octenisept® (Schülke & Mayr GmbH, Norderstedt, Germany) and washed twice with PBS (cell culture grade, Gibco® Invitrogen, Darmstadt, Germany). The epithelial cells were isolated from the connective tissue by incubation for 1 h at 37 °C with 1.4 mg/mL pronase (Sigma-Aldrich, Taufkirchen, Germany) in EBSS (Gibco® Invitrogen, Darmstadt, Germany), 20 U Penicillin-20 µg Streptomycin (PenStrep (10,000 U), AppliChem, Darmstadt, Germany), and 300 I.U./mg gentamycinsulfate (≥590 I.U./mg, Carl Roth, Karlsruhe, Germany; pronase medium, Table 1). To obtain isolated cells the pronase–mucosa suspension was gently agitated, the liquid was carefully removed, and subsequently centrifuged at 700 rpm for 3 min. The supernatant was discarded and the remaining cells resuspended in appropriate volumes of primary culture adhesion medium (DMEM:F12 (1:1), 20% FBS, 2 mM Gln, 1% NEAA, 20 U Penicillin-20 µg Streptomycin, 300 I.U./mg gentamycinsulfate, Table 1). It should be noted that the cultivation in T175 cell culture flasks was highly inefficient compared to smaller formats.

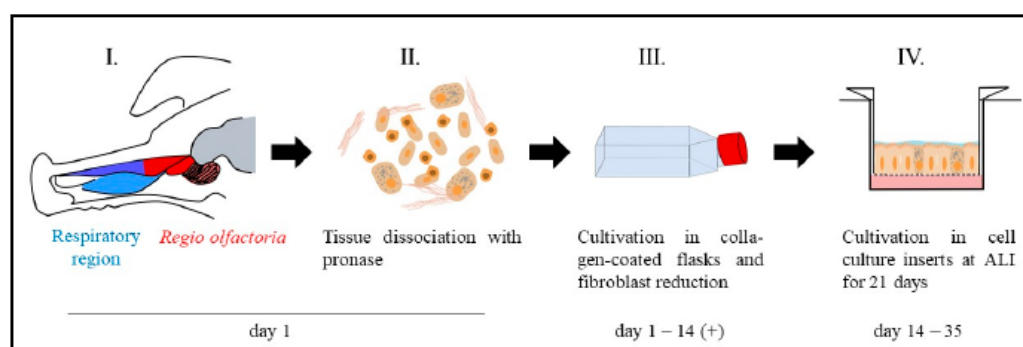


Figure 1. Workflow for primary cell isolation and cultivation under air–liquid interface (ALI) conditions. The mucosa was dissected either from the olfactory region (red) or the respiratory region (blue) (I). Single cells were obtained by pronase digestion of the mucosa explants (II). Single cells were cultivated in collagen-coated T75 cell culture flasks (III). To reduce fibroblast overgrowth, the culture was shortly trypsinated (2–4 min) to get rid of the less adherent fibroblasts and select for epithelial cells. The cells were cultivated up to 80–90% confluence in the T75 flasks and transferred into cell culture inserts to grow under ALI conditions for 21 days (IV.).

The cells were seeded in collagen-coated cell culture T flasks (T flasks were incubated in advance with 0.05 mg/mL rat tail collagen solution (Primacyte, Schwerin, Germany) for 24 h at 37 °C) with a cell density of $\sim 10^6$ cells/mL and cultivated at 37 °C, 5% CO₂ and 95% rH. The medium was changed to primary culture medium (DMEM: F12 (1:1), 10% FBS, 2 mM Gln, 1% NEAA, 20 U Penicillin-20 µg Streptomycin, 300 I.U./mg gentamycinsulfate, Table 1) after 24 h. The exchange was necessary to contain fibroblast growth due to reduced serum concentration. Cells were regularly split by trypsinization (Trypsin/EDTA, Biochrom, Berlin, Germany) for 10 min at 80% confluence.

Table 1. Composition of the cultivation media used in this work. EBSS = Earle's balanced salt solution; FBS = Foetal bovine serum; Gln = Glutamine; DMEM = Dulbecco's modified Eagle's medium; MEM = minimal essential medium.

Name	Composition
Primary culture adhesion medium	DMEM:F12 (1:1), 20% FBS, 2 mM Gln, 1% NEAA, 0.4 U/mL Penicillin-0.4 µg/mL Streptomycin, 0.6 I.U. Gentamycinsulfate
Primary culture medium	DMEM:F12 (1:1), 10% FBS, 2 mM Gln, 1% NEAA, 0.4 U/mL Penicillin-0.4 µg/mL Streptomycin, 0.6 I.U. Gentamycinsulfate
Pronase medium	EBSS + 1.4 mg/mL Pronase + 0.4 U/mL Penicillin-0.4 µg/mL Streptomycin, 0.6 I.U. Gentamycinsulfate
RPMI 2650 medium	MEM, 10% FBS, 2 mM Gln, 0.4 U/mL Penicillin-0.4 µg/mL Streptomycin

For fibroblast depletion, the culture was incubated with trypsin/EDTA solution for 4 min at 37 °C twice a week. The fact that fibroblasts adherent less strongly to the cell culture flask surface was used to reduce fibroblasts by regular short-time trypsination steps. The supernatant containing fibroblasts was discarded whereas the remaining adhered epithelial cells were washed with PBS. Fresh cultivation medium was added.

For seeding in cell culture inserts (ThinCert™, Greiner Bio-one, Frickenhausen, Germany), primary cells were isolated from T-flasks by a two-step trypsination to deplete remaining fibroblasts (Figure 1, IV). The cell culture was first treated with trypsin/EDTA solution for 4 min and the supernatant was removed. Subsequently, an additional trypsination step for 6 min was carried out to remove the epithelial cells. Membrane inserts were collagen coated as described before for the cell culture flasks and seeded with 1×10^5 cells per insert. The cells were cultured submerged for one day in the cell culture inserts. After 24 h, the apical medium was removed to cultivate cells under ALI conditions (260 µL medium per well) for 21 days. Cells were apically washed with 200 µL PBS and medium (260 µL/well) was changed every two days.

2.1.2. RPMI 2650 Cultivation

RPMI 2650 cells were cultivated in RPMI 2650 medium (MEM, 10% FBS, 2 mM Gln, 10 U Penicillin-10 µg Streptomycin, Table 1) at 37 °C, 5% CO₂ and 95% rH. Cells were regularly split at 80–90% confluency by a 5 min trypsination (trypsin/EDTA) treatment.

For permeation experiments, RPMI 2650 cells with passage numbers below 16 were seeded in cell culture inserts (ThinCert™, Greiner Bio-one, Frickenhausen, Germany) with a density of 1×10^5 cells per insert. After 24 h under submerged conditions, the apical volume was removed and the cells were cultivated under ALI conditions for 21 days. The ALI culture was washed every two days apically with 200 µL prewarmed PBS to remove diffused medium. Furthermore, 260 µL fresh medium was applied basolateral.

2.1.3. TEER Measurement

To evaluate the integrity of the cell layer the transepithelial electrical resistance measurement was used. Therefore, the cell culture inserts were filled apically with 350 µL MEM without phenol red (Gibco®, Invitrogen, Darmstadt, Germany) and basolateral filled with 500 µL MEM. For equilibration, cells were incubated for 20 min at 37 °C and 15 min cooled to room temperature (RT). The TEER value of each cell-covered membrane was determined in triplicates using an EVOM epithelial voltohmmeter and chopstick electrodes (World Precision Instruments, Sarasota, FL, USA). The raw data were processed by a blank subtraction (inserts without cells) and the multiplication by the growth area of the membrane (0.336 cm^2).

2.2. Permeation

To perform the permeation experiments, the medium was changed to 260 μ L MEM without phenol red. For primary cells 10% FBS was added to the medium. To analyse fluorescein isothiocyanate-dextran solution (FITC-dextran) permeation, 100 μ L of a solution with 500 μ g/mL FITC-dextran (Sigma Aldrich, Taufkirchen, Germany) in PBS was applied on the apical surface of the cell layer. The experiments were carried out under normal cell culture conditions at 37 °C, 5% CO₂ and 95% rH. Permeation was studied for 24 h. A volume of 20 μ L was taken as sample from the basolateral compartment at 0.5 h, 1 h, 2 h, 3 h, 4 h, 6 h, 8 h and 12 h. To keep the basolateral volume constant, 20 μ L fresh medium was added. The samples were diluted 1:5 with PBS and analysed via fluorescence spectrometry (Spectra Max M5e, Molecular Devices, San Jose, CA, USA) at 490/520 nm.

2.3. Immunofluorescence Staining

Immunofluorescence (IF) staining was performed as described previously [31], with the difference that the cell-covered membranes were stained directly in the cell culture insert and transferred to an object slide as last step. Briefly, slides were washed with PBS pH 7.4 three times for 5 min, followed by blocking with block solution (4% BSA, 0.5% Saponin and 10% normal goat serum in PBS pH 7.4) for at least 2 h or overnight. The primary antibodies (Table 2) were diluted 1:100 in blocking buffer without normal goat serum and incubated in the cell culture insert for 24 to 48 h at 4 °C. Subsequently, the slices were washed (5 min, 10 min, and 15 min) and incubated with the adequate secondary antibodies (Table 2, 1:500 diluted in PBS pH 7.4) for 2 h. After washing again three times slides were mounted with Fluoroshield™ mounting medium containing DAPI (4',6-diamidin-2-phenylindol; Sigma-Aldrich, Taufkirchen, Germany).

Table 2. List of antibodies used in this study. FITC: fluorescein-isocyanate; HRP: horseradish peroxidase; ZO-1: zonula occludens-1.

Antibody	Antigen	Immunogen	Host	Source, Cat. #
Anti-MUC5AC Antibody (45M1)	Peptide core of gastric mucin M1 (Mucin 5AC)	M1 mucin	mouse	Novus biologicals, Centennial, CO, USA, Cat. #NBP2-15196
Anti-ZO-1 (ZMD. 437)	ZO-1	synthetic peptide derived from the N-terminal region of human, dog, mouse, and rat ZO-1	rabbit	Thermo Fisher Scientific, Dreieich, Germany, Cat. #40-2300
Anti-acetylated tubulin (6-11B-1)	Acetylated tubulin	acetylated tubulin from the outer arm of <i>Strongylocentrotus purpuratus</i>	mouse	Sigma Aldrich, Taufkirchen, Germany, Cat. #T7451
Anti- β Actin (AC-15)	β Actin	not specified	mouse	Sigma Aldrich, Taufkirchen, Germany, Cat. #A5441
Anti-murine IgG-Alexa Fluor® 488	whole molecule mouse IgG	not specified	Goat	Jackson Immuno Research Europe Ltd., Cambridgeshire, UK, Cat. #115-545-003
Anti-rabbit IgG-Rhodamine Red™-X	whole molecule rabbit IgG	not specified	donkey	Jackson Immuno Research Europe Ltd., Cambridgeshire, UK, Cat. #711-295-152
Anti-murine IgG-HRP	whole molecule mouse IgG	not specified	goat	Sigma Aldrich, Taufkirchen, Germany, Cat. #AP5278
Anti-rabbit IgG-HRP	Whole molecule rabbit IgG	not specified	Goat	Jackson Immuno Research Europe Ltd., Cambridgeshire, UK, Cat. #111-035-003

2.4. Cryosectioning and Colorimetric Staining of Cell Culture Insert Membranes

Cell culture inserts were fixed in 4% paraformaldehyde for 10 min, cryo-conserved in 30% sucrose overnight and stored at 4 °C until sectioning. Before sectioning, the membranes were embedded in gelatine (7.5% gelatine and 30% sucrose in PBS [52]) to allow precise adjustment for sectioning. The membranes were cut in 14 μ m slices using a cryostat at −25 °C (HM525 NX, Thermo Fisher

Scientific, Dreieich, Germany) and mounted on Superfrost® Plus Micro slides (VWR, Darmstadt, Germany). For hematoxylin-eosin staining, slides were washed with distilled water for 1 min, followed by a 5 min hematoxylin staining step. The slides were destained under running tap water for 3 min, and counterstained with Eosin Y-0.5% acidic acid (Sigma-Aldrich, Taufkirchen, Germany) for 5 min. After an additional destaining step (0.5 min), the slides were dehydrated (75% ethanol, 96% ethanol, 100% ethanol, Xylene; 2 min each) and mounted in Eukitt®Quick hardening mounting medium (Sigma-Aldrich, Taufkirchen, Germany).

2.5. Reverse Transcription PCR (RT PCR)

The transcript analysis was carried out as described before [31]. Briefly, the total RNA was isolated from cell lysates using TRIzol (Invitrogen™, Dreieich, Germany) according to the manufacturer's instructions. For reverse transcription, 1 µg of total RNA was used. Via oligo dT15 primers (Bioron, Ludwigshafen, Germany) and 400 U Reverse® (Bioron, Ludwigshafen, Germany) mRNA was transcribed to cDNA.

For PCR analysis of the cDNA library 1 µg cDNA, 1 µM primers (see Table 3), 25 mM MgCl₂, 2.5 mM dNTP Mix and 0.5 U/µL Taq polymerase were diluted in 10× Taq-PCR buffer (all Bioron, Ludwigshafen, Germany).

Table 3. Primer sequences of the targets MUC5AC and β-actin for RT-PCR.

mRNA Targets	Forward Primer (5'-3')	Reverse Primer (5'-3')
MUC5AC	CCGGGCCTGTGCAACTA	GTTCCCAAACCTCGATAGGGC
β-actin	GACACCAGGGCGTGATGG	GCAGCTCGTAGCTCTTCTCC

The PCR reaction was performed with the following parameters: initial denaturation for 30 s at 95 °C, 40 cycles with denaturation at 95 °C for 30 s, annealing at 60 °C for 30 s, elongation at 72 °C for 60 s and a final elongation at 72 °C for 10 min. The PCR products were analysed using agarose gel electrophoresis.

2.6. Dot Blot

MUC5AC expression was analysed via dot blot as the high molecular weight protein is difficult to analyse via western blot [53]. Samples were collected from apical washing of ALI cultures with PBS as well as from tissue and cell lysates. The lysates were obtained as described before [31]. For dot blot analysis, 2 µL of these samples were applied onto a nitrocellulose membrane. The membrane was blocked by incubation with 5% skimmed milk powder (in PBS pH 7.4, 0.1% Tween20 (PBST)) for 2 h at RT. The anti-MUC5AC primary antibody (Table 2) was diluted 1:5000 in PBST and incubated for 24 h at 4 °C. The membrane was washed 4 times with PBST, and subsequently incubated with the HRP-coupled secondary antibody (dilution 1:4000 in PBST, Table 2) for 1 h at RT. After another 4 washing steps, the membrane was developed by using the chemiluminescence substrate Immobilon® (Merck Millipore, Darmstadt, Germany). The analysis was carried out by Fusion FX Imaging systems (VILBER Lourmat, Collégien, France) and Image J (java.version: 1.8.0_171, National Institute of Health, Bethesda, MD, USA).

2.7. Western Blot

The western blot was performed as described before [31]. Briefly, the cell lysates were made by using chilled RIPA cell lysis buffer (10 mM Tris-Cl, pH 8.0; 1 mM EDTA, 0.5 mM EGTA, 1% Triton X-100; 0.1% sodium deoxycholate, 0.1% SDS and 140 mM NaCl; and protease inhibitor mix (Thermo Fisher Scientific, Dreieich, Germany) and gentle agitation. Equal volumes of homogenized tissue were loaded, separated in a 12.5% SDS PAGE and blotted onto a nitrocellulose membrane (Carl Roth, Karlsruhe, Germany). The membrane was blocked (5% skimmed milk powder in PBS/0.1% Tween20, pH 7.4).

Primary antibodies (Table 2, 1:5000) were incubated overnight at 4 °C. Secondary antibodies were diluted 1:100,000 (Anti-rabbit IgG-HRP) and 1:4000 (Anti-murine IgG-HRP). Signal detection was carried out by developing the membrane with the chemiluminescence substrate Immobilon® (Merck Millipore, Darmstadt, Germany) according to the manufacturer's instructions.

2.8. Statistics

Data were assessed for significance using unpaired *t*-test (GraphPad Prism 8) comparing the primary nasal cells to the RPMI 2650 cell line. The exact repeat numbers are divided into technical replicates (*n*) and biological replicates (*N*) meaning different pigs and are addressed in the subtitles of the graphs.

3. Results

The increasing interest in intranasal delivery requires the development and the evaluation of specialized in vitro models to reduce the use of laboratory animals for drug transport and permeation studies. These models should display the main parameters of the mucosa that influence the drug permeation. Here, we defined the most important parameters as the growth in defined monolayers, the formation of cilia (drug clearance), tightly connected cell layers and the physico-chemical environment (mucus). The actual state of the art model for nasal epithelial cells is the tumour cell line RPMI 2650 [21,39]. As an alternative to tumour cells lines, primary cell models are moving more and more into focus in many fields. Here, the aim of this study was to establish a robust protocol for nasal primary epithelial cell cultivation and to develop an appropriate primary epithelial cell model. This model should especially display the first epithelial barrier during intranasal drug delivery, and hence will be compared to the standard in vitro cellular model.

3.1. Evaluation of Nasal Primary Cells and RPMI 2650 Concerning Olfactory Mucosa Model Characteristica-Monolayer, Tight Growth, Cilia and Mucus Production

A general observation of primary nasal cell cultivation was the slow growth of epithelial cells along with faster growth of undesired fibroblasts and the rapid growth of bacterial contaminations (Figure 2A,B). For fibroblast growth we have determined the content of serum in the cell culture medium to be the most influencing factor. Primary cells displayed poor adherence to the collagen coated cell culture flasks at serum levels of 10%. Increasing the serum concentration to 20% resulted in primary cells that were adherent on collagen-treated cell culture flasks after 3–4 h. However, a serum content of 30% increased, above all, the growth of fibroblasts and decreased the growth of epithelial cells. Therefore, despite the positive effects on adhesion to cell flask surface the negative effects on fibroblasts' growth counterbalanced these benefits. Hence, seeding the cells in 20% serum content followed by a change to 10% serum after adhesion (5 h) turned out to be method of choice to culture the primary porcine nasal epithelial cells.

Morphologically, a majority of respiratory epithelial primary cells (REPC) and olfactory epithelial primary cells (OEPC) appeared in the typical flat and squared cobblestone shape with sizes varying from 10 µm to 100 µm (Figure 2C,D). Particularly in REPC cultures, some cells were detected that contained larger vesicles (Figure 2E). These cells had morphological similarities to goblet or gland cells. Ciliated cells were observed in OEPC and REPC, however REPC showed considerably more cells with motile cilia, whereas in OEPC primary, non-motile cilia were also present (Figure 2F). The motile cilia showed a median length of 10 µm with a beating frequency of >5 Hz (Supplementary Materials Video S1).

To investigate the general cell growth of primary nasal epithelial cells and the tumour cell line RPMI 2650 after 21 days under ALI conditions, colorimetric staining (Hematoxylin/Eosin, Figure 3A–C) of cryosections of cell-covered membranes was performed. OEPC and REPC grew in monolayers under ALI conditions whereas the RPMI 2650 cells formed up to 10 layers. In contrast to OEPC, REPC cultures consisted of larger and smaller cells resulting in an uneven monocellular layer surface (Figure 3B). Additionally, the distribution of cilia and the formation of tight junctions were determined

using immunofluorescence (IF) staining against acetylated α -tubulin (cilia marker [54]) and ZO-1 (tight junction marker [55]) (Figure 3D–F). OEPC demonstrated the highest signal for the cilia marker acetylated α -tubulin. IF against ZO-1 showed that REPC formed the highest number of tight junctions. Only a weak signal for both marker proteins was observed in RPMI 2650.

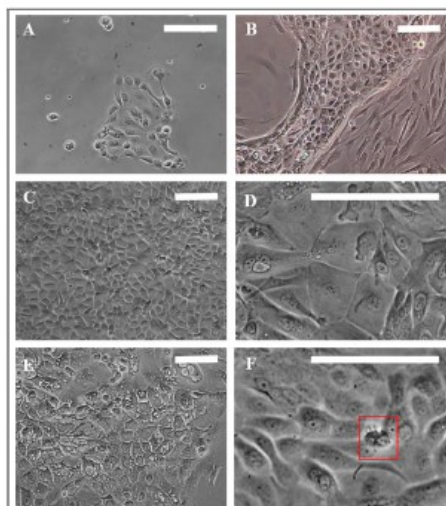


Figure 2. Morphology of porcine primary nasal epithelial cells. (A) Olfactory primary cells, 24 h in culture. (B) Fibroblast contamination in primary epithelial cells. (C,D) Morphological appearance of OEPC and REPC: small round or cobblestone shaped and big flat epithelial cells; cell membranes are clearly visible. (E) REPC: vesicular cells. (F) Red box: Ciliated cells can be motile or non-motile (beating frequency of >5 Hz). Cilia length was ~10 μ m. OEPC: olfactory epithelial primary cells; REPC: respiratory epithelial primary cells; Scale bars: 100 μ m.

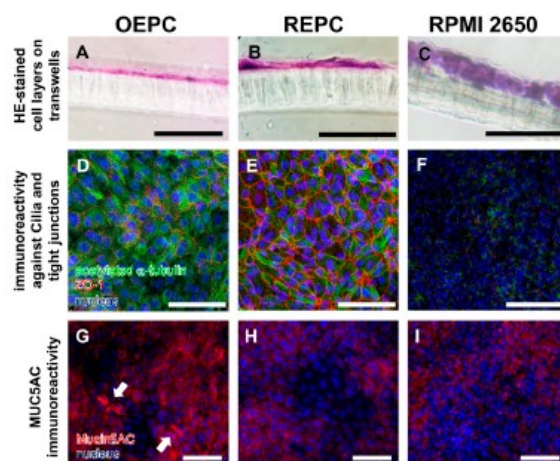


Figure 3. Characterisation of olfactory and respiratory primary cells in comparison to the standard cell line RPMI 2650. Monolayers are necessary to evaluate transport over the epithelial layer in the nasal mucosa: 14 μ m sections were made of olfactory epithelium primary cells (OEPC, A), respiratory epithelial primary cells (REPC, B) and RPMI 2650 (C) grown on a cell insert membrane for 21 days. Morphological features such as tight junctions and the formation of cilia are important influencing factors in investigations of drug permeation and clearance studies. Acetylated α -tubulin is a common marker for cilia [54]. IF double-staining of acetylated α -tubulin and the tight junction marker zonula occludens-1 (ZO-1) of ALI cultures of OEPC (D), REPC (E) and RPMI 2650 (F) after 21 days of incubation were made. An additional feature of mucosal cells is the ability to produce mucus. The marker protein mucin 5AC was used in this work, because the olfactory mucosa is to be simulated above all to investigate nose-to-brain transport. Again, IF was performed in OEPC (G), REPC (H) and RPMI 2650 (I). Scale bars: 100 μ m.

Beyond cilia and tight junctions, the physico-chemical environment of the epithelium also has an influence on intranasally administered substances. Therefore, the production of the mucin MUC5AC was investigated using IF (Figure 3G–I), RT-PCR (Figure 4A) and dot blot (Figure 4B). Both the dot blot cell lysate analysis, as well as the IF analysis, showed that OEPC have the highest immunoreactivity against MUC5AC. In the RT PCR no significant difference between *c.n. media* and the nasal primary epithelial cells could be observed. In contrast, the RPMI 2650 cells showed a significantly lower MUC5AC transcript level and no signal in the dot blot. Immunolabelling against MUC5AC resulted in weak signals in RPMI 2650 and REPC compared to OEPC.

Furthermore, we analysed the presence of secreted MUC5AC on the apical surface of the OEPC ALI cultures by washing the luminal compartment each 3 to 4 days. The supernatant of the washing buffer was then analysed by dot blot for immunoreactivity against MUC5AC (Figure 4C). At day 6 under ALI conditions the highest signal was observed. After 10 days the protein level appeared to stay at a constant level up to 20 days.

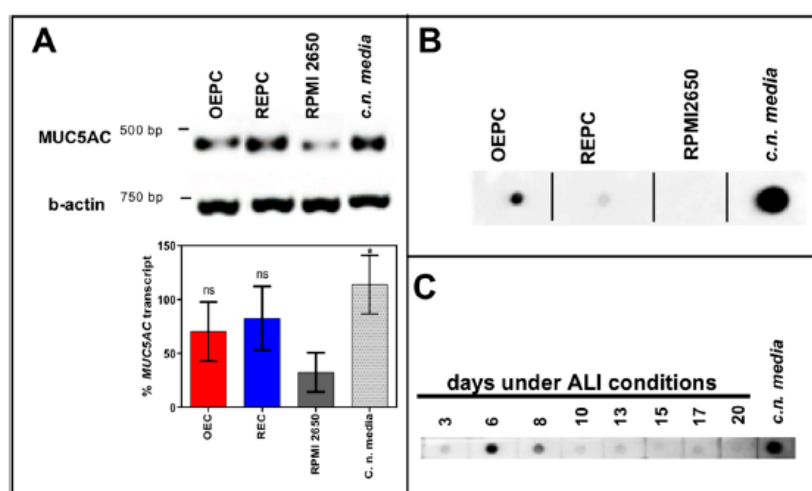


Figure 4. Mucin MUC5AC expression and immunoreactivity in primary cells of the nasal cavity. (A) Transcription analysis (RT-PCR) of MUC5AC gene in olfactory epithelial primary cells (OEPC), respiratory epithelial primary cells (REPC), tumour cell line RPMI 2650 and the *concha nasalis media* (*c.n. media*). MUC5AC transcript signal was referenced to beta-actin transcript signal. The significance was calculated by comparison of the OEPC, REPC and RPMI 2650 data with the *c.n. media* transcription data using an unpaired t-test. * $p < 0.05$; $n = 4$; error bars represent mean \pm SD. (B) Dot blot analysis of MUC5AC protein in lysates of OEPC, REPC, RPMI 2650 and *c.n. media*. All OEPC and REPC cultures shown in (A,B) were cultivated for 14 days in vitro in T flasks. (C) Immunoreactivity against MUC5AC in OEPC that were first cultured for 7 days in T flask with a minimum confluency of 70% then under ALI conditions additional 20 days. Apically secreted mucus was collected at the days indicated corresponding to a mucin production of 2 to 3 days. Statistical analysis: unpaired t-test, * $p < 0.05$ compared to the standard model RPMI 2650.

3.2. FITC-Dextran Permeation Through RPMI 2650 and Nasal Primary Cell Barriers

The analysis of the TEER values of 21 days ALI cultures of RPMI 2650, OEPC and REPC ALI revealed that REPC with $846 \pm 550 \Omega \text{ cm}^2$ displayed the highest TEER values followed by OEPC ($648 \pm 371 \Omega \text{ cm}^2$) and last RPMI 2650 ($66 \pm 5 \Omega \text{ cm}^2$; Figure 5A). Analogous to the permeation data, the nasal primary cells showed considerably higher variability displayed as higher standard deviations compared to RPMI 2650. The highest TEER value measured for OEPC was $1000 \Omega \text{ cm}^2$, whereas REPC reached a TEER value of $1600 \Omega \text{ cm}^2$.

To evaluate cell barrier function, TEER values of the cell layers after 21 days under ALI conditions were determined and permeation of FITC-dextran was analysed from the luminal/apical to the abluminal/basolateral compartment. Determination of permeability was performed over 24 h with

different sampling times. The results were compared to a diffusion control without cells (cell culture insert membrane only). Here, RPMI 2650 showed the highest permeability at all times investigated in comparison to OEPC and REPC. After 24 h, $11.7 \pm 0.9\%$ of FITC-dextran permeated through RPMI 2650 cells, whereas OEPC showed a permeation of $3.1 \pm 2.0\%$ and REPC resulted in $3.7 \pm 2.0\%$ FITC-dextran (Figure 5B). An equilibrium is obtained for FITC-dextran in the luminal and abluminal compartment of the insert. It should be noted that this equilibrium establishes earlier in the control insert without cells and limits the maximal flux of molecules in this static system (see Supplementary Materials Figure S1A,B). As the published literature usually does not acknowledge this fact, we normalized these results to the maximal concentration of FITC-dextran that is able to diffuse to the abluminal compartment within the same time (Supplementary Materials Figure S1B). The molecular flux was calculated for each cell type investigated and displayed as the amount of FITC-dextran that was able to cross the epithelial barrier per time and distance (Figure 5C). Here, it is obvious that RPMI 2650 cells are rather leaky and display a significantly higher flux compared to OEPC and REPC.

In these experiments, we observed a correlation of permeability and the TEER value for OEPC and REPC (Figure 5D). For RPMI 2650 cells no correlation occurred as the measured TEER values showed a very narrow range from $55 \Omega \text{ cm}^2$ up to $75 \Omega \text{ cm}^2$. Hereby, a higher TEER value did not result in a lower flux. In contrast to REPC and OEPC, a higher TEER value resulted in a lower flux. We determined a minimum TEER value of about $300 \Omega \text{ cm}^2$ that appears to be necessary for primary cells to achieve reproducible permeability results. Hence, all cell-layered inserts used for the flux experiments with FITC-dextran had to meet this criterion.

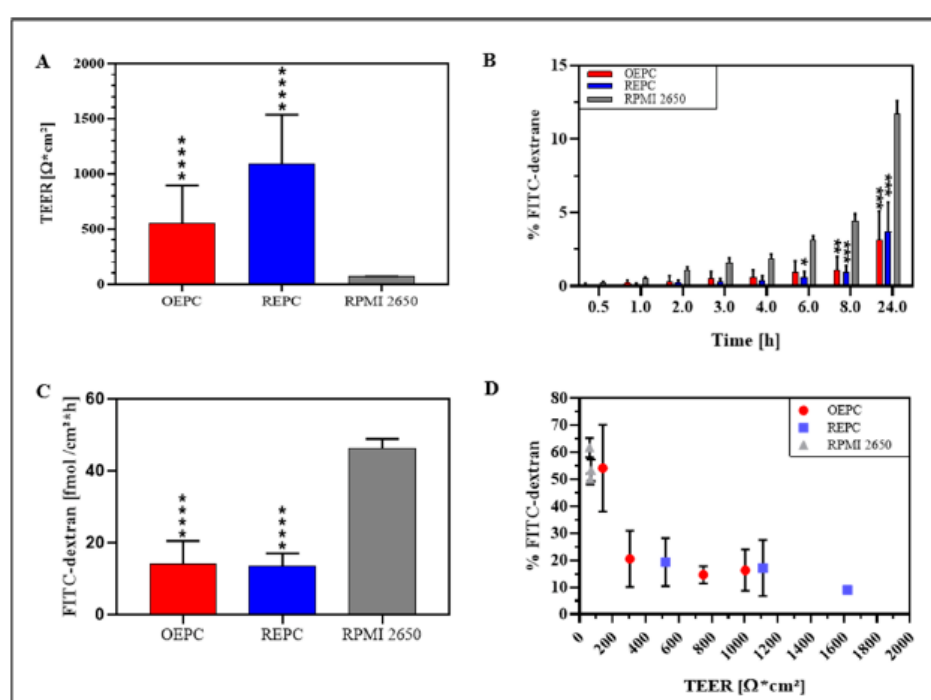


Figure 5. Comparison of FITC-dextran permeation and TEER value of nasal primary cells vs. RPMI 2650. (A) TEER values of OEPC, REPC and RPMI 2650 after 21 days ALI. (B) FITC-dextran permeation data: Values of FITC-dextran permeated through a cell layer were normalized to total of FITC-dextran. (C) Flux of FITC-dextran through an OEPC, REPC and RPMI 2650 layer after 24 h. (D) Correlation of percentage FITC-dextran permeation after 24 h and TEER value. Statistical analysis: unpaired *t*-test, * *p* < 0.05, ** *p* < 0.01, *** *p* < 0.001, **** *p* < 0.0001; all compared to the standard model RPMI 2650. OEPC: olfactory epithelial primary cells; REPC: respiratory epithelial primary cells; TEER: Transepithelial electrical resistance. FITC-dextran: Fluorescein isothiocyanate-dextran; *N* = 4, *n* = 21; error bars represent mean \pm SD of all repetitions.

4. Discussion

The increasing importance of intranasal drug delivery leads to a growing need for adequate models to test permeation of drugs through the different nasal epithelia. In the olfactory region, sensory neurons located in the epithelium were implicated to be involved in drug transport: either with a direct uptake by dendritic knobs or by epithelial or gland cells, depending highly on the molecule [5,56,57]. To display the pathway and transport of drugs to the brain in vivo studies are necessary where the intracellular transport in neurons can be determined using mucosa explants ex vivo [31,57]. However, studies on nasal olfactory epithelium are harder to perform in vivo and ex vivo as this area is rather inaccessible and difficult to reach [26,58]. In vitro models are robust tools to simulate active or passive transport through the first epithelial barrier without modelling neuronal transport. Nevertheless, in vitro cell systems can be seen as simplified models of the first epithelial barrier. They can be used to study specific transporters for high molecular weight molecules and unspecific diffusion of small molecules [59–61]. Nevertheless, considering transport mechanism and cell type specific characteristic it is necessary to set stringent criteria for these cellular models. In the nasal mucosa the epithelial cells form the first barrier for intranasal drug delivery. They are responsible for either uptake or clearance of the administered drugs [6,62]. Parameters that influence the uptake of substances with higher molecular weight are mainly the cell type (e.g., gland cells, sustentacular cells, immune-related microfold cells, etc.) and the expression of specific transport proteins such as aminopeptidases for peptide permeation studies [26,31,42,63]. Furthermore, the drug clearance alongside of nasal mucosal barriers is highly associated with cilia formation and beating [62]. In the olfactory epithelium the cells are described to form non-motile cilia. However, it was demonstrated that so called respiratory mucosa patches exist in the *regio olfactoria* that consist of epithelial cells with beating cilia. Consequently, it is harder to define the clearance rate of the olfactory mucosa only [10]. In addition, for drug stability the physico-chemical environment has to be considered which includes mucus production and the growth under ALI conditions [64]. According to these parameters that influence drug permeation on nasal mucosa, we set the following criteria for the in vitro model: tight epithelial barrier and tight junction formation, cellular monolayer, cilia formation and mucus production.

Standard nasal permeation models are often based on the tumour cell line RPMI 2650. This permanent cell line is derived from an anaplastic squamous cell carcinoma of the nasal septum, which is part of the respiratory region of the nose. Its human origin makes this cell line advantageous in terms of species comparability. Moreover, this cell line was described to mimic the human nasal mucosa and is well investigated in terms of expression of mucus-like material, aminopeptidases, ABC and SLS transporters, cytokeratin patterns, tight junctions and the growth under ALI conditions [26,41,65,66]. The good characterisation makes the RPMI 2650 cell line an established model for intranasal delivery. However, differences in the handling of this cell line have been reported to highly impact growth and protein expression, which may question the reliability of this model [37,67]. Also, we noticed that the permeation rate, as well as the TEER values, depends on the passage count of the RPMI 2650 cells; the higher the passage the lower the TEER value and the higher the permeation rate (unpublished observation). Thus, the nasal mucosa has a heterogeneous composition of several cell types such as ciliated, goblet, columnar and basal cells whereas the RPMI 2650 cell line is only composed of squamous cells which has a limiting impact on the physiology of this model. Furthermore, like most tumour cell lines also the RPMI 2650 cell line suffers from drawbacks such as genetic instability, lack of differentiation and unstable protein expression profiles [37]. The approach that probably mimics best the in vivo situation are ex vivo tissue explants from the olfactory or the respiratory mucosa. Such explants contain all features and the correct cellular composition of the nasal mucosa. However, to take specimen from human olfactory mucosa is associated with a reasonable risk. Yet, porcine nasal tissue is highly similar to the human nasal mucosa and therefore explants are available from slaughterhouse pigs [29]. However, so far there is no cultivation protocol available for long time studies with those tissue samples. We found out 8 h to be the maximum cultivation time before the tissue integrity is

highly compromised in histological sections [31]. Consequently, for long-term studies, e.g., to analyse the influence of drug formulations or drug uptake from sustained release, this model is limited.

Hence, we compared the long-term culture of primary nasal cells derived from porcine respiratory and olfactory mucosa with the standard model RPMI 2650 to gain more information about the relevance of potential artefacts due to the use of a cancer cell lines.

4.1. Comparison of OEPC and REPC: Differences in Barrier Formation and Marker Protein Expression

Our results show that there are actually differences between OEPC and REPC in terms of tight junction formation and, consequently, in TEER values, as well as in the expression of the secretory mucin MUC5AC. The permeation experiment, especially the sample time points below 8 h, resulted in a lower permeation through REPC in comparison to OEPC. This can also be related to the higher TEER values of REPC as shown in the correlation of TEER values to permeated FITC-dextran (Figure 5A). The TEER values are amongst others influenced by the thickness of the cell layer and the formation of tight junctions [68]. Both primary cell types form only monolayers that are comparable in size to mucosal epithelial cells. Thus, we conclude that REPC form a tighter barrier in comparison to the OEPC, also shown in the immunostaining of the tight junctions (ZO-1). This is in accordance with the common knowledge of the in vivo olfactory and respiratory epithelium as the epithelial cells in the respiratory epithelium are strongly connected via tight junctions, whereas epithelial cells in the olfactory epithelium are sealed to the olfactory sensory neurons neither by tight nor by gap junctions [69]. Thus, our results concerning the ZO-1 signal of the REPC are comparable to the human nasal primary cell model MucilAir™ [40]. In contrast to the respiratory epithelium, olfactory sensory neurons are located in the olfactory epithelium surrounded by sustentacular cells. The olfactory sensory neurons are sealed to those cells and span from the apical surface to the olfactory bulb [9]. Neurogenesis of olfactory neurons is known to be a continuous process to replace lost neurons in the epithelial layer, which leaves a gap in the epithelial layer until the new neuron takes its place [70]. Therefore, it might be possible that the lower number of tight junctions and the lower TEER value seen in the OEPC is correlated to the neurogenesis and the connection between the sustentacular cells and the olfactory sensory neurons. Pezzulo et al. (2010) described TEER values ranging from 700 to 1200 Ω cm² for primary cells originated from the tracheal and bronchial tract, which are similar to the TEER values for REPC in the present study [47]. However, for human nasal epithelial cells TEER values up to 3155 Ω cm² are reported [71,72]. In contrast, ex vivo TEER measurements of excised human nasal mucosa range from 60 to 180 Ω cm² [37]. The discrepancy between the excised mucosa and the primary cells could possibly be explained by damage to the axons of the olfactory sensory neurons during the dissection. These tight junctions are highly dependent on the presence of certain ions. Ca²⁺ ions were reported to be necessary to form tight barriers and a high electrical resistance. It might be possible that the excised mucosa suffers from ion depletion when it is no longer connected to blood flow and therefore shows lower TEER [73]. TEER measurements in rabbit airway epithelium in vivo resulted in a higher TEER value of 260–320 Ω cm² [74]. Besides the preparation and the tight junction formation, the cellular composition of the tissue, e.g., the presence of olfactory sensory neurons, plays an important role in the TEER measurement. Furthermore, gland ducts such as from Bowman's glands will also lower the TEER value. In the primary culture we did not observe whole glands and neurons. Hence, the higher TEER values could be a result of lacking gland ducts and void neurons.

The ability to form cilia is shared by REPC and OEPC as seen in the immunoreactivity against acetylated α -tubulin. Different groups postulated that acetylated α -tubulin might be a selective marker for primary (non-motile) and motile cilia of polarized cells [75–77]. In culture, the cilia had a mean length of 10 μ m and beating frequencies of >5 Hz. According to the literature this indicates healthy cilia formation [78–80]. In the culture flasks beating cilia were seen in patch-like clusters whereas under ALI conditions the cell layer showed a confluent signal for acetylated α -tubulin. Nevertheless, to further set up valid experiments for drug clearance studies the differentiation of the epithelial cells towards cells with motile cilia, for example by using retinoic acid, should be optimized [81]. Bateman et al.

(2013) for example published a porcine tracheal epithelial cell model to investigate virus infection and replication. They used a complex medium containing epidermal growth factor (EGF) for proliferation and retinoic acid to promote ciliogenesis [81]; similar to the present study they obtained ciliated cells. In contrast, those cells grew in multilayers with TEER values increasing up to 12 days to $800 \Omega \text{ cm}^2$ and a subsequent decrease to $250\text{--}300 \Omega \text{ cm}^2$ after 18 days. We do not observe this effect as we found TEER values around $850 \Omega \text{ cm}^2$ for REPC and $650 \Omega \text{ cm}^2$ for OEPC after 21 days of ALI cultivation. As we cultured the cells in serum-containing medium without the additional supplementation of EGF or retinoic acid there must be other factors influencing the barrier function that are present in the serum but not in serum-free bronchial epithelial growth medium. As the use of serum-free medium is rather expensive, it is of high interest to further investigate the barrier formation influencing factors present in vivo and in the serum. In contrast to our findings and the findings of Bateman et al. (2013), Delgado-Ortega et al. (2014) reported a leaky barrier model for cells from newborn pig trachea [81,82]. Probably here again the influence of the in vivo cell location and maybe also the age of the donor on the barrier model plays a role. In terms of intranasal drug delivery, using both cell types—REPC and OEPC—for barrier investigations with donor pigs with a similar age can give more detailed information of the permeation in vivo and the most efficient application site in terms of bioavailability.

In terms of mucus expression, the REPC showed lower levels of the secretory mucin MUC5AC expression but transcript levels similar to the OEPC. It has already been described in the literature that transcript expression and the actual protein amount do not always correlate [66]. The reduction of MUC5AC production in OEPC results most probably from lower amounts of glands cells over time as they do not grow under ALI conditions in vivo but in gland formations. A lack of necessary factors such as calcium can be excluded as the medium is regularly exchanged and its composition is constant. The plateau in MUC5AC production after 10 days is possibly due to the fact that also the epithelial cells (sustentacular cells) themselves are capable of producing mucus in vivo [83]. The mucin subtype MUC5AC is known to be mainly expressed in Bowman's glands of the olfactory mucosa and is therefore a rather poor marker for respiratory epithelial cells [64,84,85]. We screened for this marker protein as we are particularly interested in modelling the *regio olfactoria* for intranasal drug delivery, and therefore the application of drugs at the olfactory epithelium. The absence of MUC5AC does not mean the cells lack mucus production in general, but only this specific mucin type that is known to be highly expressed in the olfactory mucosa [84]. Aust et al. (1997) found MUC5AC to be expressed only in subpopulations of epithelial cells in the human inferior turbinate [86]. Furthermore, recent studies postulated MUC5AC to be expressed in higher amounts in the olfactory mucosa in comparison to the respiratory mucosa which is in accordance with the results of our study. Those data show clear differences in mucin type expression (MUC1, MUC2, MUC5AC and MUC5B) patterns between respiratory and olfactory epithelial cells [87]. Thus, this study supports our hypothesis that the choice of the cellular model should be based on the site of drug application. MUC5AC expression was previously found in human primary nasal epithelial cells after 21 days of cultivation under ALI conditions which is in accordance to our results with 21 day-ALI culture of OEPC [46]. Also the cultivation conditions were comparable despite of the use of serum-containing media, which however had no obvious disadvantageous effect on the porcine primary epithelial culture.

Nevertheless, taken together there are several differences concerning REPC and OEPC that can influence the drug permeation. It thus appears to be advantageous to use the cell type of the area of interest for the drug application.

4.2. Primary Cell Model Evaluation: RPMI 2650 vs. Primary Nasal Cell Barrier

The most prominent disadvantages of primary cells are the high variability between different batches and the slow and limited growth in comparison to tumour cell lines. Because of those, and other reasons, the current standard model for nasal mucosal permeation is the tumour cell line RPMI 2650 [26]. The TEER values and permeation rates measured here fit the results of other groups, showing again that the RPMI 2650 is highly reproducible [20,88,89]. Yet, several differences were

observed between RPMI 2650 and primary nasal cells that influence the permeation of molecules. Probably the most influencing factor is the lower TEER value of the RPMI 2650 cells. This goes along with the low expression of tight junction marker ZO-1 in comparison with the primary nasal cells. The paracellular permeation of molecules is highly restricted by these tight junctions in the epithelial barrier [49]. There is a high variance in the TEER values yielded for RPMI 2650 under ALI conditions in the literature from the large range observed ($41 \Omega \text{ cm}^2$ to $270 \Omega \text{ cm}^2$), which most probably depends on the size of the cellular multilayer and passage number. Compared to primary cells, RPMI 2650 forms leaky multilayered barriers as described before [22,37,39,88,90]. Mercier et al. (2018) described this discrepancy by the strong dependency on culture conditions and the experience of the operators. Therefore TEER values of 70 to $100 \Omega \text{ cm}^2$ are regarded as valid for cultures grown 21 days under ALI conditions [37]. Returning to the above-mentioned criteria for a suitable in vitro model for intranasal drug delivery, the primary nasal epithelial cells demonstrated a 10 to 13 fold higher TEER value and considerable higher signals for the ZO-1 marker protein. However, the TEER values yielded for the RPMI 2650 cells are similar to the TEER values observed in excised human nasal mucosa (TEER value: 60 to $180 \Omega \text{ cm}^2$) as described above. In addition to the possible explanations of the low TEER value of the ex vivo explants discussed above, it is in general rather questionable to compare TEER value of a single-component system such as the homogenous RPMI 2650 model or even the heterogeneous primary cell models with TEER values from multi-component systems like excised nasal mucosa, as the latter contains components such as e.g., glands and neurons that influence TEER values.

In terms of the production of MUC5AC the RPMI 2650 showed the lowest transcript level and very low signal in the immunofluorescence staining. This is in accordance with previous studies from Berger et al. (1999) who reported discrepancies between the transcript expression and the protein expression in tumour cell lines [66]. In their work they state that synthesis, maturation and secretion are most probably regulated post-transcriptionally. In general, RPMI 2650 are mostly undifferentiated, homogenous epithelial cells that originate from squamous epithelium which is part of the respiratory mucosa. Together with the lack of differentiation to form goblet cells, the lower expression of MUC5AC in comparison to OEPC is therefore explainable [20]. However, in current literature the mucus secretion pattern of RPMI 2650 cells shows discrepancies concerning the expression level and the mucin type as previously described by Mercier et al. (2018) [37]. This might be due to different culture conditions or the use of cells with different ages. To fully evaluate the mucin protein expression of the RPMI 2650 model further investigations are required.

In respect to the last criterion—the formation of cilia—our results showed very low and diffuse signals for acetylated tubulin in RPMI 2650 in comparison to well defined and fibril-shaped structures in OEPC and REPC. Several groups described the RPMI 2650's inability to differentiate and form cilia which we can support in our present study [37,90]. Furthermore, the tendency of RPMI 2650 to form homogenous multilayers is highly disadvantageous when heterogeneous epithelial layers should be simulated. Also, these cells are not polarized as described for epithelial cells but rather undifferentiated round-shaped stapled cells without a growth direction [91]. It is also questionable whether the cells located in the intermediate layers show the same phenotype as the cells grown at the ALI interface. Especially for transport mechanisms when polarized cells are required the tumour cell model is unfavoured whereas the primary cell model sufficiently fits those criteria.

5. Conclusions

In the present study, we demonstrate, for the first time, differences between primary epithelial cells from the olfactory and respiratory nasal region. Consequently, we highly recommend using primary cells originated from the equivalent tissue type for model intranasal application of drugs on the olfactory mucosa. In terms of comparability of porcine and human primary epithelial cells we obtained similar results for ciliogenesis, and mucus production as well as similar TEER values [40,71,92]. As the TEER value is the state-of-the-art parameter to evaluate barrier models, the pig is corroborated as an adequate surrogate for human tissue. Furthermore, for the investigation of complex drug transport

pathways primary cell culture should be favoured instead of RPMI 2650 tumour cell lines as those cells have different physiological features due to their growth in multilayers and their lack of differentiation ability. In general, we assume the heterogeneity of the primary cells to be advantageous compared to the RPMI 2650 as we see differences in uptake rates of molecules in different cells in our preliminary data. In conclusion, we strongly recommend the observation of several factors such as the analyte molecule, receptor or transporter expression, the importance of adequate physico-chemical environment and the impact of cilia to choose the correct model for the permeation investigation. The primary cell model is a cheap and robust alternative to the tumour cell line RPMI2650 with the advantage of having all features of epithelial cells in vivo and lacking the throwbacks of tumour cells such as genetic instability. It thus has the potential to replace the tumour cell model even in early assessment of drug development as drug efficacy and toxicity can be determined with a higher comparability to the in vivo situation. However, to fully evaluate the full potential of the primary cell model ex vivo experiments should be performed to compare the permeation of a paracellular transported molecule such as FITC-dextran. Furthermore, our study focused on the barrier function and cell type specific features of the cellular models. We only studied the paracellular transport. For further evaluation, the permeation of transcellular transported molecules such as mannitol should also be assessed.

Supplementary Materials: The following are available online at <http://www.mdpi.com/1999-4923/11/8/367/s1>, Figure S1: Permeation data referenced to control without cells vs. referencing to total FITC-dextran, Video S1: Beating cilia in submerged OEPC culture.

Author Contributions: Conceptualization, S.L., P.S. and K.S.; Methodology, S.L., P.S., J.F., H.L. and K.S.; Validation, J.F., S.L. and P.S.; Investigation, S.L. and P.S.; Resources, K.S.; Visualization, S.L. and K.S.; Writing—Original Draft Preparation, S.L., P.S. and K.S.; Writing—Review & Editing, J.F., H.L. and B.M.; Supervision, K.S. and B.M.; Project Administration, K.S.; Funding Acquisition, K.S.

Funding: This study was supported by an EU grant “N2B-patch” under the European Framework Programme for Research and Innovation Horizon 2020 (Grant No. 721,098; www.n2b-patch.eu), from a grant “FcRn in Drug Delivery” funded by the Baden-Württemberg State Ministry of Science, Research and Arts, from a grant “ALIVE” funded by the Federal Ministry for Economic Affairs and Energy (BMWi) and from fellowships from the Stiftung der Deutschen Wirtschaft (to S.L. and J.F.).

Acknowledgments: A special thanks to Rene Handrick from Biberach University for excellent advisory and technical support whenever needed. Also, special thanks to Angelika Rück, Dominik Biesinger and Sviatlana Kalinina from the core facility for confocal and multiphoton microscopy of the Ulm University. Moreover, for excellent support in microscopical questions the authors want to thank Stefan Weigel from the Technical University Munich.

Conflicts of Interest: The authors declare no conflicts of interest.

References

1. Barnabas, W. Drug targeting strategies into the brain for treating neurological diseases. *J. Neurosci. Methods* **2019**, *311*, 133–146. [[CrossRef](#)] [[PubMed](#)]
2. Illum, L. Nasal drug delivery: New developments and strategies. *Drug Discov. Today* **2002**, *7*, 1184–1189. [[CrossRef](#)]
3. Neuwelt, E.; Abbott, N.J.; Abrey, L.; Banks, W.A.; Blakley, B.; Engelhardt, B.; Grammas, P.; Nedergaard, M.; Nutt, J.; Pardridge, W.; et al. Strategies to advance translational research into brain barriers. *Lancet Neurol.* **2008**, *7*, 84–96. [[CrossRef](#)]
4. Gao, H. Progress and perspectives on targeting nanoparticles for brain drug delivery. *Acta Pharm. Sin. B* **2016**, *6*, 268–286. [[CrossRef](#)] [[PubMed](#)]
5. Illum, L. Nasal drug delivery—Possibilities, problems and solutions. *J. Control. Release* **2003**, *87*, 187–198. [[CrossRef](#)]
6. Costantino, H.R.; Illum, L.; Brandt, G.; Johnson, P.H.; Quay, S.C. Intranasal delivery: Physicochemical and therapeutic aspects. *Int. J. Pharm.* **2007**, *337*, 1–24. [[CrossRef](#)]
7. Lochhead, J.J.; Thorne, R.G. Intranasal delivery of biologics to the central nervous system. *Adv. Drug Deliv. Rev.* **2012**, *64*, 614–628. [[CrossRef](#)]

8. Harkema, J.R.; Carey, S.A.; Wagner, J.G. The Nose Revisited: A Brief Review of the Comparative Structure, Function, and Toxicologic Pathology of the Nasal Epithelium. *Toxicol. Pathol.* **2006**, *34*, 252–269. [\[CrossRef\]](#)
9. Gizurarson, S. Anatomical and histological factors affecting intranasal drug and vaccine delivery. *Curr. Drug Deliv.* **2012**, *9*, 566–582. [\[CrossRef\]](#)
10. Paik, S.; Lehman, M.; Seiden, A.M.; Duncan, H.J. Olfactory Biopsy. *Arch. Otolaryngol. Head Neck Surg.* **1992**, *118*, 731–738. [\[CrossRef\]](#)
11. Marttin, E.; Schipper, N.G.M.; Coos Verhoef, J.; Merkus, F.W.H.M. Nasal mucociliary clearance as a factor in nasal drug delivery. *Adv. Drug Deliv. Rev.* **1998**, *29*, 13–38. [\[CrossRef\]](#)
12. Graziadei, P.P.; Graziadei, G.M. Neurogenesis and neuron regeneration in the olfactory system of mammals. I. Morphological aspects of differentiation and structural organization of the olfactory sensory neurons. *J. Neurocytol.* **1979**, *8*, 1–18. [\[CrossRef\]](#)
13. Morrison, E.E.; Costanzo, R.M. Morphology of olfactory epithelium in humans and other vertebrates. *Microsc. Res. Tech.* **1992**, *23*, 49–61. [\[CrossRef\]](#)
14. Mittal, D.; Ali, A.; Md, S.; Baboota, S.; Sahni, J.K.; Ali, J. Insights into direct nose to brain delivery: Current status and future perspective. *Drug Deliv.* **2014**, *21*, 75–86. [\[CrossRef\]](#)
15. Jafek, B.W. Ultrastructure of human nasal mucosa. *Laryngoscope* **1983**, *93*, 1576–1599. [\[CrossRef\]](#)
16. Anton, F.; Poppel, P. Central projections of trigeminal primary afferents innervating the nasal mucosa: A horseradish peroxidase study in the rat. *Neuroscience* **1991**, *41*, 617–628. [\[CrossRef\]](#)
17. Deatly, A.M.; Haase, A.T.; Fewster, P.H.; Lewis, E.; Ball, M.J. Human herpes virus infections and Alzheimer's disease. *Neuropathol. Appl. Neurobiol.* **1990**, *16*, 213–223. [\[CrossRef\]](#)
18. Balin, B.J.; Broadwell, R.D.; Salcmant, M.; El-Kalliny, M. Entry of peripherally administered protein to the CNS in mouse, rat and squirrel monkey. *J. Comp. Neurol.* **1986**, *251*, 260–280. [\[CrossRef\]](#)
19. Bahadur, S.; Pathak, K. Physicochemical and physiological considerations for efficient nose-to-brain targeting. *Expert Opin. Drug Deliv.* **2011**, *9*, 19–31. [\[CrossRef\]](#)
20. Wengst, A.; Reichl, S. RPMI 2650 epithelial model and three-dimensional reconstructed human nasal mucosa as in vitro models for nasal permeation studies. *Eur. J. Pharm. Biopharm.* **2010**, *74*, 290–297. [\[CrossRef\]](#)
21. Gonçalves, V.S.S.; Matias, A.A.; Poejo, J.; Serra, A.T.; Duarte, C.M.M. Application of RPMI 2650 as a cell model to evaluate solid formulations for intranasal delivery of drugs. *Int. J. Pharm.* **2016**, *515*, 1–10. [\[CrossRef\]](#)
22. Kürti, L.; Veszelka, S.; Bocsik, A.; Dung, N.T.K.; Ózsvári, B.; Puskás, L.G.; Kittel, Á.; Szabó-Révész, P.; Deli, M.A. The effect of sucrose esters on a culture model of the nasal barrier. *Toxicol. Vitro.* **2012**, *26*, 445–454. [\[CrossRef\]](#)
23. Nakamura, K.; Maitani, Y.; Takayama, K. The enhancing effect of nasal absorption of FITC-dextran 4400 by β -sitosterol β -D-glucoside in rabbits. *J. Control. Release* **2002**, *79*, 147–155. [\[CrossRef\]](#)
24. Grainger, C.I.; Greenwell, L.L.; Martin, G.P.; Forbes, B. The permeability of large molecular weight solutes following particle delivery to air-interfaced cells that model the respiratory mucosa. *Eur. J. Pharm. Biopharm.* **2009**, *71*, 318–324. [\[CrossRef\]](#)
25. Nicolazzo, J.A.; Reed, B.L.; Finnin, B.C. The Effect of Various in Vitro Conditions on the Permeability Characteristics of the Buccal Mucosa. *J. Pharm. Sci.* **2003**, *92*, 2399–2410. [\[CrossRef\]](#)
26. Schmidt, M.C.; Peter, H.; Lang, S.R.; Ditzinger, G.; Merkle, H.P. In vitro cell models to study nasal mucosal permeability and metabolism. *Adv. Drug Deliv. Rev.* **1998**, *29*, 51–79. [\[CrossRef\]](#)
27. Kim, K.-J.; Malik, A.B. Protein transport across the lung epithelial barrier. *Am. J. Physiol. Cell. Mol. Physiol.* **2015**, *284*, L247–L259. [\[CrossRef\]](#)
28. Moran, D.T.; Rowley, J.C., 3rd; Jafek, B.W. Electron microscopy of human olfactory epithelium reveals a new cell type: The microvillar cell. *Brain Res.* **1982**, *253*, 39–46. [\[CrossRef\]](#)
29. Wadell, C.; Björk, E.; Camber, O. Nasal drug delivery—Evaluation of an in vitro model using porcine nasal mucosa. *Eur. J. Pharm. Sci.* **1999**, *7*, 197–206. [\[CrossRef\]](#)
30. Samson, G.; De La Calera, A.G.; Dupuis-Girod, S.; Faure, F.; Decullier, E.; Paintaud, G.; Vignault, C.; Scoazec, J.Y.; Pivot, C.; Plauchu, H.; et al. Ex vivo study of bevacizumab transport through porcine nasal mucosa. *Eur. J. Pharm. Biopharm.* **2012**, *80*, 465–469. [\[CrossRef\]](#)
31. Ladel, S.; Flamm, J.; Zadeh, A.S.; Filzwieser, D.; Walter, J.C.; Schlossbauer, P.; Kinscherf, R.; Lischka, K.; Luksch, H.; Schindowski, K. Allogenic fc domain-facilitated uptake of IgG in nasal Lamina propria: Friend or foe for intranasal CNS delivery? *Pharmaceutics* **2018**, *10*, 107. [\[CrossRef\]](#)

32. Glorieux, S.; Van den Broeck, W.; van der Meulen, K.M.; Van Reeth, K.; Favoreel, H.W.; Nauwynck, H.J. In vitro culture of porcine respiratory nasal mucosa explants for studying the interaction of porcine viruses with the respiratory tract. *J. Virol. Methods* **2007**, *142*, 105–112. [\[CrossRef\]](#)
33. Tulinski, P.; Fluit, A.C.; van Putten, J.P.M.; de Bruin, A.; Glorieux, S.; Wagenaar, J.A.; Duim, B. An Ex Vivo Porcine Nasal Mucosa Explants Model to Study MRSA Colonization. *PLoS ONE* **2013**, *8*, e53783. [\[CrossRef\]](#)
34. Moore, G.E.; Sandberg, A.A. Studies of a human tumor cell line with a diploid karyotype. *Cancer* **1964**, *17*, 170–175. [\[CrossRef\]](#)
35. Moorhead, P.S. Human tumor cell line with a quasi-diploid karyotype (RPMI 2650). *Exp. Cell Res.* **1965**, *39*, 190–196. [\[CrossRef\]](#)
36. Hayflick, L.; Moorhead, P.S. The serial cultivation of human cell strains. *Exp. Cell Res.* **1961**, *621*, 585–621. [\[CrossRef\]](#)
37. Mercier, C.; Perek, N.; Delavenne, X. Is RPMI 2650 a Suitable In Vitro Nasal Model for Drug Transport Studies? *Eur. J. Drug Metab. Pharmacokinet.* **2018**, *43*, 13–24. [\[CrossRef\]](#)
38. Na, K.; Lee, M.; Shin, H.; Chung, S. In vitro nasal mucosa gland-like structure formation on a chip. *Lab Chip* **2017**. [\[CrossRef\]](#)
39. Mercier, C.; Hodin, S.; He, Z.; Perek, N.; Delavenne, X. Pharmacological Characterization of the RPMI 2650 Model as a Relevant Tool for Assessing the Permeability of Intranasal Drugs. *Mol. Pharm.* **2018**, *15*, 2246–2256. [\[CrossRef\]](#)
40. Mercier, C.; Jacquerooux, E.; He, Z.; Hodin, S.; Perek, N.; Boudard, D.; Delavenne, X.; Constant, S. Pharmacological characterization of the 3D MucilAir™ nasal model. *Eur. J. Pharm. Biopharm.* **2019**, *139*, 186–196. [\[CrossRef\]](#)
41. Moll, R.; Krepler, R.; Franke, W.W. Complex Cytokeratin Polypeptide Patterns Observed in Certain Human Carcinomas. *Differentiation* **1982**, *23*, 256–269. [\[CrossRef\]](#)
42. Peter, H.G. *Cell Culture Sheets to Study Nasal Peptide Metabolism the Human Nasal RPMI 2650 Cell Line Model*; ETH Zürich: Zürich, Switzerland, 1996.
43. Stratford, R.E.; Lee, V.H.L. Amino-peptidase activity in homogenates of various absorptive mucosae in the albino rabbit: Implications in peptide delivery. *Int. J. Pharm.* **1986**, *30*, 73–82. [\[CrossRef\]](#)
44. Tchao, R. Epithelial cell interaction in air-liquid interface culture. *Vitro Cell. Dev. Biol.* **1989**, *25*, 460–465. [\[CrossRef\]](#)
45. de Jong, P.M.; van Sterkenburg, M.A.; Hesselink, S.C.; Kempenaar, J.A.; Mulder, A.A.; Mommaas, A.M.; Dijkman, J.H.; Ponc, M. Ciliogenesis in human bronchial epithelial cells cultured at the air-liquid interface. *Am. J. Respir. Cell Mol. Biol.* **1994**, *10*, 271–277. [\[CrossRef\]](#)
46. Lee, M.K.; Yoo, J.W.; Lin, H.; Kim, Y.S.; Kim, D.D.; Choi, Y.M.; Park, S.K.; Lee, C.H.; Roh, H.J. Air-liquid interface culture of serially passaged human nasal epithelial cell monolayer for in vitro drug transport studies. *Drug Deliv. J. Deliv. Target. Ther. Agents* **2005**, *12*, 305–311. [\[CrossRef\]](#)
47. Pezzulo, A.A.; Starmer, T.D.; Scheetz, T.E.; Traver, G.L.; Tilley, A.E.; Harvey, B.-G.; Crystal, R.G.; McCray, P.B.; Zabner, J. The air-liquid interface and use of primary cell cultures are important to recapitulate the transcriptional profile of in vivo airway epithelia. *Am. J. Physiol. Cell. Mol. Physiol.* **2010**, *300*, L25–L31. [\[CrossRef\]](#)
48. Chen, S.; Einspanier, R.; Schoen, J. Transepithelial electrical resistance (TEER): A functional parameter to monitor the quality of oviduct epithelial cells cultured on filter supports. *Histochem. Cell Biol.* **2015**, *144*, 509–515. [\[CrossRef\]](#)
49. Van Itallie, C.M.; Anderson, J.M. Claudins and Epithelial Paracellular Transport. *Annu. Rev. Physiol.* **2005**, *68*, 403–429. [\[CrossRef\]](#)
50. Flamm, J.; Boscher, M.; Maigler, F.; Akana, C.; Lindemann, J.; Kleiner, S.; Sommer, F.; Schindowski, K. Standardized refined intranasal administration for region-specific intranasal drug deposition in mice established with 3D rapid prototypes under 3R criteria. *Berl. Munch. Tierarztl. Wochenschr.* **2018**, *131*, 408–416. [\[CrossRef\]](#)
51. Röhm, M.; Carle, S.; Maigler, F.; Flamm, J.; Kramer, V.; Mavoungou, C.; Schmid, O.; Schindowski, K.; Schmid, O.; Mavoungou, C.; et al. A comprehensive screening platform for aerosolizable protein formulations for intranasal and pulmonary drug delivery. *Int. J. Pharm.* **2017**, *532*, 537–546. [\[CrossRef\]](#)
52. Nieder, B.; Wagner, H.; Luksch, H. Development of output connections from the inferior colliculus to the optic tectum in barn owls. *J. Comp. Neurol.* **2003**, *464*, 511–524. [\[CrossRef\]](#)

53. Troxler, R.F.; Offner, G.D.; Nunes, D.P.; Oppenheim, F.G.; Iontcheva, I. Molecular characterization of a major high molecular weight mucin from human sublingual gland. *Glycobiology* **2007**, *7*, 965–973. [\[CrossRef\]](#)
54. Shah, A.S.; Ben-Shahar, Y.; Moninger, T.O.; Kline, J.N.; Welsh, M.J. Motile Cilia of Human Airway Epithelia Are Chemosensory. *Science* **2009**, *325*, 1131–1134. [\[CrossRef\]](#)
55. Heijink, I.H.; Brandenburg, S.M.; Noordhoek, J.A.; Postma, D.S.; Slebos, D.J.; Van Oosterhout, A.J.M. Characterisation of cell adhesion in airway epithelial cell types using electric cell-substrate impedance sensing. *Eur. Respir. J.* **2010**, *35*, 894–903. [\[CrossRef\]](#)
56. Crowe, T.P.; Greenlee, M.H.W.; Kanthasamy, A.G.; Hsu, W.H. Mechanism of intranasal drug delivery directly to the brain. *Life Sci.* **2018**, *195*, 44–52. [\[CrossRef\]](#)
57. Baker, H.; Spencer, R.F. Transneuronal transport of peroxidase-conjugated wheat germ agglutinin (WGA-HRP) from the olfactory epithelium to the brain of the adult rat. *Exp. Brain Res.* **1986**, *63*, 461–473. [\[CrossRef\]](#)
58. Jorissen, M.; Van Der Schueren, B.; Van Den Berghe, H.; Cassiman, J.J. Contribution of in vitro culture methods for respiratory epithelial cells to the study of the physiology of the respiratory tract. *Eur. Respir. J.* **1991**, *4*, 210–217.
59. Bhowmick, R.; Gappa-Fahlenkamp, H. Cells and Culture Systems Used to Model the Small Airway Epithelium. *Lung* **2016**, *194*, 419–428. [\[CrossRef\]](#)
60. Even-Tzur, N.; Jaffa, A.; Gordon, Z.; Gottlieb, R.; Kloog, Y.; Einav, S.; Wolf, M.; Elad, D. Air-liquid interface culture of nasal epithelial cells on denuded amniotic membranes. *Cell. Mol. Bioeng.* **2010**, *3*, 307–318. [\[CrossRef\]](#)
61. Jeliakova-Mecheva, V.V.; Bobilya, D.J. A porcine astrocyte/endothelial cell co-culture model of the blood-brain barrier. *Brain Res. Protoc.* **2003**, *12*, 91–98. [\[CrossRef\]](#)
62. Pardeshi, C.V.; Belgamwar, V.S. Direct nose to brain drug delivery via integrated nerve pathways bypassing the blood–brain barrier: An excellent platform for brain targeting. *Expert Opin. Drug Deliv.* **2013**, *10*, 957–972. [\[CrossRef\]](#)
63. Rath, T.; Kuo, T.T.; Baker, K.; Qiao, S.W.; Kobayashi, K.; Yoshida, M.; Roopenian, D.; Fiebiger, E.; Lencer, W.I.; Blumberg, R.S. The immunologic functions of the neonatal FC receptor for IGG. *J. Clin. Immunol.* **2013**, *33*, 9–17. [\[CrossRef\]](#)
64. Gänger, S.; Schindowski, K. Tailoring formulations for intranasal Nose-to-Brain delivery via the olfactory area: A review on physico-chemical characteristics and mucociliary clearance of the nasal olfactory mucosa. *Pharmaceutics* **2018**, *10*, 116. [\[CrossRef\]](#)
65. Dolberg, A.M.; Reichl, S. Expression of P-glycoprotein in excised human nasal mucosa and optimized models of RPMI 2650 cells. *Int. J. Pharm.* **2016**, *508*, 22–33. [\[CrossRef\]](#)
66. Berger, J.T.; Voynow, J.A.; Peters, K.W.; Rose, M.C. Respiratory carcinoma cell lines MUC genes and glycoconjugates. *Am. J. Respir. Cell Mol. Biol.* **1999**, *20*, 500–510. [\[CrossRef\]](#)
67. Kreft, M.E.; Lasi, E.; Kristan, K. The Characterization of the Human Nasal Epithelial Cell Line RPMI 2650 Under Different Culture Conditions and Their Optimization for an Appropriate in vitro Nasal Model. *Pharm. Res.* **2015**, *32*, 665–679. [\[CrossRef\]](#)
68. Srinivasan, B.; Kolli, A.R.; Esch, M.B.; Abaci, H.E.; Shuler, L.; Hickman, J.J.; Srinivasan, B.; Kolli, A.R.; Esch, M.B.; Abaci, H.E.; et al. TEER Measurement Techniques for in vitro barrier model systems. *J. Lab. Autom.* **2016**, *20*, 107–126. [\[CrossRef\]](#)
69. Engström, B.; Ekblom, A.; Hansson, P. The Olfactory and Respiratory Epithelium in Rhesus and Squirrel Monkeys Studied with Freeze-fracture Technique. *Acta Otolaryngol.* **2009**, *108*, 259–267. [\[CrossRef\]](#)
70. Holcomb, J.D.; Graham, S.; Calof, A.L. Neuronal homeostasis in mammalian olfactory epithelium: A review. *Am. J. Rhinol.* **1996**, *10*, 125–134. [\[CrossRef\]](#)
71. Yoo, J.-W.; Kim, Y.-S.; Lee, S.-H.; Lee, M.-K.; Roh, H.-J.; Jhun, B.-H.; Lee, C.-H.; Kim, D.-D. Serially passaged human nasal epithelial cell monolayer for in vitro drug transport studies. *Pharm. Res.* **2003**, *20*, 1690–1696. [\[CrossRef\]](#)
72. Kim, N.; Hee, D.; Suh, M.; Ho, J.; Oh, S.; Kyun, M. Effect of lipopolysaccharide on diesel exhaust particle-induced junctional dysfunction in primary human nasal epithelial cells. *Environ. Pollut.* **2019**, *248*, 736–742. [\[CrossRef\]](#)
73. Farshori, P.; Kachar, B. Redistribution and Phosphorylation of Occludin During Opening and Resealing of Tight Junctions in Cultured Epithelial Cells. *J. Membr. Biol.* **1999**, *170*, 147–156. [\[CrossRef\]](#)

74. Bhat, M.; Toledo-Velasquez, D.; Wang, L.; Malanga, C.J.; Ma, J.K.; Rojanasakul, Y. Regulation of tight junction permeability by calcium mediators and cell cytoskeleton in rabbit tracheal epithelium. *Pharm. Res.* **1993**, *10*, 991–997. [\[CrossRef\]](#)
75. Piperno, G.; Fuller, M.T. Monoclonal antibodies specific for an acetylated form of alpha-tubulin recognize the antigen in cilia and flagella from a variety of organisms. *J. Cell Biol.* **1985**, *101*, 2085–2094. [\[CrossRef\]](#)
76. Quinones, G.B.; Danowski, B.A.; Devaraj, A.; Singh, V.; Ligon, L.A. The posttranslational modification of tubulin undergoes a switch from detyrosination to acetylation as epithelial cells become polarized. *Mol. Biol. Cell* **2011**, *22*, 1045–1057. [\[CrossRef\]](#)
77. Zholos, A.V.; Atherton-Watson, H.; Elborn, J.S.; Ennis, M.; de Courcey, F.; Danahay, H.L.; Canning, P.; Williams, M.T.S. Development of primary human nasal epithelial cell cultures for the study of cystic fibrosis pathophysiology. *Am. J. Physiol. Physiol.* **2012**, *303*, C1173–C1179. [\[CrossRef\]](#)
78. Jorissen, M.; Bessems, A. Normal ciliary beat frequency after ciliogenesis in nasal epithelial cells cultured sequentially as monolayer and in suspension. *Acta Otolaryngol.* **1995**, *115*, 66–70. [\[CrossRef\]](#)
79. Salathe, M.; Bookman, R.J. Coupling of $[Ca^{2+}]_i$ and ciliary beating in cultured tracheal epithelial cells. *J. Cell Sci.* **1995**, *108*, 431–440.
80. Yager, J.; Chen, T.M.; Dulfano, M.J. Measurement of frequency of ciliary beats of human respiratory epithelium. *Chest* **1978**, *73*, 627–633. [\[CrossRef\]](#)
81. Bateman, A.C.; Karasin, A.I.; Olsen, C.W. Differentiated swine airway epithelial cell cultures for the investigation of influenza A virus infection and replication. *Infl. Other Respir. Viruses* **2013**, *7*, 139–150. [\[CrossRef\]](#)
82. Delgado-Ortega, M.; Olivier, M.; Sizaret, P.-Y.; Simon, G.; Meurens, F. Newborn pig trachea cell line cultured in air-liquid interface conditions allows a partial in vitro representation of the porcine upper airway tissue. *BMC Cell Biol.* **2014**, *15*, 14. [\[CrossRef\]](#)
83. Getchell, M.L.; Getchell, T.V. Fine structural aspects of secretion and extrinsic innervation in the olfactory mucosa. *Microsc. Res. Tech.* **1992**, *23*, 111–127. [\[CrossRef\]](#)
84. Solbu, T.T.; Holen, T. Aquaporin pathways and mucin secretion of bowman's glands might protect the olfactory mucosa. *Chem. Senses* **2012**, *37*, 35–46. [\[CrossRef\]](#)
85. Kim, C.-H.; Song, K.S.; Kim, S.-S.; Kim, H.-U.; Seong, J.-K.; Yoon, J.-H. Expression of MUC5AC mRNA in the Goblet Cells of Human Nasal Mucosa. *Laryngoscope* **2000**, *110*, 2110–2113. [\[CrossRef\]](#)
86. Aust, M.R.; Madsen, C.S.; Jennings, A.; Kasperbauer, J.L.; Gendler, S.J. Mucin mRNA Expression in Normal and Vasomotor Inferior Turbinates. *Am. J. Rhinol.* **1997**, *11*, 293–302. [\[CrossRef\]](#)
87. Kennel, C.; Gould, E.A.; Larson, E.D.; Salcedo, E.; Vickery, T.W.; Restrepo, D.; Ramakrishnan, V.R. Differential Expression of Mucins in Murine Olfactory Versus Respiratory Epithelium. *bioRxiv* **2019**, 1–32. [\[CrossRef\]](#)
88. Reichl, S.; Becker, K. Cultivation of RPMI 2650 cells as an in-vitro model for human transmucosal nasal drug absorption studies: Optimization of selected culture conditions. *J. Pharm. Pharmacol.* **2012**, *64*, 1621–1630. [\[CrossRef\]](#)
89. Pozzoli, M.; Sonvico, F.; Ong, H.X.; Traini, D.; Bebaawy, M.; Young, P.M. Optimization of RPMI 2650 Cells as a Model for Nasal Mucosa. *Respir. Drug* **2014**, *2*, 739–742.
90. De Fraissinette, A.; Brun, R.; Felix, H.; Vonderscher, J.; Rummelt, A. Evaluation of the human cell line RPMI 2650 as an in vitro nasal model. *Rhinology* **1995**, *33*, 194–198.
91. Werner, U.; Kissel, T. In-vitro cell culture models of the nasal epithelium: A comparative histochemical investigation of their suitability for drug transport studies. *Pharm. Res.* **1996**, *13*, 978–988. [\[CrossRef\]](#)
92. Yoon, J.-H.; Moon, H.-J.; Seong, J.-K.; Kim, C.-H.; Lee, J.-J.; Choi, J.-Y.; Song, M.S.; Kim, S.-H. Mucociliary differentiation according to time in human nasal epithelial cell culture. *Differentiation* **2002**, *70*, 77–83. [\[CrossRef\]](#)



Simone Ladel, Frank Maigler, Johannes Flamm, Patrick Schlossbauer, Alina Handl, Rebecca Hermann, Helena Herzog, Thomas Hummel, Boris Mizaikoff, and Katharina Schindowski. 2020. Impact of Glycosylation and Species Origin on the Uptake and Permeation of IgG's through the Nasal Airway Mucosa. *Pharmaceutics* 12, 11: 1014. <https://doi.org/10.3390/pharmaceutics12111014>

© 2020 by the authors. Licensee MDPI, Basel, Switzerland. This article is an open access article distributed under the terms and conditions of the Creative Commons Attribution 4.0 International (CC BY 4.0) license (<http://creativecommons.org/licenses/by/4.0/>).



Article

Impact of Glycosylation and Species Origin on the Uptake and Permeation of IgGs through the Nasal Airway Mucosa

Simone Ladel ^{1,2}, Frank Maigler ^{1,2}, Johannes Flamm ^{1,2}, Patrick Schlossbauer ¹, Alina Handl ^{1,2}, Rebecca Hermann ¹, Helena Herzog ^{1,2}, Thomas Hummel ³, Boris Mizaikoff ⁴ and Katharina Schindowski ^{1,*}

¹ Institute of Applied Biotechnology, University of Applied Science Biberach, Hubertus-Liebrecht Straße 35, 88400 Biberach, Germany; ladel@hochschule-bc.de (S.L.); maigler@hochschule-bc.de (F.M.); flamm@hochschule-bc.de (J.F.); schlossbauer@hochschule-bc.de (P.S.); handl@hochschule-bc.de (A.H.); rebecca.hermann96@gmail.com (R.H.); helena.herzog@uni-ulm.de (H.H.)

² Faculty of Natural Science, University of Ulm, Albert-Einstein-Allee 11, 89081 Ulm, Germany

³ Smell & Taste Clinic, Department of Otorhinolaryngology, TU Dresden, Fetscherstraße 74, 01307 Dresden, Germany; thummel@mx.tu-dresden.de

⁴ Institute of Analytical and Bioanalytical Chemistry, University of Ulm, Albert-Einstein-Allee 11, 89081 Ulm, Germany; boris.mizaikoff@uni-ulm.de

* Correspondence: schindowski@hochschule-bc.de; Tel.: +49-7351-582-498

Received: 26 September 2020; Accepted: 21 October 2020; Published: 23 October 2020



Abstract: Although we have recently reported the involvement of neonatal Fc receptor (FcRn) in intranasal transport, the transport mechanisms are far from being elucidated. Ex vivo porcine olfactory tissue, primary cells from porcine olfactory epithelium (OEPC) and the human cell line RPMI 2650 were used to evaluate the permeation of porcine and human IgG antibodies through the nasal mucosa. IgGs were used in their wild type and deglycosylated form to investigate the impact of glycosylation. Further, the expression of FcRn and Fc-gamma receptor (FCGR) and their interaction with IgG were analyzed. Comparable permeation rates for human and porcine IgG were observed in OEPC, which display the highest expression of FcRn. Only traces of porcine IgGs could be recovered at the basolateral compartment in ex vivo olfactory tissue, while human IgGs reached far higher levels. Deglycosylated human IgG showed significantly higher permeation in comparison to the wild type in RPMI 2650 and OEPC, but insignificantly elevated in the ex vivo model. An immunoprecipitation with porcine primary cells and tissue identified FCGR2 as a potential interaction partner in the nasal mucosa. Glycosylation sensitive receptors appear to be involved in the uptake, transport, but also degradation of therapeutic IgGs in the airway epithelial layer.

Keywords: IgG permeation; barrier model; nose-to-brain; primary cells; RPMI 2650; olfactory epithelium; respiratory epithelium; drug delivery; blood-brain barrier

1. Introduction

In the last 30 years, the rise in the importance of therapeutic immunoglobulin G (IgG) has been exceptional. Two Nobel prizes have been awarded to scientists for antibody-related discoveries so far, over 80 antibodies have entered clinical trials and the approval success rates have been near one in four [1,2]. The use of therapeutic IgGs in indications such as oncology, autoimmune diseases and inflammatory diseases represented revolutionary innovations in the treatment of chronic and acute conditions. However, up to now, the use of IgGs in central nervous system (CNS)-related diseases is severely hampered due to the low blood–brain barrier (BBB) permeability and the poor

brain permeability in general. The four distinct and highly restrictive barrier structures, the BBB, the blood–CSF (cerebrospinal fluid) barrier, the meningeal barrier and the ventricular barrier, are the most limiting factors in successful IgG-based therapy of CNS-related diseases. Amongst them, the BBB is the most relevant as it provides access to the entire brain [3]. There are several mostly experimental strategies to overcome this barrier. One strategy is to disrupt the tight junctions in the BBB to allow paracellular passage of molecules [4]. Furthermore, mannitol, an osmotic agent that leads to a shrinkage of the brain endothelial cells or focused ultrasound can be used to increase the permeability to the brain [5,6]. However, the unspecific disruption of the BBB harbors the risk of exposing the brain to potentially harmful bloodborne substances [3]. Besides the unspecific trafficking strategies to the brain, also selective approaches were performed using receptors, such as the transferrin receptor, that are known to undergo transcytosis in the brain endothelial cells [3,7–9]. Alongside the strategies described, there are also ideas to circumvent the BBB, including the concept of nose-to-brain (N2B) drug delivery. In theory, N2B is most likely mediated along the olfactory or the trigeminal nerve pathways that are located in the neuroepithelium of the nasal cavity or by paracellular transport [10–12]. In a former IgG permeation study through ex vivo porcine olfactory mucosa explants, IgGs were found in olfactory epithelial cells, glands and in neuronal fiber tracts [13]. Hereby, differences between the permeation of allogenic porcine IgGs and xenogenic human IgGs have been shown. It was assumed that the neonatal Fc receptor (FcRn), a specialized IgG transporter that is expressed mainly in endothelial and epithelial cells as well as monocytes, is involved in IgG uptake and trafficking in the neuroepithelium. Accordingly, Stirling et al. showed higher uptake of human IgG compared to porcine IgG in porcine kidney cells expressing the FcRn [14]. In accordance, our previous data may indicate the faster penetration of human IgG through porcine olfactory mucosa explants compared to the permeation of porcine IgG in the same set-up [13].

In general, several studies show the involvement of FcRn in IgG transport in different tissues and cell types [15–19]. Thus, FcRn was also found to be expressed in the BBB. The role of FcRn in the BBB appears to be mainly as an efflux transporter; however, some studies suggest that FcRn may also take part in IgG distribution within the brain [20–22]. There are many controversial studies concerning the influence of these Fc receptors in IgG distribution in the brain. Recently, Ruano-Salguero and Lee showed in an in vitro BBB model that antibody transcytosis across brain endothelial-like cells is not dependent on FcRn transport [23]. However, they also highlighted the need for clarifying the transcytosis mechanism in general. Nevertheless, the function of FcRn as IgG transporter in the mucosal epithelium was proven in several studies focusing on gut or lung mucosa [16,24]. As the nasal mucosa displays the first barrier to overcome for intranasally administered therapeutic IgGs, it is of great interest to evaluate if FcRn function is similar to other reported mucosal sites or if the function of FcRn in the neuroepithelium is comparable to neuronal tissue. Other candidates that are discussed to have potential IgG transport functions and could be involved in mucosal IgG trafficking are Fc gamma receptors (FCGRs), particularly FCGR2b [25,26]. Again, the influence of these FCGRs on the transport of antibodies has not been clarified yet. These receptors are mainly known to mediate immunological effector functions and are highly dependent on IgG glycosylation [27,28]. Several studies show altered interaction of FCGR with deglycosylated IgGs. EndoS deglycosylation of IgG1 leads to decreased binding to human FCGR2a/b and FCGR3a, whereas binding to FCGR1 is not affected. Interestingly, reduced fucosylation leads to increased FCGR3a binding, as shown by Cambay et al. [27,29–32].

The present study focuses on the difference in permeation rates of different IgGs (allogenic porcine IgG and xenogenic human IgG, both glycosylated and deglycosylated) through different models for nasal drug delivery: ex vivo specimens of porcine olfactory mucosa, primary epithelial cells derived from porcine olfactory mucosa and the human cell line derived from a squamous nasal epithelial cancer, RPMI 2650. Furthermore, the influence of IgG glycosylation on permeation was investigated by comparing the normally glycosylated (wild type, WT) IgG and enzymatically deglycosylated (DG) IgG. Because of the lack of commercially available monoclonal porcine IgGs, a biosimilar of a well characterized human IgG against vascular endothelial growth factor (VEGF), named hIgG in the

following, was used for the deglycosylation study as a defined glycopattern was preferable. Porcine mucosa was used for modeling the human nasal mucosa as its high similarity was described before in other studies and the cross-species transport of human IgG by the porcine FcRn has been already shown by Stirling et al. [13,14,33–35]. In addition, the permeation experiments were also performed in porcine olfactory epithelial primary cells (OEPC) and in the human cell line RPMI 2650 (ACC 287, DSMZ, Braunschweig, Germany) [36–39]. The most important factor limiting the nasal absorption of high molecular weight molecules is the low epithelial membrane permeability and the mucociliary clearance [40]. Both factors were included in the cellular OEPC model, displaying the first barrier for N2B. In the ex vivo model, more complex factors interfere with IgG permeation, such as the interaction with the local immune system and the uptake in neuronal fibers, which makes it more similar to the in vivo and, hence, clinical situation.

2. Materials and Methods

2.1. IgGs Used in This Study

To evaluate the permeation kinetics of a human IgG, hIgG was produced in an in-house project according to standard procedures and purified with Protein A MabSelect SuRe™ resin (GE Healthcare, Solingen, Germany) on an ÄKTA Purifier system (GE Healthcare, Solingen, Germany). The antibody was eluted with 50 mM sodium acetate buffer pH 4.0. The concentration was determined at 280 nm using a NanoDrop™ (Thermo Fisher Scientific, Dreieich, Germany) spectrophotometer applying the extinction coefficient 1.54 L/(mol × cm).

Porcine serum IgGs were purchased from Sigma-Aldrich (Taufkirchen, Germany).

2.2. IgG Deglycosylation

IgGs were deglycosylated by the enzyme Endo S (NEB, Ipswich, UK) according to the manufacturer's protocol. Briefly, 500 µg IgG was incubated with 340 U Endo S for 2 h at 37 °C. Endo S was separated from the IgG by ultrafiltration (100 kDa MWCO, Satorius, Göttingen, Germany). The deglycosylation was confirmed by hydrophobic interaction liquid chromatography (HILIC, see Supplementary Figure S1). Hereby, the exact glycopattern was determined by analyzing the cut-off Fc-glyco-residues. The identification of the glycosylation pattern is both a quality control for the IgG itself, as the glycopattern highly depends on the production process, and a verification of a successful deglycosylation process as, otherwise, no glycan-residues would be found by HILIC.

2.3. Tissue Preparation and Ex Vivo Permeation

The mucosa explants were harvested and placed upside-down in a side-by-side set-up, as described before [13]. In brief, tissue specimens (2 cm²) were excised from the *concha nasalis media* (c.n. media) of slaughterhouse pigs (postmortem delay < 1.5 h). To simulate the upside-down conditions at the olfactory region, the mucosa specimens were placed into a self-made side-by-side cell system consisting of two 1.5 mL microreaction tubes. The upper compartment was filled with 0.26 mL DMEM/F12 (Gibco® Invitrogen, Darmstadt, Germany) supplemented with 20 U penicillin, 20 µg streptomycin (PenStrep (U), AppliChem, Darmstadt, Germany) and 300 I.U./mg gentamycinsulfate (≥590 I.U./mg, Carl Roth, Karlsruhe, Germany). Then, 30 µL of 1.5 mg/mL IgG solution in PBS pH 6.5 was applied onto the epithelial layer (lower compartment). The system was incubated at 35 °C and >90% humidity for 5 h. As negative/vehicle control PBS without IgG was used. After permeation, the mucosa explants were directly fixed in 4% paraformaldehyde for 2 h and cryoconserved in 30% sucrose overnight. Then, 14 µm slices were prepared in a cryostat at −25 °C (HM525 NX, Thermo Fisher Scientific, Dreieich, Germany) and mounted on Superfrost® Plus Micro Slides (VWR International GmbH, Darmstadt, Germany). To verify tissue integrity, adjacent or following slides from each sample were hematoxylin–eosin stained (HE; Gil III, Merck Millipore, Darmstadt, Germany, data not shown).

as described previously [13]. Ex vivo permeation was performed in four independent experiments at least. Samples with damaged epithelial layers were excluded from the study as described [13].

2.4. Cell Culture

2.4.1. Primary Cells

Porcine olfactory epithelial primary cells (OEPC) were prepared and cultured as described recently [36]. Briefly, cells were harvested from mucosal explants originating from the dorsal part of the *concha nasalis dorsalis* (*c.n. dorsalis*) and the *c.n. media*. The cells were disinfected with Octenisept (Schülke, Noederstedt, Germany), washed and isolated by pronase digestion (1.4 mg/mL in EBSS (Gibco® Invitrogen, Darmstadt, Germany), 20 U penicillin, 20 µg streptomycin (PenStrep (U), AppliChem, Darmstadt, Germany), 300 I.U./mg gentamycinsulfate (≥590 I.U./mg, Carl Roth, Karlsruhe, Germany) for 1 h at 37 °C) and agitation. The suspension was carefully removed from the remaining tissue and centrifuged at 700 rpm for 3 min. The sedimented cells were taken up in appropriate volumes of primary cell culture adhesion medium (DMEM:F12 (1:1), 20% fetal bovine serum (FBS) 2 mM Gln, 1% non-essential amino acids (NEAA), 20 U penicillin, 20 µg streptomycin, 300 I.U./mg gentamycinsulfate) and seeded in T75 flasks coated with 0.05 mg/mL rat tail collagen solution (Primacyte, Schwerin, Germany). Cells were cultivated at 37 °C, 5% CO₂ and 95% rH. The medium was changed to primary cell culture medium (DMEM:F12 (1:1), 10% FBS, 2 mM Gln, 1% NEAA, 20 U penicillin, 20 µg streptomycin, 300 I.U./mg gentamycinsulfate) after 6 h. Fibroblasts were removed by regular Trypsin/EDTA incubation for 4 min at 37 °C.

2.4.2. RPMI 2650

RPMI 2650 cells were cultivated in MEM medium (BioWest, Nuaille, France) containing 10% FBS, 2 mM Gln and 10U penicillin, 10 µg streptomycin at 37 °C, 5% CO₂, 95% rH. Cells were split on a regular basis at 80–90% confluency by trypsinization (Trypsin/EDTA, Biochrom, Stockelsdorf, Germany).

2.4.3. Air–Liquid Interface (ALI) Cell Culture

To expose airway epithelial cells with their apical sides to the air, while their basolateral sides still have contact with the medium, the cells were cultured on cell culture inserts at the air–liquid interface (ALI). This procedure mimics the conditions in the airways. For permeation experiments, primary cells and RPMI 2650 cells were seeded in collagen-coated (0.05 mg/mL rat tail collagen solution) cell culture inserts (ThinCert™, Greiner Bio-one, Frickenhausen, Germany) with a density of 1×10^5 cells (diluted in culture medium), and 260 µL cultivation medium was applied in the basolateral compartment. The apical volume was removed after 24 h of cultivation under submerged conditions. For an additional 21 days, the cells were cultivated under ALI conditions. To remove diffused medium (and prevent fibroblast outgrowth in the primary cell culture), the apical side of the ALI cultures was washed every other day with 200 µL pre-warmed PBS. After 24 h, the cells were adherent and were not removed by the washing steps. In addition, the basolateral medium was also replenished every other day. The ALI procedure is visualized in Figure 1A–C.

2.5. In Vitro Permeation

2.5.1. TEER Measurement

The trans-epithelial electrical resistance (TEER) measurement was used to confirm cell layer integrity (Figure 1D). Cell culture inserts were apically filled with 350 µL MEM without phenol red (Gibco®, Invitrogen, Schwerte, Germany) and the abluminal/basolateral compartment filled with 500 µL MEM. With incubation for 20 min at 37 °C and 15 min at room temperature (RT), the cells were allowed to equilibrate to the new conditions. The TEER values were determined in triplicate using an EVOM epithelial voltohmmeter and chopstick electrodes (World Precision Instruments, Friedberg,

Germany). The raw data were processed by subtracting the blank (inserts without cells) and by multiplying with the area of the insert's membrane (0.336 cm^2). The cut-off values for OEPC and RPMI 2650 confluent cell layers were determined as described previously [36].

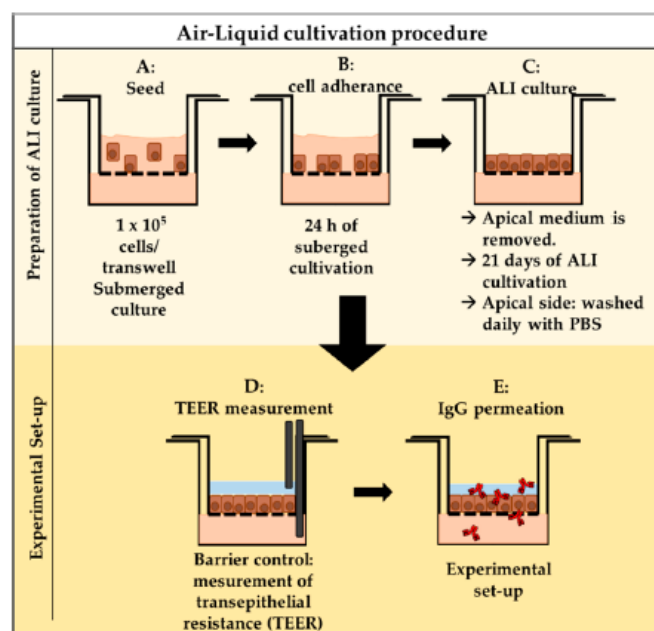


Figure 1. Workflow for air–liquid interface (ALI)-based in vitro permeation experiments. (A) Cells were seeded in a concentration of 1×10^5 cells/transwell. (B) Cell were incubated for 24 h to adhere to the inserts. (C) After 24 h under submerged conditions, the medium from the apical side was removed to achieve ALI conditions. The cells were washed once daily with PBS to avoid the medium draining from the bottom to the apical surface. Cells were differentiated for 21 days at ALI conditions for an optimal and tight barrier. (D) Barrier integrity was confirmed by transepithelial resistance (TEER) measurement. (E) Experimental set-up of IgG permeation.

2.5.2. In Vitro Permeation—Experimental Procedure

To carry out the permeation experiments, the medium was changed to 260 μL cultivation medium without FBS to avoid potential interference of traces of bovine IgGs within the FBS. To analyze IgG permeation, 100 μL of 0.5 mg/mL IgG in PBS was applied at the apical surface of the cell layer (Figure 1E). The experiments were executed under normal cell culture conditions at 37°C , 5% CO_2 , 95% rH. Permeation was performed for 48 h. For sampling, a volume of 20 μL was taken from the basolateral compartment at 0.5, 2, 4, 8, 12, 24 and 48 h. Then, 20 μL fresh medium was added to keep the basolateral volume constant. The samples were analyzed via enzyme-linked immunosorbent assay (ELISA). The remaining cell culture inserts were fixed in 4% paraformaldehyde for 10 min, cryoconserved in 30% sucrose overnight and stored at 4°C until sectioning.

The samples were analyzed by ELISA. For the quantitative analysis of hIgG, a sandwich set-up was used. High-binding 96-well plates (Microton, Greiner Bio-one, Frickenhausen, Germany) were coated with 0.05 $\mu\text{g/mL}$ of recombinant VEGF (Sino Biologicals, Beijing, China) using a 0.1 M bicarbonate buffer pH 9.6 overnight at 4°C . Plates were washed four times with PBS supplemented with 0.3% Tween (PBST) for 1 min, followed by a blocking step with 1% bovine serum albumin (BSA) in PBST and incubated for at least 2 h at 37°C or overnight at 4°C . Samples were diluted in coating buffer, added to the wells and incubated for 45 min at 37°C . Plates were washed again four times as described before. The detection antibody anti-human κ (from goat) conjugated with horseradish peroxidase (HRP; Table 1) was diluted 1:4000 in coating buffer, added to the wells and incubated for 30 min at

37 °C. After extensive washing with PBST, TMB chromogenic substrate (Thermo Fisher/Pierce™, Dreieich, Germany) was used for detection according to the manufacturer's protocol.

Table 1. List of secondary antibodies used in this study.

Antibody	Antigen	Host	Source, Catalog Number
Anti-rabbit IgG-Rhodamine Red™-X	Whole molecule rabbit IgG	Donkey	Jackson Immuno Research Europe Ltd., Cambridgeshire, UK, Cat. #711-295-152
Anti-murine IgG-Alexa Fluor® 488	Whole molecule mouse IgG	Goat	Jackson Immuno Research Europe Ltd., Ely, UK, Cat. #115-545-003
AffiniPure Anti swine IgG (H+L)-Alexa Fluor® 647	Whole molecule porcine IgG	Goat	Jackson Immuno Research Europe Ltd., Ely, UK, Cat. #114-605-003
AffiniPure Anti human-Alexa Fluor® 647	Whole molecule human IgG	Donkey	Jackson Immuno Research Europe Ltd., Ely, UK, Cat. #709-605-149
Anti-rabbit IgG-HRP	Whole molecule rabbit IgG	Goat	Jackson Immuno Research Europe Ltd., Ely, UK, Cat. #111-035-003
Anti-murine IgG-HRP	Whole molecule rabbit IgG	Goat	Sigma Aldrich, Taufkirchen, Germany, Cat. #AP5278
Anti-human κ light chain IgG-HRP	Human κ light chain	Goat	SouthernBiotech, Birmingham, AL, USA, Cat. #2060-05
AffiniPure Anti swine IgG (H+L)-HRP	Whole molecule porcine IgG	Goat	Jackson Immuno Research Europe Ltd., Ely, UK, Cat. #114-035-003
AffiniPure Anti swine IgG (H+L)	Whole molecule porcine IgG	Goat	Jackson Immuno Research Europe Ltd., Ely, UK, Cat. #114-005-003

The quantitative analysis of porcine IgGs was also carried out using the sandwich ELISA (company, city, country) used for hIgG despite the coating protein and the detection antibody. Here, AffiniPure goat anti-swine IgG (H + L) (Table 1) was coated with a concentration of 1 µg/mL. For detection, the goat anti-swine Fc conjugated with HRP (EMD Millipore, Darmstadt, Germany) was used in a 1:50,000 dilution. Absorbance was read at 450 nm using the SpectraMax M Series (molecular devices, San Jose, CA, USA).

2.6. Immunofluorescence Staining of Tissue Explants and Cell Culture Insert Membranes

The immunofluorescence (IF) staining was performed as described previously [13,36]. Briefly, sections/membranes were washed three times with PBS pH 7.4 for 5 min, followed by blocking with 4% BSA, 0.5% saponin and 10% normal goat serum in PBS pH 7.4 overnight. The primary antibodies against FcRn (Pirbright Institute, Woking, UK) and against FCGR2/CD32 (Novus Biologicals/Bio-Techne GmbH, Wiesbaden, Germany) were diluted 1:100 in PBS pH 7.4 containing 4% BSA and 0.5% saponin and incubated for 24 to 48 h at 4 °C. Afterwards, the sections/membranes were washed again three times and incubated with the corresponding secondary antibody (Table 1, 1:500 diluted in PBS pH 7.4) for 2 h. Subsequently, three additional washing steps were performed. Nuclei were stained via DAPI (20 µg/mL in PBS, Thermo Fisher, Dreieich, Germany) for 10 min and washed in PBS pH 7.4. After three additional washing steps, slides were mounted with Fluoromount G mounting medium (Sigma-Aldrich, Taufkirchen, Germany).

2.7. Western Blot Analysis

The Western blot was performed as described before [36]. Briefly, the cell and tissue lysates with equal weight or cell count were extracted by using ice-cold RIPA cell lysis (10 mM Tris-Cl, pH 8.0; 1 mM EDTA, 0.5 mM EGTA, 1% Triton X-100; 0.1% sodium deoxycholate, 0.1% SDS, 140 mM NaCl; protease

inhibitor mix (Thermo Fisher Scientific, Dreieich, Germany) and ultrasound (Hielscher, Stuttgart, Germany)). Equal volumes of homogenized tissue were loaded, separated in a 12.5% SDS PAGE and blotted onto a nitrocellulose membrane (Carl Roth, Karlsruhe, Germany). The membrane was blocked with 5% skimmed milk powder (TSI GmbH, Zeven, Germany) in PBS-0.1% Tween20, pH 7.4 for 1 h at room temperature (RT). Primary antibodies against FcRn [14]; for human: Sigma Aldrich, Taufkirchen, Germany) and against β -Actin (Sigma Aldrich, Taufkirchen, Germany) were diluted 1:5000 in blocking buffer and incubated overnight at 4 °C. Secondary antibodies were diluted 1:5000 (Anti-human IgG-HRP, SouthernBiotech, Birmingham, AL, USA), 1: 50000 (Anti-rabbit IgG-HRP, Jackson Immuno Research, Ely, UK) and 1:4000 (Anti-murine IgG-HRP, Sigma Aldrich, Taufkirchen, Germany). For signal detection, the chemiluminescence substrate Immobilon® (Merck Millipore, Darmstadt, Germany) was used according to the manufacturer's instructions.

2.8. Immunoprecipitation

Immunoprecipitation was performed to identify interaction partners of IgG in cells and the tissue. Tissue and cell lysates were prepared as described in Section 2.7 with 1% Triton X-100, 20 mM Tris, 150 mM NaCl, pH 6.5 as lysis buffer. Pierce™ Protease and Phosphatase Inhibitor (Thermo Scientific, Dreieich, Germany) was freshly added 1:1000 to the working solution. Lysates were centrifuged in a microcentrifuge (Eppendorf, Hamburg, Germany) at maximum speed for 15 min at 4 °C. Then, 500 μ L of the supernatant was added to 50 μ g of the capture antibody and incubated by overhead agitation for 1 h at 4 °C. Then, 20 μ L of Protein A agarose beads (Cell Signaling Technology, Frankfurt, Germany) was added and incubated under agitation overnight at 4 °C. Beads were washed four times with 500 μ L ice-cold lysis buffer. The pellet was resuspended with 20 μ L 3 \times SDS sample buffer, mixed by vortexing and centrifuged for 30 s at maximum speed. Proteins were eluted from the beads by boiling for 5 min at 95 °C and centrifuged again for 30 s at maximum speed. The analysis for FcRn and FCGR2 (1:100) was performed by Western blot, as described in Section 2.7.

2.9. Statistics

Data were assessed for statistical significance using unpaired t-test or Mann–Whitney test (GraphPad Prism 8, Version 8.3.0 (538), San Diego, CA, USA). The number of experimental repetitions is divided into technical replicates (*n*) and biological replicates (*N*). Biological replicates represent different batches of primary cells, different pigs or the number of newly cultured RPMI 2650 cells.

3. Results

So far, the transport pathways of IgGs through the nasal mucosa remain to be elucidated. Previous studies identified that FcRn appears to be involved in IgG trafficking [15]. Therefore, the focus of the present study is the interaction of IgGs with Fc receptors in models of the olfactory mucosa. In former studies, especially the glycosylation status of IgGs affects the binding to Fc receptors [31,41]. Several models have been developed so far to test the permeation of drugs through the olfactory epithelium with ex vivo tissue explants, primary nasal cells and tumor cell lines such as RPMI 2650 [13,36,39,42,43]. Here, the IgG permeation was evaluated in these models as well as the relevance of using allo- or xenogenic IgGs and their glycosylation.

3.1. IgG Permeation through Different Models of the Olfactory Mucosa and Olfactory Epithelium

3.1.1. Impact of IgG Species Origin on Trans-Epithelial Permeation of IgGs

To evaluate whether there is a difference between the permeation of porcine serum IgGs (pIgG) and a human IgG (hIgG) through porcine nasal mucosa models, the permeation was determined using in vitro ALI cultures of OEPC and RPMI2650 as well as ex vivo tissue explants (Figure 2A–D). The results can give further information about the validity of the porcine model to develop nasal

drug delivery with human antibodies since the human nasal olfactory mucosa is limited for such experimental models. All antibodies used here were normally glycosylated (wild types, WT).

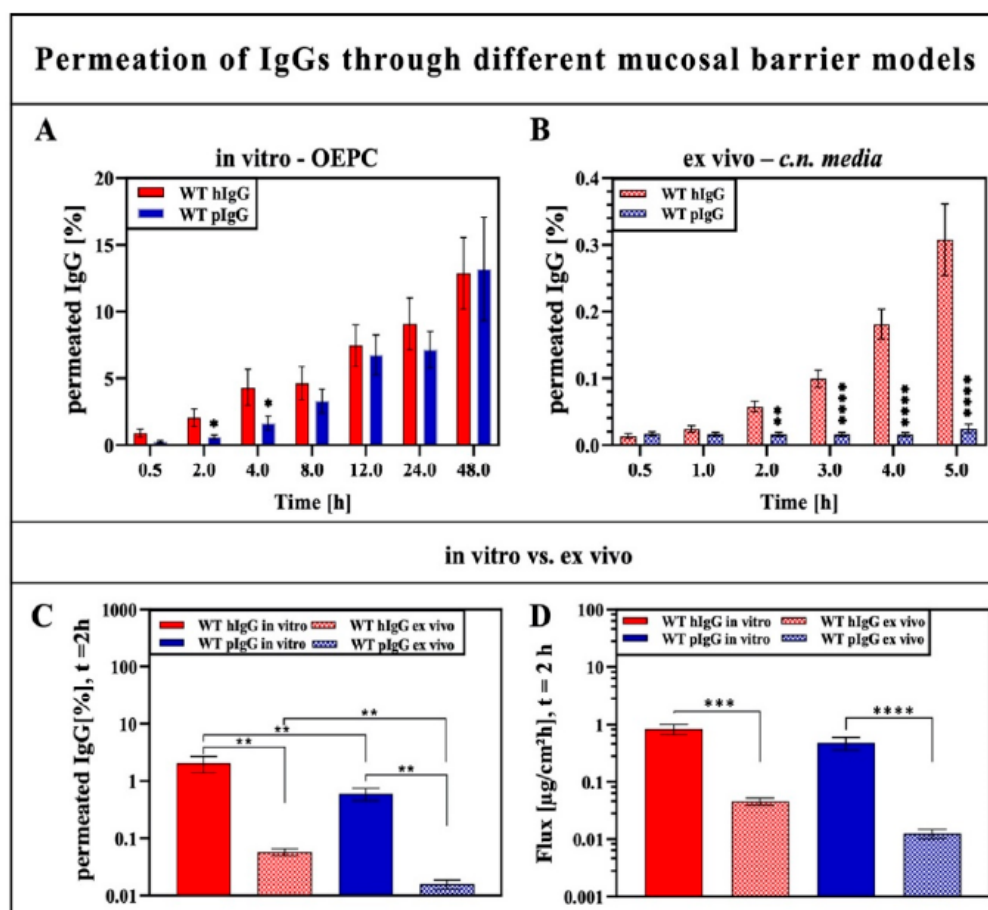


Figure 2. Cumulated permeation of allogenic porcine serum IgG (pIgG) and xenogenic human IgG (hIgG) through in vitro porcine olfactory epithelial primary cells (OEPC) and ex vivo porcine olfactory mucosa (*conchae nasalis media* (*c.n. media*)). (A) Percentage permeation of wild-type hIgG (WT hIgG) and porcine serum IgG (WT pIgG) through olfactory epithelial primary cells (OEPC) over 48 h. Error bars represent mean \pm SEM. $N = 4$, $n = 21$. (B) Percentage permeation of WT hIgG and WT pIgG through excised nasal mucosa tissue explants (ex vivo—*c.n. media*) over 5 h. Error bars represent mean \pm SEM. WT hIgG: $N = 4$, $n = 29$, WT pIgG: $N = 4$, $n = 12$. (C) Comparison of percentage permeated IgG through the OEPC in vitro model and the ex vivo model after 2 h. (D) Comparison of the flux of the IgGs through the in vitro and the ex vivo model. The significance was analyzed by unpaired t-test. * $p < 0.05$, ** $p < 0.001$, *** $p < 0.0001$; **** $p < 0.00001$, error bars represent mean \pm SEM.

Using OEPC ALI cultures derived from primary epithelial cells of the porcine olfactory mucosa cultured at the air–liquid barrier, the permeation of the hIgG was significantly faster over the first four hours in comparison to pIgGs. From 8 to 48 h, the permeation rate of pIgGs converges (Figure 2A). By contrast, using an ex vivo model derived from a specimen of the porcine olfactory mucosa, the hIgG permeation was 12 times higher after 5 h than the permeation of pIgG (Figure 2B). A comparison of the ex vivo and the primary cell in vitro model shows 35-fold higher permeation for hIgG and 1.8-fold higher flux in the in vitro model. For pIgGs, 35-fold higher flux and 37-fold higher permeation could be determined in the in vitro model compared to the ex vivo model. In brief, a difference in the permeation behavior of pIgG and hIgG was shown for the uptake at earlier time points in the epithelial layer model OEPC. This might indicate either different binding affinities to transport-related receptors

or differences in the intracellular IgG trafficking. Furthermore, when using the ex vivo model of the *c.n. media*, pIgG can be hardly found at the basolateral/abluminal compartment in contrast to hIgG. Again, this suggests that species-dependent binding to IgG receptors or species-dependent IgG trafficking and/or degradation pathways influences the permeation of IgGs through the olfactory mucosa.

3.1.2. Impact of IgG Glycosylation on Permeation through the Nasal Epithelium or Nasal Mucosa

The glycosylation of IgG was shown to have a high impact on Fc receptor binding in several studies [18,27,30]. However, the common opinion is that binding to the IgG transporter FcRn is not affected by deglycosylation of the IgG [44]. To evaluate the involvement of IgG glycosylation sensitive receptors in intranasal IgG permeation, a study was performed using a deglycosylated monoclonal hIgG (DG hIgG). The enzyme used for deglycosylation was EndoS, which hydrolyses the asparagine-linked glycans on IgG [41,45,46]. The experiment was not performed with polyclonal porcine serum IgGs, as a defined glycopattern was desired to simplify the analysis. The (de-)glycosylation of hIgG was evaluated by hydrophilic interaction liquid chromatography (HILIC, see Supplementary Figure S1).

To avoid experimental bias due to cross-species binding, the permeation was performed in RPMI 2650 with allogenic human IgGs in addition to the permeation through OEPC and *c.n. media*. The cell line RPMI 2650 was derived from cancerous human nasal squamous epithelium and is currently used as a standard model for intranasal drug delivery since specimens of human nasal mucosa are unfortunately hardly available [47–49]. Comparable to the in vitro permeation through OEPC layers (Figure 3B), DG hIgG showed a higher permeation rate and flux than wild-type IgG in the RPMI 2650 ALI model (Figure 3A). In detail, the percentage permeation of DG hIgG was two times higher compared with the WT hIgG. The permeation of DG hIgG and WT hIgG through OEPC resulted in three times higher permeation of the DG hIgG after 48 h (Figure 3B). By contrast, the permeation rate of DG hIgG and WT hIgG did not show significant differences in the ex vivo model but a tendency towards higher permeation was observed for DG hIgG (Figure 3C). Considering the direct comparison of the permeation results after two hours, the permeation of WT hIgG through the primary cell in vitro model was 40 times higher than the permeation through the tissue explant (Figure 3D). For DG hIgG, the percentage in vitro permeation was over 80 times higher than the ex vivo permeation after 2 h (Figure 3D). Compared to the ex vivo permeation, both variants of the IgG showed a higher permeation rate and higher flux in the RPMI 2650 model at 2 h. In contrast, the permeation and the flux through the primary cell model was significantly higher than the permeation through RPMI 2650 cells for both the DG hIgG and the WT hIgG. This was surprising as the barrier tightness of RPMI 2650 (transepithelial resistance: 50–70 Ωcm^2) is much lower than OEPC (transepithelial resistance: 800–1000 Ωcm^2) and therefore the RPMI 2650 was suspected to show higher IgG flux due to paracellular transport [36].

In contrast to the interspecies differences in permeation from Figure 2, the permeation behavior of DG und WT hIgG displayed similar patterns in the in vitro (OEPC, RPMI 2650) and ex vivo (*c.n. media*) models. In all in vitro models, deglycosylation of hIgG did result in higher permeation of hIgG from the apical to the basolateral side. Moreover, in the ex vivo model, the tendency of higher permeation of DG hIgG is visible but not significant due to the usually high standard variations in this model type. The higher permeation rate of DG IgG could indicate a glycosensitive mechanism in IgG trafficking. Receptors which are known to be sensitive to Fc glycosylation are FCGRs. The significantly higher permeation of DG hIgG could imply the involvement of FCGRs either in IgG recycling or degradation.

3.2. Analysis of IgG Transporter in Porcine Nasal Mucosa, Primary Epithelial Cells and the RPMI 2650 Model

3.2.1. FcRn Expression in OEPC and RPMI 2650

Up to now, FcRn is the best described protein, which has an important role in IgG transport. Further, enhanced transport via FcRn was shown by Fc engineering [16,50]. We recently described the expression of FcRn in porcine nasal mucosa explants [13]. Therefore, we now focused on the primary cell model (OEPC) and the human nasal cell line RPMI 2650.

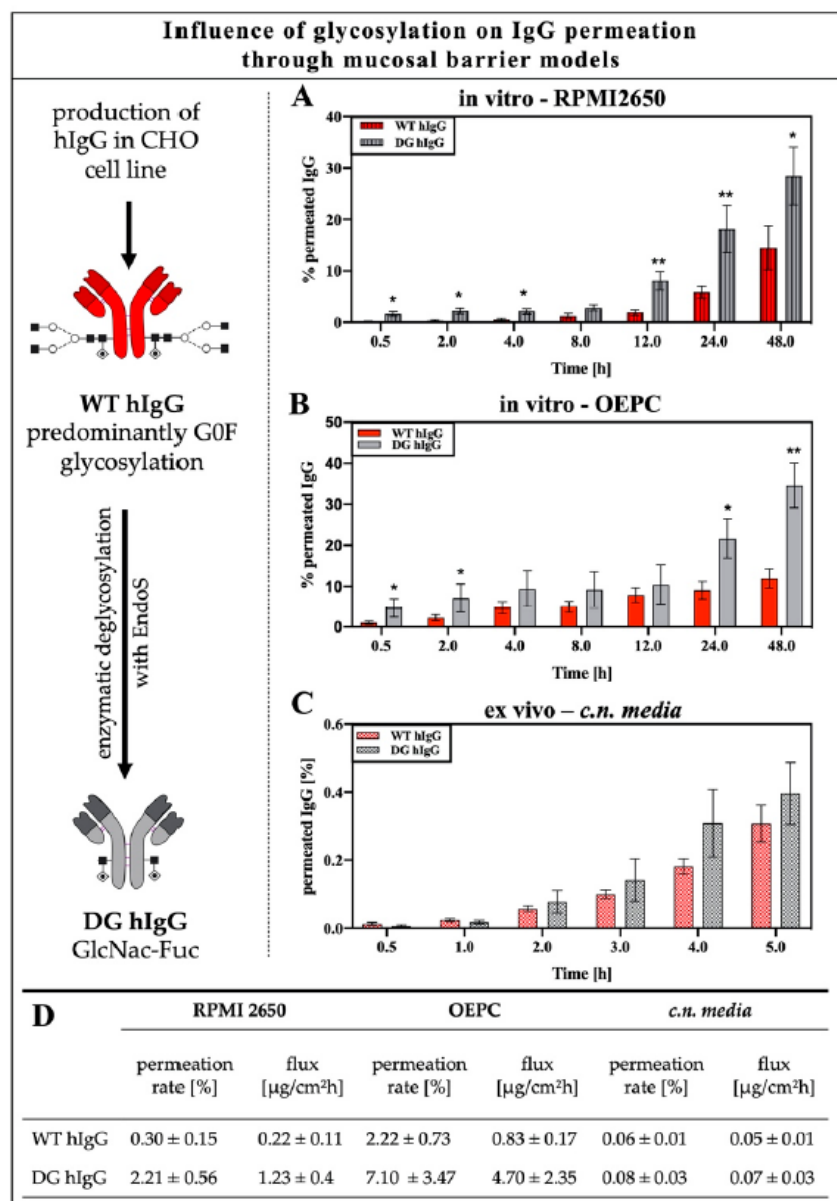


Figure 3. Permeation of wild-type (WT hIgG) and deglycosylated human IgG (DG hIgG) through RPMI 2650, porcine olfactory epithelial primary cells (OEPC) and porcine olfactory mucosa (c.n.media) (A) Percentage permeation of WT hIgG and DG hIgG through RPMI 2650 cells over 48 h. Error bars represent mean \pm SEM. $N = 3$, $n = 11$. (B) Percentage permeation of WT hIgG and DG hIgG through olfactory epithelial primary cells (OEPC) in vitro model over 48 h. Error bars represent mean \pm SEM. WT hIgG: $N = 4$, $n = 21$, DG hIgG: $N = 3$, $n = 10$. (C) Percentage permeation of WT hIgG and DG hIgG through excised nasal mucosa tissue explants (ex vivo) over 5 h. Error bars represent mean \pm SEM. WT hIgG: $N = 4$, $n = 29$, DG hIgG: $N = 3$, $n = 10$. (D) Tabular summary of permeation rate and flux of WT and DG hIgG in the in vitro models RPMI 2650 and OEPC and the ex vivo model c.n. media after 2 h. Results represent mean values \pm SEM. Permeation of wild-type (WT hIgG) and Endo S digested deglycosylated human IgG (DG hIgG) through porcine olfactory epithelial primary cells and porcine olfactory mucosa. Both in vitro models show significant differences ($p < 0.001$) in permeation rate and flux compared to the ex vivo model. Furthermore, the permeation through the OEPC model resulted in significantly higher permeation and flux compared to the RPMI 2650 model ($p < 0.001$). The significance was calculated by unpaired t-test. * $p < 0.05$, ** $p < 0.001$, error bars represent mean \pm SEM.

The transcription (Figure 4A,B) and the expression of *FCGRT* (gene of FcRn) in OEPC and RPMI 2650 (Figure 4C,D) were determined by RT PCR and Western blot and compared to porcine olfactory mucosa (*c.n. media*) as a reference [13]. There was a tendency observable for a lower expression level of FcRn in RPMI 2650 in comparison to OEPC and porcine *c.n. media* tissue, but this failed to reach statistical significance. FcRn expression in OEPC was comparable to *c.n. media* as the reference tissue. In both models, the intensity of FcRn immunofluorescence (Figure 4E,F) was roughly comparable with the semi-quantification by Western blot. It should be noted that different secondary antibodies had to be used to detect human and porcine FcRn and should hence not be compared head-to-head (Figure 4C–G). The differences in the cell morphology and size of RPMI 2650 and OEPC were described in detail recently [36]. In summary, FcRn expression was found in each of the three models even though differences in the expression levels were observed.

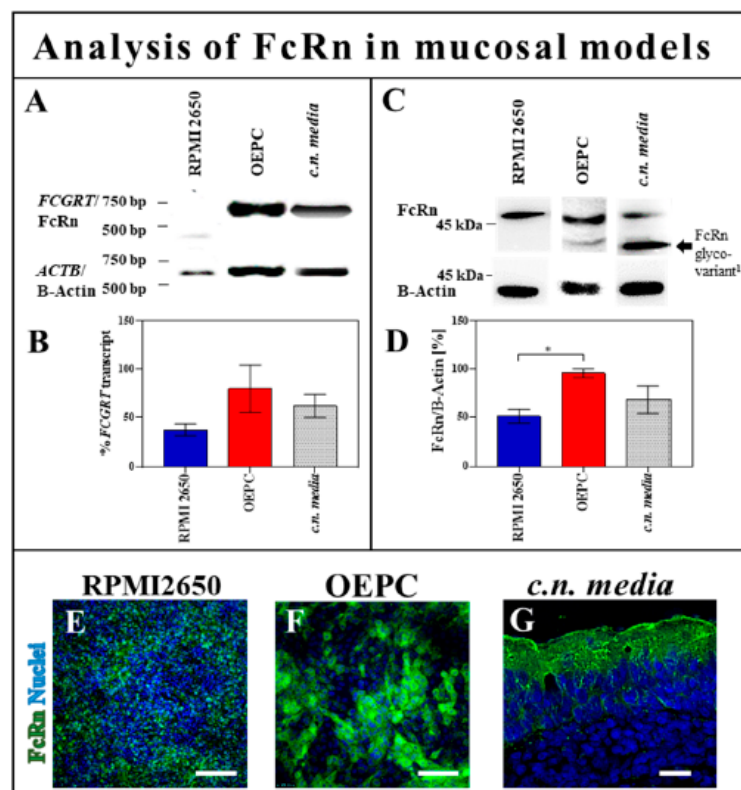


Figure 4. FcRn expression in olfactory epithelial primary cells and RPMI 2650 cells. (A) Reverse transcription PCR: *FCGRT* (gene of FcRn) transcription analysis in porcine olfactory epithelial primary cells (OEPC; expected size of amplified cDNA: *FCGRT* 635 bp, *ACTB* (gene of B-Actin): 612 bp), the human cell line RPMI 2650 (expected band size: *FCGRT*: 403 bp, *ACTB*: 612 bp) and the reference tissue from porcine olfactory mucosa (*c.n. media*). (B) A relative quantification was carried out by comparing the band intensity with a housekeeping gene. The significance was calculated by comparison of the OEPC and RPMI 2650 data with the *c.n. media* transcription data using an unpaired t-test. $n = 4$; error bars represent mean \pm SEM. (C) Western blot: FcRn expression analysis in OEPC, RPMI 2650 and *c.n. media* (B-Actin: 42 kDa., human and porcine FcRn: 42 kDa–46 kDa¹ depending on glycovariant) (D) For the quantification of multiple bands due to different glycovariants of the FcRn [14], intensities were summed up. Statistical analysis was performed as described for the transcription analysis using an unpaired t-test. * $p < 0.05$, $n = 4$; error bars represent mean \pm SEM. (E) Immunofluorescence study of FcRn expression (green) in RPMI 2650, OEPC (F) and *c.n. media* (G). Differences in cell morphology and size of OEPC and RPMI 2650 were discussed recently [36]. Scale bar: 50 µm.

3.2.2. Protein Interaction Study of FcRn and FCGR2 with Wild-Type and Deglycosylated IgG

It was previously demonstrated that the affinity of FcRn to IgGs with G0F-glycosylation is not significantly altered to Endo S digested (deglycosylated) IgGs deglycosylation, leaving a GlcNac-Fuc glycosylation pattern, as was the case for DG IgG in this study [51]. Hence, the significantly higher levels of DG IgG compared to WT IgG in both epithelial models (Figure 3A,B) appear to be linked to a glycosylation dependent Fc-interacting molecule, which allows faster and more efficient transport of DG IgG through the epithelial layer. Further, we may exclude that nasal epithelial IgG trafficking is only dependent on FcRn because of the insensitivity of FcRn to alteration of Fc-glycosylation [52]. To narrow down the number of potential glycosylation-sensitive Fc-interaction molecules, we focused here on FCGR, since their dependence on glycosylation was well demonstrated in many studies. Table 2 details and justifies why a particular focus was placed on FCGR2. Briefly, FCGR subclasses have a different level of sensitivity to Fc-glycosylation patterns. While FCGR1 is largely independent of Fc glycosylation, especially FCGR3a shows high sensitivity to fucose residues. Even when the Fc was trimmed back by Endo S to a GlcNac-Fuc residue, a 10-fold reduction in affinity was reported [53]. In general, FCGR2 and FCGR3a show almost a complete loss of affinity towards deglycosylated IgG [29].

Table 2. Fc receptors and their potential relevance in epithelial IgG trafficking.

Fc Receptor	Sensitivity to Deglycosylated IgG	Potential Relevance in Epithelial IgG Trafficking	Refs.
FCGR1	Rather insensitive due alternative binding domain.	Has not yet been implicated in IgG trafficking; expression in epithelial has not yet been demonstrated.	[30,32,53]
FCGR2	Endo S treatment of IgG decreases their interaction with FCGR2, but fucose does not alter the affinity to FCGR2.	Expression in epithelial cells from placenta was shown in several studies. Was linked to IgG trafficking of maternal IgG to the fetus in placental cell lines (FCGR2b).	[26,29,32,53,54]
FCGR3a	Endo S treatment abolishes the interaction with FCGR3, but also fucosylated IgGs such as hIgG used here were shown to bind with significantly decreased affinity.	Expression in human nasal epithelium was demonstrated. Controversially discussed for placental IgG trafficking.	[32,53,55,56]

As FCGR1 is insensitive to the Fc-glycopattern and FCGR3a is highly fucose sensitive, we assumed that the involvement of these receptors would not yield a remarkable difference in the permeation pattern of the fucosylated hIgG WT and the still fucosylated hIgG DG (GlcNac-Fuc) [29,53]. With this conclusion and due to the link between FCGR2 and IgG trafficking observed before in placenta, we focused here on FCGR2 [26].

FCGR2-immunoreactivity is rather low in comparison to FcRn (Figure 5A,B); therefore, the signal intensity was amplified using Image J software (Figure 5A) in order to visualize potential co-localization of FCGR2 with IgG. Nevertheless, co-localization of FcRn and FCGR2 could be shown in OEPC in permeation experiments of pIgG (Figure 5E) and hIgG (Figure 5H). Unfortunately, for pigs, only an antibody against both variants of the FCGR2 is commercially available and therefore the results cannot distinguish between FCGR2a and b variants. By RT-PCR, we could detect FCGR2b in *c.n. media* (data not shown). Interestingly, not all epithelial cells that appeared to have taken up IgG showed immunoreactivity against one or both of the Fc receptors (Figure 5E,H).

To investigate the interaction between allogenic pIgG and xenogenic hIgG with porcine FcRn, immunoprecipitation was performed (Figure 5I–K). IgGs were bound to Protein A agarose beads, and a pull down with lysates from OEPC containing endogenous levels of FcRn was performed. To yield enough cell lysate for the experiment, each analyte IgG was incubated with OEPC cell lysate from different batches. We found protein interaction of porcine and human IgG in their wild-type form as well as in their deglycosylated form with the FcRn (Figure 5J). The analysis resulted in two bands because of the different glycopatterns of the FcRn, as described above [14]. However, the human IgGs did not show the lower band, indicating that human IgGs bind only to one of the two glycovariants. Differences in band intensity were inconsistent between repetitive experiments. Therefore, no quantification was performed. Most probably, the batch-to-batch variability of the primary cell composition and cell count

used for the cell lysates causes these problems which we have not solved so far. This heterogeneity of OEPC cell lysates was described in more detail before [36]. However, the interaction of the WT and the DG variants for pIgG and hIgG with FcRn could be shown in OEPC cell lysates.

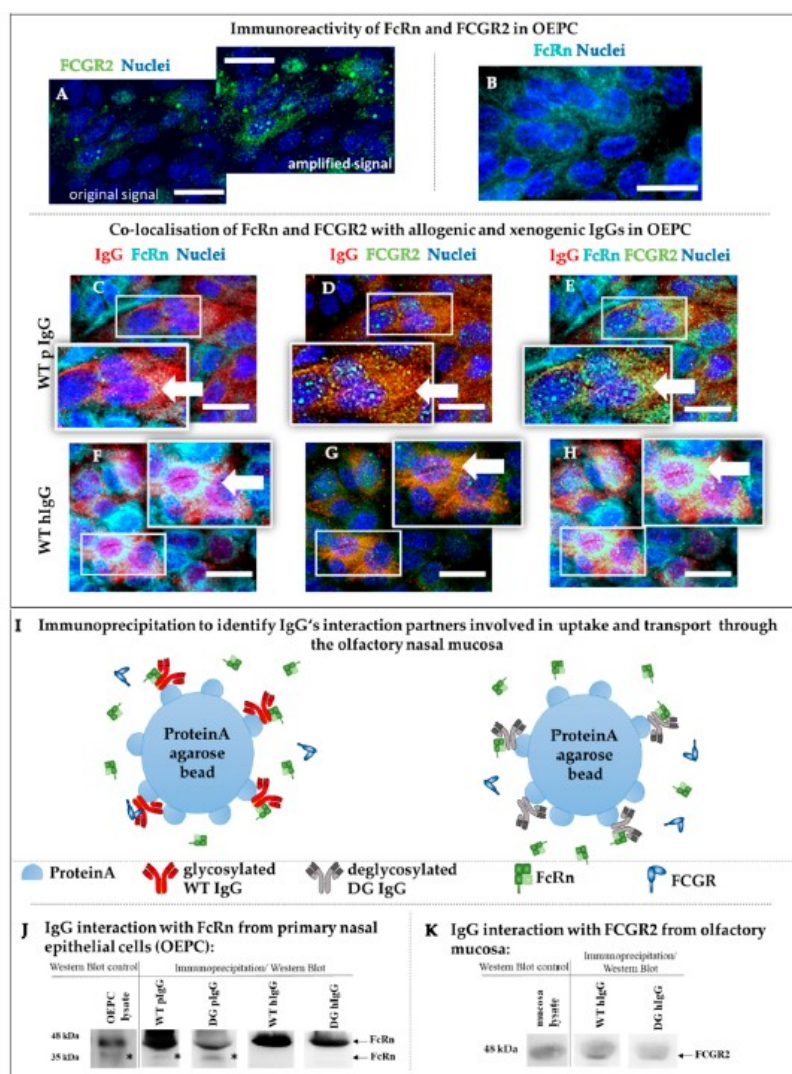


Figure 5. Analysis of IgG transporter expression and protein–protein interaction. (A–H) Co-localization study of FcRn (B,C,F) and FCGR2 (A,D,G) with porcine (D,E) and human (F–H) IgG in primary cells from olfactory epithelium (OEPC) (representative data are shown, $N = 3$, $n = 3$). (A) To visualize the low amount of FCGR2 (original), the intensity was highly increased (increased intensity) to evaluate co-localization with FcRn and IgG. FCGR2 expression was found to be mainly intracellular. (B) FcRn was found to be intracellular and on the cell's surface with sufficient immunoreactivity. (C–E) Co-localization of FCGR2 (green), FcRn (cyan) and pIgG (red). (F–H) Co-localization of FCGR2 (green), FcRn (cyan) and hIgG (red). Scale bar: 20 μ m, arrows mark sites of co-localization. (I) Underlying principle of the immunoprecipitation (IP) to evaluate the binding of wild-type (WT hIgG) and deglycosylated human IgG (DG hIgG) and porcine IgG (WT pIgG, DG pIgG) to the porcine FcRn. (J) IP study of FcRn interaction with wild-type and deglycosylated allogenic pIgG and xenogenic hIgG using primary cell lysate (OEPC, origin: porcine nasal mucosa, olfactory region) ($N = 3$). IgGs were incubated with OEPC cell lysate and captured using Protein A agarose beads. The resulting bands could not be quantified due to high batch-to-batch variations in the cell lysates. * The additional bands in the line of the WT and DG pIgG is caused by different glycovariants of the porcine FcRn [14]. hIgGs seem to bind only to one of the variants. (K) Interaction study (IP) of WT hIgG and DG hIgG with FCGR2 using whole mucosa lysate from *c.n. media*.

Due to the co-localization observed in Figure 5H, we performed immunoprecipitation also for interaction with FCGR2. However, immunoprecipitation for interaction of IgG and FCGR2 failed in OEPC cell lysates (data not shown), while a detection was possible in lysates of *c.n. media* whole tissue explants (Figure 5K). This could indicate a problem with the detection limit as FCGR2 is low expressed in epithelial cells (see Figure 5A). Unfortunately, there are no studies reported that have previously compared FcRn and FCGR expression head-to-head in pigs. Indeed, there is evidence that the expression level of FCGR2 is directly linked to cytokine expression in the organism [57]. As slaughterhouse pigs were used in this study, we cannot exclude experimental bias due to the health state of the pig. Furthermore, the choice and availability of antibodies against porcine FCGR is rather limited and, hence, no other antibodies against these antigens could be tested. Therefore, the interaction signals might be below detection limit of the Western blot.

4. Discussion

The understanding of IgG transport processes from the nasal mucosa to the brain is an important step on the way to developing specialized, intranasally applied, therapeutic IgGs against CNS-related and oncologic diseases. Many studies have used different approaches to investigate the general transport processes of antibodies in mucous membranes. Most of these studies concluded that FcRn plays a key role in antibody transport [58–62]. Hereby, apical monomeric IgGs are taken up via pinocytosis and are bound intracellularly by the FcRn under slightly acidic conditions in early endosomes [15]. Afterwards, the IgGs are recycled, as is known for endothelial cells, or transcytosed to the lamina propria in polarized epithelial cells [63].

In this study, first, the involvement of FcRn in IgG transport through porcine olfactory mucosa was evaluated in vitro via OEPC ALI culture models and ex vivo models. According to common knowledge, the FcRn is the main transporter in terms of IgG trafficking in epithelial and endothelial barriers. However, there are still open questions concerning IgG trafficking, especially from the nasal mucosa to the brain [23,25,64]. To simplify the complex mucosa with the highly heterogeneous epithelial layer containing gland cells, ciliated cells, immune-related cells, the mucous layer and the underlying lamina propria including blood vessels, glands and the local immune system, permeation experiments were performed in an epithelial primary cell ALI culture model to display only the first barrier of the mucosa. According to the literature, mucosal epithelial cells express the FcRn and are able to perform transcytosis to the underlying tissue [17,65]. The binding of IgGs to FcRn shows high cross-species reactivity; however, the binding affinities differ depending on the species [66–68]. It is known that the binding affinity and the FcRn-related transport is fairly similar for hIgG and pIgG in porcine epithelial cells. However, Stirling et al. showed that hIgGs are taken up more rapidly by porcine FcRn [14]. To gain further information about IgG transport in the epithelial barrier of porcine olfactory mucosa, the permeation rate and flux of hIgG and pIgGs were compared. The results shown in Figure 2A,B support the findings of faster uptake of hIgG. In early time points, the permeation rate as well as the flux of hIgG was higher compared to the pIgG but both assimilated after 8 h. We concluded in general that the permeation in the first epithelial barrier is not strongly dependent on IgG species origin. Nevertheless, by immunoprecipitation and immunofluorescence, we are the first to show an interaction of FcRn and IgG in the olfactory epithelial barrier roughly similar to other mucosal sites [14,15,69]. It must be mentioned that we used porcine serum IgGs and therefore cannot exclude IgG subclass-specific effects in our experiment as FcRn binding affinity depends on the IgG subclass [55]. However, there are still open questions in terms of the transcytosis process of IgG. It is, for example, unknown how the intracellular sorting of IgG is proceeded and how monoclonal IgG and immune complexes are distinguished [55]. In this context, also the pinocytosis uptake of IgGs in the epithelial cells can be addressed, as there is an acidic environment on the apical surface of the mucosal epithelium. Therefore, FcRn-mediated uptake would be possible as the binding affinity for IgG is highest around pH 6 to 6.5, which matches the pH of the mucous layer [70]. In contrast, Hornby et al. found evidence in 2014 for low FcRn surface expression in Caco-2 cells and a surface FcRn-IgG binding

that was inconsequential for overall transcytosis [71]. In addition, immunofluorescence staining against FcRn in OEPC shows that FcRn is not expressed in all epithelial cells but varied heavily in the cellular monolayer, indicating that FcRn expression is highly dependent on the cell type [72]. Again, this supports the common assumption of an uptake based mainly on pinocytosis. However, there is evidence for a bidirectional transport of IgG mediated by FcRn in the MDCK cell line expressing human FcRn [63]. If there is FcRn-mediated IgG transport from the basolateral to the acidic apical side in the nasal epithelial layer, how does the release of the IgG take place? Again, the involvement of an additional mechanism including a factor X receptor protein might be possible, as postulated before by Sockolovsky and Szoka in 2016 for the IgG recycling pathway [52].

Interestingly, in the complex ex vivo model, the permeation rate varies widely between the porcine and the human IgGs. Flux and permeation rates of the human IgG were significantly higher after 1 h in comparison to porcine IgG. This result is in accordance with a former immunofluorescence study in porcine olfactory mucosa and apparent degradation in lymphoid follicles [13]. Our data support the thesis of porcine IgG remaining in the tissue as the amount of porcine IgG recovered from the basolateral compartment was below or near to the detection limit and did not increase during the course of the experiment. In the former study, it was suggested that the species origin of the IgG is highly important for IgG transport and clearance in the nasal olfactory mucosa [13]. The data gained in the present study further indicate species-dependent IgG trafficking—however, not in the epithelial layer but in cellular structures of the underlying lamina propria. If FcRn would be the only transporter involved in IgG trafficking at the olfactory mucosa, it should be species-independent (regarding human and porcine IgG), as proven here in the in vitro model and by Stirling et al. in 2005 in tumor cells transfected with porcine FcRn [14]. Here, again, such a co-factor X involved in IgG trafficking could be considered.

In general, the permeation rate in the epithelial barrier model (OEPC ALI culture) was more than 35-fold higher for both IgGs compared to the ex vivo mucosa model after 2 h. Hereby, influencing factors such as the longer distance through the whole tissue, the connective underlying tissue as well as recycling and clearance at blood vessels or glands will reduce the amount of permeated IgG. However, the big difference between the human and the porcine IgG cannot be explained by these parameters if FcRn is assumed to be the only transporter involved. Instead, the missing link might be the mucosal immune system. The immune system in the porcine and human nasal mucosa is organized in so-called lymphoid follicles (LF) [13,73–75]. These LFs consist of B and T cell agglomerates as well as isolated monocytes and dendritic cells (DCs) [74,75]. Furthermore, beneath the epithelial layer, DCs and macrophages are located and involved in immune surveillance at the mucosal barrier [75–77]. We have shown recently that LF areas are spared from permeated IgG, indicating immune-related uptake and degradation processes [13]. Further, it is known from intestinal mucosal sites that transcytosed immune complexes are taken up by DCs directly beneath the epithelial layer. These immune complexes are taken up by other Fc binding receptors: the FCGRs. FCGRs are a heterogeneous group of cell surface glycoproteins that interact with antibody–antigen complexes and initiate defending responses in effector cells of the immune system. FCGRs regulate a variety of immune responses such as phagocytosis, degranulation, antibody-dependent cellular cytotoxicity, transcriptional regulation of cytokine and chemokine expression, B cell activation and immune complex clearance [78]. A hint of a direct or indirect interaction of FcRn with FCGRs is the FcRn-mediated intracellular routing to cross-presentation compartments in DCs [55]. However, the exact intracellular mechanism responsible for directing immune complexes remains largely unclear.

Are FCGRs the missing factor X and are they involved in IgG trafficking in the epithelia? In 2019, Golebski et al. published the involvement of FCGR3 and TLR4 in discrimination between commensal and invading bacteria in human nasal epithelial cells [56]. The expression of FCGR in the nasal epithelium strengthens the hypothesis of crosstalk of FCGR and FcRn in IgG transport and sorting processes in the epithelium. Another interesting study was carried out by Ishikawa et al. in 2015 that demonstrated maternal IgG trafficking in human placental endothelial cells mediated by FCGR2b in

the absence of FcRn [26]. They further suggest that IgG internalization and transcytosis is mediated rather by FCGR2b than FcRn in the placental endothelium. This could explain why serum albumin, which is also recycled by FcRn, is not transcytosed across the placental barrier [79]. Hence, based on the expression of FCGR2 in OEPC, FCGR2 could be a possible candidate in the search for factor X (see Figure 6). However, species-related special has to be considered as, for example, unlike in humans, maternal IgGs do not cross the porcine placenta to reach the fetus, even though FcRn is expressed there [80].

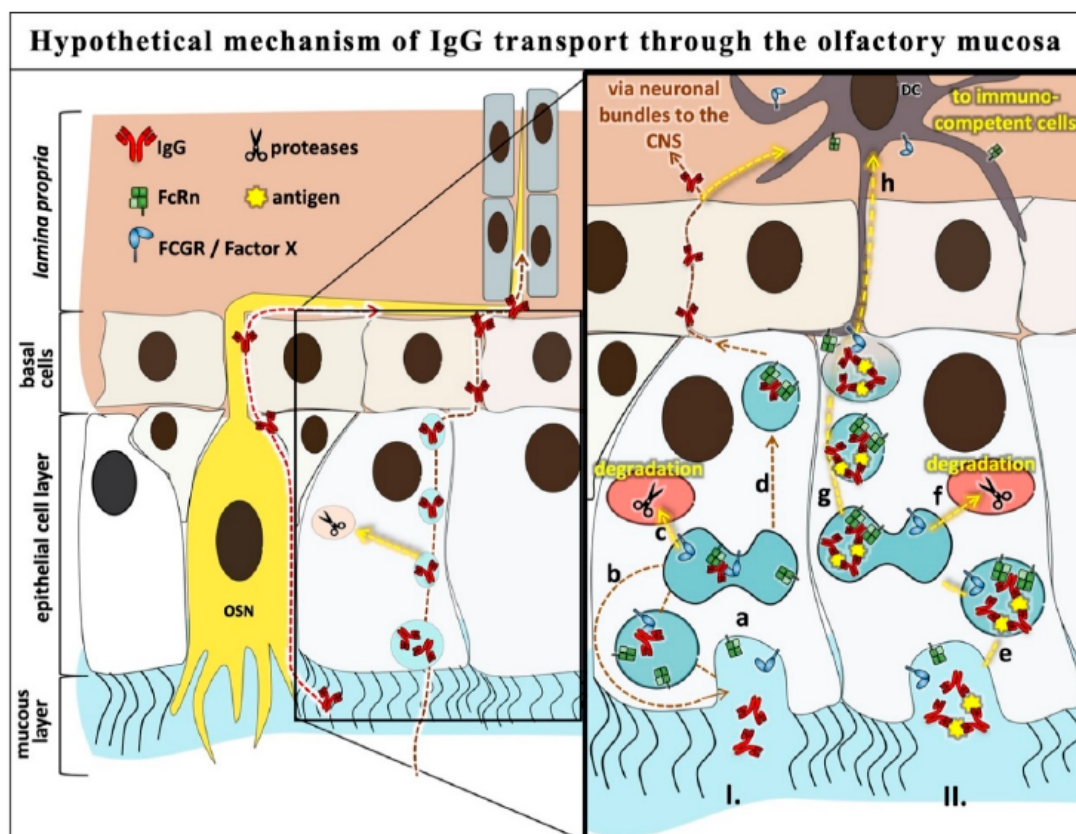


Figure 6. Cross-binding hypothesis: hypothetical mechanism of IgG transport through the olfactory mucosa. I. (a) Uptake of monomeric IgGs was presumably via pinocytosis, but FcRn was also found at the apical surface [13] and vesicle transport to the sorting compartment. (b) Cross-binding of IgG with FcRn and a second Fc receptor such as FCGR2, which might be factor X as suggested [52]; recycling back to the apical surface or (c) lysosomal degradation. Alternatively, a second FcRn replaces FCGR2/factor X and (d) the monomeric IgG is transcytosed to the lamina propria/basolateral side. II. (e) Uptake of immune complexes similar to monomeric IgG and vesicle transport to the sorting compartment. Binding to FCGR2/factor X is not possible due to steric hindrance; therefore, double binding of FcRn to one Fc part is possible. The complex can either (f) be degraded in the lysosome or (g) transcytosed to the lamina propria and (h) taken up by dendritic cells (DC) via different FCGRs or FcRn. Further studies are needed to confirm the role of FCGR2 in IgG trafficking in the airway epithelia. Due to limitations of the commercially available anti-porcine FCGR2 antibodies, we could not distinguish between FCGR2a and FCGR2b. Nevertheless, other studies suggest FCGR2b to be expressed in epithelial cells.

The binding of IgG to low-affinity FCGRs is highly dependent on the glycosylation of the IgG despite the binding to the high-affinity receptor FCGR1 [53]. To directly gain some ideas regarding which FCGR type might be involved in nasal IgG transport, a fucosylated human IgG1 was deglycosylated using the enzyme Endo S that leaves a glycan residue of N-Acetylglucosamine (GlcNAc) and fucose at asparagine 297 (see Supplemental Figure S1; for details concerning the Fc-glycosylation

sensitivity of different FCGR types, see Table 2). This IgG and its glycosylation pattern were described previously [41,46]. It should be noted that a human IgG was used due to the lack of commercially available monomeric porcine IgGs with a defined glycopattern. However, a recent study showed comparable binding of human and porcine IgG to the porcine FCGR1, FCGR2a and FCGR2b but no interaction with the porcine FCGR3a [35]. Therefore, we cannot make any assumptions about the involvement of this receptor type. However, as the human IgG used in this study is fucosylated (GalNac-Fuc) and the common IgG fucosylation patterns are known to highly decrease the affinity to FCGR3a, an interaction is rather unlikely [53]. If the high-affinity FCGR1 would be the only FCGR involved in nasal IgG trafficking, no difference between the WT IgG and the DG IgG should be detected as it is known to be mainly unaffected by deglycosylation in human. Hence, since FCGR2b was the only FCGR described to be involved in epithelial IgG trafficking we focused on this subclass.

Significantly higher levels of DG IgG were detected in the epithelial models compared to WT IgG (Figure 3). In the ex vivo nasal mucosa model, a tendency towards higher levels was detected; however, due to the high standard variation, this failed to demonstrate statistical significance. It was demonstrated that the affinity of FcRn to IgG is rather unaffected by deglycosylation of IgG; hence, we can exclude the notion that nasal epithelial IgG trafficking is only dependent on FcRn [51,52]. Further, the higher flux of DG IgG in the ex vivo mucosa model may indicate that other Fc receptors like FCGRs are not only involved in IgG trafficking through the epithelial layer but also in crosstalk to cells of the *lamina propria* (Figure 6).

To exclude interspecies effects due to the use of human IgG in porcine tissue and cells, the permeation experiments were repeated using the nasal mucosa standard cell line RPMI 2650 [37,39,49]. The results from the OEPC model could be confirmed in the RPMI 2650 model, indicating again a cross-species mechanism for IgG trafficking. The permeation rate in RPMI 2650 was unexpectedly low compared to the permeation rate through the primary cell layer. It was shown before that OEPC forms a much tighter barrier compared to the RPMI 2650 cells [34]. Furthermore, RPMI 2650 cells grow in multilayers and do not completely polarize like primary epithelial cells [36,37,81]. Apparently, the amount of FcRn directly correlates with IgG flux even in this rather leaky model. OEPC demonstrated the highest protein expression followed by RPMI 2650 cells and olfactory mucosa (Figure 4). In an immunoprecipitation study using OEPC lysates, little tendency of lower FcRn interaction when using deglycosylated IgG could be shown. However, due to high variabilities between the samples with cells of different batches, it cannot be considered as a significant result. Nevertheless, a clear interaction between IgG and FcRn was shown. The correlation between IgG uptake and FcRn expression, together with the results from the immunoprecipitation study and the permeation study using DG IgG, suggest that it is likely that FcRn is involved in IgG trafficking in the nasal mucosa, but not exclusively.

Since deglycosylated IgGs show higher permeation rates in all models, there was the assumption of an IgG glycosylation sensitive factor X that is involved in the transport. As FCGR2 was already identified to be involved in IgG trafficking in the placenta, this target was the first attempt to identify the factor X [26].

So far, identification of FCGR2 transcripts has yet not given any reliable results, possibly due to the lack of valid mRNA sequences for porcine FCGR transcripts. Therefore, an immunofluorescence study was performed to check for FCGR2 expression. Unfortunately, we cannot distinguish between the subtypes a, b and c of FCGR2 in this study. Nevertheless, co-localization was found between FcRn, IgG and FCGR2 for both IgGs in the OEPC model (Figure 5C–H). Without interaction studies of FcRn together with FCGR2b and IgG, a final conclusion cannot be made. As described above, also FCGR3a was found in nasal epithelial cells. However, we can exclude this receptor from being involved in this study as we used deglycosylated hIgGs that still contain a fucose residue in their glycosylation pattern. As mentioned before, even a small glycosylation residue containing fucose will significantly reduce interaction with FCGR3 and therefore the permeation pattern in this study should not have changed between hIgG WT and hIgG DG [82]. There are several facts in favor for the hypothesis of

FCGR involvement. For example, an IgG3 variant with hinge-region deletions that prevent binding to FCGR but not to FcRn was still transported across the human placenta [83]. Likewise, deglycosylated IgGs were transported in mice [84]. Furthermore, a comparison of glycosylation patterns between fetal and maternal IgG by Stapelton et al. in 2018 concluded that IgG transport was not glycosylation selective [85]. Regardless, the differences in permeation rate between WT and DG IgG, together with the differential transport of IgG subclasses described in several studies, suggests that there is at least one factor X involved in IgG transport in the nasal mucosa in addition to FcRn [61,86,87].

5. Conclusions

In the present study, we showed, for the first time, the differences in permeation rate between allogenic and xenogenic IgGs as well as WT IgG and DG IgG in ex vivo olfactory mucosa, primary olfactory epithelial cells and RPMI 2650.

In this study, we present new insights into IgG trafficking. On the one hand, we showed that permeation with IgG from alien species did not result in an altered permeation rate in the epithelial barrier but in the underlying lamina propria. In more detail, the permeation rate of pIgG and hIgG did not differ in the epithelial barrier model but in the whole tissue explant. Hereby, as seen in immunofluorescence studies before, pIgG crosses the mucosa in very low amounts or not at all, whereas hIgG was detectable in higher levels at the basolateral side [13]. Most probably, this effect could be explained by the immune-related uptake of the pIgGs and the different binding affinities to the porcine FCGR2 and FCGR3 [35]. On the other hand, we show strong evidence for the dependence of IgG transport on the glycosylation status of the IgG.

DG IgG showed significantly higher permeation rates in all models compared to the WT IgG. The highest difference was shown in the primary cell model and therefore in the first epithelial layer of the mucosa. These results could hint at an additional mechanism including a still unknown factor X involved in IgG trafficking in epithelial cells that is dependent on the IgG glycosylation. In Figure 6, the cross-binding hypothesis that is derived from the data of this study is displayed.

The underlying principle of the cross-binding hypothesis is the idea that antibody agglomerates that have bound to an antigen, so-called immune complexes, are transferred to immune competent cells such as DCs in the lamina propria. Such a mechanism would ensure that the mucosal surface is monitored by the underlying immune system to prevent infection. In contrast, the transcytosis of unbound, monomeric IgGs from the apical to the basolateral side may not be very important for immune surveillance. Therefore, it would make sense that it may occur as an occasional event or due to a high antibody concentration on the apical surface as it can occur during intranasal delivery. It may also be possible that the suggested factor X is expressed in a substantially lower amount compared to FcRn and therefore a double binding of Fc by two FcRn proteins is enabled if a high amount of IgG is present on the apical side of the epithelial cell. To distinguish between monomeric IgG and multimeric immune complexes, the additional factor X might be involved. In this hypothesis, factor X binds to the glycosylated hinge region of IgG in combination to FcRn to ensure either lysosomal IgG degradation or recycling back to the apical surface (Figure 6I). In immune complexes, the hinge region might not be freely accessible and may not bind to factor X due to steric hindrance. In this case, double binding or multiple binding of FcRn could be possible and might give the signal for transcytosis. The basolateral endocytosed immune complex could then be taken up by DCs via FCGRs (Figure 6II).

Due to the fact that, for most FCGRs, their affinity to IgG Fc is dependent on Fc glycosylation, it is likely that the suggested factor X could be one of the FCGRs or a not yet identified Fc binding protein. Because of literature based data, we made the first attempt to verify the involvement of FCGR2 not only in the placenta but also in the olfactory epithelium [26]. However, further research is needed to confirm these observations and the use of this transcytosis mechanism for IgG drug delivery in the airway.

Supplementary Materials: The following are available online at <http://www.mdpi.com/1999-4923/12/11/1014/s1>, Figure S1: HILIC analysis of hIgG glycan pattern digested either in total (PNGaseF) or by Endo S.

Author Contributions: Conceptualization, S.L., K.S.; Methodology, S.L., J.F.; Validation, S.L., P.S., R.H., F.M., A.H.; Investigation, S.L., R.H., P.S., H.H.; Resources, K.S.; Visualization, S.L., K.S.; Writing—Original Draft Preparation, S.L., K.S.; Writing—Review and Editing, J.F., F.M., R.H., P.S., A.H., T.H., B.M.; Supervision, K.S., B.M.; Project Administration, K.S.; Funding Acquisition, K.S. All authors have read and agreed to the published version of the manuscript.

Funding: This study was supported by an EU grant “N2B-patch” under the European Framework Programme for Research and Innovation Horizon 2020 (Grant No. 721098; www.n2b-patch.eu), from a grant “FcRn in Drug Delivery” funded by the Baden-Württemberg State Ministry of Science, Research and Arts, from a grant “ALIVE” funded by the Federal Ministry for Economic Affairs and Energy (BMWi) and from fellowships from the Stiftung der Deutschen Wirtschaft (to S.L. and J.F.).

Acknowledgments: Special thanks to Rene Handrick from Biberach University for excellent advisory and technical support whenever needed. Furthermore, special thanks to Angelika Rück and Sviatlana Kalinina from the core facility for confocal and multiphoton microscopy of the Ulm University. In addition, the authors thank Lena Spindler and Jerome Egli for their excellent revision of the manuscript. Many thanks also to the Pirbright Institute and Probiogen for kindly providing us with the antibodies used in this study.

Conflicts of Interest: The authors declare no conflict of interest.

References

- Kaplan, H.; Reichert, J.M. Antibodies to watch in 2019. *MAbs* **2019**, *11*, 219–238. [[CrossRef](#)] [[PubMed](#)]
- Hay, M.; Thomas, D.W.; Craighead, J.L.; Economides, C.; Rosenthal, J. Clinical development success rates for investigational drugs. *Nat. Biotechnol.* **2014**, *32*, 40–51. [[CrossRef](#)] [[PubMed](#)]
- Freskgård, P.O.; Urich, E. Antibody therapies in CNS diseases. *Neuropharmacology* **2017**, *120*, 38–55. [[CrossRef](#)] [[PubMed](#)]
- Carman, A.J.; Mills, J.H.; Krenz, A.; Kim, D.-G.; Bynoe, M.S. Adenosine Receptor Signaling Modulates Permeability of the Blood-Brain Barrier. *J. Neurosci.* **2011**, *31*, 13272–13280. [[CrossRef](#)]
- Rodriguez, A.; Tatter, S.B.; Debinski, W. Neurosurgical techniques for disruption of the blood–brain barrier for glioblastoma treatment. *Pharmaceutics* **2015**, *7*, 175–187. [[CrossRef](#)]
- Burgess, A.; Shah, K.; Hough, O.; Hynynen, K.; Burgess, A. Expert Review of Neurotherapeutics through the blood—Brain barrier Focused ultrasound-mediated drug delivery through the blood – brain barrier. *Expert. Rev. Neurother.* **2015**, *17*, 477–491. [[CrossRef](#)]
- Manich, G.; Cabezon, I.; del Valle, J.; Duran-Vilaregut, J.; Camins, A.; Pallàs, M.; Pelegrí, C.; Vilaplana, J. Study of the transcytosis of an anti-transferrin receptor antibody with a Fab’ cargo across the blood–brain barrier in mice. *Eur. J. Pharm. Sci.* **2013**, *49*, 556–564. [[CrossRef](#)]
- Fishman, J.B.; Rubin, J.B.; Handrahan, J.V.; Connor, J.R.; Fine, R.E. Receptor-mediated transcytosis of transferrin across the blood-brain barrier. *J. Neurosci. Res.* **1987**, *18*, 299–304. [[CrossRef](#)]
- Urayama, A.; Grubb, J.H.; Sly, W.S.; Banks, W.A. Mannose 6-Phosphate Receptor–mediated Transport of Sulfamidase Across the Blood–brain Barrier in the Newborn Mouse. *Mol. Ther.* **2008**, *16*, 1261–1266. [[CrossRef](#)]
- Gänger, S.; Schindowski, K. Tailoring formulations for intranasal Nose-to-Brain delivery via the olfactory area: A review on physico-chemical characteristics and mucociliary clearance of the nasal olfactory mucosa. *Pharmaceutics* **2018**, *10*, 116. [[CrossRef](#)]
- Mittal, D.; Ali, A.; Md, S.; Baboota, S.; Sahni, J.K.; Ali, J. Insights into direct nose to brain delivery: Current status and future perspective. *Drug Deliv.* **2014**, *21*, 75–86. [[CrossRef](#)] [[PubMed](#)]
- Pardeshi, C.V.; Belgamwar, V.S. Direct nose to brain drug delivery via integrated nerve pathways bypassing the blood–brain barrier: An excellent platform for brain targeting. *Expert Opin. Drug Deliv.* **2013**, *10*, 957–972. [[CrossRef](#)] [[PubMed](#)]
- Ladel, S.; Flamm, J.; Zadeh, A.S.; Filzwieser, D.; Walter, J.C.; Schlossbauer, P.; Kinscherf, R.; Lischka, K.; Luksch, H.; Schindowski, K. Allogenic fc domain-facilitated uptake of IgG in nasal Lamina propria: Friend or foe for intranasal CNS delivery? *Pharmaceutics* **2018**, *10*, 107. [[CrossRef](#)] [[PubMed](#)]
- Stirling, C.M.A.; Charleston, B.; Takamatsu, H.; Claypool, S.; Lencer, W.; Blumberg, R.S.; Wileman, T.E. Characterization of the porcine neonatal Fc receptor—Potential use for trans-epithelial protein delivery. *Immunology* **2005**, *114*, 542–553. [[CrossRef](#)] [[PubMed](#)]

15. Spiekermann, G.M.; Finn, P.W.; Ward, E.S.; Dumont, J.; Dickinson, B.L.; Blumberg, R.S.; Lencer, W.I. Receptor-mediated Immunoglobulin G Transport Across Mucosal Barriers in Adult Life. *J. Exp. Med.* **2002**, *196*, 303–310. [\[CrossRef\]](#) [\[PubMed\]](#)
16. Yoshida, M.; Masuda, A.; Kuo, T.T.; Kobayashi, K.; Claypool, S.M.; Takagawa, T.; Kutsumi, H.; Azuma, T.; Lencer, W.I.; Blumberg, R.S. IgG transport across mucosal barriers by neonatal Fc receptor for IgG and mucosal immunity. *Springer Semin. Immunopathol.* **2006**, *28*, 397–403. [\[CrossRef\]](#)
17. Roopenian, D.C.; Akilesh, S. FcRn: The neonatal Fc receptor comes of age. *Nat. Rev. Immunol.* **2007**, *7*, 715–725. [\[CrossRef\]](#)
18. de Taeye, S.W.; Rispen, T.; Vidarsson, G. The Ligands for Human IgG and Their Effector Functions. *Antibodies* **2019**, *8*, 30. [\[CrossRef\]](#)
19. Zhang, W.; Wang, W.; Li, S.; Jia, S.; Zhang, X.; Cao, T. Localization of neonatal Fc receptor for IgG in aggregated lymphoid nodules area in abomasum of Bactrian camels (*Camelus bactrianus*) of different ages. *BMC Vet. Res.* **2016**, *237*. [\[CrossRef\]](#)
20. Xiao, G.; Gan, L.-S. Receptor-mediated endocytosis and brain delivery of therapeutic biologics. *Int. J. Cell Biol.* **2013**, *2013*, 703545. [\[CrossRef\]](#)
21. Iwasaki, A. Immune Regulation of Antibody Access to Neuronal Tissues. *Trends Mol. Med.* **2017**, *23*, 227–245. [\[CrossRef\]](#) [\[PubMed\]](#)
22. Garg, A.; Balthasar, J.P. Investigation of the influence of FcRn on the distribution of IgG to the brain. *AAPS J.* **2009**, *11*, 553–557. [\[CrossRef\]](#) [\[PubMed\]](#)
23. Ruano-salguero, J.S.; Lee, K.H. Antibody transcytosis across brain endothelial-like cells occurs nonspecifically and independent of FcRn. *Sci. Rep.* **2020**, *1–10*. [\[CrossRef\]](#) [\[PubMed\]](#)
24. Guilleminault, L.; Azzopardi, N.; Arnoult, C.; Sobilo, J.; Herve, V.; Montharu, J.; Diot, P. Fate of inhaled monoclonal antibodies after the deposition of aerosolized particles in the respiratory system. *J. Control Release* **2014**, *196*, 344–354. [\[CrossRef\]](#)
25. Abuqayyas, L.; Balthasar, J.P. Investigation of the role of FcγR and FcRn in mAb distribution to the brain. *Mol. Pharm.* **2013**, *10*, 1505–1513. [\[CrossRef\]](#)
26. Ishikawa, T.; Takizawa, T.; Iwaki, J.; Mishima, T.; Ui-Tei, K.; Takeshita, T.; Matsubara, S.; Takizawa, T. Fc gamma receptor IIb participates in maternal IgG trafficking of human placental endothelial cells. *Int. J. Mol. Med.* **2015**, *35*, 1273–1289. [\[CrossRef\]](#)
27. Subedi, G.P.; Barb, A.W. The immunoglobulin G1 N-glycan composition affects binding to each low affinity Fc γ receptor. *MAbs* **2016**, *8*, 1512–1524. [\[CrossRef\]](#)
28. Stewart, R.; Hammond, S.A.; Oberst, M.; Wilkinson, R.W. The role of Fc gamma receptors in the activity of immunomodulatory antibodies for cancer. *J. Immunother. Cancer* **2014**, *2*, 9. [\[CrossRef\]](#)
29. Allhorn, M.; Olin, A.I.; Nimmerjahn, F.; Colin, M. Human IgG/FcγR interactions are modulated by streptococcal IgG glycan hydrolysis. *PLoS ONE* **2008**, *3*. [\[CrossRef\]](#)
30. Hayes, J.M.; Wormald, M.R.; Rudd, P.M.; Davey, G.P. Fc gamma receptors: Glycobiology and therapeutic prospects. *J. Inflamm. Res.* **2016**, *9*, 209–219. [\[CrossRef\]](#)
31. Lux, A.; Yu, X.; Scanlan, C.N.; Nimmerjahn, F. Impact of Immune Complex Size and Glycosylation on IgG Binding to Human FcγRs. *J. Immunol.* **2013**, *190*, 4315–4323. [\[CrossRef\]](#) [\[PubMed\]](#)
32. Cambay, F.; Raymond, C.; Brochu, D.; Gilbert, M.; Tu, T.M.; Cantin, C.; Lenferink, A.; Grail, M.; Henry, O.; De Crescenzo, G.; et al. Impact of IgG1 N-glycosylation on their interaction with Fc gamma receptors. *Curr. Res. Immunol.* **2020**, *1*, 23–37. [\[CrossRef\]](#)
33. Franz-Montan, M.; Serpe, L.; Martinelli, C.C.M.; Da Silva, C.B.; dos Santos, C.P.; Novaes, P.D.; Volpato, M.C.; De Paula, E.; Lopez, R.F.V.; Groppo, F.C. Evaluation of different pig oral mucosa sites as permeability barrier models for drug permeation studies. *Eur. J. Pharm. Sci.* **2016**, *81*, 52–59. [\[CrossRef\]](#) [\[PubMed\]](#)
34. Tulinski, P.; Fluit, A.C.; van Putten, J.P.M.; de Bruin, A.; Glorieux, S.; Wagenaar, J.A.; Duim, B. An Ex Vivo Porcine Nasal Mucosa Explants Model to Study MRSA Colonization. *PLoS ONE* **2013**, *8*, e053783. [\[CrossRef\]](#) [\[PubMed\]](#)
35. Egli, J.; Schlothauer, T.; Spick, C.; Seeber, S.; Singer, T.; Odermatt, A.; Iglesias, A. The Binding of Human IgG to Minipig FcγRs—Implications for Preclinical Assessment of Therapeutic Antibodies. *Pharm. Res.* **2019**, *36*, 47. [\[CrossRef\]](#) [\[PubMed\]](#)

36. Ladel, S.; Schlossbauer, P.; Flamm, J.; Luksch, H.; Mizaikoff, B.; Schindowski, K. Improved In Vitro Model for Intranasal Mucosal Drug Delivery: Primary Olfactory and Respiratory Epithelial Cells Compared with the Permanent Nasal Cell Line RPMI 2650. *Pharmaceutics* **2019**, *11*, 367. [\[CrossRef\]](#)
37. Schmidt, M.C.; Peter, H.; Lang, S.R.; Ditzinger, G.; Merkle, H.P. In vitro cell models to study nasal mucosal permeability and metabolism. *Adv. Drug Deliv. Rev.* **1998**, *29*, 51–79. [\[CrossRef\]](#)
38. Pozzoli, M.; Sonvico, F.; Ong, H.X.; Traini, D.; Bebawy, M.; Young, P.M. Optimization of RPMI 2650 Cells as a Model for Nasal Mucosa. *Respir. Drug Deliv.* **2014**, *2*, 739–742.
39. Mercier, C.; Hodin, S.; He, Z.; Perek, N.; Delavenne, X. Pharmacological Characterization of the RPMI 2650 Model as a Relevant Tool for Assessing the Permeability of Intranasal Drugs. *Mol. Pharm.* **2018**, *15*, 2246–2256. [\[CrossRef\]](#)
40. Jadhav, K.; Gambhire, M.; Shaikh, I.; Kadam, V.; Pisal, S. Nasal Drug Delivery System-Factors Affecting and Applications. *Curr. Drug Ther.* **2008**, *2*, 27–38. [\[CrossRef\]](#)
41. Collin, M.; Shannon, O.; Björck, L. IgG glycan hydrolysis by a bacterial enzyme as a therapy against autoimmune conditions. *Proc. Natl. Acad. Sci. USA* **2008**, *105*, 4265–4270. [\[CrossRef\]](#) [\[PubMed\]](#)
42. Samson, G.; García De La Calera, A.; Dupuis-Girod, S.; Faure, F.; Decullier, E.; Paintaud, G.; Vignault, C.; Scoazec, J.Y.; Pivot, C.; Plauchu, H.; et al. Ex vivo study of bevacizumab transport through porcine nasal mucosa. *Eur. J. Pharm. Biopharm.* **2012**, *80*, 465–469. [\[CrossRef\]](#) [\[PubMed\]](#)
43. de Courcey, F.; Zholos, A.V.; Atherton-Watson, H.; Williams, M.T.S.; Canning, P.; Danahay, H.L.; Elborn, J.S.; Ennis, M. Development of primary human nasal epithelial cell cultures for the study of cystic fibrosis pathophysiology. *Am. J. Physiol. Physiol.* **2012**, *303*, C1173–C1179. [\[CrossRef\]](#)
44. Mackness, B.C.; Jaworski, J.A.; Boudanova, E.; Park, A.; Valente, D.; Mauriac, C.; Pasquier, O.; Schmidt, T.; Kabiri, M.; Kandira, A.; et al. Antibody Fc engineering for enhanced neonatal Fc receptor binding and prolonged circulation half-life. *MAbs* **2019**, *11*, 1276–1288. [\[CrossRef\]](#) [\[PubMed\]](#)
45. Collin, M.; Olsén, A. Effect of SpeB and EndoS from *Streptococcus pyogenes* on human immunoglobulins. *Infect. Immun.* **2001**, *69*, 7187–7189. [\[CrossRef\]](#)
46. Collin, M.; Björck, L. Toward Clinical use of the IgG Specific Enzymes IdeS and EndoS against Antibody-Mediated Diseases. *Methods Mol. Biol.* **2017**, *1535*, 357. [\[CrossRef\]](#)
47. Reichl, S.; Becker, K. Cultivation of RPMI 2650 cells as an in-vitro model for human transmucosal nasal drug absorption studies: Optimization of selected culture conditions. *J. Pharm. Pharmacol.* **2012**, *64*, 1621–1630. [\[CrossRef\]](#)
48. Wengst, A.; Reichl, S. RPMI 2650 epithelial model and three-dimensional reconstructed human nasal mucosa as in vitro models for nasal permeation studies. *Eur. J. Pharm. Biopharm.* **2010**, *74*, 290–297. [\[CrossRef\]](#)
49. Mercier, C.; Perek, N.; Delavenne, X. Is RPMI 2650 a Suitable In Vitro Nasal Model for Drug Transport Studies? *Eur. J. Drug Metab. Pharmacokinet.* **2018**, *43*, 13–24. [\[CrossRef\]](#)
50. Foss, S.; Grevys, A.; Sand, K.M.K.; Bern, M.; Blundell, P.; Michaelsen, T.E.; Pleass, R.J.; Sandlie, I.; Andersen, J.T. Enhanced FcRn-dependent transepithelial delivery of IgG by Fc-engineering and polymerization. *J. Control Release* **2016**, *223*, 42–52. [\[CrossRef\]](#) [\[PubMed\]](#)
51. Wada, R.; Matsui, M.; Kawasaki, N. Influence of N-glycosylation on effector functions and thermal stability of glycoengineered IgG1 monoclonal antibody with homogeneous glycoforms. *MAbs* **2019**, *11*, 350–372. [\[CrossRef\]](#) [\[PubMed\]](#)
52. Sockolosky, J.T.; Szoka, F.C. The neonatal Fc receptor, FcRn, as a target for drug delivery and therapy. *Adv. Drug Deliv. Rev.* **2016**, *91*, 109–124. [\[CrossRef\]](#) [\[PubMed\]](#)
53. Hanson, Q.M.; Barb, A.W. A perspective on the structure and receptor binding properties of immunoglobulin G Fc. *Biochemistry* **2015**, *54*, 2931–2942. [\[CrossRef\]](#) [\[PubMed\]](#)
54. Hayes, J.M.; Cosgrave, E.F.J.; Struwe, W.B.; Wormald, M.; Davey, G.P.; Jefferis, R.; Rudd, P.M. *Fc Receptors: Humanized Mice to Study FcγR Function*; SpringerLink: New York, NY, USA, 2014; Volume 382, ISBN 978-3-319-07910-3.
55. Pyzik, M.; Sand, K.M.K.; Hubbard, J.J.; Andersen, J.T.; Sandlie, I.; Blumberg, R.S. The Neonatal Fc Receptor (FcRn): A Misnomer? *Front. Immunol.* **2019**, *10*. [\[CrossRef\]](#)
56. Golebski, K.; Hoepel, W.; van Egmond, D.; de Groot, E.J.; Amatngalim, G.D.; Beekman, J.M.; Fokkens, W.J.; van Drunen, C.M.; den Dunnen, J. FcγRIII stimulation breaks the tolerance of human nasal epithelial cells to bacteria through cross-talk with TLR4. *Mucosal Immunol.* **2019**, *12*, 425–433. [\[CrossRef\]](#)

57. Nimmerjahn, F.; Ravetch, J.V. Fcγ receptors: Old friends and new family members. *Immunity* **2006**, *24*, 19–28. [\[CrossRef\]](#)
58. Ye, L.; Zeng, R.; Bai, Y.; Roopenian, D.C.; Zhu, X. Efficient mucosal vaccination mediated by the neonatal Fc receptor. *Nat. Biotechnol.* **2011**, *29*, 158–165. [\[CrossRef\]](#)
59. Tzaban, S.; Massol, R.H.; Yen, E.; Hamman, W.; Frank, S.R.; Lapierre, L.A.; Hansen, S.H.; Goldenring, J.R.; Blumberg, R.S.; Lencer, W.I. The recycling and transcytotic pathways for IgG transport by FcRn are distinct and display an inherent polarity. *J. Cell Biol.* **2009**, *185*, 673–684. [\[CrossRef\]](#)
60. Schlachetzki, F.; Zhu, C.; Pardridge, W.M. Expression of the neonatal Fc receptor (FcRn) at the blood-brain barrier. *J. Neurochem.* **2002**, *81*, 203–206. [\[CrossRef\]](#)
61. Stapleton, N.M.; Brinkhaus, M.; Armour, K.L.; Bentlage, A.E.H.; de Taeye, S.W.; Temming, A.R.; Mok, J.Y.; Brasser, G.; Maas, M.; van Esch, W.J.E.; et al. Reduced FcRn-mediated transcytosis of IgG2 due to a missing Glycine in its lower hinge. *Sci. Rep.* **2019**, *9*, 1–10. [\[CrossRef\]](#)
62. Schneider, Z.; Jani, P.K.; Szikora, B.; Végh, A.; Kövesdi, D.; Iliás, A.; Cervenak, J.; Balogh, P.; Kurucz, I.; Kacskovics, I. Overexpression of bovine FcRn in mice enhances T-dependent immune responses by amplifying T helper cell frequency and germinal center enlargement in the spleen. *Front. Immunol.* **2015**, *6*, 357. [\[CrossRef\]](#) [\[PubMed\]](#)
63. Claypool, S.M.; Dickinson, B.L.; Wagner, J.S.; Johansen, F.; Venu, N.; Borawski, J.A.; Lencer, W.I.; Blumberg, R.S. Bidirectional Transepithelial IgG Transport by a Strongly Polarized Basolateral Membrane Fcγ-Receptor. *Mol. Biol. Cell* **2004**, *15*, 1746–1759. [\[CrossRef\]](#) [\[PubMed\]](#)
64. Zhang, Y.; Pardridge, W.M. Mediated efflux of IgG molecules from brain to blood across the blood–brain barrier. *J. Neuroimmunol.* **2001**, *114*, 168–172. [\[CrossRef\]](#)
65. Dickinson, B.L.; Blumberg, R.S.; Wayne, I.; Invest, J.C.; Dickinson, B.L.; Badizadegan, K.; Wu, Z.; Ahouse, J.C.; Zhu, X.; Simister, N.E.; et al. Bidirectional FcRn-dependent IgG transport in a polarized human intestinal epithelial cell line. *J. Clin. Invest.* **1999**, *104*, 903–911. [\[CrossRef\]](#)
66. Neuber, T.; Frese, K.; Jaehrling, J.; Jäger, S.; Daubert, D.; Felderer, K.; Linnemann, M.; Höhne, A.; Kaden, S.; Kölln, J.; et al. Characterization and screening of IgG binding to the neonatal Fc receptor. *MAbs* **2014**, *6*, 928–942. [\[CrossRef\]](#)
67. Kacskovics, I. Fc receptors in livestock species. *Vet. Immunol. Immunopathol.* **2004**, *102*, 351–362. [\[CrossRef\]](#)
68. Ober, R.J.; Radu, C.G.; Ghetie, V.; Ward, E.S. Differences in promiscuity for antibody–FcRn interactions across species: Implications for therapeutic antibodies. *Int. Immunol.* **2001**, *13*, 1551–1559. [\[CrossRef\]](#)
69. Martins, J.P.; Kennedy, P.J.; Santos, H.A.; Barrias, C.; Sarmiento, B. A comprehensive review of the neonatal Fc receptor and its application in drug delivery. *Pharmacol. Ther.* **2016**, *161*, 22–39. [\[CrossRef\]](#)
70. England, R.J.; Homer, J.J.; Knight, L.C.; Ell, S.R. Nasal pH measurement: A reliable and repeatable parameter. *Clin. Otolaryngol. Allied Sci.* **1999**, *24*, 67–68. [\[CrossRef\]](#)
71. Hornby, P.J.; Cooper, P.R.; Kliwinski, C.; Ragwan, E.; Mabus, J.R.; Harman, B.; Thompson, S.; Kauffman, A.L.; Yan, Z.; Tam, S.H.; et al. Human and non-human primate intestinal FcRn expression and immunoglobulin G transcytosis. *Pharm. Res.* **2014**, *31*, 908–922. [\[CrossRef\]](#)
72. Cianga, C.; Cianga, P.; Plamadeala, P.; Amalinei, C. Nonclassical major histocompatibility complex I-like Fc neonatal receptor (FcRn) expression in neonatal human tissues. *Hum. Immunol.* **2011**, *72*, 1176–1187. [\[CrossRef\]](#) [\[PubMed\]](#)
73. Debertin, A.S.; Tschernig, T.; Tönjes, H.; Kleemann, W.J.; Tröger, H.D.; Pabst, R. Nasal-associated lymphoid tissue (NALT): Frequency and localization in young children. *Clin. Exp. Immunol.* **2003**, *134*, 503–507. [\[CrossRef\]](#) [\[PubMed\]](#)
74. Debertin, A.S.; Tschernig, T.; Schürmann, A.; Bajanowski, T.; Brinkmann, B.; Pabst, R. Coincidence of different structures of mucosa-associated lymphoid tissue (MALT) in the respiratory tract of children: No indications for enhanced mucosal immunostimulation in sudden infant death syndrome (SIDS). *Clin. Exp. Immunol.* **2006**, *146*, 54–59. [\[CrossRef\]](#)
75. Brandtzaeg, P.; Pabst, R. Let's go mucosal: Communication on slippery ground. *Trends Immunol.* **2004**, *25*, 570–577. [\[CrossRef\]](#) [\[PubMed\]](#)
76. Iwasaki, A. Mucosal Dendritic Cells. *Annu. Rev. Immunol.* **2007**, *25*, 381–418. [\[CrossRef\]](#)
77. Kang, H.; Yan, M.; Yu, Q.; Yang, Q. Characteristics of nasal-associated lymphoid tissue (NALT) and nasal absorption capacity in chicken. *PLoS ONE* **2013**, *8*, e084097. [\[CrossRef\]](#)

78. Li, X.; Ptacek, T.S.; Brown, E.E.; Edberg, J.C. Fcγ receptors: Structure, function and role as genetic risk factors in SLE. *Genes Immun.* **2009**, *10*, 380–389. [[CrossRef](#)]
79. Gitlin, D.; Koch, C. On the mechanisms of maternofetal transfer of human albumin and gamma-G globulin in the mouse. *J. Clin. Investig.* **1968**, *47*, 1204–1209. [[CrossRef](#)]
80. Jacobsen, B.; Hill, M.; Reynaud, L.; Hey, A.; Barrow, P. FcRn Expression on Placenta and Fetal Jejunum during Early, Mid-, and Late Gestation in Minipigs. *Toxicol. Pathol.* **2016**, *44*, 486–491. [[CrossRef](#)]
81. De Fraissinette, A.; Brun, R.; Felix, H.; Vonderscher, J.; Rummelt, A. Evaluation of the human cell line RPMI 2650 as an in vitro nasal model. *Rhinology* **1995**, *33*, 194–198.
82. O'Connell, L.Y.; Lai, J.; Presta, L.G.; Keck, R.; Meng, Y.G.; Hong, K.; Weikert, S.H.A.; Shields, R.L. Lack of Fucose on Human IgG1 N-Linked Oligosaccharide Improves Binding to Human FcγRIII and Antibody-dependent Cellular Toxicity. *J. Biol. Chem.* **2002**, *277*, 26733–26740. [[CrossRef](#)]
83. Mathiesen, L.; Nielsen, L.K.; Andersen, J.T.; Grevys, A.; Sandlie, I.; Michaelsen, T.E.; Hedegaard, M.; Knudsen, L.E.; Dziegiel, M.H. Maternofetal transplacental transport of recombinant IgG antibodies lacking effector functions. *Blood* **2013**, *122*, 1174–1181. [[CrossRef](#)] [[PubMed](#)]
84. Bakchoul, T.; Walek, K.; Krautwurst, A.; Rummel, M.; Bein, G.; Santoso, S.; Sachs, U.J. Glycosylation of autoantibodies: Insights into the mechanisms of immune thrombocytopenia. *Thromb. Haemost.* **2013**, *110*, 1259–1266. [[CrossRef](#)] [[PubMed](#)]
85. Stapleton, N.M.; Armstrong-Fisher, S.S.; Andersen, J.T.; van der Schoot, C.E.; Porter, C.; Page, K.R.; Falconer, D.; de Haas, M.; Williamson, L.M.; Clark, M.R.; et al. Human IgG lacking effector functions demonstrate lower FcRn-binding and reduced transplacental transport. *Mol. Immunol.* **2018**, *95*, 1–9. [[CrossRef](#)] [[PubMed](#)]
86. Malek, A. Ex vivo human placenta models: Transport of immunoglobulin G and its subclasses. *Vaccine* **2003**, *21*, 3362–3364. [[CrossRef](#)]
87. Stapleton, N.M.; Andersen, J.T.; Stemerding, A.M.; Bjarnarson, S.P.; Verheul, R.C.; Gerritsen, J.; Zhao, Y.; Kleijer, M.; Sandlie, I.; de Haas, M.; et al. Competition for FcRn-mediated transport gives rise to short half-life of human IgG3 and offers therapeutic potential. *Nat. Commun.* **2011**, *2*, 599. [[CrossRef](#)]

Publisher's Note: MDPI stays neutral with regard to jurisdictional claims in published maps and institutional affiliations.



© 2020 by the authors. Licensee MDPI, Basel, Switzerland. This article is an open access article distributed under the terms and conditions of the Creative Commons Attribution (CC BY) license (<http://creativecommons.org/licenses/by/4.0/>).

Lena Marie Spindler, Andreas Feuerhake, **Simone Ladel**, Cemre Günday, Johannes Flamm, Nazende Günday-Türel, Emre Türel, Günter E.M. Tovar, Katharina Schindowski & Carmen Gruber-Traub. (2021). Nano-in-Micro-Particles Consisting of PLGA Nanoparticles Embedded in Chitosan Microparticles via Spray-Drying Enhances Their Uptake in the Olfactory Mucosa. *Frontiers in Pharmacology*, 12. <https://doi.org/10.3389/fphar.2021.732954>

© 2021 by the authors. This article is an open access article distributed under the terms and conditions of the Creative Commons Attribution 4.0 International (CC BY 4.0) license (<http://creativecommons.org/licenses/by/4.0/>).



Nano-in-Micro-Particles Consisting of PLGA Nanoparticles Embedded in Chitosan Microparticles via Spray-Drying Enhances Their Uptake in the Olfactory Mucosa

Lena Marie Spindler^{1,2}, Andreas Feuerhake¹, Simone Ladel^{3,4}, Cemre Günday⁵, Johannes Flamm^{3,4}, Nazende Günday-Türel⁵, Emre Türel⁵, Günter E. M. Tovar^{1,2}, Katharina Schindowski³ and Carmen Gruber-Traub^{1*}

OPEN ACCESS

Edited by:

Christoph Eugen Hagemeyer,
Monash University, Australia

Reviewed by:

Haitao Yu,
The University of Melbourne, Australia
Ernesto Reverchon,
University of Salerno, Italy
Christina Karavasili,
Aristotle University of Thessaloniki,
Greece

*Correspondence:

Carmen Gruber-Traub
carmen.gruber-traub@
igb.fraunhofer.de

Specialty section:

This article was submitted to
Translational Pharmacology,
a section of the journal
Frontiers in Pharmacology

Received: 29 June 2021

Accepted: 16 August 2021

Published: 01 September 2021

Citation:

Spindler LM, Feuerhake A, Ladel S, Günday C, Flamm J, Günday-Türel N, Türel E, Tovar GEM, Schindowski K and Gruber-Traub C (2021) Nano-in-Micro-Particles Consisting of PLGA Nanoparticles Embedded in Chitosan Microparticles via Spray-Drying Enhances Their Uptake in the Olfactory Mucosa. *Front. Pharmacol.* 12:732954. doi: 10.3389/fphar.2021.732954

¹Fraunhofer Institute for Interfacial Engineering and Biotechnology, Innovation Field Functional Surfaces and Materials, Fraunhofer-Gesellschaft, Stuttgart, Germany, ²Institute of Interfacial Process Engineering and Plasma Technology, University of Stuttgart, Stuttgart, Germany, ³Institute for Applied Biotechnology, Biberach University of Applied Science, Biberach, Germany, ⁴Faculty of Natural Science, University of Ulm, Ulm, Germany, ⁵MyBiotech GmbH, Überherrn, Germany

Intranasal delivery has gained prominence since 1990, when the olfactory mucosa was recognized as the window to the brain and the central nervous system (CNS); this has enabled the direct site specific targeting of neurological diseases for the first time. Intranasal delivery is a promising route because general limitations, such as the blood-brain barrier (BBB) are circumvented. In the treatment of multiple sclerosis (MS) or Alzheimer's disease, for example, future treatment prospects include specialized particles as delivery vehicles. Poly(lactic-co-glycolic acid) (PLGA) nanoparticles are well known as promising delivery systems, especially in the area of nose-to-brain (N2B) delivery. Chitosan is also broadly known as a functional additive due to its ability to open tight junctions. In this study, we produced PLGA nanoparticles of different sizes and revealed for the first time their size-time-dependent uptake mechanism into the *lamina propria* of porcine olfactory mucosa. The intracellular uptake was observed for 80 and 175 nm within only 5 min after application to the epithelium. After 15 min, even 520 nm particles were detected, associated with nuclei. Especially the presence of only 520 nm particles in neuronal fibers is remarkable, implying transcellular and intracellular transport via the olfactory or the trigeminal nerve to the brain and the CNS. Additionally, we developed successfully specialized Nano-in-Micro particles (NiMPs) for the first time via spray drying, consisting of PLGA nanoparticles embedded into chitosan microparticles, characterized by high encapsulation efficiencies up to 51%, reproducible and uniform size distribution, as well as smooth surface. Application of NiMPs accelerated the uptake compared to purely applied PLGA nanoparticles. NiMPs were spread over the whole transverse section of the olfactory mucosa within 15 min. Faster uptake is attributed to additional paracellular transport, which was examined via tight-junction-opening. Furthermore, a separate chitosan penetration gradient of ~150 µm caused by dissociation from PLGA nanoparticles was observed within 15 min in the *lamina propria*, which was demonstrated to be proportional to an immunoreactivity

gradient of CD14. Due to the beneficial properties of the utilized chitosan-derivative, regarding molecular weight (150–300 kDa), degree of deacetylation (80%), and particle size (0.1–10 μm) we concluded that M2-macrophages herein initiated an anti-inflammatory reaction, which seems to already take place within 15 min following chitosan particle application. In conclusion, we demonstrated the possibility for PLGA nanoparticles, as well as for chitosan NiMPs, to take all three prominent intranasal delivery pathways to the brain and the CNS; namely transcellular, intracellular via neuronal cells, and paracellular transport.

Keywords: intranasal application, mucosal uptake, poly lactic-co-glycolic acid particles, chitosan coating, nasal delivery, nano-in-micro particles, spray drying, olfactory transport mechanism

INTRODUCTION

Intranasal delivery became more prominent in the last decades because modern treatments focus on biopharmaceuticals and concurrently reveal opportunities, but also provide challenges. Intranasal delivery is a promising route to overcome general limitations such as the blood-brain barrier (BBB). In the treatment of neurological disorders, for example multiple sclerosis or Alzheimer's disease. Future prospective treatments may also include not only proteins or antibodies, but also specialized particles as delivery vehicles, but the BBB is shielding the central nervous system (CNS) and the brain from the blood stream. Modern therapeutics, such as antibodies and proteins, are therefore banned through size exclusion and surface charge (Wolburg et al., 1994; Stützel et al., 2015), which is problematic for intravenous and oral administration in current therapeutic approaches. More than one billion people are currently affected by neurological diseases with a rising tendency (WHO 2006). Further, the global need displays a great demand for effective treatments of the upper airways, such as the nasal cavity. Covid-19 infections, as one prominent example, occur mainly from the initial contact to the nasal mucosa and can harm the brain (Yu et al., 2020; Layden et al., 2020). Therefore, to prevent greater damage, effective treatments should also occur along this route. As a consequence, the actual need for innovative intranasal delivery systems is rapidly increasing.

The nasal mucosa, as the first biological barrier in the nose to target the brain and the CNS, consists of respiratory and olfactory mucosa. The respiratory epithelium covers approximately 97% of the nasal cavity in humans and is necessary for respiration (Ugwoke et al., 2005). Further, rapid clearance of dust and other foreign substances occurs via the directed movement of millions of cilia (Menache et al., 1997). In contrast to this, the olfactory mucosa is characterized by fewer long cilia, specialized to detect odorants, initializing an electric signal in olfactory sensory neurons to maintain olfaction (Ugwoke et al., 2005). The olfactory sensory neurons are located between epithelial cells and underlying basal cells, forming neuronal bundles, which protrude through the ethmoid bone and therefore directly connect the olfactory mucosa to the brain and the CNS (Morrison and Costanzo 1990; Morrison and Costanzo 1992). Further, the olfactory mucosa consists of a *lamina propria* mainly built of fibroblastic cells. The olfactory epithelium covers 4–5 cm^2

in humans. Up to approximately 10 cm^2 of the olfactory mucosa can be excised from the dorsal part of the *concha nasalis dorsalis* in pigs (Getty 1975; Mistry 2009; Ladel et al., 2018). The olfactory epithelium can be distinguished from the respiratory epithelium due to fewer blood capillaries and hence brighter color (Mistry 2009; Stützel et al., 2015).

Polymeric nanoparticles embody convincing advantages such as stability, high loading capacity, and controlled drug release (Bourganis et al., 2018; Rabiee et al., 2020). Poly(lactic-co-glycolic acid) (PLGA) nanoparticles especially are widely known as promising delivery vehicles. PLGA, consisting of lactic and glycolic acid, is a biodegradable biopolymer already approved by the Food and Drug Administration (FDA) and the European Medicine Agency (EMA) (Danhier et al., 2012). Its release properties are tunable due to the mass ratio of lactic and glycolic acid. Exemplarily, a mass ratio of 50% each results in a controlled release over several days. Degradation occurs through hydrolysis and the decomposition products are further metabolized. U. Seju et al. (2011) reported PLGA nanoparticles as promising delivery systems for nose-to-brain delivery because drug release of olanzapine occurs over several days due to slow swelling of PLGA and long-term residence of the resulting gel at the site of action, further 8-fold drug concentrations, compared to the solute form, have been achieved (Seju et al., 2011). Muntimadugu et al. (2016) reported the transport of PLGA nanoparticles with diameters below 200 nm along axons within the nasal mucosa (Muntimadugu et al., 2016). Neuronal bundles within the olfactory mucosa being directly connected to the olfactory or trigeminal nerve is identified as one transport route to the brain and the CNS (Anderson et al., 2008; Stützel et al., 2015; Gänger and Schindowski 2018). PLGA and chitosan particles up to 250 μm were recently reported to be mainly transported via the olfactory route (Rabiee et al., 2020); however, uptake and distribution examinations of PLGA and chitosan particles in nasal mucosa samples are still rare.

Additional nose-to-brain delivery routes are intracellular uptake and further transcytosis, as well as paracellular transport. Other research groups focused on the paracellular route in epithelial cell cultures and mucosal tissues (Sadeghi et al., 2008; Fazil et al., 2012; Sonaje et al., 2012; Rassu et al., 2016). Herein chitosan-based carriers have become one of the most promising and intensively-studied mucosal drug delivery systems (Garcia-Fuentes and Alonso 2012). This is attributed to

their mild and simple preparation technique as well as their capacity to associate biologics and enable transport across mucosal barriers. Chitosan is a renewable biopolymer, which is gained from the naturally occurring chitin of crustaceans, extracted by deacetylation (Wenling et al., 2005; Yuan et al., 2011; Sarmento and Neves 2012). With at least 50% N-deacetylated chemical groups, it is referred to as chitosan. The origin, as well as the degree of deacetylation, affects the polymer properties, such as solubility, swelling, and adhesion. The interaction between the positive amino groups of chitosan and several negative groups in the mucosa enables mucoadhesion, which is further dependent on the molecular weight of the chitosan (Henriksen et al., 1996). The length of the chitosan polymer chains and their average molecular weight can be controlled by enzyme-mediated decomposition or acid hydrolysis (Ilium 1998). The chitosan utilized in this study, for example, has 80% deacetylated residues and is; therefore, mucoadhesive and well soluble in acidic solutions. Chitosan can open tight junctions (Fazil et al., 2012; Sonaje et al., 2012; Rassu et al., 2016), which are the characteristic intercellular connections present in epithelial cells and endothelial cells. One major component *Zonula occludens* protein 1 (ZO-1) was initially explored, in 1986, by Stevenson et al. (1986) in epithelial cells (Stevenson et al., 1986), it was later also documented in endothelial cells (Anderson et al., 1988) and fibroblasts (Itoh et al., 1991; Howarth et al., 1992). The above-mentioned research groups described the ability of chitosan to open tight junctions in cell culture, studying the impact of chitosan solutions on cellular interconnections. Further, other research groups have postulated that chitosan nanoparticles open tight junctions and; therewith, affect increased drug levels in the brain and the CNS, but did not directly prove the tight junction opening (Rassu et al., 2016; Bourganis et al., 2018; Rabiee et al., 2020). Further experimental investigations of tight junction opening are, therefore, still needed to fully clarify intranasal transport routes of chitosan particles and encapsulated active pharmaceutical ingredients.

Together with the application of particles to the nasal mucosa, it is important to consider particle distribution in the olfactory tissue, biocompatibility, biodegradation, and especially immune response. Nevertheless, these aspects are rarely reported in literature for intranasal delivery and more research is needed (Rabiee et al., 2020). The nasal mucosa, as a biological barrier directly exposed to the environment, is a well-known immune active tissue (Morrison and Costanzo 1990; Doty, 2015; Stützle et al., 2015; Bourganis et al., 2018; Ladel et al., 2018). Nasal-associated lymphoid tissue (NALT) includes immune active cells, either present between the epithelial layer and the *lamina propria*, infiltrated from blood vessels, or directly produced inside of lymphoid follicles located in the mucosa itself. Moreover, recent studies have revealed the still incomplete understanding of intranasal pathways and distribution routes of individual compounds, as well as formulation compositions (Rabiee et al., 2020; Keller et al., 2021). Which drug delivery system exactly triggers what specific pathway is mainly unclear up to now. Consequently, clarification of distribution routes of individual compounds as well as formulation composition, such as the herein investigated prominent particle materials PLGA and

chitosan, are needed to develop suitable drug delivery systems in the future.

Within this study, we examined size- and time- dependent particle permeation studies on porcine olfactory mucosa. We compared the permeation of pure PLGA nanoparticles of different diameters up to 520 nm to spray-dried nano-in-micro particles (NiMPs) coated with chitosan to identify chitosan-mediated mechanisms important for intranasal delivery. Additionally, we utilized the unique benefits of the controlled release of PLGA nanoparticles over several days combined with the aforementioned abilities of chitosan. Moreover, we investigated organoid accumulation, such as in glands and neuronal bundles as well as the local initial immune response within the olfactory mucosa.

MATERIALS AND METHODS

Nanoparticle Preparation

Poly(lactic-co-glycolic acid) PLGA nanoparticles with 80 and 175 nm diameter were prepared by precipitation. 5 mg ml⁻¹ PLGA 50:50 (Evonik, Essen, Germany) and 14 µg ml⁻¹ Lumogen (BTC Europe, Monheim, Germany), or 10 mg ml⁻¹ PLGA 50:50 (Evonik, Essen, Germany) and 28 µg ml⁻¹ Lumogen (BTC Europe, Monheim, Germany) were dissolved in Acetone for 80 and 175 nm particles respectively. This solution was mixed in a 1:2 solvent:nonsolvent ratio with distilled water containing 2.5 mg ml⁻¹ Pluronic F68 (Sigma-Aldrich, St. Louis, United States) by the use of a magnetic stirrer.

PLGA nanoparticles with 520 nm diameter were prepared by two-step double emulsification to obtain water-oil-water emulsions (w/o/w). The first emulsification step was performed with Milli-Q water and 5 mg ml⁻¹ PLGA (Evonik, Essen, Germany) solution in Dichloromethane:Ethylacetate (1:3) as solvent. The water to organic phase ratio was 1:10. For labeling 28 µg ml⁻¹ Lumogen F Red (BTC Europe, Monheim, Germany) was added to the formulation dissolved in the organic phase. As a surfactant polyvinyl alcohol (PVA) with a molecular weight of 27 kDa (Sigma-Aldrich, St. Louis, United States) was used in the second emulsification. Therefore 1 %wt. PVA was dissolved in water at 80°C. The obtained primary emulsion and PVA containing aqueous phase were emulsified to achieve a w/o/w emulsion at a ratio of 1:10. Both emulsification steps were performed at the highest speed (26,000 rpm) for 1 min by using Silence Crusher M (Heidolph Instruments GmbH & Co. KG, Schwabach, Germany) homogenization device. The finally obtained w/o/w emulsion was stirred moderately overnight to evaporate the organic phase.

Nano-in-Micro Particle Preparation via Spray Drying

A Büchi B-290 mini spray dryer (Büchi Labortechnik AG, Flawil, Switzerland) was used to encapsulate the previously prepared PLGA nanoparticles into a chitosan matrix. Chitosan 80/200 (Chitoceuticals, Heppe Medical Chitosan GmbH, Halle, Germany), with a degree of deacetylation of 80% and a

molecular weight of 150–300 kDa, was dissolved in 0.5 %vol. acetic acid at a concentration of 1 %wt. The chitosan matrix was labeled with fluorescein sodium salt (Honeywell Fluka, New Jersey, United States) at a concentration of $260 \mu\text{g ml}^{-1}$ in the spray drying solution. The nanoparticle suspension (6.25 mg ml^{-1} PLGA in Milli-Q water) was then mixed with the fluorescein labelled chitosan solution at a mass ratio of 1/3 or 2/3 before spray drying. Spray drying was performed with a two-fluid nozzle and a nozzle cap diameter of 1.5 mm. The inlet temperature was set to 100°C at a fluid feed rate of 4.46 ml min^{-1} , gas feed rate of 12.94 g min^{-1} , and an aspiration rate of 100% equating with $\sim 700 \text{ g min}^{-1}$. The system was equilibrated before use and washed after spray drying with Milli-Q water.

Scanning Electron Microscopy

For Scanning Electron Microscopy (SEM) analysis, PLGA nanoparticle suspension (6.25 mg ml^{-1} PLGA in Milli-Q water) was vortexed and $10 \mu\text{l}$ of the suspension was pipetted onto a clean silicon wafer, covered with a petri dish, and dried overnight at room temperature. Nano-in-micro particle powders were fixed with conductive electron microscopy tape directly onto a sample holder. A thin layer of platinum was sputtered on all samples before measurement. Measurements were performed at different magnifications with a Leo Gemini 1530 VP (Carl Zeiss Microscopy Deutschland GmbH, Oberkochen, Germany) microscope at 5.00 kV using the InLens detector and SE2 for signal B.

Laser Scanning Microscopy

For Confocal Laser Scanning Microscopy (CLSM) the nanoparticle suspension (6.25 mg ml^{-1} PLGA in Milli-Q water) was vortexed and $10 \mu\text{l}$ were applied to a cover glass, which was then covered with a petri dish and dried at room temperature protected from light. Completely dried samples were measured upside down with a 63x water immersion objective. Nano-in-micro particles were deposited rarely with a sieve and a spatula onto a cover glass, covered with an additional cover glass and sealed gently with tape, to avoid contamination during analysis. Powder samples were measured immediately after preparation with the 63x water immersion objective. Most tissue samples have been measured with a 20x objective. All measurements have been performed with a confocal LSM 710 (Carl Zeiss Microscopy Deutschland GmbH, Oberkochen, Germany). The utilized lasers and the corresponding emission filters for CLSM imaging are displayed in **Supplementary Table S1**. For three-dimensional information, z-stack measurements with a pitch of $0.5 \mu\text{m}$ for 63x recordings and $1 \mu\text{m}$ for 20x images were recorded and stitched together in a maximum intensity projection. For picture analysis and post-processing, ZEN software (Carl Zeiss Microscopy Deutschland GmbH, Oberkochen, Germany) was used.

Particle Size Distribution

PLGA nanoparticles were measured as a suspension in Milli-Q water via dynamic light scattering using a Zetasizer Nano ZS (Malvern Instruments, Malvern, United Kingdom). Mean particle size and Polydispersity Index (PI), referred to as

squared difference between standard deviation and average decay rate, were reported (ISO 2017). The average decay rate is defined by diffusion coefficient and scattering vector as written in ISO standard 22412:2017. Since the Stokes-Einstein hydrodynamic diameter is inversely proportional to the decay rate, the average diameter is equal to the average decay rate.

Nano-in-micro particles were measured via static light scattering at 1,500 rpm stirring velocity performed with a Mastersizer 2000 (Malvern Instruments, Malvern, United Kingdom) using its μP 2000 measurement cell. The spray-dried powder sample was first dispersed in 2-propanol via ultrasonic treatment for 3 s in an ultrasonic bath. Additional measurements at 1,500 rpm were performed after 1 min ultrasonic treatment in the measurement cell. Measuring chitosan particles is reported with the organic solvent ethanol (Kašpar et al., 2013; Tokárová et al., 2013), but we detected swelling of chitosan particles within several minutes in ethanol falsifying the particle size measurement as a result. Therefore, we only used 2-propanol as a solvent for static light scattering measurements. We calculated the mean particle diameter from the volume distribution output. Additionally, Scanning Electron Microscopy (SEM) images were analyzed with ImageJ software (Wayne Rasband, 1997). Particle diameters were extracted, plotted, and fitted with a Gaussian fit in Origin Pro 2019 (Origin Lab, 1992).

Further, the Polydispersity Index (PDI) also for nano-in-micro particles (NiMPs) was calculated with **Eq. 1** using the mean particle diameter d_m and the standard deviation of the particle size σ (Clayton et al., 2016), which is not automatically reported within the Mastersizer software (Malvern Instruments, Malvern, United Kingdom).

$$PDI = \left(\frac{\sigma}{d_m} \right)^2 \quad (1)$$

Zeta Potential

Zeta potential was examined for PLGA nanoparticles and nano-in-micro particles (NiMPs) with a Zetasizer Nano ZS (Malvern Instruments, Malvern, United Kingdom) utilizing a folded capillary cell DTS 1070 (Malvern Instruments, Malvern, United Kingdom). The instrument was calibrated routinely with a -50 mV latex standard. PLGA nanoparticles were suspended in Milli-Q water, as well as in 2-propanol as comparison. Due to initially occurring agglomeration and swelling of chitosan NiMPs in Milli-Q water, NiMPs were suspended and measured only in 2-propanol via ultrasonic treatment of 30 s in an ultrasonic bath. For measurements in aqueous media Smoluchowski approximation and Huckel approximation for non-aqueous measurements in 2-propanol was used. The measurements were repeated five times at neutral pH and 25°C after 600 s equilibration time.

Encapsulation Efficiency

The encapsulation efficiency of nano-in-micro particles (NiMPs) was examined via image analysis from Confocal Scanning Electron Microscopy images using the software ImageJ

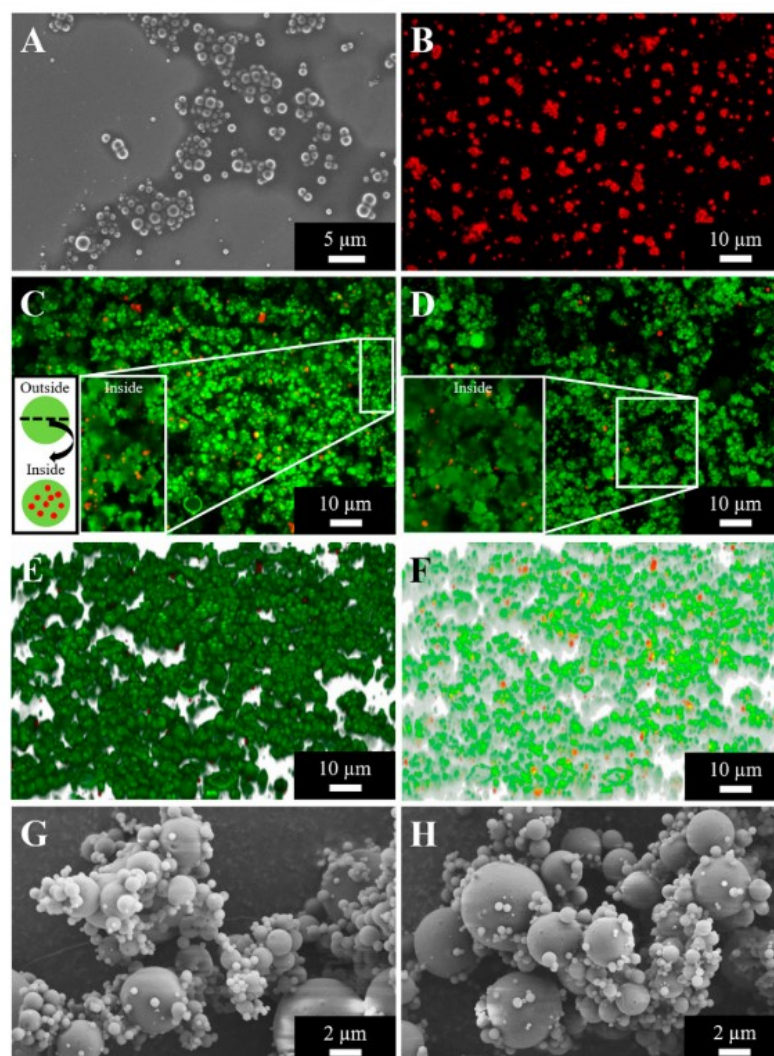


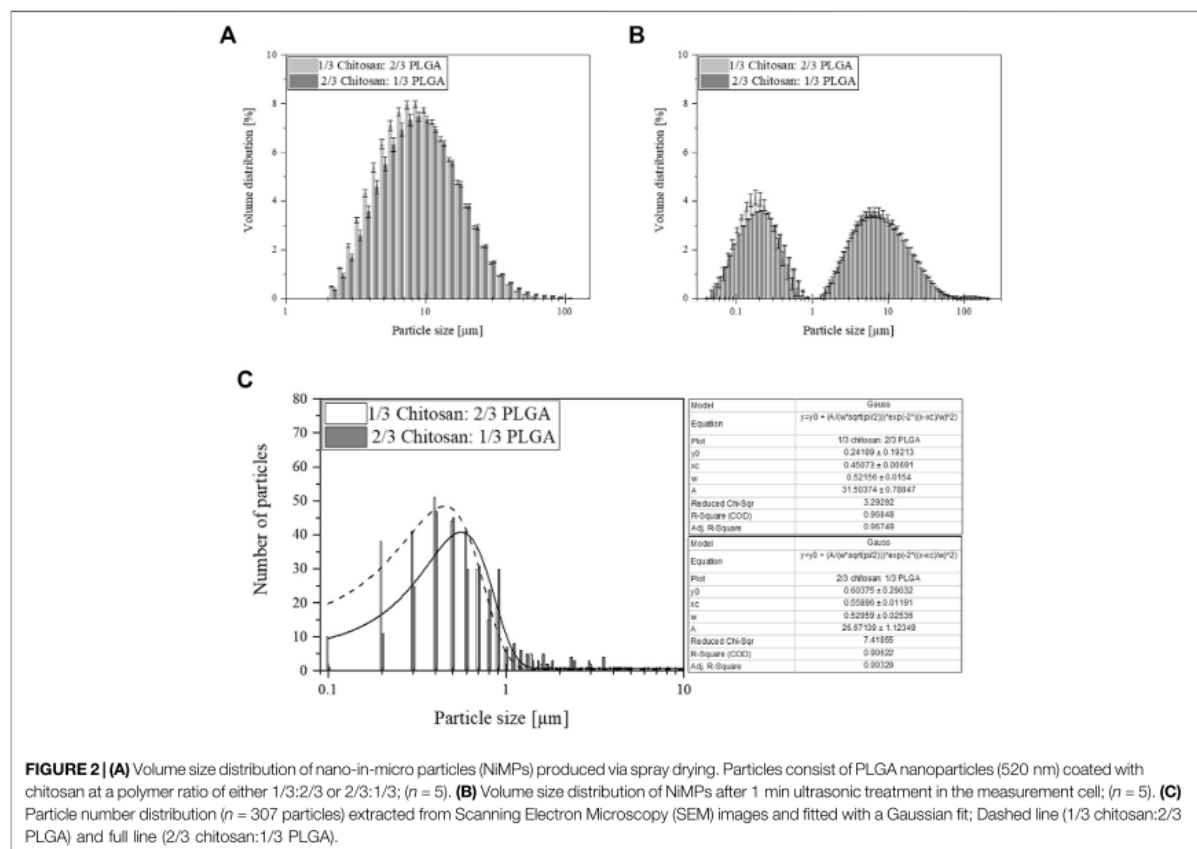
FIGURE 1 | PLGA nanoparticles prepared by double emulsion technique (**A, B**) and spray dried nano-in-micro particles (NiMPs) prepared by spray drying at two different polymer ratios consisting of PLGA nanoparticles (520 nm) and chitosan as matrix material (**C–H**). **(A)** Scanning Electron Microscopy (SEM) image, magnification 5 kX. **(B)** Confocal Laser Scanning Microscopy (CLSM) picture, mag. 630 X, maximum intensity projection (MIP) stitched together from a z-stack, particles labeled with Lumogen F Red. **(C)** CLSM image of NiMPs 1/3 chitosan:2/3 PLGA, mag. 630 X, MIP; Enlarged cross-section of particles and particle schematic; Chitosan (green) and PLGA nanoparticles (red). **(D)** CLSM image of NiMPs 2/3 chitosan:1/3 PLGA, mag. 630 X, MIP. **(E)** 3D projection of CLSM images (green: chitosan; red: PLGA) stitched together from a z-stack, mag. 630 X, external view. **(F)** Transparent 3D projection of CLSM images (green: chitosan; red: PLGA) stitched together from a z-stack, mag. 630 X, internal view. **(G)** SEM image of NiMPs 1/3 chitosan:2/3 PLGA, mag. 10 kX. **(H)** SEM picture of NiMPs 2/3 chitosan:1/3 PLGA, mag. 10 kX. 3D projections (external, transparent) of CLSM images from 2/3 chitosan:1/3 PLGA NiMPs displayed in **Supplementary Figure S1**.

(Wayne Rasband, 1997) and two different calculations. First, the average number of PLGA nanoparticles colored in red incorporated in green stained chitosan microparticles was determined using the assumption of particles equal in size with the mean diameters extracted from light scattering measurements for nanoparticles and microparticles, respectively ($n = 5$). In the second calculation, the relative encapsulation efficiency was observed relating the total cross-section area of PLGA nanoparticles (red) to the cross-section area

of nanoparticles solely outside of chitosan microparticles ($n = 5$). Consequently, the difference between total cross-section area of nanoparticles and cross-section area of nanoparticles outside of microparticles revealed the percentage of successfully encapsulated nanoparticles through spray drying.

Tissue Preparation

Pig snouts were purchased from a local slaughterhouse. Mucosa specimens were excised from the dorsal part of the *concha nasalis*



dorsalis (Getty 1975; Mistry 2009). The olfactory mucosa was gently removed from the underlying cartilage with the help of forceps (Ladel et al., 2018). Excised specimens were further dissected into 1–2 cm² samples. *Post mortem* delay of the mucosa was below 2 h.

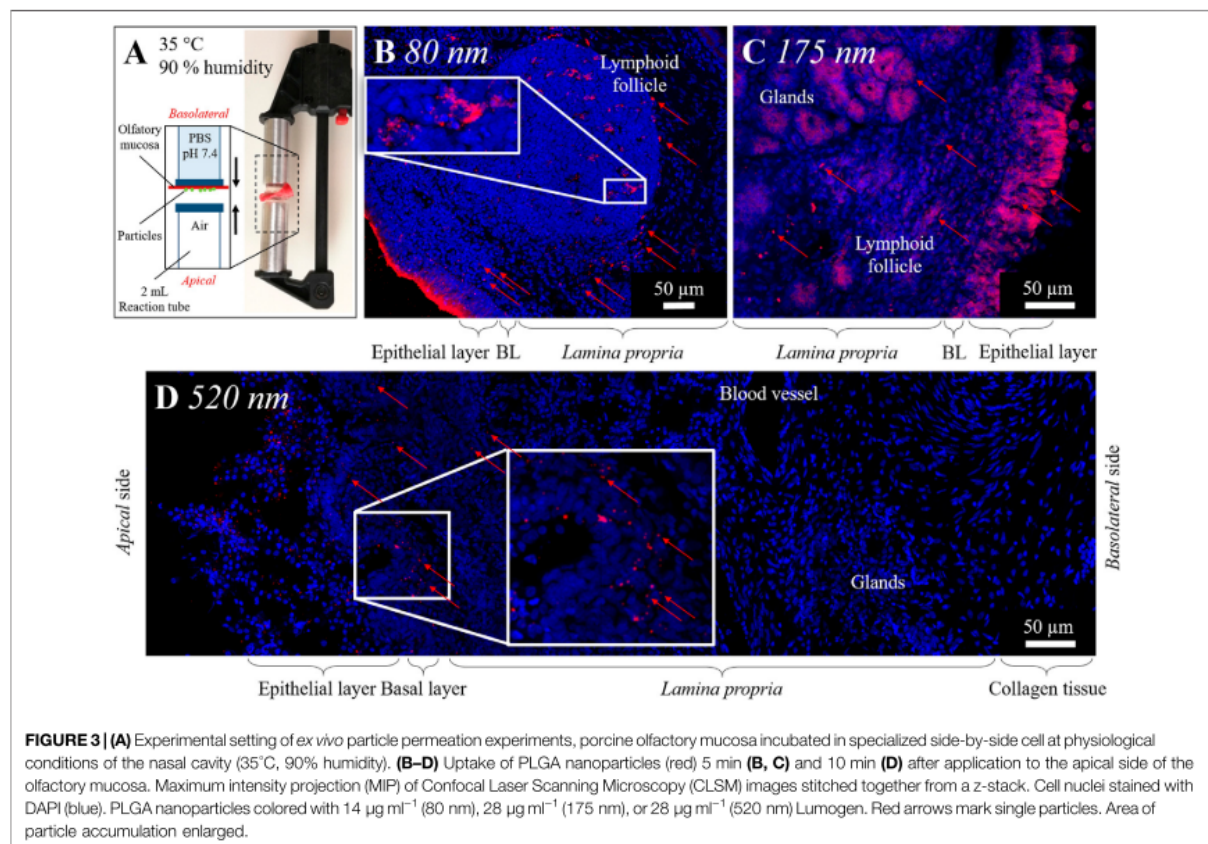
Ex vivo Permeation Studies

For particle application, prepared mucosa specimens were put into a Petri dish. ~12 mg of NiMPs were administered to the olfactory mucosa, which due to the chitosan coating is equivalent to ~4 mg of PLGA particles for NiMPs with low chitosan ratio and ~2 mg for NiMPs with high chitosan content, examined from the actual encapsulation efficiency evaluated via image analysis from Confocal Laser Scanning Microscopy images (chapter 2.7). The mucosa was then placed into a modified side-by-side cell consisting of two micro reaction tubes (1.5 ml) between clamping tongs (Figure 3A), resulting with the inner radius 5 mm in a permeation area of 78.5 mm². The bottom microtube was filled with 260 μ l of phosphate-buffered saline (PBS) at pH 7.4 before placing the mucosa with its basolateral side on top of it. The system was sealed to avoid leakage by closing the cell. Finally, the cell was put upside down into an incubator at 35°C and 90% humidity to simulate the natural conditions within the nasal cavity for 5 min to 2 h. As a comparison, 20 μ l of the PLGA

nanoparticle suspension was applied similarly; however, due to the production procedure ~0.2 mg particles were applied in this case, which does hence only allow a quantitative comparison among similar applied samples. Due to the sensitivity of PLGA nanoparticles they could not be dried and applied as a powder; however, the NiMPs could not be suspended in aqueous media due to the intense swelling of chitosan. Consequently, PLGA nanoparticles and NiMPs were treated differently in the experiments, which is considered in the comparison of the results. Control samples were taken respectively at time point 0 min directly after application. After the respective incubation times, the mucosa specimens were immediately fixed in 4 %wt. paraformaldehyde for at least 2 h and stored in 30%wt. sucrose at 4°C until sectioning. The tissue samples were cut in 20 μ m slices at the site of applied particles in a cryostat at –25°C (HM560, Thermo Fisher Scientific, Dreieich, Germany) and mounted on Superfrost®Plus Micro slides (Thermo Fisher Scientific, Waltham, United States).

Immunohistochemistry and Histological Staining

The structural integrity of the epithelial layer was confirmed by hematoxylin-eosin (HE) staining. HE-stained slides were dehydrated



in ethanol and 2-propanol. Finally, they were embedded with Eukitt[®] Quick-hardening mounting medium (Sigma-Aldrich, St. Louis, United States) and covered with a coverslip.

For observation via confocal laser scanning microscopy either solely cell nuclei were stained with DAPI (4',6-Diamidin-2-phenylindol 2HCl; Serva Electrophoresis GmbH, Heidelberg, Germany) or DAPI staining was performed after the immunohistochemistry staining procedure. Tissue explants viability was verified with control samples live-stained after incubation up to 5 h with Hoechst 33342 (Cell Signaling Technology Inc., Danvers, United States). To visualize the initial immune reaction, CD14⁺ cells were stained via CD14 primary antibody (#NB100-77758, Novus Biologicals, Littleton, United States) and goat anti-mouse secondary IgG (H+L) Alexa Fluor[®] 647 (#A-21235, Thermo Fisher Scientific, Waltham, United States). Neurofilament heavy protein (200 kDa) NF-H was marked to visualize co-localization with neuronal bundles and therefore stained with NF-H primary antibody (#PA1-10002, Thermo Fisher Scientific, Waltham, United States) and goat anti-chicken secondary IgY (H+L) FITC (#A16055, Thermo Fisher Scientific, Waltham, United States). Cell-cell junction protein 1 (Zonula

occludens protein 1; ZO-1) was detected via ZO-1 primary antibody (#NBP1-85047, Novus Biologicals, Littleton, United States) and secondary goat anti-rabbit IgG (H+L) Alexa Fluor[®] 647 (#ab150083, Abcam, Cambridge, United Kingdom). The fluorescently stained samples were fixated with Fluoroshield[™] mounting medium (Sigma-Aldrich, St. Louis, United States) and covered with a coverslip.

RESULTS

Nanoparticles

Particle Size Distribution

The particle size of the poly(lactic-co-glycolic acid) PLGA nanoparticles manufactured with precipitation was adjusted by the variation of PLGA concentration in the solvent phase. 5 mg ml⁻¹ PLGA starting concentration resulted in an average particle size of 81.6 nm with a Polydispersity index (PI) of 0.071, whereas characterization of the particles manufactured with 10 mg ml⁻¹ PLGA starting concentration revealed a mean particle size of 174.4 nm and a PI value of 0.037. Hence, both samples produced via precipitation resulted in monodisperse size distributions below the critical value of 0.1 (Hughes et al., 2015). PLGA

nanoparticles produced via the double emulsion method resulted in a medium size of 519.7 nm with a narrow size distribution characterized by a PI of 0.28.

Zeta Potential

The Zeta potential was characteristically negative for all prepared PLGA nanoparticles (Vila et al., 2002; Ravi Kumar et al., 2004). However, 2-propanol is less polar than water and has a lower dielectric constant of 18.0 As Vm⁻¹ at 25°C compared to 78.5 As Vm⁻¹ of water (Akerlof 1932), the resulting zeta potential in both investigated solvents did not differ significantly.

Morphology

PLGA nanoparticle morphology was examined using Scanning Electron Microscopy (SEM) and Confocal Laser Scanning Microscopy (CLSM). As presented in **Figure 1A**, nanoparticles prepared by the double emulsion technique are spherical and show a smooth surface. Further, their successful labeling with Lumogen F Red was confirmed with their intense and homogenous color (**Figure 1B**).

Nano-in-Micro Particles

Particle Size Distribution

Herein prepared nano-in-micro particles (NiMPs) consisting of PLGA nanoparticles (520 nm) coated via spray-drying with chitosan varying the chitosan:PLGA polymer ratio. First, NiMPs with 1/3 chitosan:2/3 PLGA were prepared and analyzed via static light scattering (SLS), while stirring at 1,500 rpm in the μ P2000 measurement cell. The resulting Gaussian shaped volume size distribution is presented in **Figure 2A**. Compared to the NiMPs with 2/3 chitosan:1/3 PLGA, the particle size increased with a higher chitosan ratio and the histogram is; therefore, shifted to the right towards bigger particle sizes.

Further, we calculated the d(0.5) value for both types of NiMPs representing 50% of the particle populations respectively, as well as the mean particle size and thereof the Polydispersity Index (PDI) to characterize the homogeneity of the particle population. These values are presented in **Table 1**. NiMPs with a higher chitosan ratio resulted in a d(0.5) particle size of 8.65 μ m (**Table 1**) compared to the slightly smaller particles with less chitosan characterized by a d(0.5) diameter of 8.10 μ m. Both spray-dried samples resulted in a unidisperse particle size distribution; however, the population of NiMPs with less chitosan is more homogenous than the sample with a higher chitosan ratio, characterized by a smaller PDI (**Table 1**).

Second, the samples were treated with ultrasound for 1 min in the μ P2000 measurement cell and afterwards measured again at 1,500 rpm. The second measurement cycle revealed a bidisperse size distribution for both sample types displayed in **Figure 2B**. The volume fraction is divided equally in a nanoparticle and a microparticle fraction, due to the split up of agglomerates. The nanoparticle fraction of NiMPs with low chitosan ratio (1/3 chitosan:2/3 PLGA) is characterized by a mean particle diameter of 0.18 μ m compared to 0.21 μ m of NiMPs with high chitosan ratio (2/3 chitosan:1/3 PLGA) (**Table 1**). Due to the previously described mean size of 519.7 nm of PLGA nanoparticles, the nanoparticle fractions of both NiMP samples should mainly consist of pure chitosan. Further, the nanoparticle fraction resulted in slightly bigger particles due to the higher chitosan ratio and the size distribution of this fraction is broader (**Table 1**). In contrast, the microparticle fraction of NiMPs with less chitosan is characterized by a mean particle diameter of 6.61 μ m, whereas NiMPs consisting of more chitosan have a smaller mean diameter of 5.75 μ m. Additionally, the microparticle fraction of NiMPs with high chitosan ratio is narrower than the microparticle fraction of NiMPs with low chitosan ratio (**Table 1**). These findings imply that additional chitosan in the spray drying process is mainly forming pure chitosan nanoparticles, not NiMPs. Therefore, it is important to compare the encapsulation efficiencies and understand, whether a higher matrix ratio is beneficial to encapsulate nanoparticles via spray drying, which is explained below.

Additionally, we measured the size distribution of NiMPs in representative Scanning Electron Microscopy (SEM) images using ImageJ software and plotted their resulting diameters against frequency. The following size distributions are presented in **Figure 2C** together with a non-linear Gaussian fit performed in OriginPro software. The majority of 1/3 chitosan:2/3 PLGA-NiMPs has a diameter of 0.45 μ m. NiMPs with high chitosan ratio (2/3 chitosan:1/3 PLGA) resulted in a slightly greater mean diameter of 0.52 μ m (**Table 1**), which confirms that more chitosan available during spray-drying as matrix material results mainly in bigger nanoparticles. Further, the displayed size distribution is monodisperse; however, very broad. This additional analysis shows, NiMPs (2/3 chitosan:1/3 PLGA) consisting of more chitosan result in a broader size distribution than NiMPs produced with less chitosan (1/3 chitosan:2/3 PLGA), which is attributed to the smaller sample size of the image analysis. In the size distribution extracted from SEM images further only few microparticles occur. In contrast to this, the size distributions examined via static light scattering

TABLE 1 | Characteristic parameters of nano-in-micro particles (NiMPs) obtained from static light scattering measurements. d(0.5) value represents the diameter of 50% of the particle population. The Polydispersity index (PDI) characterizes the homogeneity of the particle population; 1 min ultrasonic treatment (US).

Method	SLS	SLS	SLS	SEM
Condition	Agglomerated suspension in 2-propanol	Suspension in 2-propanol	Suspension in 2-propanol	Dry
Treatment	1,500 rpm	After US (First Peak)	After US (Second Peak)	None
d [μ m] 1/3 chitosan: 2/3 PLGA	8.10	0.18	6.61	0.45
d [μ m] 2/3 chitosan: 1/3 PLGA	8.65	0.21	5.75	0.56
PDI 1/3 chitosan: 2/3 PLGA	0.99	0.70	1.89	0.6
PDI 2/3 chitosan: 1/3 PLGA	1.17	0.87	1.84	1.3
Distribution	Monodisperse	Bidisperse	Bidisperse	Monodisperse

represent the samples volume fraction. In volumetric size distributions, few bigger particles represent a bigger fraction than in frequency displaying distributions, where the volume of the measured particles within the sample is not considered.

Zeta Potential

The examination of chitosan NiMPs in contrast to PLGA nanoparticles revealed an overall positive zeta potential, which is characteristically for chitosan (Vila et al., 2002; Ravi Kumar et al., 2004) and proves the successful encapsulation of PLGA nanoparticles into the chitosan matrix by spray drying.

Encapsulation Efficiency

Comparing both spray-dried NiMP samples with different polymer ratios, in NiMPs with less chitosan and higher PLGA ratio (1/3 chitosan:2/3 PLGA) generally about seven 519.7 nm PLGA nanoparticles (NP) per single chitosan 6.61 μ m microparticle (MP) have been encapsulated (Figure 1C). Red nanoparticles are distributed inside of green chitosan microparticles (Figure 1F). Solely, a few nanoparticles remained on the surface (Figure 1E) and hence most nanoparticles were encapsulated successfully.

Due to the higher chitosan ratio NiMPs with 2/3 chitosan:1/3 PLGA showed an average of only two 519.7 nm PLGA NP in one chitosan 5.75 μ m MP (Figure 1D). Both samples further resulted in similar encapsulation efficiencies; however, NiMPs with a lower chitosan ratio were produced with proportionally less matrix material to cover PLGA nanoparticles. NiMPs consisting of 1/3 chitosan:2/3 PLGA resulted in an encapsulation efficiency of $39 \pm 19\%$ (Figure 1C). NiMPs with a higher chitosan ratio (2/3 chitosan:1/3 PLGA) yielded in a higher encapsulation efficiency of $51 \pm 16\%$ (Figure 1D), however this is not significant. Consequently, PLGA nanoparticles were successfully encapsulated into chitosan via spray drying, but a 1/3 higher matrix composition did not significantly improve the encapsulation efficiency. Proportionally, even more nanoparticles were encapsulated with a lower chitosan amount.

Morphology

NiMPs were further investigated via Scanning Electron Microscopy (SEM). Exemplary pictures, at a magnification of 10 kX, are displayed in Figure 1E (1/3 chitosan:2/3 PLGA) and Figure 1F (2/3 chitosan: 1/3 PLGA). The previously-described effect, causing slightly bigger particles due to the increase in chitosan ratio during spray drying, can also be supported by the SEM analysis. Samples prepared with a ratio of 1/3 chitosan:2/3 PLGA show more particles below one micron (Figure 1G), which is additionally proved with the size distribution in Figure 2C. In contrast, spray-dried NiMPs with the opposite polymer ratio (2/3 chitosan:1/3 PLGA) are slightly bigger (Figure 1H, Figure 2C).

Further, NiMPs are, independent of their polymer ratio, spherically shaped and show a smooth surface, which can be attributed to the spray drying inlet temperature of 100°C and a resulting outlet temperature of $45 \pm 1^\circ\text{C}$, which allows continuous evaporation of the water phase and results in homogenous particles with dense pores and hence smooth appearing surface (Paudel et al., 2013).

Mucosal Uptake of PLGA Nanoparticles

In this study, we examined the uptake of PLGA nanoparticles with diameters of 80, 175, and 520 nm into olfactory mucosa tissue. Therefore, nanoparticle suspensions have been applied onto the apical site of explanted porcine mucosa specimens and incubated in specialized side-by-side cells at physiological conditions of 35°C and 90% humidity (Figure 3A) mimicking the nasal cavity. Quality control of olfactory mucosa biopsy and further processing steps including cutting, particle application, fixation, and cryo-sectioning occurred via hematoxylin-eosin (HE) staining. Only specimens with an intact epithelial layer were analyzed; those with a damaged epithelial layer were excluded from the study because a compromised epithelial layer could enhance particulate uptake. Further, sample thickness of *ex vivo* specimens was $1,273 \pm 356 \mu\text{m}$, whereas individual samples were not significantly different in thickness (Shapiro-Wilk normality test, One-Way-ANOVA with Levene's variance test and Bonferroni posthoc test; $\alpha = 0.05$ respectively). Detailed thickness data and statistical analysis are presented in Supplementary Figure S2.

PLGA nanoparticles, with a diameter of 80 and 175 nm have been taken up immediately into the *lamina propria* of the olfactory mucosa within 5 min after application. Particles are spread over the *lamina propria*. 80 nm nanoparticles, co-localized with cell nuclei, have been observed in lymphoid follicles (Figure 3B) and the epithelial cell layer, which implies spontaneous cellular uptake of these nanoparticles. 175 nm particles have additionally been documented more prominent in glands than in lymphoid follicles (Figure 3C).

In general, it is reported that cells can take up nanoparticles, with a diameter below 200 nm, intracellularly after intranasal administration (Mistry et al., 2009; Bourganis et al., 2018; Rabiee et al., 2020). Muntimadugu et al. (2016) has further already reported the transport of PLGA nanoparticles, with diameters below 200 nm, along axons within the nasal mucosa (Muntimadugu et al., 2016). This was also proven within our experiments for porcine olfactory mucosa. We further investigated PLGA nanoparticles with a 520 nm diameter. In contrast to intranasal application, K. Y. Win and S. S. Feng et al. (2005) proved the intracellular uptake of 500 nm polymer particles into Caco-2 epithelial cells (Win and Feng 2005). In our study, 10 min after application to the olfactory mucosa explants, cells also seemed able to take up 520 nm nanoparticles; these were found distributed in the epithelial layer and mainly in the outer 150 μ m of the *lamina propria* (Figure 3D). Overall, the uptake of the larger-size particles occurred in slower motion compared to 80 and 175 nm particles. Further, 520 nm particles have not, in contrast to smaller nanoparticles, been observed primarily near nuclei within the first 15 min but between, hence intercellularly. Within 15 min, further 520 nm particles have been detected only sparsely in glands, not in deeper layers of the *lamina propria*, nor in the collagen tissue, which connects the porcine mucosa with the nasal septum *in vivo*.

An overview of size- and time-dependent PLGA nanoparticle uptake and distribution is presented in Table 2:

In summary, the uptake of PLGA nanoparticles, displayed in Table 2, is fast, within only 5 min after application to the apical side of olfactory mucosa, of PLGA nanoparticles up to a diameter of 520 nm, into the epithelial cell layer. Further size dependent penetration occurs within 10 min to the underlying *lamina propria*. Herein, 80 nm particles penetrate to a high extent, whereas similar

TABLE 2 | Size- and time-dependent uptake, as well as co-localization with sub structures in the olfactory mucosa, of PLGA nanoparticles (suspension) and spray dried nano-in-micro particles (NiMPs) (powder) consisting of 520 nm PLGA particles embedded in chitosan. 5 min, 10 min, or 15 min after particle application to the apical side and incubation at physiological conditions of the nasal cavity (35°C, 90% humidity). (+) rarely, (++) intermediately, (+++) often particles observed, or (–) no particles observed. Examined samples: PLGA nanoparticles ($n = 3$), respectively; NiMPs ($n = 6$). Quantitative comparison only applicable for PLGA nanoparticles among each other and NiMPs separately due to different applied particle amounts (suspension versus powder).

5 min after application	Epithelium (apical)	<i>Lamina propria</i>	Lymphoid follicle	Gland	Neuronal bundle	Collagen tissue (basolateral)
10 min after application						
15 min after application						
PLGA 80 nm	+++	++	+++	-	-	-
PLGA 175 nm	+++	++	+	++	-	-
PLGA 520 nm	+++	+	-	+	+	-
NiMP (PLGA+chitosan)	+++	+	+++	++	+	++

amounts of 175 nm particles were taken up. 520 nm, in contrast, penetrated to a very low extent and, hence, were also slower. Further, many 80 nm particles were detected within 5 min, especially intracellularly within lymphoid follicles, which can imply an interaction with immune cells. In contrast, 175 nm particles were only rarely found associated with lymphoid follicles and 520 nm particles were, even within 15 min, not detected co-localized with lymphoid follicles. This indicates a size dependent relation in transport. The initial immune reaction was investigated within this study and is described below. Supplementary, 175 nm particles have been detected after 5 min in glands, 520 nm particles only after 15 min, and 80 nm particles were not detected at all. This again implies a size dependent differentiation in transport routes, but does not impact transport towards the brain or the central nervous system (CNS). In contrast, gland associated nanoparticles might stuck in the mucosa and are, therefore, less effective as drug delivery system. Additionally, only 520 nm nanoparticles have been detected in neuronal bundles, which could enable further transport to the brain or the CNS. Consequently, especially 520 nm particles seem to have the ability for transcellular neuronal transport, in contrast, 80 and 175 nm do not. Those seem to be transported only transcellular across other cell types. Finally, none of the investigated pure PLGA nanoparticle samples were detected within the basolateral collagen tissue and, thereof, none of these penetrated the whole transverse section of the tissue samples within 15 min following application.

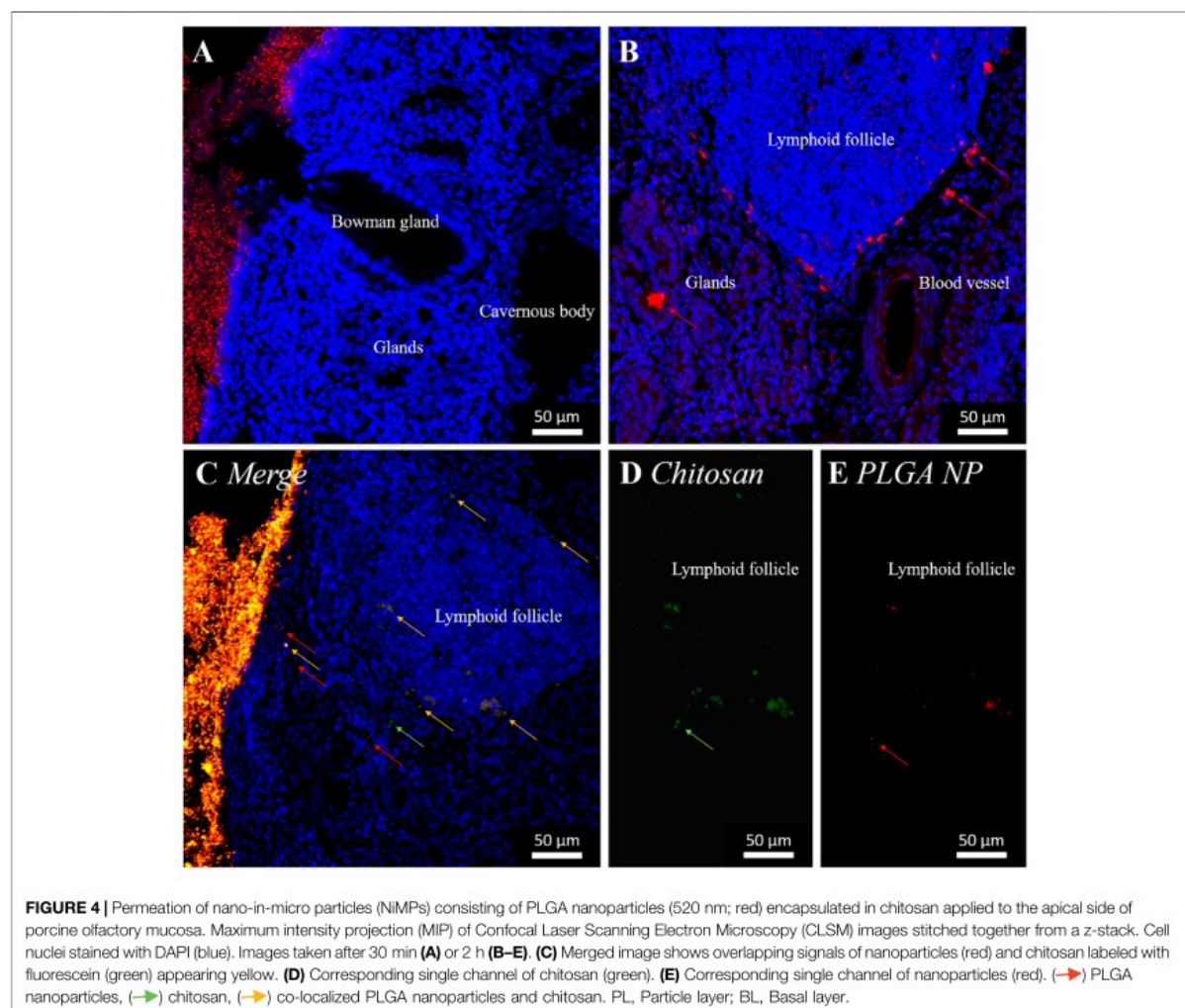
Nano-in-Micro Particle Uptake

PLGA nanoparticles, with a 520 nm diameter, were embedded in a second production step via spray drying in chitosan. The previously-

described variation of polymer ratio PLGA:chitosan showed no impact on olfactory uptake. Therefore, the following results are true for all, herein produced and described, nano-in-micro particles (NiMPs). ~12 mg NiMPs were applied onto porcine olfactory mucosa specimens and incubated similarly to pure nanoparticles, in a side-by-side cell at 35°C and 90% humidity, mimicking the nasal cavity (**Figure 3A**). Due to the different application of PLGA nanoparticle suspensions as powder here, only the occurrence of NiMPs and chitosan-coated PLGA particles is examined, but not the quantitative particle amount. This is because more PLGA particles have been applied, respectively, on powder samples.

The applied particle patch (red) covered the epithelial layer completely (**Figure 4**). In contrast to the above, chapter 3.3 described the distribution of purely applied 520 nm PLGA particles in the outer ~150 μm of the *lamina propria*, chitosan-coated NiMPs have been detected 15 min after application spread deep within the *lamina propria* even distributed over the entire width of the olfactory mucosa sample reaching the collagen tissue at the basolateral side (**Supplementary Figure S3**). All findings of NiMP-uptake within the initial 15 min after application to the olfactory mucosa are summarized and displayed in **Table 2**.

Due to the complete coverage of the epithelial layer with the applied particle layer, initially within 5 min, many NiMPs were found associated with the epithelium. Fewer NiMPs were found in the *lamina propria*; however, the penetration occurred faster than for pure 520 nm PLGA particles without chitosan coating. Within 10 min, NiMPs were mainly detected associated with lymphoid follicles (**Supplementary Figure S4**). After 15 min, NiMPs were

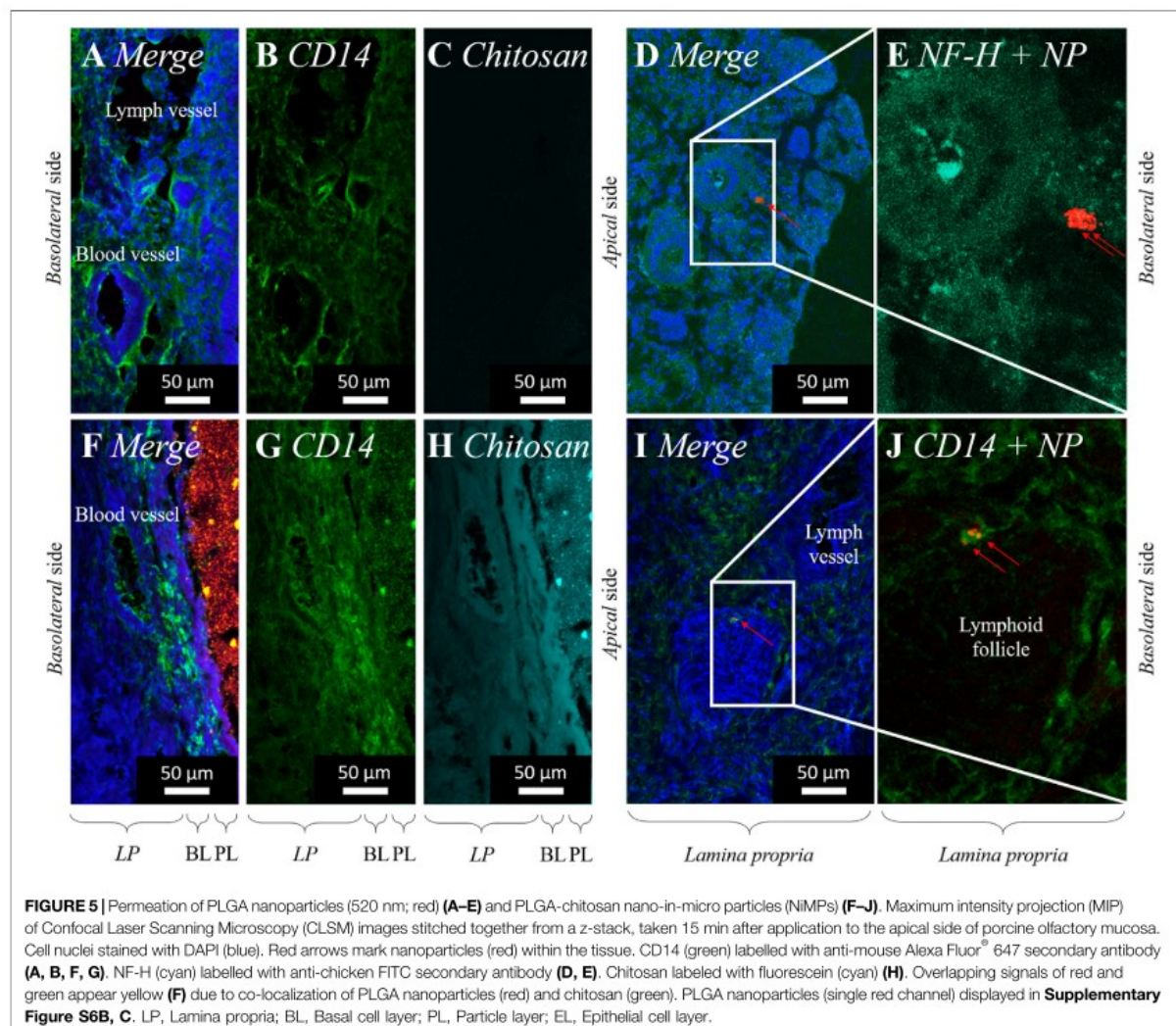


finally detected in glands and neuronal bundles to a slightly lower extent. Finally, within 15 min, NiMPs were detected spread over the whole transverse section of the mucosal tissue sample, even distributed at the basolateral side in the collagen tissue. Consequently, the chitosan-coating herein accelerated the uptake of NiMPs, compared to the identical purely-applied PLGA particles, with 520 nm in the initial 15 min after application. However, to analyze the quantitative amount further investigations are needed, due to the different particle amounts applied, caused by the sampling procedure.

30 min following particle application, surface located bowman glands have been detected, where the gland-overlying particle patch was cleared (**Figure 4A** and **Supplementary Figure S6**). Therefore, epithelial glands seem to be able to either take up particles within 30 min, resulting in enhanced uptake compared to the surrounding epithelial layer, or transport overlying particles away due to the ongoing mucus production mechanism (Sadé et al., 1970; Aspden et al., 1995; Aspden et al., 1997). For this reason, we

additionally stained control samples, after 5 h incubation, with Hoechst 33342 dye, which solely stains intact cell nuclei to prove cell viability within and after the experiments. This live-stain experiment proved that cells of the excised mucosa samples were alive throughout the whole duration of the experiments (data not shown). As a result, it could be assumed that the monitored glands were also able to produce mucus during the experiment and, therefore, possibly transported overlying particles away.

Samples examined 2 h after particle application showed similar results to the above described results 15 min following application. NiMPs were observed over the whole transverse section of the porcine olfactory mucosa, including collagen tissue layers at the basolateral side of the sample (**Supplementary Figure S5**). Furthermore, 520 nm particles were detected in mucus-producing glands within the tissue (**Figure 4B**), and in the outer zone of lymphoid follicles (**Figures 4B–E**). Therefore, NiMPs also seem to be transported



to lymphoid follicles, as similar behavior was found after 5 min for nanoparticles with 80 nm diameter. Due to the green labeling of chitosan in NiMPs, we were able to additionally prove the co-localization of chitosan (**Figures 4C,D**) with PLGA nanoparticles (red) (**Figures 4C,E**) in the outer zone of lymphoid follicles. Consequently, not only the pure PLGA particles were transported there but also chitosan-coated NiMPs. Co-localization with glands (**Figure 4B**) could also be attributed to the mucoadhesive properties of chitosan (Henriksen et al., 1996). When passing glands, mucus in these glands seems to hold up chitosan-coated nanoparticles due to mucoadhesion.

Influence of Chitosan Coating

In general, the interaction of chitosan and PLGA nanoparticles within mucosal tissues is not yet well characterized. We, therefore, examined the following immunohistochemistry studies and compared purely applied 80, 175, and 520 nm PLGA particles

with nano-in-micro particles (NiMPs) consisting of 520 nm PLGA nanoparticles embedded in chitosan via spray drying.

Co-Localization With Initial Immune Cells and Neuronal Fibers

When pure PLGA nanoparticles were applied to the porcine olfactory mucosa sample, several nanoparticles were taken up into the epithelial layer, these also passed the basal cell layer (BL), and permeated into outer layers of the *lamina propria* (LP) as already described in the previous chapter. We additionally labeled CD14⁺ cells via immunofluorescence staining. As shown in **Figure 5A** (merge) and **Figure 5B** (single channel), CD14 was mostly detected homogeneously distributed within the olfactory mucosa, since this biological barrier is an important immunologically-active tissue. Further, an increased signal was detected, particularly within blood vessels and lymphatic vessels, because CD14⁺ monocytes roll along with endothelial cells and are

moving from the immunogenic active tissue site into the bloodstream. Due to the application of pure 80, 175 and 520 nm PLGA nanoparticles without chitosan, no chitosan signal was detectable in this kind of sample, which serves as a control here (Figure 5C).

Significant agglomerates of several nanoparticles have been further observed near nuclei (Figure 5D), 520 nm particles especially in neuronal bundles (Figure 5E) stained against the marker neuronal filament heavy protein (NF-H). Neuronal bundles are axonal fibers of primary neurons that merge in the *lamina propria* and connect the olfactory mucosa via the olfactory or the trigeminal nerve directly to the brain (Morrison and Costanzo 1990; Morrison and Costanzo 1992).

When chitosan-coated NiMPs have been applied to the porcine olfactory mucosa, within 15 min several chitosan-coated nanoparticles were also detected in the outer area of the sample, including the epithelial layer, basal cell layer (BL), and the outer layers of the *lamina propria* (LP) (previous chapter). NiMPs have also been observed in neuronal bundles (data not shown) and could, therefore, possibly be also transported along the olfactory and trigeminal nerve to the brain and the central nervous system (CNS). As stated in chapter 3.4, we have already proved that not only pure PLGA nanoparticles can penetrate the olfactory mucosa, but also chitosan associated with these nanoparticles, and even to a faster extent. In Figure 5H, we solely displayed the penetration of chitosan labeled with fluorescein, which indicates, that chitosan is also able to dissociate from PLGA nanoparticles and independently penetrate the outer ~150 µm of the olfactory mucosa within 15 min after application to the apical side of the sample. Further, an intensity gradient of chitosan is visible decreasing to deeper layers within the tissue.

In the examination of CD14⁺ cells after application of chitosan-coated NiMPs, a CD14⁺ signal was detected on the surface of single epithelial cells; however, the epithelial layer herein was completely covered by the particle patch (Figure 5F). Further, CD14⁺ monocytes were again detected at the inner wall of blood vessels. Additionally, an accumulation of CD14⁺ immunoreactivity was monitored in the outer layers of the *lamina propria* (Figure 5G), where no blood or lymphatic vessel is present. Moreover, in Figure 5I, we found a CD14⁺ signal surrounding a lymphoid follicle present in the *lamina propria*; especially one CD14⁺ cell directly associated with NiMPs on its surface, as well as intracellularly, seems to express CD14 on its cell surface (Figure 5J). In contrast to this, direct cellular CD14-association with pure 520 nm PLGA particles could not be found. Bringing this together with the described chitosan penetration gradient (Figure 5H), we conclude that an attraction of immune cells occurred due to the presence of chitosan recognized by CD14⁺ monocytes or macrophages. This could be assigned to the lipopolysaccharide-receptor, which CD14 is part of, resulting in either a pro-inflammatory event triggered by M1-macrophages, or a wound healing procedure described by the increased presence of M2-macrophages (Davis et al., 2018).

Cell Junction Opening

Chitosan can open tight junctions (Fazil et al., 2012; Sonaje et al., 2012; Rassu et al., 2016), which are the characteristic intercellular

connections present in epithelial cells and endothelial cells. We, therefore, stained the prominent component *Zonula occludens* protein 1 *ZO-1* via immunohistochemistry.

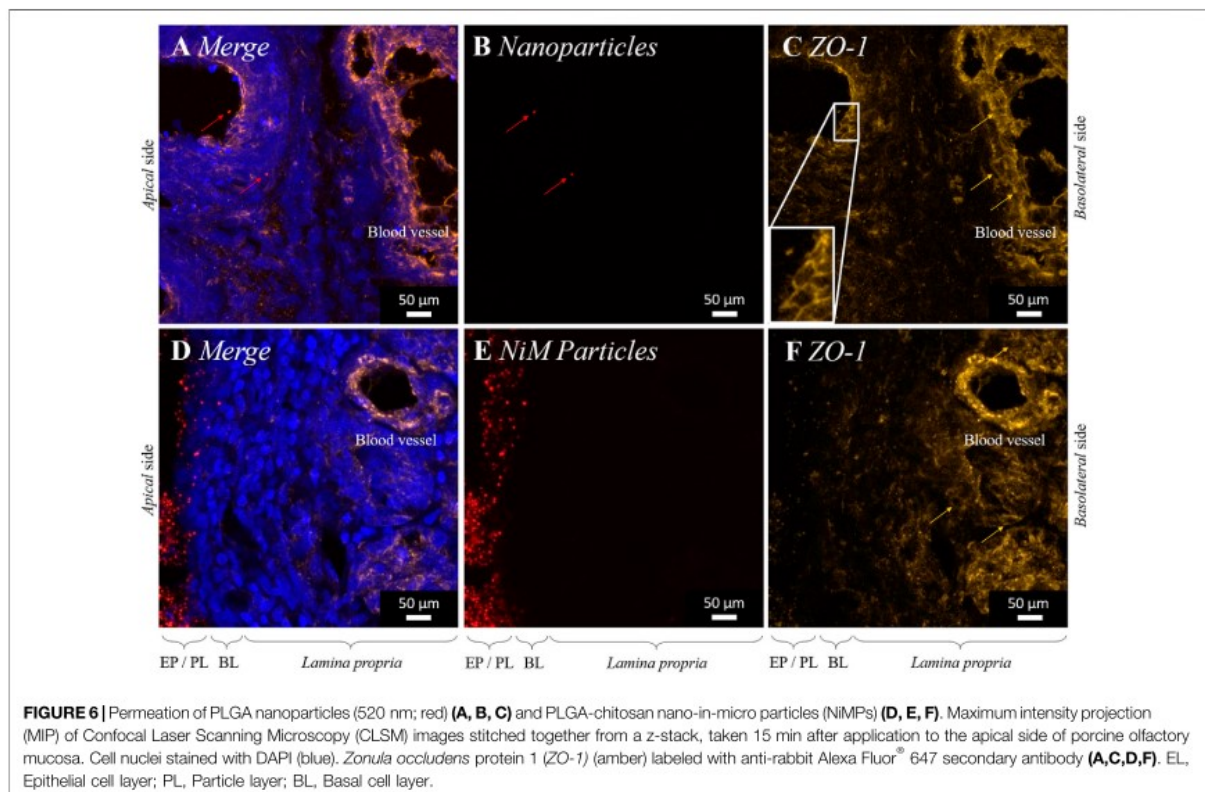
As already described in chapter 3.3, within 15 min after application PLGA nanoparticles (520 nm) permeated into the olfactory tissue sample (Figures 6A,B). *ZO-1* protein was detected mainly between epithelial cells forming the well-known tight junctions (Figures 6A,C). When pure PLGA nanoparticles have been applied, higher magnification revealed characteristically honeycomb-like staining resulting from intercellular present *ZO-1*, which was earlier described in cell culture (Stevenson et al., 1986; Anderson et al., 1988). The underlying *lamina propria* consists, to large extent, of fibroblastic cells, where *ZO-1* is mainly localized in endothelial cells. The localization in blood vessels was also proven in this study (Figures 6A,D). Open tight junctions are characterized by another conformation than in the closed stage. The membrane protein *ZO-1* is internalized into the cytoplasm, resulting in loosening of the intercellular connection (Smith et al., 2004). Consequently, due to the internalization of the former membrane protein, immunohistochemically targeting of *ZO-1* in the open conformation is hence not possible anymore, which results in discoloring.

Comparing the results of nanoparticle permeation to the application of chitosan-embedded NiMPs, we not only detected the above described uptake of PLGA nanoparticles associated with chitosan polymer molecules, we additionally displayed the ability of chitosan to penetrate the *lamina propria* dissociated from nanoparticles, approximately 150 µm, within 15 min after particle application to the olfactory epithelium (Figure 5H). Additionally, we investigated the presence of *ZO-1* signal in tight junctions. Following the application of NiMPs, we again detected a gradient signal (Figure 6F) reverse to the above-shown chitosan gradient (Figure 5H); therefore, matching the previously-described chitosan penetration of approximately 150 µm into the *lamina propria*, which caused *ZO-1* internalization and tight junction opening. Foremost in deeper layers of the *lamina propria*, *ZO-1* signal was still apparent proving working cell-cell junctions. Especially in the wall of blood vessels, the *ZO-1* immunoreactivity (Figures 6D,F) indicated still active tight junctions. Epithelial cells, which directly underlie the applied NiMPs faded also within 15 min and were therefore found discolored (Figures 6D,F) caused by chitosan mediated tight junction opening.

DISCUSSION

In this study, we successfully prepared poly(lactic-co-glycolic acid) PLGA nanoparticles of different sizes (80, 175, and 520 nm) using the precipitation and double emulsion method. Further, we produced specialized nano-in-micro particles (NiMPs) via spray drying, consisting of PLGA nanoparticles (520 nm), embedded into the matrix polymer chitosan.

NiMPs have in this study been produced via spray drying. In contrast to other innovative methods for nano- and



microparticle production, e.g. electrospraying or supercritical CO₂ assisted electrohydrodynamic processes (Jaworek and Sobczyk 2008; Baldino et al., 2019a; Baldino et al., 2019b), spray drying is an even commercially used formulation process. Especially the pharmaceutical industry (Stahl 1980; Lee et al., 2002) benefits from high throughput production of spray drying, concurrently resource-friendly, as well as from high resulting encapsulation efficiencies of up to 100% (Walz et al., 2018). Spray drying of chitosan has been already reported in the literature; however, ineffective process parameters or inhomogeneous particles have mainly been documented (He et al., 1999; Tokárová et al., 2013). To achieve a robust production process and reproducible particles, with homogenous size distribution and morphology, it is necessary to choose suitable process parameters, such as inlet temperature, feed rate, and gas flow (Paudel et al., 2013). The crucial factors in this process are droplet atomization followed by feed evaporation. To generate homogenous particles, atomization should be uniform, resulting in fine droplets at the first stage. These droplets then need to evaporate continuously in the second step, to achieve homogenous particles with smooth surface. Droplets dry from the outer to the inner phase, meaning that the remaining liquid in the center of the particle needs to evaporate through the already partly dried matrix. When evaporation takes place too fast at inlet temperatures above 100°C, either hollow particles are formed

through the so-called Rush-hour effect (Paudel et al., 2013), or they even burst and empty shells remain. Contrary to common knowledge, wrinkled surfaces of spray-dried chitosan particles do not occur from the polymeric properties of chitosan itself, but mainly from the process parameters of spray-drying. When particles cool down at the end of the process, they shrink and characteristic wrinkles occur. Hence, it is possible to prepare reproducible smooth chitosan particles utilizing suitable spray drying parameters like the ones reported herein. With moderate evaporation rates, dense and homogenous particles were achieved. Consequently, we developed a robust spray drying process. The morphology of all particulate samples in this study was spherical, with smooth surfaces because we optimized the spray drying process performed with a Büchi B-290 Mini-Spray dryer. An inlet temperature of 100°C was identified, as a crucial parameter, which resulted in an outlet temperature of 45 ± 1°C. This allowed the polymer droplets to continuously evaporate, ultimately resulting in homogenous and smooth particles.

For the chitosan:PLGA polymer ratio of NiMPs, a higher chitosan ratio resulted in increased particle diameters determined via image analysis of Scanning Electron Microscopy images and static light scattering; however, NiMPs tend to agglomerate in suspension. They were split up during static light scattering after an additional ultrasonic treatment within the measurement cell, which then revealed a bidisperse size distribution with a nanoparticle and a microparticle fraction. A higher chitosan

ratio mainly influenced the nanoparticle fraction, which is attributed to the formation of additional, and slightly bigger pure chitosan nanoparticles during spray drying. Generally, due to the higher PLGA content about seven PLGA nanoparticles with a mean diameter of 519.7 nm were found in one chitosan microparticle with a mean diameter of 6.61 μm for low chitosan ratio, whereas, high chitosan ratio during spray drying resulted in an encapsulation of about two 519.7 nm-PLGA-nanoparticles per chitosan microparticle with a mean diameter of 5.75 μm . The achieved encapsulation efficiency of NiMPs was either $39 \pm 19\%$ (1/3 chitosan:2/3 PLGA) or $51 \pm 16\%$ (2/3 chitosan:1/3 PLGA); and therefore, not significantly different. Although, 1/3 more chitosan as matrix material was present, the encapsulation efficiency did not significantly increase. This is again attributed to the formation of additional pure chitosan nanoparticles, which were determined via static light scattering measurements after additional ultrasonic treatment. Consequently, spray drying is a very efficient method to encapsulate nanoparticles up to a mass ratio of 2/3, covering them successfully with the added matrix polymer, even more beneficial when using less matrix material. The polymer ratio variation had no impact on the following *ex vivo* experiments.

Mucosal uptake of PLGA nanoparticles and NiMPs was investigated, with porcine olfactory mucosa specimens, in specialized side-by-side cells, mimicking the upside-down orientation and physiological conditions within the nasal cavity at 35°C and 90% humidity. Overall, a size- and time-dependent uptake of PLGA nanoparticles was observed. Smaller PLGA nanoparticles, with 80 nm diameter, were taken up immediately deep into the *lamina propria* 5 min after application to the epithelium. Fewer 175 nm particles penetrated the epithelial and the basal layer within 5 min. For 520 nm PLGA nanoparticles, slower uptake was observed, reaching the outer ~150 μm of the *lamina propria* within 10 min. Additionally, 80 and 175 nm particles were documented to directly associate with cell nuclei within 5 min, which implies intracellular uptake. In contrast, 520 nm particles have not initially been observed near nuclei, but after 15 min, and to lower amounts, compared to the smaller nanoparticles. The occurring decelerated penetration due to increasing particle size is already reported in the literature (Mistry et al., 2009; Bourganis et al., 2018). Further, reported critical particle size enabling transcellular transport after intranasal administration is 200 nm (Bourganis et al., 2018; Rabiee et al., 2020). However, Musumeci et al. (2018) reported that PLGA nanoparticles, up to 300 nm, reach and accumulate in the brain of rats, but did not clarify the occurring transport mechanism (Musumeci et al., 2018). Nanoparticles with diameters greater than 500 nm have not yet been reported for nose-to-brain (N2B) targeting (Bourganis et al., 2018; Rabiee et al., 2020), but size-dependent intracellular uptake is possible also for 200, 500 and even 1,000 nm particles in epithelial cells (Caco-2) (Win and Feng 2005).

Remarkably, we reported herein co-localization of 520 nm PLGA particles with nuclei, especially accumulated in neuronal bundles, which implies intracellular uptake in neuronal axons and could enable transcellular transport within the olfactory, or

trigeminal nerve pathway to reach the brain and the central nervous system (CNS) (Gänger and Schindowski 2018; Bourganis et al., 2018; Rabiee et al., 2020; Keller et al., 2021). The diameter of axons in humans ranges from 100 to 700 nm (Morrison and Costanzo 1990; Morrison and Costanzo 1992; Mistry et al., 2009). It is broadly reported that directed transport along with neuronal cells and posterior neuronal bundles is one of the most promising routes for nose-to-brain delivery. To further investigate this phenomenon, additional experiments visualizing the exact cellular uptake and transport mechanism could be helpful. Hence, live imaging or *in vivo* experiments with particle sizes above 200 nm should again also be taken into account.

Contrasting the observations of 520 nm pure PLGA particles to the similar 520 nm PLGA particles embedded into chitosan, NiMPs were taken up faster and deeper in the *lamina propria*. A quantitative analysis was herein not possible because sample sizes differed between PLGA nanoparticle suspension and NiMP powder samples. The effect of applied polymer amount and sample condition needs hence to be investigated in future studies. Within 15 min high amounts of NiMPs were detected spread over the whole olfactory mucosa section, reaching the collagen tissue at the basolateral side, where none of the purely applied PLGA nanoparticles were found. Furthermore, chitosan has been detected associated with the penetrated PLGA nanoparticles within the olfactory mucosa. Especially after 2 h, several 520 nm particles have been found together with chitosan in the outer zone of lymphoid follicles, where usually T-cells and B-cells are present in the porcine olfactory mucosa (Ladel et al., 2018). Small pure PLGA nanoparticles (80 and 175 nm) have also been detected in this area after approximately 5 min. In contrast to this, purely applied 520 nm PLGA particles were not found associated with lymphoid follicles. Ladel et al. (2018) showed CD3⁺, CD20⁺, and CD14⁺ cells in the outer area of the porcine olfactory epithelium-associated lymphoid follicles (Ladel et al., 2018). This finding further matches the subepithelial dome more prominent in intestinal Peyer's patch but also found in young adults and sheep.

Also within this study, we consequently examined the general initial immune reaction, which is mediated by CD14⁺ immune cells, namely monocytes and macrophages. It takes place within the first few hours after contact with a biomaterial (Anderson et al., 2008). We further monitored the presence of CD14 around lymphoid follicles. In our study, PLGA was not found co-localized with CD14⁺ cells, thus seems not to be recognized by CD14. Therefore, it is assumed that PLGA nanoparticles can pass the olfactory epithelium reaching for example, neuronal bundles, and could then be further transported to the brain and the CNS. Nevertheless, 80 nm PLGA nanoparticles especially have been documented associated with lymphoid follicles, which should be further clarified. Although this result is not attributable to the recognition by monocytes or macrophages, an interaction mechanism with other present immune cells could still be possible and should be explored in future studies.

The chitosan penetration gradient within the olfactory mucosa was found in our study to be proportional to a gradient of the initial immune response. Chitosan, therefore, seemed to cause a migration of CD14⁺ cells to the particles underlying the *lamina*

propria within 15 min after particle application to the epithelium. The membrane located glycoprotein CD14 forms together with the lipopolysaccharide-binding protein (LPB), the lipopolysaccharide-receptor (LPR), which recognizes bacterial endotoxin lipopolysaccharides lipopolysaccharide-receptor present on the surface of Gram-negative bacteria (Wright et al., 1990). Lipopolysaccharide-induced upregulation of the CD14 membrane receptor is known as an initial immune reaction in mucosal tissues, such as the intestine (Funda et al., 2001); (Frolova et al., 2008). Otterlei et al. (1994) initially described chitosan-recognition by CD14 on monocytes (Otterlei et al., 1994). To the contrary, Qiao et al. (2010) reported the reduction of pro-inflammatory cytokines through chitosan oligosaccharides (Qiao et al., 2010). Recently, Chang et al. (2019) differentiated between low molecular (below 7.1 kDa) and high molecular (above 72 kDa) chitosan in the macrophage-binding mechanism. They reported that only low molecular weight chitosan up to 7.1 kDa could bind CD14 and interpreted it as an activation of a pro-inflammatory cascade. Studies describing the immune reaction of applied chitosan microparticles are still rather poor. Solely, S. Davis et al. (2018) proved chitosan particles with a high degree of deacetylation with sizes of 1–10 μm causing less M1-macrophage activation than similar chitin particles (Davis et al., 2018). Consequently, either the pro- or anti-inflammatory ability of chitosan particles is dependent on molecular weight, particle size, and degree of deacetylation. Taking this into account, we assume that in our study the observed CD14⁺ signal should be anti-inflammatory inducing a wound healing cascade, because the herein utilized chitosan has a molecular weight of 150–300 kDa. This should hence not be critical because Chang et al. (2019) reported for chitosans with molecular weights above 72 kDa solely anti-inflammatory reactions. Further, a high degree of 80% deacetylation and lastly a particle size ranging through agglomerates from approximately one micron up to 100 μm supports this reasoning. Nevertheless, the herein investigated CD14 immunohistochemical staining does not allow us to distinguish between M1- and M2-macrophages, which should be further evaluated in cell culture experiments, because, for example, a quantitative cell assay with altering cytokine concentrations would be needed as a reference (Zarif et al., 2016). This was not possible with the *ex vivo* samples of this study.

Moreover, the chitosan coating of NiMPs revealed several other interesting findings different from the purely applied identical PLGA nanoparticles. Chitosan was found to penetrate the olfactory mucosa approximately ~150 μm within 15 min. Further, it accelerated the penetration of coated nanoparticles significantly and enables transport over the whole transverse tissue section within 15 min as described above. This is attributed to the swelling of chitosan on the top of the mucosa because the naturally occurring pH value in the nose of healthy individuals ranges around pH 6 (England et al., 1999). Unmodified chitosan does not completely dissolve at physiological pH values in the nose due to its pKa value of ~6.5 but it is swelling and single chitosan polymer chains can move into the tissue. One explanation of enhanced uptake and accelerated permeation into the olfactory mucosa could be attributed to the well-

known ability of chitosan to open tight junctions or more general cell-cell junctions enabling paracellular transport. The membrane protein *Zonula occludens* protein 1 (ZO-1) is part of tight junctions within the epithelial cell layer as well as endothelial cells, and adherens junctions within the *lamina propria* (Steinke et al., 2008; Wolburg et al., 2008). When tight junctions are opened due to chitosan treatment, the membrane protein ZO-1 immunohistological staining fades. V. Dodane et al. previously reported this in 1999 in the cell culture of Caco-2 cells. The underlying mechanism caused by the internalization of this specific protein from the membrane to the cytoskeleton was later clarified by Smith et al. (2004) (Smith et al., 2004). This ability in cell culture has been proved by several research groups in the past decades (Dodane et al., 1999; Rassi et al., 2016); nevertheless, the chitosan application onto tissues is rarely reported. The opening mechanism in epithelial cells, previously reported by Dodane et al. (1999) to take place after 1 h and regenerate within 24 h also observed through fading and recovery of ZO-1 staining (Dodane et al., 1999), however, they investigated acidic solutions at low chitosan concentrations. Smith et al., 2004 further described a concentration-dependent internalization of ZO-1 on Caco2-monolayers within 1 h. M. Fazil et al. (2012) additionally showed increased brain uptake caused by chitosan particles but did not show ZO-1 staining as reference (Fazil et al., 2012). We, herein, showed for the first time that this is also true in the naturally occurring environment of porcine olfactory mucosa as a prominent biological barrier. The ZO-1 discoloring is attributed to internalization and opening of cell-cell junctions occurring in the *ex vivo* setting within only 15 min, including swelling of the dry chitosan-coated particles, which was never previously reported. To better understand which dosage of chitosan is most effective to promote paracellular transport, further experiments with different concentrations, particle amounts, as well as shorter timeframes would be interesting.

Finally, local particle clearance was observed above surface-located Bowman glands. NiMPs have been cleared completely within 30 min, which could be attributed either to accelerated particle uptake within glands or ongoing mucus production resulting in continuously pushing away the overlying particle layer. Ongoing mucus production even in *ex vivo* setting was already early described to last at least 4–5 h for frog palate mucosa (Sadé et al., 1970; Aspden et al., 1995), later also for human specimens (Aspden et al., 1997) and ferret trachea with velocities up to $9.5 \pm 3.5 \text{ mm min}^{-1}$ (Abanses et al., 2009; Jeong et al., 2014). Further, chitosan was found to reduce mucociliary transport rate (MTR) proportionally to its molecular weight (Aspden et al., 1995), which was attributed only to its physical interaction with mucins not harming the mucosa itself (Aspden et al., 1997). Unfortunately, no further tracking of particles was possible in this study because no particles have been detected directly associated with the gland ensheathing cells, or the underlying cells of the *lamina propria*, and continuous monitoring was not possible due to the sampling procedure. As Raber et al. (2014) also described enhanced uptake of chitosan-coated PLGA nanoparticles in glandular ducts of hair follicles (Raber et al., 2014), mucosal glands could also function as uptake enhancing mucosa components. For the clarification of the role of surface-associated glands, it would be

interesting to continuously monitor the site of action. It would be beneficial to monitor organoids, such as glands, using a complex model of the olfactory mucosa. For example an organ-on-a-chip model, a so-called nose-on-a-chip.

CONCLUSION

Within this study, we successfully developed specialized Nano-in-Micro particles (NiMPs) consisting of PLGA nanoparticles embedded into chitosan microparticles via spray drying. We evolved a robust spray-drying process resulting in homogenous microparticles with high encapsulation efficiency, uniform size distribution, smooth surface, and dense pores. We demonstrated, that not only 80 and 175 nm PLGA nanoparticles purely applied to the olfactory mucosa can be taken up intracellularly within only 5 min, but also 520 nm PLGA particles are associated with nuclei and neuronal fibers after 15 min, which can imply transcellular transport within the olfactory epithelium and intracellular uptake into neuronal cells following transport along those to the olfactory or trigeminal nerve, which finally enables targeting of the brain and the central nervous system (CNS). These findings were further proved to be size-time-proportional, resulting in smaller particles moving faster (within only 5 min) and to a higher extent into the *lamina propria*. Chitosan-coated NiMPs were identified as even more interesting nanoparticle carriers and are auspicious delivery vehicles themselves. Their chitosan coating is subsequently swelling on the mucosal barrier; therefore, single chitosan polymer chains penetrate within 15 min approximately 150 μ m into the olfactory mucosa. With this, the chitosan penetration affects the opening of tight junctions and, therefore, can additionally enable paracellular transport through the olfactory epithelium. Consequently, the accelerated uptake of chitosan-coated nanoparticles was examined.

PLGA nanoparticles, as well as, NiMPs were found in lymphoid follicles; however, only NiMPs were co-localized after 15 min with the immunoreactivity signal of membrane protein CD14 present on monocytes and macrophages. Hence, we assume any other interaction for PLGA nanoparticles e.g., T- or B-cell mediated binding, which needs to be investigated in future studies. NiMPs herein showed the ability to initialize an anti-inflammatory cascade within 15 min after particle application, due to the beneficial properties of the herein utilized chitosan (molecular weight, degree of deacetylation, and particle size). However, CD14⁺ macrophages could be either pro-inflammatory M1-macrophages or anti-inflammatory M2-macrophages effecting wound healing, which could not be fully clarified within this study because therefore cytokine levels are needed as a reference, which should be investigated in cell culture. Additionally, particle clearance of gland overlaying particles was herein documented, but could not be fully enlightened, because the sampling procedure was limited and continuously monitoring was not possible.

In conclusion, within this study, we demonstrated the possibility for PLGA nanoparticles as well as for chitosan NiMPs to take all three prominent pathways to the brain and the CNS, namely transcellular, intracellular via neuronal cells, and paracellular transport. Overall, although polymeric particles are broadly reported as promising drug delivery systems, not only for intranasal application the usage in the clinic is still lacking. Up to now, no nano-based system has entered advanced clinical trials. Consequently, still more research is needed to collect additional data and unravel the complex phenomena within the nasal mucosa, to clarify the different transport mechanisms and the role of special organoids, like bowman glands. Further, verifying specific influences of particle material, other formulation components, and particle sizes.

DATA AVAILABILITY STATEMENT

The original contributions presented in the study are included in the article/**Supplementary Material**, further inquiries can be directed to the corresponding author.

AUTHOR CONTRIBUTIONS

Conceptualization, CG-T, KS, NG-T, and ET; methodology, LS, SL, JF, and NG-T; investigation, LS, AF, SL, and CG; writing - original draft preparation, LS and AF; writing - review and editing, all authors; visualization, LS, AF, and SL; supervision, CG-T, KS, ET, and GT; funding acquisition, CG-T, KS, LS, SL, and JF. All authors have read and agreed to the published version of the manuscript.

FUNDING

This study has received funding from the European Union's Horizon 2020 research and innovation programme under grant agreement No. 721098 (www.n2b-patch.eu) to AF, CG, NG-T, ET, GT, KS and CG-T.

ACKNOWLEDGMENTS

LS thanks the Studienstiftung des deutschen Volkes for her PhD scholarship. SL and JF thank the Stiftung der deutschen Wirtschaft for their PhD fellowships. All authors thank Sue Child and Matthew Burton for their language review.

SUPPLEMENTARY MATERIAL

The Supplementary Material for this article can be found online at: <https://www.frontiersin.org/articles/10.3389/fphar.2021.732954/full#supplementary-material>

REFERENCES

- Abanses, J. C., Arima, S., and Rubin, B. K. (2009). Vicks VapoRub Induces Mucin Secretion, Decreases Ciliary Beat Frequency, and Increases Tracheal Mucus Transport in the Ferret Trachea. *CHEST* 135 (1), 143–148. doi:10.1378/chest.08-0095
- Akerlof, G. (1932). Dielectric Constants of Some Organic Solvent-Water Mixtures at Various Temperatures. *J. Am. Chem. Soc.* 54 (11), 4125–4139. doi:10.1021/ja01350a001
- Anderson, J. M., Rodriguez, A., and Chang, D. T. (2008). Foreign Body Reaction to Biomaterials. *Semin. Immunol.* 20 (2), 86–100. doi:10.1016/j.smim.2007.11.004
- Anderson, J. M., Stevenson, B. R., Jesaitis, L. A., Goodenough, D. A., and Mooseker, M. S. (1988). Characterization of ZO-1, a Protein Component of the Tight Junction from Mouse Liver and Madin-Darby Canine Kidney Cells. *J. Cell Biol.* 106, 1141–1149. doi:10.1083/jcb.106.4.1141
- Aspden, T. J., Mason, J. D., Jones, N. S., Lowe, J., Skaugrud, O., and Illum, L. (1997). Chitosan as a Nasal Delivery System: The Effect of Chitosan Solutions on *In Vitro* and *In Vivo* Mucociliary Transport Rates in Human Turbinates and Volunteers. *J. Pharm. Sci.* 86 (4), 509–513. doi:10.1021/js960182o
- Aspden, T. J., Adler, J., Davis, S. S., Skaugrud, O., and Illum, L. (1995). Chitosan as a Nasal Delivery System: Evaluation of the Effect of Chitosan on Mucociliary Clearance Rate in the Frog Palate Model. *Int. J. Pharmaceutics* 122 (1–2), 69–78. doi:10.1016/0378-5173(95)00036-i
- Baldino, L., Cardea, S., and Reverchon, E. (2019a). Supercritical Assisted Electrospray: An Improved Micronization Process. *Polymers (Basel)* 11 (2). doi:10.3390/polym11020244
- Baldino, L., Cardea, S., and Reverchon, E. (2019b). A Supercritical CO₂ Assisted Electrohydrodynamic Process Used to Produce Microparticles and Microfibers of a Model Polymer. *J. CO₂ Utilization* 33, 532–540. doi:10.1016/j.jcou.2019.08.013
- Bourganis, V., Kammona, O., Alexopoulos, A., and Kiparissides, C. (2018). Recent Advances in Carrier Mediated Nose-To-Brain Delivery of Pharmaceuticals. *Eur. J. Pharm. Biopharm.* 128, 337–362. doi:10.1016/j.ejpb.2018.05.009
- Chang, S.-H., Lin, Y.-Y., Wu, G.-J., Huang, C.-H., and Tsai, G. J. (2019). Effect of Chitosan Molecular Weight on Anti-Inflammatory Activity in the RAW 264.7 Macrophage Model. *Internat. J. Biol. Macromol.* 131, 167–175. doi:10.1016/j.ijbiomac.2019.02.066
- Clayton, K. N., Salameh, J. W., Wereley, S. T., and Kinzer-Ursem, T. L. (2016). Physical Characterization of Nanoparticle Size and Surface Modification Using Particle Scattering Diffusometry. *Biomicrofluidics* 10 (5), 054107. doi:10.1063/1.4962992
- Danhier, F., Ansorena, E., Silva, J. M., Coco, R., Le Breton, A., and Préat, V. (2012). PLGA-based Nanoparticles: An Overview of Biomedical Applications. *J. Control. Release* 161 (2), 505–522. doi:10.1016/j.jconrel.2012.01.043
- Davis, S., Cirone, A. M., Menzie, J., Russell, F., Dorey, C. K., Shibata, Y., et al. (2018). Phagocytosis-mediated M1 Activation by Chitin but Not by Chitosan. *Am. J. Physiol. Cell Physiol.* 315 (1), C62–C72. doi:10.1152/ajpcell.00268.2017
- Dodane, V., Amin Khan, M. J. R., and Merwin, J. R. (1999). Effect of Chitosan on Epithelial Permeability and Structure. *Int. J. Pharm.* 182, 21–32. doi:10.1016/s0378-5173(99)00030-7
- Doty, R. L. (2015). *Handbook of Olfaction and Gustation*. New Jersey, United States: John Wiley & Sons.
- Eliezer, N., Sadé, J., Silberberg, A., and Nevo, A. C. (1970). The Role of Mucus in Transport by Cilia. *Am. Rev. Respir. Dis.* 102 (1), 48–52. doi:10.1164/arrd.1970.102.1.48
- England, R. J., Homer, J. J., Knight, L. C., and Ell, S. R. (1999). Nasal pH Measurement: a Reliable and Repeatable Parameter. *Clin. Otolaryngol. Allied Sci.* 24 (1), 67–68. doi:10.1046/j.1365-2273.1999.00223.x
- Fazil, M., Md, S., Haque, S., Kumar, M., Baboota, S., Sahni, J. K., et al. (2012). Development and Evaluation of Rivastigmine Loaded Chitosan Nanoparticles for Brain Targeting. *Eur. J. Pharm. Sci.* 47 (1), 6–15. doi:10.1016/j.ejps.2012.04.013
- Frolova, L., Drastich, P., Rossmann, P., Klimesova, K., and Tlaskalova-Hogenova, H. (2008). Expression of Toll-like Receptor 2 (TLR2), TLR4, and CD14 in Biopsy Samples of Patients with Inflammatory Bowel Diseases: Upregulated Expression of TLR2 in Terminal Ileum of Patients with Ulcerative Colitis. *J. Histochem. Cytochem.* 56 (3), 267–274. doi:10.1369/jhc.7A7303.2007
- Funda, D. P., Tucková, L., Farré, M. A., Iwase, T., Moro, I., and Tlaskalová-Hogenová, H. (2001). CD14 Is Expressed and Released as Soluble CD14 by Human Intestinal Epithelial Cells *In Vitro*: Lipopolysaccharide Activation of Epithelial Cells Revisited. *Infect. Immun.* 69 (6), 3772–3781. doi:10.1128/IAI.69.6.3772-3781.2001
- Gänger, S., and Schindowski, K. (2018). Tailoring Formulations for Intranasal Nose-To-Brain Delivery: A Review on Architecture, Physico-Chemical Characteristics and Mucociliary Clearance of the Nasal Olfactory Mucosa. *Pharmaceutics* 10 (3), 116. doi:10.3390/pharmaceutics10030116
- Garcia-Fuentes, M., and Alonso, M. J. (2012). Chitosan-based Drug Nanocarriers: where Do We Stand? *J. Control. Release* 161 (2), 496–504. doi:10.1016/j.jconrel.2012.03.017
- Getty, R. (1975). *Sisson and Grossman's: The Anatomy of the Domestic Animals*. Philadelphia: W. B. Saunders Company.
- He, P., Davis, S. S., and Illum, L. (1999). Chitosan Microspheres Prepared by spray Drying. *Int. J. Pharm.* 187, 53–65. doi:10.1016/s0378-5173(99)00125-8
- Henriksen, L., Green, K. L., Smart, J. D., Smista, G., and Karlsen, J. (1996). Bioadhesion of Hydrated Chitosans: an *In Vitro* and *In Vivo* Study. *Int. J. Pharmaceutics* 145, 231–240. doi:10.1016/s0378-5173(96)04776-x
- Howarth, A. G., Hughes, M. R., and Stevenson, B. R. (1992). Detection of the Tight junction-associated Protein ZO-1 in Astrocytes and Other Nonepithelial Cell Types. *Am. J. Physiol.* 262 (2), C461–C469. doi:10.1152/ajpcell.1992.262.2.C461
- Hughes, J. M., Budd, P. M., Tiede, K., and Lewis, J. (2015). Polymerized High Internal Phase Emulsion Monoliths for the Chromatographic Separation of Engineered Nanoparticles. *J. Appl. Polym. Sci.* 132 (1). doi:10.1002/app.41229
- Illum, L. (1998). Chitosan and its Use as a Pharmaceutical Excipient. *Pharm. Res.* 15, 1326–1331. doi:10.1023/a:1011929016601
- ISO (2017). *Particle Size Analysis — Dynamic Light Scattering (DLS)*. 22412. Geneva, Switzerland: International Standard, 44.
- Itoh, M., Yonemura, S., Nagafuchi, A., Tsukita, S., and Tsukita, S. (1991). A 220-kD Undercoat-Constitutive Protein: its Specific Localization at Cadherin-Based Cell-Cell Adhesion Sites. *J. Cell Biol.* 115 (5), 1449–1462. doi:10.1083/jcb.115.5.1449
- Jaworek, A., and Sobczyk, A. T. (2008). Electrospraying Route to Nanotechnology: An Overview. *J. Electrostatics* 66 (3–4), 197–219. doi:10.1016/j.elstat.2007.10.001
- Jeong, J. H., Joo, N. S., Hwang, P. H., and Wine, J. J. (2014). Mucociliary Clearance and Submucosal Gland Secretion in the *Ex Vivo* Ferret Trachea. *Am. J. Physiol. Lung Cell Mol. Physiol.* 307 (1), L83–L93. doi:10.1152/ajplung.00009.2014
- Kašpar, O., Tokárová, V., Nyanhongo, G. S., Gübitz, G., and Štěpánek, F. (2013). Effect of Cross-Linking Method on the Activity of spray-dried Chitosan Microparticles with Immobilized Laccase. *Food Bioprocesses* 91 (4), 525–533. doi:10.1016/s0960-3085(12)00110-1
- Keller, L. A., Merkel, O., and Popp, A. (2021). *Intranasal Drug Delivery: Opportunities and Toxicologic Challenges during Drug Development*. Cham, Switzerland: Springer Nature Switzerland AG.
- Ladel, S., Flamm, J., Zadeh, A. S., Filzwieser, D., Walter, J. C., Schlossbauer, P., et al. (2018). Allogenic Fc Domain-Facilitated Uptake of IgG in Nasal Lamina Propria: Friend or Foe for Intranasal CNS Delivery? *Pharmaceutics* 10 (3). doi:10.3390/pharmaceutics10030107
- Layden, J. E., Ghinai, I., Pray, I., Kimball, A., Layer, M., Tenforde, M. W., et al. (2020). Pulmonary Illness Related to E-Cigarette Use in Illinois and Wisconsin - Final Report. *N. Engl. J. Med.* 382 (10), 903–916. doi:10.1056/NEJMoa1911614
- Lee, G., Carpenter, J. F., and Manning, M. C. (2002). "Spray-drying of Proteins," in *Pharmaceutical Biotechnology* (Boston: Springer), 135–158. doi:10.1007/978-1-4615-0557-0_6
- Ménache, M. G., Hanna, L. M., Gross, E. A., Lou, S. R., Zinreich, S. J., Leopold, D. A., et al. (1997). Upper Respiratory Tract Surface Areas and Volumes of Laboratory Animals and Humans: Considerations for Dosimetry Models. *J. Toxicol. Environ. Health* 50 (5), 475–506. doi:10.1080/00984109708984003
- Mistry, A., Stolnik, S., and Illum, L. (2009). Nanoparticles for Direct Nose-To-Brain Delivery of Drugs. *Int. J. Pharm.* 379 (1), 146–157. doi:10.1016/j.ijpharm.2009.06.019
- Mistry, A. (2009). *The Development and Application of Biological Models for Evaluation of Direct Nose-To-Brain Drug Delivery Systems*. Nottingham, United Kingdom: Doctor of Philosophy, University of Nottingham.
- Morrison, E. E., and Costanzo, R. M. (1992). Morphology of Olfactory Epithelium in Humans and Other Vertebrates. *Microsc. Res. Tech.* 23 (23), 49–61. doi:10.1002/jemt.1070230105

- Morrison, E. E., and Costanzo, R. M. (1990). Morphology of the Human Olfactory Epithelium. *J. Comp. Neurol.* 297, 1–13. doi:10.1002/cne.902970102
- Muntimadugu, E., Dhommatti, R., Jain, A., Challa, V. G., Shaheen, M., and Khan, W. (2016). Intranasal Delivery of Nanoparticle Encapsulated Tarenflurbil: A Potential Brain Targeting Strategy for Alzheimer's Disease. *Eur. J. Pharm. Sci.* 92, 224–234. doi:10.1016/j.ejps.2016.05.012
- Musumeci, T., Serapide, M. F., Pellicteri, R., Dalpiaz, A., Ferraro, L., Dal Magro, R., et al. (2018). Oxcarbazepine Free or Loaded PLGA Nanoparticles as Effective Intranasal Approach to Control Epileptic Seizures in Rodents. *Eur. J. Pharm. Biopharm.* 133, 309–320. doi:10.1016/j.ejpb.2018.11.002
- Otterlei, M., Vårum, K. M., Ryan, L., and Espevik, T. (1994). Characterization of Binding and TNF-Alpha-Inducing Ability of Chitosans on Monocytes: the Involvement of CD14. *Vaccine* 12 (9), 825–832. doi:10.1016/0264-410x(94)90292-5
- Paudel, A., Worku, Z. A., Meeus, J., Guns, S., and Van den Mooter, G. (2013). Manufacturing of Solid Dispersions of Poorly Water Soluble Drugs by spray Drying: Formulation and Process Considerations. *Int. J. Pharm.* 453 (1), 253–284. doi:10.1016/j.ijpharm.2012.07.015
- Qiao, Y., Ruan, Y., Xiong, C., Xu, Q., Wei, P., Ma, P., et al. (2010). Chitosan Oligosaccharides Suppressant LPS Binding to TLR4/MD-2 Receptor Complex. *Carbohydr. Polym.* 82 (2), 405–411. doi:10.1016/j.carbpol.2010.04.079
- Raber, A. S., Mittal, A., Schäfer, J., Bakowsky, U., Reichrath, J., Vogt, T., et al. (2014). Quantification of Nanoparticle Uptake into Hair Follicles in Pig Ear and Human Forearm. *J. Control. Release* 179, 25–32. doi:10.1016/j.jconrel.2014.01.018
- Rabiee, N., Ahmadi, S., Afshari, R., Khalaji, S., Rabiee, M., Bagherzadeh, M., et al. (2020). Polymeric Nanoparticles for Nasal Drug Delivery to the Brain: Relevance to Alzheimer's Disease. *Adv. Ther.* 4 (3). doi:10.1002/adtp.202000076
- Rassu, G., Soddu, E., Cossu, M., Gavini, E., Giunchedi, P., and Dalpiaz, A. (2016). Particulate Formulations Based on Chitosan for Nose-To-Brain Delivery of Drugs. A Review. *J. Drug Deliv. Sci. Tech.* 32, 77–87. doi:10.1016/j.jddst.2015.05.002
- Ravi Kumar, M. N., Bakowsky, U., and Lehr, C. M. (2004). Preparation and Characterization of Cationic PLGA Nanospheres as DNA Carriers. *Biomaterials* 25 (10), 1771–1777. doi:10.1016/j.biomaterials.2003.08.069
- Sadeghi, A. M., Dorkosh, F. A., Avadi, M. R., Weinhold, M., Bayat, A., Delie, F., et al. (2008). Permeation Enhancer Effect of Chitosan and Chitosan Derivatives: Comparison of Formulations as Soluble Polymers and Nanoparticulate Systems on Insulin Absorption in Caco-2 Cells. *Eur. J. Pharm. Biopharm.* 70 (1), 270–278. doi:10.1016/j.ejpb.2008.03.004
- Sarmiento, B., and Neves, J. d. (2012). *Chitosan-based Systems for Biopharmaceuticals: Delivery, Targeting, and Biopolymer Therapeutics*. Chichester, United Kingdom: John Wiley & Sons.
- Seju, U., Kumar, A., and Sawant, K. K. (2011). Development and Evaluation of Olanzapine-Loaded PLGA Nanoparticles for Nose-To-Brain Delivery: *In Vitro* and *In Vivo* Studies. *Acta Biomater.* 7 (12), 4169–4176. doi:10.1016/j.actbio.2011.07.025
- Smith, J., Wood, E., and Dornish, M. (2004). Effect of Chitosan on Epithelial Cell Tight Junctions. *Pharm. Res.* 21, 43–49. doi:10.1023/b:pham.0000012150.60180.e3
- Sonaje, K., Chuang, E. Y., Lin, K. J., Yen, T. C., Su, F. Y., Tseng, M. T., et al. (2012). Opening of Epithelial Tight Junctions and Enhancement of Paracellular Permeation by Chitosan: Microscopic, Ultrastructural, and Computed-Tomographic Observations. *Mol. Pharm.* 9 (5), 1271–1279. doi:10.1021/mp200572t
- Stahl, P. H. (1980). *Feuchtigkeit und Trockenheit in der pharmazeutischen Technologie*. Heidelberg: Springer-Verlag.
- Steinke, A., Meier-Stiegen, S., Drenckhahn, D., and Asan, E. (2008). Molecular Composition of Tight and Adherens Junctions in the Rat Olfactory Epithelium and Fila. *Histochem. Cel Biol* 130 (2), 339–361. doi:10.1007/s00418-008-0441-8
- Stevenson, B. R., Siliciano, J. D., Mooseker, M. S., and Goodenough, D. A. (1986). Identification of ZO-1: a High Molecular Weight Polypeptide Associated with the Tight junction (Zonula Occludens) in a Variety of Epithelia. *J. Cel Biol* 103, 755–766. doi:10.1083/jcb.103.3.755
- Stützel, M., Flamm, J., Carle, S., and Schindowski, K. (2015). Nose-to-Brain Delivery of Insulin for Alzheimer's Disease. *Admet & Dmpk* 3 (3). doi:10.5599/admet.3.3.184
- Tokárová, V., Kašpar, O., Knejzlik, Z., Ulbrich, P., and Štěpánek, F. (2013). Development of spray-dried Chitosan Microcarriers for Nanoparticle Delivery. *Powder Tech.* 235, 797–805. doi:10.1016/j.powtec.2012.12.005
- Ugwoke, M. I., Agu, R. U., Verbeke, N., and Kinget, R. (2005). Nasal Mucoadhesive Drug Delivery: Background, Applications, Trends and Future Perspectives. *Adv. Drug Deliv. Rev.* 57 (11), 1640–1665. doi:10.1016/j.addr.2005.07.009
- Vila, A., Sánchez, A., Tobio, M., Calvo, P., and Alonso, M. J. (2002). Design of Biodegradable Particles for Protein Delivery. *J. Control. Release* 78 (15–24), 15–24. doi:10.1016/s0168-3659(01)00486-2
- Walz, M., Hirth, T., and Weber, A. (2018). Investigation of Chemically Modified Inulin as Encapsulation Material for Pharmaceutical Substances by spray-drying. *Colloids Surf. A: Physicochemical Eng. Aspects* 536, 47–52. doi:10.1016/j.colsurfa.2017.07.072
- Wenling, C., Duohui, J., Jiamou, L., Yandao, G., Nanming, Z., and Xiufang, Z. (2005). Effects of the Degree of Deacetylation on the Physicochemical Properties and Schwann Cell Affinity of Chitosan Films. *J. Biomater. Appl.* 20 (2), 157–177. doi:10.1177/0885328205049897
- WHO (2006). "Neurological Disorders: Public Health Challenges," in *WHO Library Cataloguing-In-Publication Data* (Geneva: World Health Organization).
- Win, K. Y., and Feng, S. S. (2005). Effects of Particle Size and Surface Coating on Cellular Uptake of Polymeric Nanoparticles for Oral Delivery of Anticancer Drugs. *Biomaterials* 26 (15), 2713–2722. doi:10.1016/j.biomaterials.2004.07.050
- Wolburg, H., Neuhaus, J., Kniesel, U., Krauss, B., Schmid, E. M., Öcalan, M., et al. (1994). Modulation of Tight junction Structure in Blood-Brain Barrier Endothelial Cells. Effects of Tissue Culture, Second Messengers and Cocultured Astrocytes. *J. Cel Sci* 107 (5), 1347–1357. doi:10.1242/jcs.107.5.1347
- Wolburg, H., Wolburg-Buchholz, K., Sam, H., Horvát, S., Deli, M. A., and Mack, A. F. (2008). Epithelial and Endothelial Barriers in the Olfactory Region of the Nasal Cavity of the Rat. *Histochem. Cel Biol* 130 (1), 127–140. doi:10.1007/s00418-008-0410-2
- Wright, S. D., Ramos, R. A., Tobias, P. S., Ulevitch, R. J., and Mathison, J. C. (1990). CD14, a Receptor for Complexes of Lipopolysaccharide (LPS) and LPS Binding Protein. *Science* 249 (4975), 1431–1433. doi:10.1126/science.1698311
- Yu, F., Yan, L., Wang, N., Yang, S., Wang, L., Tang, Y., et al. (2020). Quantitative Detection and Viral Load Analysis of SARS-CoV-2 in Infected Patients. *Clin. Infect. Dis.* 71 (15), 793–798. doi:10.1093/cid/ciaa345
- Yuan, Y., Chesnutt, B. M., Haggard, W. O., and Bumgardner, J. D. (2011). Deacetylation of Chitosan: Material Characterization and *In Vitro* Evaluation via Albumin Adsorption and Pre-osteoblastic Cell Cultures. *Materials (Basel)* 4 (8), 1399–1416. doi:10.3390/ma4081399
- Zarif, J. C., Hernandez, J. R., Verdone, J. E., Campbell, S. P., Drake, C. G., and Pienta, K. J. (2016). A Phased Strategy to Differentiate Human CD14+monocytes into Classically and Alternatively Activated Macrophages and Dendritic Cells. *Biotechniques* 61 (1), 33–41. doi:10.1214/000114435

Conflict of Interest: The authors CG, NG-T, and ET are employed by MyBiotech GmbH (66802 Überherrn, Germany).

The remaining authors declare that the research was conducted in the absence of any commercial or financial relationships that could be construed as a potential conflict of interest.

Publisher's Note: All claims expressed in this article are solely those of the authors and do not necessarily represent those of their affiliated organizations, or those of the publisher, the editors and the reviewers. Any product that may be evaluated in this article, or claim that may be made by its manufacturer, is not guaranteed or endorsed by the publisher.

Copyright © 2021 Spindler, Feuerhake, Ladel, Günday, Flamm, Günday-Türel, Türel, Tovar, Schindowski and Gruber-Traub. This is an open-access article distributed under the terms of the Creative Commons Attribution License (CC BY). The use, distribution or reproduction in other forums is permitted, provided the original author(s) and the copyright owner(s) are credited and that the original publication in this journal is cited, in accordance with accepted academic practice. No use, distribution or reproduction is permitted which does not comply with these terms.



Frank Maigler, **Simone Ladel**, Johannes Flamm, Stella Gänger, Barbara Kurpiers, Stefanie Kiderlen, Ronja Völk, Carmen Hamp, Sunniva Hartung, Sebastian Spiegel, Arghavan Soleimanizadeh, Katharina Eberle, Rebecca Hermann, Lukas Krainer, Claudia Pitzer, Katharina Schindowski. (2021). Selective CNS Targeting and Distribution with a Refined Region-Specific Intranasal Delivery Technique via the Olfactory Mucosa. *Pharmaceutics*, 13(11), 1904. <https://doi.org/10.3390/pharmaceutics13111904>

© 2021 by the authors. Licensee MDPI, Basel, Switzerland. This article is an open access article distributed under the terms and conditions of the Creative Commons Attribution 4.0 International (CC BY 4.0) license (<http://creativecommons.org/licenses/by/4.0/>).



Article

Selective CNS Targeting and Distribution with a Refined Region-Specific Intranasal Delivery Technique via the Olfactory Mucosa

Frank Maigler ^{1,2,†}, Simone Ladel ^{1,2,†}, Johannes Flamm ^{1,2,†}, Stella Gänger ^{1,3}, Barbara Kurpiers ⁴, Stefanie Kiderlen ⁵, Ronja Völk ¹, Carmen Hamp ¹, Sunniva Hartung ¹, Sebastian Spiegel ¹, Arghavan Soleimanizadeh ¹, Katharina Eberle ¹, Rebecca Hermann ¹, Lukas Krainer ⁵, Claudia Pitzer ⁴  and Katharina Schindowski ^{1,*} 

- ¹ Institute of Applied Biotechnology, University of Applied Science Biberach, Hubertus-Liebrecht Straße 35, 88400 Biberach, Germany; maigler@hochschule-bc.de (F.M.); ladel@hochschule-bc.de (S.L.); flamm@hochschule-bc.de (J.F.); gaenger@hochschule-bc.de (S.G.); voelk.ronja@web.de (R.V.); carmen.mirjam.hamp@t-online.de (C.H.); sunnivahartung@web.de (S.H.); spiegel@hochschule-bc.de (S.S.); soleimani@hochschule-bc.de (A.S.); kathy-eberle@web.de (K.E.); rebecca.hermann96@gmail.com (R.H.)
- ² Faculty of Natural Science, University of Ulm, Albert-Einstein-Allee 11, 89081 Ulm, Germany
- ³ Medical Faculty, University of Ulm, Albert-Einstein-Allee 11, 89081 Ulm, Germany
- ⁴ Interdisciplinary Neurobehavioral Core, Heidelberg University, Im Neuenheimer Feld 515, 69120 Heidelberg, Germany; barbara.kurpiers@pharma.uni-heidelberg.de (B.K.); claudia.pitzer@pharma.uni-heidelberg.de (C.P.)
- ⁵ Prospective Instruments LK OG, Stadtstraße 33, 6850 Dornbirn, Austria; sk@p-inst.com (S.K.); lk@p-inst.com (L.K.)

* Correspondence: schindowski@hochschule-bc.de

† These authors contributed equally to this work.



Citation: Maigler, F.; Ladel, S.; Flamm, J.; Gänger, S.; Kurpiers, B.; Kiderlen, S.; Völk, R.; Hamp, C.; Hartung, S.; Spiegel, S.; et al. Selective CNS Targeting and Distribution with a Refined Region-Specific Intranasal Delivery Technique via the Olfactory Mucosa. *Pharmaceutics* **2021**, *13*, 1904. <https://doi.org/10.3390/pharmaceutics13111904>

Academic Editors: Tomoyuki Furubayashi and Daisuke Inoue

Received: 1 October 2021

Accepted: 5 November 2021

Published: 10 November 2021

Publisher's Note: MDPI stays neutral with regard to jurisdictional claims in published maps and institutional affiliations.



Copyright: © 2021 by the authors. Licensee MDPI, Basel, Switzerland. This article is an open access article distributed under the terms and conditions of the Creative Commons Attribution (CC BY) license (<https://creativecommons.org/licenses/by/4.0/>).

Abstract: Intranasal drug delivery is a promising approach for the delivery of drugs to the CNS, but too heterogeneous, unprecise delivery methods without standardization decrease the quality of many studies in rodents. Thus, the lack of a precise and region-specific application technique for mice is a major drawback. In this study, a previously developed catheter-based refined technique was validated against the conventional pipette-based method and used to specifically reach the olfactory or the respiratory nasal regions. This study successfully demonstrated region-specific administration at the olfactory mucosa resulting in over 20% of the administered fluorescein dose in the olfactory bulbs, and no peripheral bioactivity of insulin detemir and Fc-dependent uptake of two murine IgG1 (11C7 and P3X) along the olfactory pathway to cortex and hippocampus. An scFv of 11C7 showed hardly any uptake to the CNS. Elimination was dependent on the presence of the IgG's antigen. In summary, it was successfully demonstrated that region-specific intranasal administration via the olfactory region resulted in improved brain targeting and reduced peripheral targeting in mice. The data are discussed with regard to their clinical potential.

Keywords: CNS drug delivery; nose to brain drug delivery; biopharmaceuticals; therapeutic antibodies; CNS targeting; refined drug delivery

1. Introduction

With growing numbers of patients suffering from neurological disorders, the need arises for treatment and administration approaches with the ability to deliver drug molecules in therapeutic quantities to the central nervous system (CNS). Yet, this need is nearly unmet [1]. Drug delivery technologies are of high relevance as they ensure that a pharmaceutical compound can reach its pharmacological target, and thereby safely achieve its desired therapeutic effect [2]. A highly critical point in drug delivery is the low availability of drugs in the CNS due to the blood brain barrier (BBB). The purpose of the BBB is to protect the brain by restricting the entry of neurotoxic substances. This is achieved by the

tightly composed endothelial barrier, a structure that represents a major hurdle for drug molecules to enter the CNS [3]. While for small molecule drugs, chemical modification may improve CNS delivery, nearly all macromolecules such as proteins and antibodies fail to cross the BBB in therapeutically relevant amounts [4,5]. Drugs with a low central bioavailability are currently delivered via intrathecal, intracerebroventricular or intraparenchymal injections. In this way, they are delivered directly to the cerebrospinal fluid (CSF) of the CNS. However, such invasive delivery systems are also accompanied with lower patient compliance and a documented risk of infections and side effects [6].

In recent past decades, the minimally-invasive approach of intranasal drug administration from the nose to the brain (N2B) has gained considerable attention as an alternative drug delivery route. The nasal cavity is highly suitable for minimally-invasive drug delivery, since the airway mucosa presents a good permeability and efficient absorption of both small molecule drugs and biopharmaceuticals [7]. Intranasal drug transport via neuronal connections such as the olfactory and trigeminal nerves appears to be the most relevant pathway to reach the CNS [8,9]. Moreover, the human nasal cavity has an impressively large mucosal surface area of about 160 cm². Further advantages include the rapid drug uptake after administration and avoidance of the hepatic first-pass elimination [10]. Challenges of intranasal N2B drug administration are mainly represented by the mucociliary clearance, limited administrable volume, enzymatic degradation and physico-chemical properties of the mucus layer, such as low pH [11,12].

In more detail, the nasal mucosa is not uniform and consists of different epithelia [6]. The two predominant epithelial types are described as respiratory and olfactory epithelium, and most likely constitute the main areas of substance absorption. Nasal respiratory epithelium is formed by ciliated cells, goblet cells, intermediate cells, and basal cells. Its further constituents are the various serous glands that produce the nasal mucus and nasal secretions that are propelled from the ciliated cells to the nasopharynx [13,14]. The respiratory mucosa covers up to 90% of the nasal cavity in humans and up to 50% in rodents [12] and is highly perfused, hence very suitable for the systemic absorption of drugs [15].

The human olfactory cleft extends from the roof of the nasal cavity down to the superior parts of the turbinates and is covered with olfactory mucosa [16]. The olfactory mucosa covers about 50% of the nasal cavity in rodents and less than 10% in humans [17]. It is formed by pseudo stratified columnar epithelial cells, olfactory sensory neurons (OSN), supporting cells, basal cells and Bowman's glands [15]. The unmyelinated axons of OSN spread through the basal lamina and form the *fila olfactoria* nerve bundles enclosed by olfactory ensheathing cells (OEC) and olfactory nerve fibroblasts. OECs are suggested to be a part of the innate immune system and their uptake of particles is well described [18,19]. The ensheathed nerve bundles travel through the cribriform plate of the ethmoid bone into the CNS where they terminate at the olfactory bulb. Hence, OSN are exceptional neurons that have their cell bodies located in a distal epithelium while their non-motile cilia processes extend into the mucus and allow them to be in direct contact with the environment. Interestingly, the olfactory nerve bundles appear to play a major role in N2B drug delivery. The intranasal delivery of drugs to the CNS has been pinpointed to the upper third of the nasal cavity, thus the olfactory region [4,6,12].

To reach the nerves, the drug must pass the epithelial tight junctions, which poses a hurdle that could limit the drug uptake [12]. However, the neuronal turnover within the olfactory epithelial layer is rather high, and dying cells may leave a gap that renders the epithelium sufficiently porous [20]. Although new OSN regrow in the gaps, the clefts may still allow an efficient drug uptake for larger particles. In addition, the formation of tight junctions lining the apical layer has been reported to be delayed [21]. Despite these observations, it should be noted that the passage through the *lamina propria* does not consequently imply that the total applied dose of the drug will arrive in the CNS. It may also be absorbed by blood vessels, enter glands, lymphatic/glymphatic vessels, the cranial nerves or interact with mucosal immune cells [6]. However, mathematical predictions

strongly suggest a transport along the olfactory and trigeminal neural pathways [22]. Taking the trigeminal or olfactory route, the drug can reach the subarachnoid space adjacent to the pons or the olfactory bulb. From here, the further distribution of a drug in the CNS appears to be mediated via bulk flow of the CSF [23].

Owing to the promising features of intranasally delivered CNS-active drugs, there has been a rise in publications on intranasal drug delivery experiments in rodents. However, a literature search on *in vivo* experiments that use intranasal drug delivery has revealed one concerning condition. Nearly every intranasal administration approach is performed by pouring a drop of drug solution onto, or into, the nostril of a mouse or rat. In this scenario, even the administration of volumes of 20 μ L, or less, lead to a flooding of the murine nostril, so that the total amount of deposited drug remains unknown. Furthermore, this approach is also accompanied with safety issues for the laboratory animals such as the swallowing or inhalation of administered drug solution. Further, the assessment of pharmacokinetic data and of quantitative readouts cannot be determined when using this conventional technique [24].

Recently, the authors of this study have suggested a region-specific administration approach utilizing a catheter to either target the respiratory or olfactory mucosa [25]. This approach was developed with the aid of a 3D cast of the murine nasal cavity. As the flow chart in Figure 1 summarizes, the conventional and refined region-specific intranasal administration were first compared to examine the novel administration approach in more detail and to verify its suitability and feasibility. Then, the potential uptake to the periphery after intranasal delivery was explored. Here, insulin was used as it is well described with the conventional intranasal method [26] and as it provides peripheral bioactivity. Finally, the time-dependent distribution of modern biopharmaceutics within the CNS was evaluated using the novel intranasal technique. In accordance with former investigations, different molecular sizes were compared [27]. In summary, the data indicated that this novel refined intranasal technique is highly suitable for further studies to understand the N2B transport mechanisms and to explore the pharmacokinetics of complex biopharmaceutics after region-specific intranasal delivery.

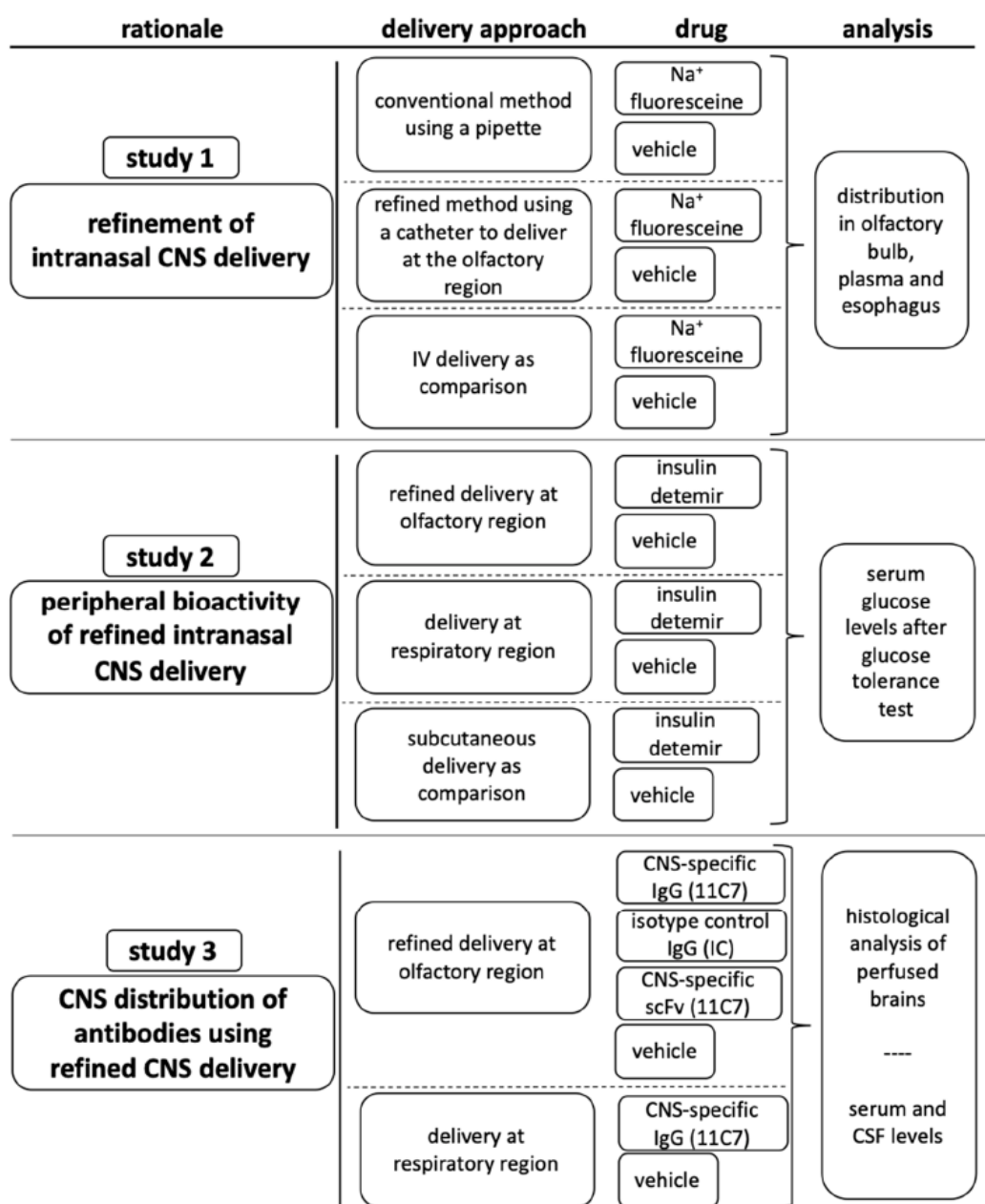


Figure 1. Study design of three studies with the aim of validating the previously refined intranasal region-specific administration technique [25] in vivo at the olfactory mucosa (study 1), determining the extent of molecules that are delivered to the periphery when administered at the olfactory mucosa (study 2) and analyzing the distribution of IgGs in the CNS after intranasal administration at the olfactory region (study 3).

2. Materials and Methods

Unless stated elsewhere, all chemicals were purchased from Sigma Aldrich, Taufkirchen, Germany.

2.1. Manufacturing of the Antibodies 11C7, P3X (Isotype Control) and 11C7 scFv

The hybridoma cell line 11C7 producing a murine IgG1 directed against Nogo-A was kindly provided by Prof. Dr. Martin Schwab/NovaGo Therapeutics AG (Schlieren,

Switzerland). Hybridoma cells were cultivated on an orbital shaker (Kuhner, Herzogenrath, Germany) at 140 rpm and 37 °C in a humidified atmosphere with 5% CO₂ within serum-free TurboDoma TP-6 medium (Cell Culture Technologies LLC, Gravesano, Switzerland) supplemented with 0.1% (*v/v*) Pluronic F-68 (Merck, Darmstadt, Germany) and 4 mM L-Glutamine (Lonza, Basel, Switzerland). Batch production processes were performed within 1000 mL disposable Erlenmeyer shake flasks with vented caps (Corning, New York City, NY, USA) and a working volume of 350 mL with an initial seeding density of 4×10^5 cells/mL. A murine IgG1 was used as non-binding isotype control and produced with the hybridoma cell line P3X63Ag8 (ATCC, Manassas, VA, USA). Cells were cultivated under static conditions at 37 °C in a humidified atmosphere with 5% CO₂ within T175 flasks with vented caps (Greiner Bio-one, Frickenhausen, Germany). Cultivation and production were performed in Dulbecco's modified Eagles's medium supplemented with 4 mM L-Glutamine and 10% (*v/v*) XerumFreeTM (Amsbio, Cambridge, MA, USA) with a working volume of 40 mL and an initial seeding density of 5×10^5 cells/mL. Cultivation parameters for both cell lines were assessed daily and the harvesting procedure was initiated prior to when the viability declined to ~70%.

Prior purification, cell culture broth was cleared by centrifugation at $3000 \times g$ for 15 min and subsequent microfiltration by using a Sartopore[®] 2 capsule (Sartorius, Göttingen, Germany) with a heterogeneous PES double layer. The purification was performed using a ProteinA MabSelect SuReTM resin (GE Healthcare, Solingen, Germany) packed into a XK 16/40 column (GE Healthcare, Solingen, Germany) and an ÄKTA Purifier system (GE Healthcare, Solingen, Germany). After finishing the clearing procedure, culture broth was loaded on the pre-equilibrated resin, which was performed with 10 mM phosphate buffer and 140 mM NaCl pH 7.0. To remove unbound material, the resin was washed with the equilibration buffer and finally antibody was eluted using 20 mM sodium acetate buffer with pH 3.0. Subsequently, elution fractions were pooled and introduced to diafiltration via tangential flow filtration using a Sartocon[®] slice 200 stainless steel holder (Sartorius, Göttingen, Germany), equipped with a 30 kDa molecular weight cut-off Hydrosart[®] ultrafiltration cassette (Sartorius, Göttingen, Germany). Diafiltration of both antibody solutions was performed against phosphate buffered saline (PBS) at pH 6.5 with concomitant concentration up to a final concentration of 10 mg/mL. Continuous determination of antibody concentrations was facilitated by using a NanoDropTM (Thermo Fisher Scientific, Dreieich, Germany) spectrophotometer at 280 nm and applying the mass extinction coefficient 13.7 L/(g·cm).

The recombinant His-tagged 11C7 scFv (approximately 31 kDa) was produced in a stable and monoclonal CHO-K1 cell line by batch cultivation in 1000 mL shake flasks (Omnilab, Munich, Germany) under orbital shaking conditions (50 mm orbit) at 140 rpm, 37 °C within a moist saturated atmosphere and 5% CO₂ saturation. With an initial seeding density of 4×10^5 cells/mL, 400 mL HyClone SFM4CHO (Cytiva, Freiburg, Germany) supplemented with 4 mM L-Glutamine and 500 µg/mL G418 were inoculated and cultivated until the viability declined to ~70%. Cell culture broth was cleared by centrifugation at $3000 \times g$ for 15 min and subsequent microfiltration by using a Sartopore[®] 2 capsule (Sartorius, Göttingen, Germany) with a heterogeneous PES double layer. The purification was performed using a HisTrapTM FF 5 mL prepacked column (GE Healthcare, Solingen, Germany) and an ÄKTA Purifier system (GE Healthcare, Solingen, Germany). The cleared culture broth was loaded onto preequilibrated resin (equilibration buffer: 20 mM tris (hydroxymethyl) aminomethane, 300 mM NaCl, 10 mM imidazole, pH 8.0). To remove unbound material, a washing step with equilibration buffer and a total of 20 mM imidazole was performed. Elution of bound 11C7 scFv was initiated by gradually increasing imidazole concentration to 500 mM. Subsequently, elution fractions were pooled and introduced to diafiltration via tangential flow filtration using a Sartocon[®] slice 200 stainless steel holder (Sartorius, Göttingen, Germany), equipped with a 10 kDa molecular weight cut-off Hydrosart[®] ultrafiltration cassette (Sartorius, Göttingen, Germany). Diafiltration of 11C7 scFv was performed against phosphate buffered saline (PBS) at pH 6.5 with concomitant concentration up to a final

concentration of 2.4 mg/mL. Continuous determination of antibody fragment concentration was facilitated by using a NanoDrop™ (Thermo Fisher Scientific, Dreieich, Germany) spectrophotometer at 280 nm and applying the mass extinction coefficient 3.4 L/(g·cm).

2.2. Animal Housing and Ethics

Breeding pairs from male and female C57BL/6N mice were purchased from Charles River Laboratories (Sulzfeld, Germany) at the age of 8 weeks. Mice were expanded for one generation at the Interdisciplinary Neurobehavioral Core (INBC), University of Heidelberg. Male mice at the age of 11 weeks were used for the study. Mice were housed in groups of four per cage, with food and water ad libitum under a standard 12 h light/dark cycle (7:00 p.m.–7:00 a.m.) with a regulated ambient temperature of 22 °C and at a relative humidity of 40–50%. All procedures were conducted in strict compliance with national and international guidelines for the Care and Use of Laboratory Animals. Animal experiments were approved by the local governing body (Regierungspräsidium, Karlsruhe, Germany, under the ethical approval number G-92/19) and were carried out in compliance with the ARRIVE guidelines.

2.3. Study 1: Refined Region-Specific Catheter-Based Intranasal Administration of Sodium Fluorescein

A total number of 24 C57BL/6 mice were randomized to receive vehicle (PBS) or sodium fluorescein (10 mg/mL in PBS; Sigma Aldrich, Taufkirchen, Germany) solution administered either via the conventional or refined intranasal application or via intravenous (IV) injections. For the conventional application, animals were anesthetized with Isoflurane and placed in a supine position, with the head supported at a 45 degree angle to the body. Volumes of 2 µL of either vehicle or sodium fluorescein were applied to the nostril and repeated with the other nostril. The refined region-specific administration was established with 3D cast reproduced from a CT scan of murine skull [25]. Animals were anesthetized with Isoflurane and placed in a supine position, with the head supported at a 45 degree angle to the body. Volumes of 2 µL were applied to one ethmoid turbinate through the nostrils using a neonatal catheter (Nutraline, Vygon GmbH und Co KG, Aachen, Germany) with a Hamilton 10 µL-syringe (VWR International GmbH, Darmstadt, Germany). For an irritation-free application, a nasal balm (Bepanthen Augen- und Nasensalbe, Bayer Vital GmbH, Leverkusen, Germany) was applied at the sides of the catheter. The catheter was inserted 8 mm ± 0.1 mm from the nostril and with an insertion angle of 60 degrees. Fifteen seconds after application, the catheter was slowly removed and the procedure was repeated with the other nostril. For IV application the dose was administered via the tail vein according to standard procedures for mice. Samples (blood) and organs (brain, olfactory bulbs, esophagus, stomach) were collected at 10 and 30 min after administration. Organs were minced with chilled PBS (pH 7.4) in a Potter–Elvehjem homogenizer and centrifuged. The supernatant was transferred to a 96 well plate (Greiner Bio-One Fluotrac) and analyzed in a fluorescence plate reader with λ_{ex} 460 nm and λ_{em} 515 nm (SpectraMax M Series Multi-Mode Microplate Reader, Molecular Devices, San Jose, CA, USA). Quantification was performed with serial dilution of sodium fluorescein in the respective organ matrix. Blood samples were collected in tubes, (S-Monovette Sarstedt, Nümbrecht, Germany), centrifuged, and the plasma samples were analyzed as described above.

2.4. Study 2: Region-Specific Administration of Insulin Detemir (Levemir®)

Animals were randomized in groups to receive either saline (0.9% NaCl saline, Miniplasco connect, B.Braun AG, Melsungen, Germany) or insulin detemir (Levemir®, NovoNordisk, Denmark) with the refined technique at the respiratory or olfactory region. Blood samples were collected from the saphenous vein 5 min prior to dosing and baseline blood glucose levels were determined with Contour® blood glucose test strips (Ascensia Diabetes Care, Parsippany, NJ, USA). Region-specific administration at the olfactory area was performed as stated above (study 1) by introducing the catheter 8 mm into the nostril and

applying 2.5 μ L per nostril. To target the respiratory region, the catheter was introduced only 2 mm. Blood glucose levels were determined 10 min after the intranasal delivery. Animals were challenged with a glucose tolerance test by intraperitoneal administration of 3 g/kg glucose 15 min after intranasal delivery and blood glucose levels were determined 30 and 75 min after intranasal dosing.

2.5. Study 3: CNS Distribution of Monoclonal Antibodies and a scFv after Region-Specific Administration

Application procedures at the olfactory and respiratory region were performed with 3 μ L per nostril as described above. Amounts of 11C7 and P3X as isotype control were formulated in PBS pH 6.5 at 10 mg/mL and 11C7 scFv at 2.4 mg/mL to provide equimolar doses. Animals were anesthetized, CSF was collected from the cisterna magna and finally mice were transcardially perfused with saline. CSF samples were stored at -20°C until analysis. The skin of the mouse heads was removed and the heads stored in 4% paraformaldehyde until further processing. Mice heads were dehydrated with sucrose and 14 μ m sagittal cryosections were cut at -25°C from the nostril through the cerebellum (cryostat HM525 NX Thermo Fisher Scientific, Dreieich, Germany) and dried at 60°C (UFB400, Memmert GmbH & Co KG, Schwabach, Germany).

2.6. Staining Procedures and Microscopy

Thawed sections were washed three times with PBS (5 min, 10 min and 15 min) and blocked with blocking buffer (PBS, 4% fetal bovine serum, 0.5% Triton X-100 and 5% normal goat serum) for 3 h. For the detection of 11C7 full IgG and P3X, AF647 alpaca anti-mouse (#615-605-214, Jackson Immuno Research, Cambridgeshire, UK) was diluted 1:500 in PBS and incubated for 2.5 h at room temperature. Following three washing steps, sections were counterstained with 20 μ g/mL DAPI (4',6-diamidin-2-phenylindol; Sigma Aldrich, Taufkirchen, Germany) in PBS for 10 min. Slides were washed with PBS for 10 min, followed by washing with water for 1 min and mounted in Fluoromount G (Thermo Fisher Scientific, Dreieich, Germany). The images were captured with a confocal laser microscope (LSM 710, Zeiss, Jena, Germany) at the Core Facility Confocal and Multiphoton Microscopy at Ulm University, Germany, and with the MPX-1040 multi-modal microscope (Prospective Instruments, Dornbirn, Austria) for whole slide images. Whole slide images were acquired using a $4\times$ (Thorlabs, Super Apochromatic, Air, NA 0.2) and a $16\times$ (Nikon LWD Plan Fluorite, Water, NA 0.8) objective at three excitation channels: blue ($\lambda_{\text{ex/em}}$ 395/432 nm), green ($\lambda_{\text{ex/em}}$ 475/515 nm) and red ($\lambda_{\text{ex/em}}$ 637/681 nm). Whole slide images were scanned using an xyz-stage and an in-house developed software routine (Prospective Instruments, Dornbirn, Austria). All images were saved as TIF-files and postprocessed using ImageJ (v1.53c) as previously described [28].

2.7. Statistics

Data were assessed for statistical significance using Prism Version 8.3.0 (GraphPad, San Diego, CA, USA). All data are presented as mean \pm SEM. Statistical significance was calculated with ANOVA or Student's *t*-test as indicated.

3. Results

3.1. Refinement of Intranasal Delivery and Establishing a Region-Specific Administration at the Olfactory Region (Study 1)

The nasal cavity is covered by different epithelia and different nerve endings such as the olfactory and the trigeminal nerve, which are embedded in the mucosa at different anatomical regions (Figure 2A). In order to gain a profound understanding of the fate and pathways of intranasally administered molecules, a region-specific administration technique enabling the discrimination between different nasal epithelia is of high importance. The conventional technique to deliver drugs intranasally is to administer drops to the nostrils with the aid of a pipette (Figure 2B). Despite the fact that in most published studies the administered volumes exceed the volume of a murine nasal cavity, this method is not

suitable to target only one region covered predominantly with a specific epithelium such as olfactory or respiratory mucosa (Figure 2A). Lochhead and Thorne suggested a potential pathway for drug delivery into the CNS via the olfactory mucosa [12]. Therefore, the authors of this study recently developed a novel catheter-based technique in vitro to target the olfactory or respiratory region only, with a smaller volume and with high specificity and reproducibility (Figure 2C) [25].

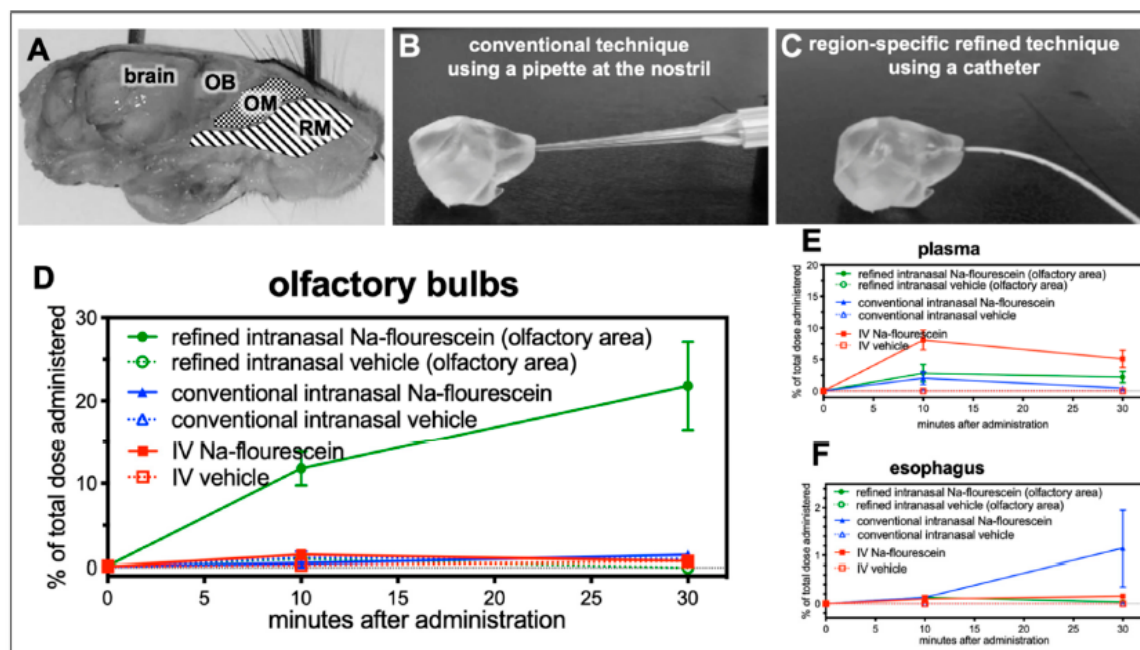


Figure 2. The refined technique results in up to 21% of the dose in the olfactory bulbs, when administered at the olfactory region (study 1). (A) Sagittal view on a murine head with highlighted areas for catheter-based administration at either respiratory mucosa (RM) or olfactory mucosa (OM) with adjacent olfactory bulb (OB) as part of the brain. As previously described, a region-specific technique was developed with the aid of 3D-printed models of the murine nasal cavity reconstructed from CT scans of a mouse head [25]. (B) demonstrates the conventional technique using a pipette with usually a rather high volume, from 20 to 30 μ L. With this method, no selective delivery to the respiratory or olfactory mucosa is possible. Therefore, the intranasal delivery (C) has been refined by using a catheter with an adjusted smaller administered volume, which can deliver the drug region-specific either at the olfactory or respiratory area. The aim of study 1 was to validate the region-specificity of the refined catheter-based technique with fluorescein in vivo. (D) 10 min after administration, the levels reached with the refined technique were significantly higher than achieved with the conventional method or IV delivery (* $p < 0.04$, Student's t -test). At 30 min after administration at the olfactory region, 21.8 \pm 5.34% of the dose was recovered at the olfactory bulbs while administration with a pipette at the nostrils resulted in only 1.5 \pm 0.05% ($n = 2$; $p = 0.0626$) and intravenous (IV) delivery resulted in 0.7 \pm 0.07% ($n = 2$; $p = 0.0587$). (E) Elevated levels of fluorescein were detected in serum after IV administration and after intranasal delivery with the conventional pipette-based method. (F) Interestingly, higher levels of traces of the intranasally administered doses were swallowed and ingested with the conventional method than with the refined method (conventional: 1.15 \pm 0.804% vs. refined: 0.03 \pm 0.078% vs. IV: 0.078 \pm 0.078%). Due to the limited number of animals per group this study shows tendencies, but fails to demonstrate statistical significance (mean \pm SEM; $n = 2$). (A–C) are adapted with permission from ref. [25]. 2021, Nicole Lange et al.

Here, this refined technique was evaluated for the first time in vivo in a small pilot study (study 1; Figure 1). A solution containing 20 μ g of sodium fluorescein or vehicle (PBS) was administered either to the nostril (conventional technique) or via a catheter to the olfactory area (refined technique). Although, volumes of 20 to 40 μ L per nostril had been reported for the conventional technique, here the same volume as for the refined technique was used to enable a direct comparison. Finally, a group of animals received

fluorescein or vehicle intravenously (IV) into the tail vein. Due to the rather fast elimination of fluorescein, animals were sacrificed 10 and 30 min after application and the fluorescence was determined in olfactory bulbs, whole brains (without olfactory bulbs), serum and esophagus. No relevant increase in fluorescence levels was found in any sample from animals which have received vehicle (data not shown). As demonstrated in Figure 2D significant levels of sodium fluorescein were detected with the refined technique in olfactory bulbs ($11.76 \pm 2.05\%$ of the total administered dose after 10 min, and $21.81 \pm 5.34\%$ after 30 min) while the conventional method ($0.50 \pm 0.50\%$ after 10 min, and $1.48 \pm 0.05\%$ after 30 min) and IV administration ($1.49 \pm 0.12\%$ of the total administered dose after 10 min, and $0.74 \pm 0.07\%$ after 30 min) revealed only slightly elevated levels compared with vehicle.

Levels in whole brains were marginally elevated up to 3.6% in the refined and IV groups after 10 min and in all three after 30 min (data not shown). As seen for olfactory bulbs, the levels in the IV group declined with time, apparently due to the short half-life of fluorescein. The similarly low levels of both intranasal groups may represent transport via the trigeminal nerve that has terminal endings in the respiratory and the olfactory region. In addition, the amount of fluorescein that could be detected in serum after both delivery techniques was determined. While $8.1 \pm 1.57\%$ were found in the serum 10 min after IV delivery, only $2.84 \pm 1.38\%$ (refined) and $2.04 \pm 1.02\%$ (conventional) could be detected. These values decreased after 30 min for the conventional technique and IV administration and remained rather stable with the refined technique (Figure 2E).

A high risk of the conventional technique is that a significant amount of the delivered dose is swallowed and ingested or even inhaled and thereby life-threatening for the animals [25]. Therefore, esophagus and stomach were analyzed for potential ingested traces of fluorescein. Samples from the stomach could not be used since the animals had not been fasted for a sufficient time, but increased levels up to $1.15 \pm 0.80\%$ were found in animals treated with the conventional technique compared with refined (0.13%) and IV (0.16%; Figure 2F) delivery. It should be noted that only a small volume was used for the conventional technique, while in published studies 10 to 20 times higher volumes are used. Therefore, the percentage of swallowed and ingested drug solution can be estimated to be rather high. In summary, the present data demonstrate that the refined technique is a suitable method to investigate drug delivery via the olfactory region.

3.2. Peripheral Bioactivity after Region-Specific Intranasal Administration of Insulin Detemir (Study 2)

In general, mucosal tissues are well perfused and harbor several capillaries and blood vessels in their *lamina propria*. However, it is known that respiratory mucosa at the lower parts of the nasal cavity contains more and larger glands and more cavernous bodies than the olfactory mucosa [15]. Therefore, the aim of study 2 was to determine the peripheral bioactivity of a drug, which was administered at the olfactory or respiratory regions of the nasal cavity. Insulin was chosen as the drug since its peripheral bioactivity (lowering blood glucose levels) can be sensitively and easily assessed. Since the half-life of insulin is rather short, insulin detemir with a prolonged half-life was used [29]. Hence, mice were challenged with a high dose of glucose to uncover the amounts of insulin that was distributed to the periphery. As positive control, insulin detemir was administered subcutaneously (SC). As demonstrated previously, by introducing the catheter with the refined technique either 2 or 8 mm from the nostrils, different regions of the nasal cavity were targeted (Figure 3A) [25].

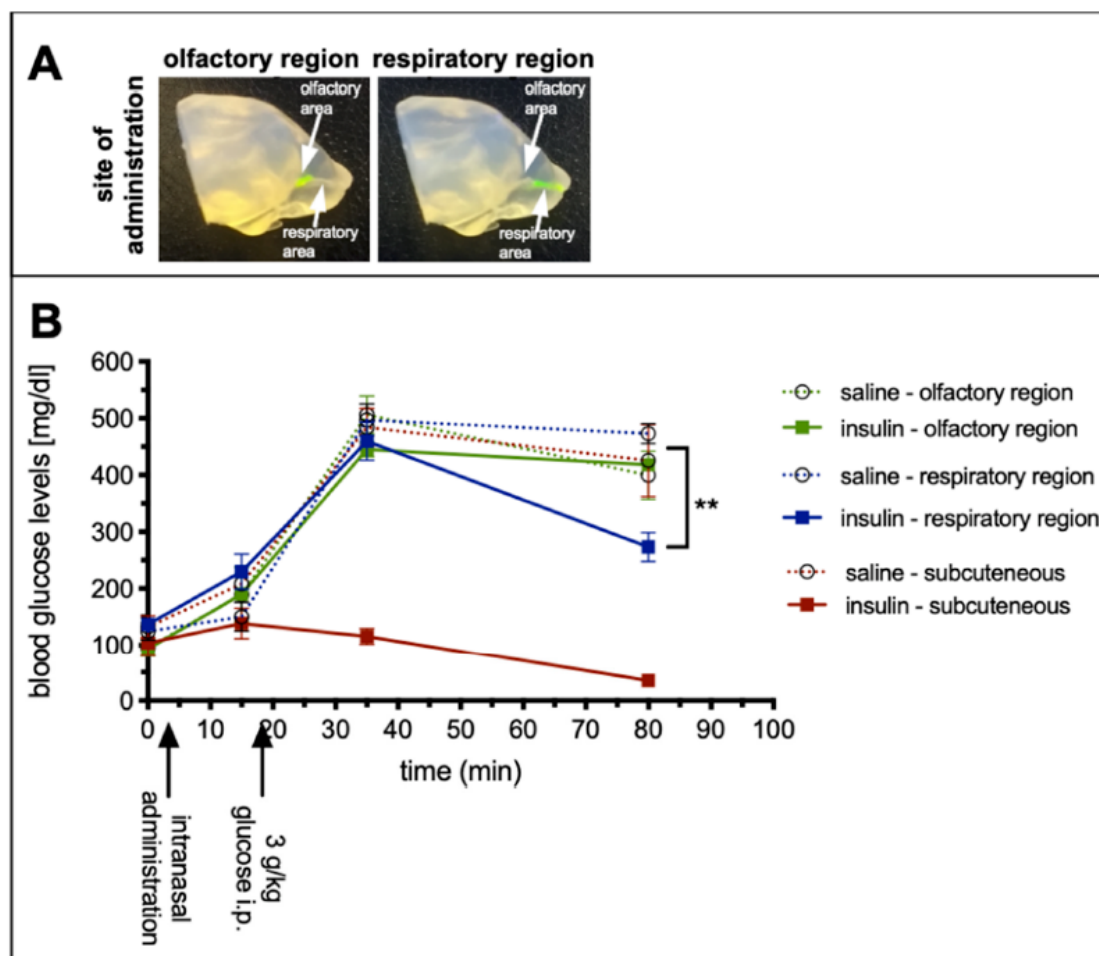


Figure 3. No peripheral bioactivity after region-specific delivery of insulin detemir to the olfactory region (study 2). Silicone based 3D-model made by vacuum cast method (A), for the visualization of the targeted regions [25]. Adapted with permission from ref. [25]. 2021, Nicole Lange et al. Glucose tolerance test to examine the peripheral effects after region-specific administration of insulin detemir versus vehicle (B), monitored via blood glucose levels. Black arrows highlight catheter-based refined administration to the respiratory or olfactory nasal regions or subcutaneous injections of insulin detemir or vehicle. Mice were challenged with a high dose of intraperitoneal glucose to determine the peripheral activity of insulin detemir. As expected, subcutaneously delivered insulin demonstrated a high peripheral bioactivity by lowering the blood glucose levels. Interestingly, insulin delivered via the respiratory regions covered predominantly with respiratory mucosa was also distributed from the nose to the periphery and displayed 40.2% of the subcutaneously delivered activity. Insulin targeted to the olfactory regions did not show any statistically significant bioactivity in the periphery. Error bars represent mean \pm SEM, $n = 3$. Data were analyzed with two-way ANOVA with multiple comparisons. ** $p < 0.009$. A is reproduced from [25] with kind permission from the rights owner.

Blood samples were taken from the saphenous vein prior to catheter-based intranasal delivery to the respiratory or the olfactory region via both nostrils or SC delivery with a total dose of 0.5 IU = 71 μ g insulin detemir). Saline was used as vehicle control. The basal blood glucose levels of all groups were comparable (Figure 3B) and also 10 min after intranasal or SC delivery no statistically significant changes were observed. Fifteen min after drug delivery all animals were challenged with 3 g/kg glucose injected intraperitoneally (IP) and subsequently bled after 30 and 75 min. While the glucose levels of the SC insulin detemir group remained stable, all other groups, regardless of whether vehicle or drug, displayed a strong and significant increase in blood glucose. However, 75 min after drug delivery, the blood glucose concentration of the animals, which received the insulin via

the respiratory area displayed significantly lower levels compared with vehicle control (273 ± 25 mg/dL vs. 433 ± 25 mg/dL; $** p < 0.009$), while the levels from the olfactory targeted group were unaffected with 418 ± 10 mg/dL ($p = 0.86$; Figure 3B). The lowered glucose level of the respiratory targeted groups corresponded to 40.2% of the peripheral bioactivity of the 0.5 IU insulin detemir administered SC (3.8% for olfactory targeting). All vehicle groups displayed similar values that did not differ significantly from each other. Therefore, all vehicle groups were pooled for statistical analysis.

These results imply that insulin detemir was absorbed from the respiratory nasal mucosa and distributed to the periphery to a significantly higher extent than when administered to the olfactory mucosa. In combination with the result from study 1 showing a specific targeting of the olfactory bulbs as parts of the CNS, the catheter-based refined method was highly specific for intranasal CNS targeting with low peripheral effects.

3.3. Antibody CNS Distribution after Region-Specific Intranasal Administration (Study 3)

Modern biopharmaceutics such as antibodies and antibody-derived formats such as single chain variable fragments (scFv) have a very low bioavailability in the CNS when delivered intravenously [30]. Therefore, intranasal delivery to the CNS could be an attractive minimally invasive option. To explore the transport path from the olfactory region to the brain and to study kinetics of distribution and elimination, study 3 was designed with two different murine IgG antibodies and a scFv. The IgG1 antibody 11C7 binds to Nogo-A, which is predominantly expressed within the CNS but some reports have detected it in OSN [31,32]. The 11C7 was used as it is a promising antibody for multiple sclerosis or similar neurodegenerative diseases as it was shown that 11C7 therapy induces neuronal outgrowth in studies performed by Schwab and coworkers [33–37]. In general, the Fc part of IgGs is mentioned by other studies to be possibly involved in IgG uptake and transport either intra- or paracellularly [38–40]. However, there are conflicting data showing that the Fc binding neonatal Fc receptor (FcRn), which is the most prominent IgG transporter in mammals, functions mainly as an efflux transporter [40–42]. To investigate not only the impact of molecular size but also the presence of an Fc domain on molecular transport from the nose to the brain, the 11C7 N2B uptake was compared with an scFv from the same IgG. Furthermore, to exclude bias due to 11C7 binding potentially to Nogo-A on OSN, an isotype control antibody was used that does not bind to murine tissue. Therefore, the IgG1 antibody P3X was defined as the isotype control, since the absence of binding to murine brain, nasal mucosa or other investigated murine tissues in a dot blot (data not shown) could be confirmed. Both IgG antibodies were used at 10 mg/mL and the mice received 3 μ L per nostril at the olfactory region using the catheter-based refined technique (total dose of 60 μ g). The 11C7 scFv was delivered at equimolar concentrations with 2.4 mg/mL. PBS was delivered as vehicle control and one cohort received 11C7 at the respiratory region for comparison. Although 11C7 and P3X were biotinylated at the hinge region, detection was performed with polyclonal antibodies against murine IgG heavy and light chains since detection with streptavidin produced a rather high background. Mice were transcardially perfused in deep anesthesia, however, traces of endogenous murine IgGs could be found in particular in the nasal mucus and the choroid plexus (Figure 4A,F). Therefore, vehicle control showed baseline levels even if traces of endogenous IgGs were present.

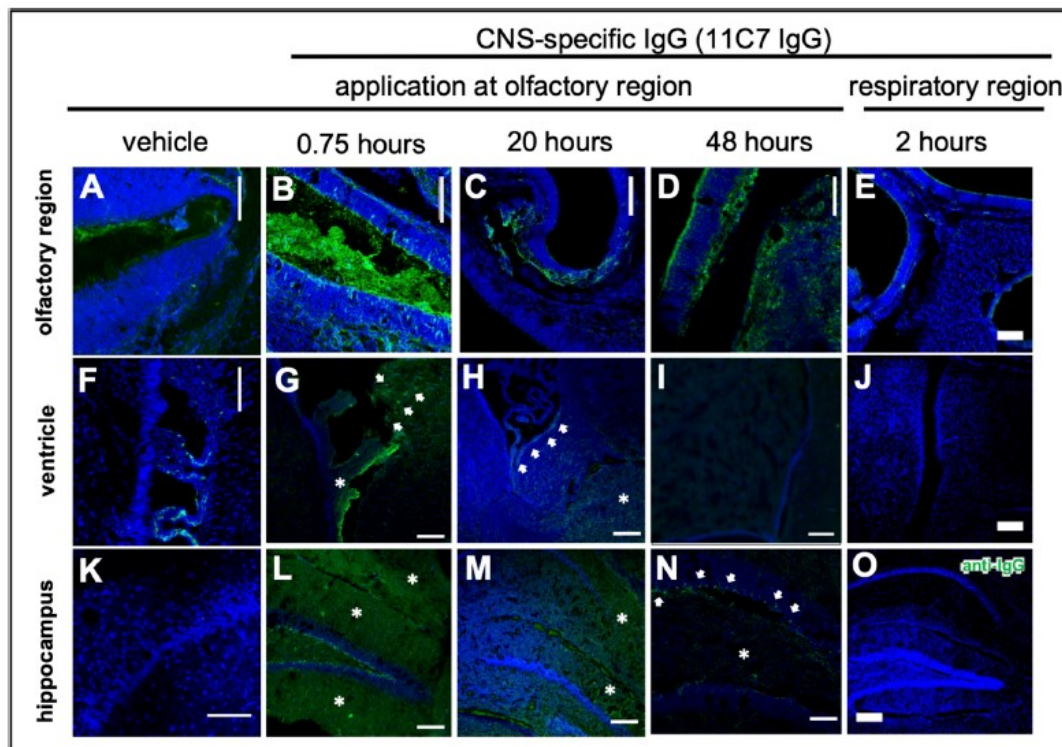


Figure 4. Distribution of the CNS-specific IgG1 antibody 11C7 in the nasal mucosa after region-specific intranasal delivery (study 3). A total dose of 60 μ g 11C7 per mouse was administered at the olfactory (B–D,G–I,L–N) and respiratory (E,J,O) regions. The vehicle control was administered at the olfactory region and displays background staining from endogenous murine IgGs in the nasal mucus (A), and the choroid plexus (F), which was not removed after transcardial perfusion. The region-specificity became obvious in an investigation of the upper nasal cavity with its ethmoid turbinates: while after administration at the olfactory region the antibody was detectable at the olfactory mucosa (B), and showed a time-dependent clearance (C,D), no elevated levels of IgG were observed at the ethmoid turbinates after administration at the respiratory region. Further, none of the animals from the respiratory delivery group displayed any signs of a CNS delivery of 11C7 (J,O). A rapid distribution to the subventricular zones (see arrowheads) of the ventricles was found (G), that lasted up to 20 h (H), but was undetectable after 48 h (I). In addition, 11C7 was observed diffusely (see asterisks) in the hippocampus shortly after administration (L). The diffuse pattern disappeared within 20 h (M) and after 48 h distinct cells (see arrowheads) and neuronal projections were observed (N), highly similar to what was reported from Nogo-A expression studies [43]. Scale bar, 100 μ m.

The distribution in the nasal mucosa and to the CNS is shown in Figure 4 taken by confocal microscopy. In summary, the region-specificity was well demonstrated since no traces of 11C7 were found after administration at the respiratory region (Figure 4E) nor any distribution to the brain (Figure 4J,O). Compared with vehicle control levels, a rather rapid distribution to the subventricular zones and the hippocampus was observed. While in the beginning the staining pattern was rather diffuse (Figure 4G,L,M), within 48 h no 11C7 was detectable at the subventricular zones (Figure 4I) and a highly specific pattern remained in the hippocampus (Figure 4N) and cortex, similar to what was previously reported for Nogo-A expression, the antigen of 11C7 [43]. In addition, a similar rapid distribution to the olfactory bulb and midbrain followed by a fast elimination was recently observed with radiolabeled IgGs [44].

3.4. Fc-Dependent Uptake into Olfactory Mucosa and Transport along Neuronal Bundles to the CNS

Recently, the transport of exogenously administered IgGs along neuronal bundles projecting from olfactory sensory neurons of the olfactory mucosa to the olfactory bulb in an ex vivo model of porcine olfactory mucosa [38] has been described. Excitingly, the Fc domain of IgGs appeared to play a major role in the transmucosal transport. Therefore, in study 3 the focus was also on the in vivo transport mechanisms from the olfactory region to the CNS (Figure 5) and the difference of full IgGs and a scFv devoid of Fc. After a single dose with 60 µg, a rapid uptake of both IgGs via intracellular pathways to the *lamina propria* (Figure 5A–D) and then along neuronal bundles to the brain, was observed (Figure 5G). As expected, the immunoreactivity of the IgGs along the neuronal projections decreased time dependently (Figure 5H–K). The 11C7 scFv with only 31 kDa and devoid of an Fc domain showed a distinct uptake pattern with evidence for an extracellular pathway and a decreased uptake (Figure 5E,F). Nevertheless, it should be noted that IgGs and scFv were detected with anti-IgG and anti-His-Tag antibodies, respectively. Therefore, no direct comparison of the staining intensity could be performed.

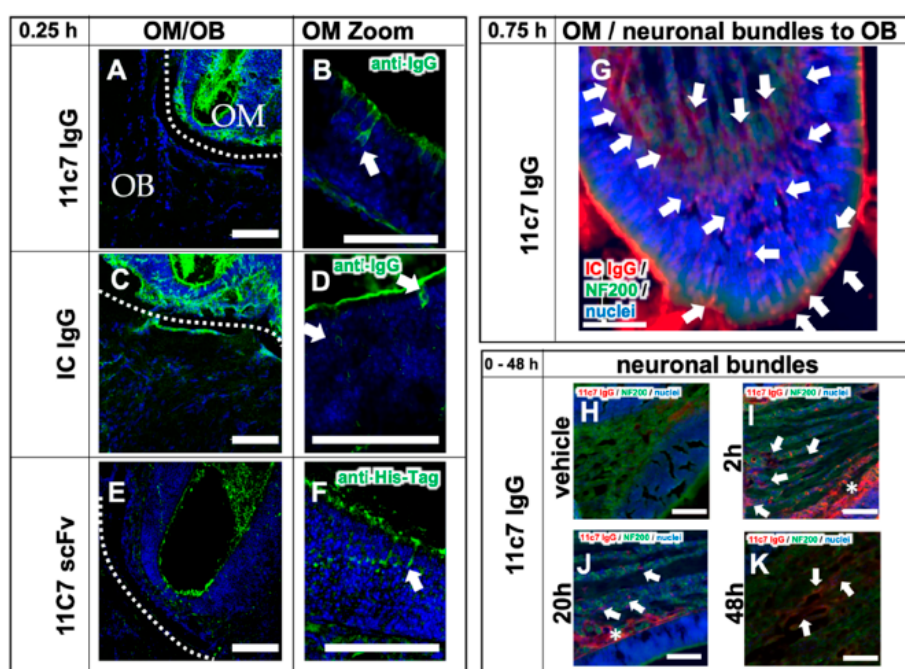


Figure 5. Transport mechanisms of both the full IgGs 11C7 and the isotype (IC) control, and the 11C7 scFv (study 3). Images from confocal microscopy show the rapid uptake of 11C7 and IC into the olfactory mucosa (OM) and also traces in the olfactory bulb (OB) after only 15 min (A,C). Higher magnification shows evidence for a predominantly intracellular pathway as previously reported from ex vivo olfactory mucosa (see arrowheads) (B,D) [38,39]. In contrast, the 11C7 scFv devoid of an Fc domain appears to be taken up to a lower extent (E) and displays more evidence for a transcellular transport (F). However, it should be noted that IgGs and scFv were visualized with different detection systems (anti-IgG vs. anti-His-Tag) and, hence, the fluorescence intensity should be evaluated with caution. Epifluorescence microscopy demonstrates, 45 min after administration, the full transport scheme with intracellular uptake at the apical mucosa, distribution to the *lamina propria* and transport along neuronal bundles from the *lamina propria* to the olfactory bulb (G). For a better visualization, anti-IgG immunoreactivity is displayed here in red, and neurofilament (NF200)-immunoreactivity in green. Transport kinetics along neuronal bundles after a single dose (H–K): while only background is observed in the vehicle control animals (H), decreasing levels of 11C7 are observed within 48 h (I–K). Arrowheads point to distinct stained structures while asterisk show diffuse staining pattern. Scale bar, 100 µm.

3.5. Reduced Elimination from CNS of Nogo-A-Binding IgG

To investigate the CNS distribution after region-specific catheter-based administration at the olfactory mucosa, sagittal sections through a whole mouse head from the nostrils to the cerebellum were performed, and whole section images were captured with a multi-modal microscope (Figure 6). The vehicle control demonstrated the background immunoreactivity against murine IgGs (Figure 6A): No specific staining was observed within the CNS, but endogenous IgGs could be detected in the nasal mucus, in particular at the respiratory mucosa (RM). A rather high staining was observed in muscle tissue of the neck, jaw and cheeks in all animals investigated with a similar intensity (Figure 6A–C), however, this did not interfere with the analysis of the brain and nasal mucosa. In general, the intranasally administered antibody distributed through the brain in a rostral to caudal direction (Figure 6B,C and Figure 7) with more diffuse staining shortly after administration in the olfactory bulbs (Figure 7G,L), anterior olfactory nucleus (AON) or olfactory tubercle (OT), Figure 7H,M) in the subventricular zones (Figure 7I,N), while after several hours a more distinct staining pattern developed dependent on the antigen localization (Figure 6C). Both IgGs showed mostly similar levels in the rostral brain subsequent to administration, however, a majority of mice that received the IC antibody tended to display a somewhat stronger immunoreactivity in the olfactory bulbs compared with 11C7. The elimination of the full IgGs appeared to be strongly dependent on the presence of the antigen in the CNS. While 11C7 is an antibody with a high affinity against its CNS-specific antigen Nogo-A (in-house data revealed a K_D of 14 pM, data not shown), P3X served as isotype control (IC) with no antigen in the murine brain and nasal mucosa. Indeed, immunoreactivity against P3X is absent in both hippocampus (Figure 7O) and cortex (data not shown) up to 48 h after application while 11C7-immunoreactivity is still detectable (Figures 4N, 6C and 7J). It can be estimated that different antibodies with other CNS-specific antigens would display different distribution patterns. In some sections, the staining pattern of 11C7 in hippocampus (Figure 7J) and cortex (data not shown) implicated its presence in blood vessel. This was probably due to 11C7 elimination from the CNS via FcRn uptake, a process that is, amongst others, localized in endothelial cells [45]. Interestingly, staining of blood vessels was not observed in animals treated with P3X, possibly due to the relative low amounts of P3X that reached these brain areas. In a previous study from Thorne and coworkers using radiolabeled IgGs administered via the conventional technique in rats, a similar distribution pattern in olfactory bulbs and midbrain was demonstrated [44,46]. While the study by Thorne et al. demonstrated the occurrence of IgG transport via the trigeminal nerve, no evidence for such transport was found in this study. Additionally, in the above-mentioned study, the radiolabeled IgGs appeared within 10 min in the blood in similar levels as in the olfactory bulbs after intranasal delivery with the conventional technique [44,46].

Interestingly, not only the antigen and its specific expression in the CNS played a role in the distribution and pharmacokinetics after intranasal delivery to the olfactory region, but also the presence of an Fc domain appeared to be an important factor. Hence, while the 11C7 scFv targeted the same antigen Nogo-A within the CNS, its uptake into the nasal mucosa and from there to the olfactory bulbs appeared to be significantly reduced when compared with both full IgGs (Figures 5E,F and 7P–Q). As mentioned above, the detection of full IgG and scFv was not identical, so fluorescence intensities should be interpreted with caution, but also the localization within the epithelial layer of the olfactory mucosa differs dramatically (Figure 5F). In previous studies, it has already been speculated that the presence of the Fc domain plays a pivotal role in a successful mucosal uptake and these data confirm this [38,39].

It should be noted that CSF samples were also analyzed from the mice in study 3 by ELISA, but no significant amounts of 11C7, IC, or 11C7 scFv could be determined. It cannot be excluded that methodological issues interfered with the analysis since the samples had to be frozen for logistical reasons. Possibly, this may hint that the distribution to the CNS does not include drainage to the CSF or is rapidly cleared from the CSF [47–49]. Further

studies are necessary to elucidate the involvement of the CSF, but also of the glymphatic system [50–53].

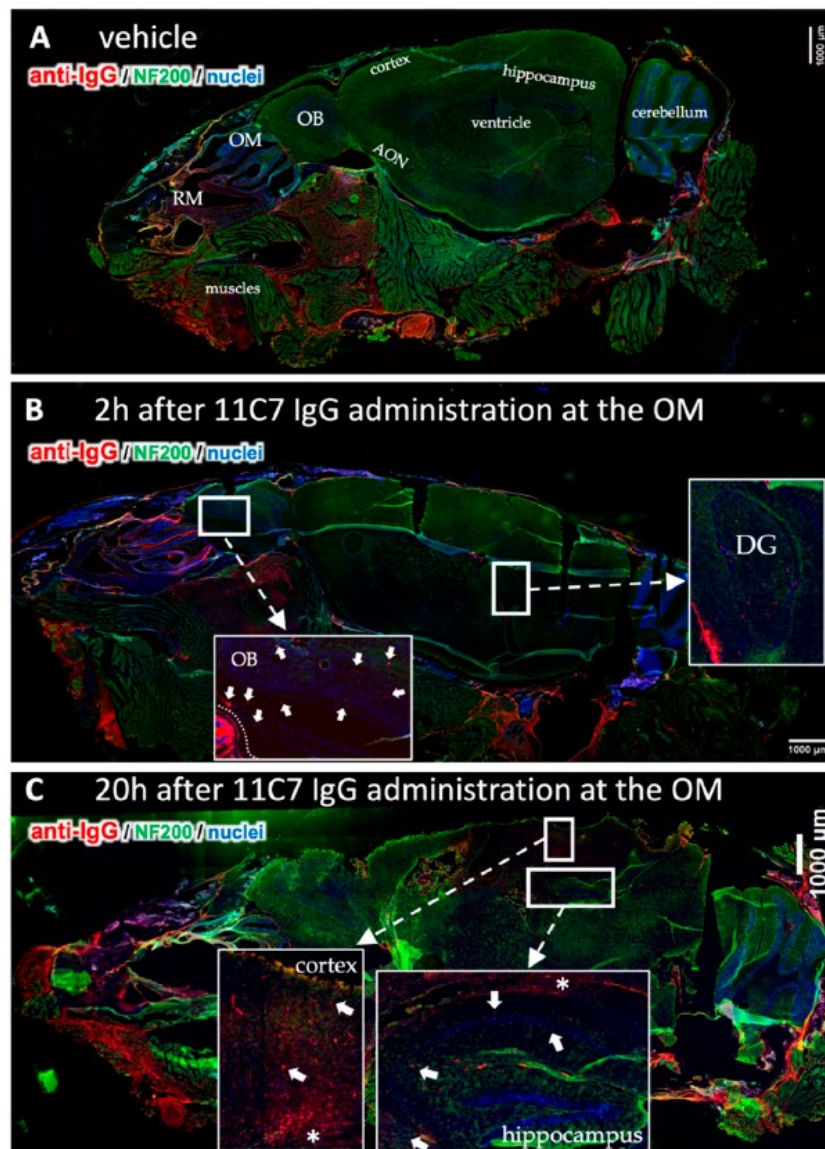


Figure 6. Time-dependent CNS distribution analyzed in sagittal section from mouse heads after region-specific delivery at the olfactory mucosa (OM, study 3). Whole slide images of a vehicle treated animal demonstrate endogenous IgGs in the nasal mucus, but also in the muscles underneath the nasal cavity and at the neck (A). This immunoreactivity was observed in all animals investigated. No background staining was observed in the CNS except for choroid plexus in all vehicle animals. The 11C7 could clearly be detected in the olfactory bulbs (arrowheads) and in the dentate gyrus of the hippocampus (B). At 20 h after administration the distribution pattern shifted into the caudal direction with lower intensities in the olfactory bulbs, but higher and more distinct staining in the cortex and the hippocampus where the antigen of 11C7 was expressed. Arrowheads point to distinct stained structures while asterisk show diffuse staining pattern. (C). OM, olfactory mucosa; RM, respiratory mucosa; OB, olfactory bulb; AON, anterior olfactory nucleus; DG, dentate gyrus. Scale bars, 1000 μm.

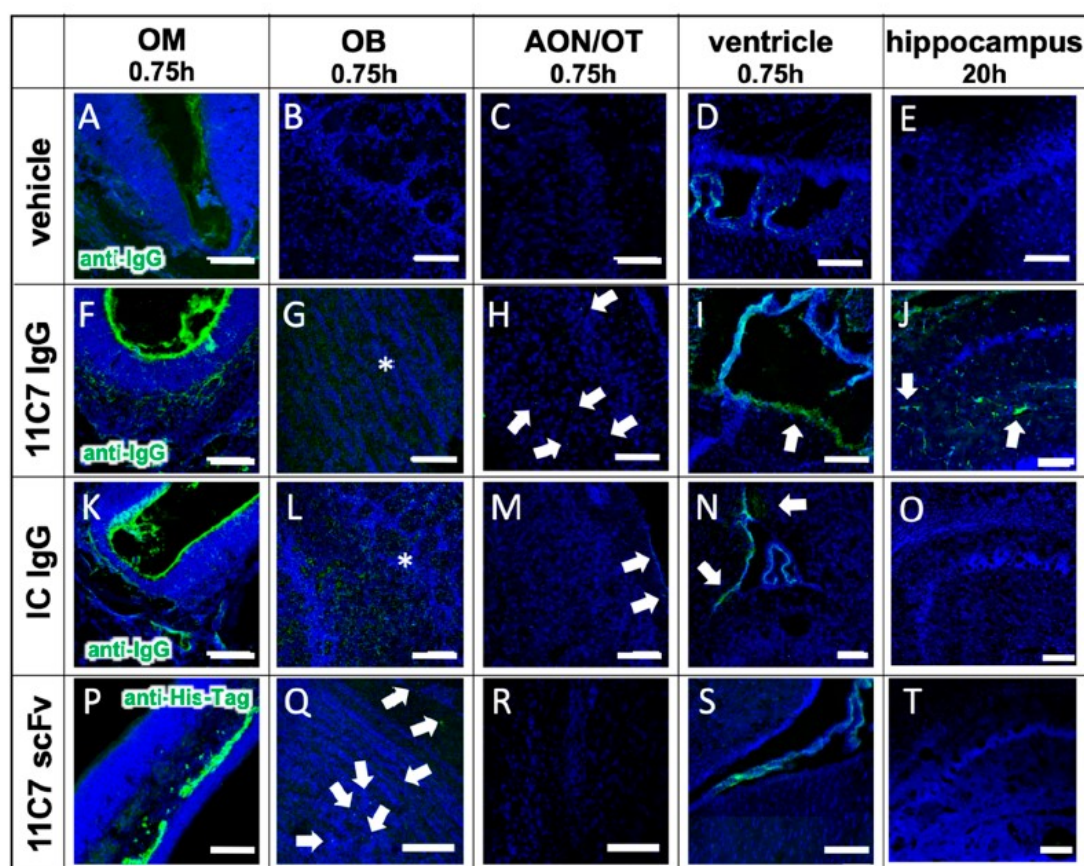


Figure 7. Antibody distribution is dependent on the presence of the antigen in the CNS and the presence of an Fc domain (study 3). The distribution and clearance in the murine OM and CNS are shown 45 min and 20 h (E,J,O,T) after directed intranasal administration at the olfactory region (OM). All images were captured with a confocal microscope. Arrowheads point to distinct stained structures while asterisk show diffuse staining pattern. (A–E) Background signal due to endogenous IgGs, that have not been cleared by transcardial perfusion, and autofluorescence in the tissue of an animal, which received a vehicle control (PBS). (F–J) distribution of anti-Nogo-A monoclonal full antibody 11C7. The 11C7 was detected in the OM (F), the OB (G), the AON/OT (anterior olfactory nucleus/olfactory tubercle) (H), the choroid plexus in the ventricles (I), and after 20 h in the hippocampus (J). The strongest signal was detected in the olfactory epithelium followed by the olfactory bulb and the choroid plexus. In the hippocampus, the signals were amplified for a better visualization. (K–O) Distribution of the isotype control (IC) antibody, which does not recognize any structure of the murine CNS as antigen. The distribution profile within 45 min was similar to 11C7 however the immunoreactivity in the AON/OT was lower in all animals investigated. The similar distribution pattern in OM, OB, AON and the subventricular zones imply the relevance of the Fc receptor system. The absence of IC in hippocampus (O) is a strong indication that the presence of the antigen is critical to avoid rapid elimination. (P–T) A scFv format of 11C7 was distributed to the OB to a lesser extent than the IgGs. In addition, hardly any signals higher than the vehicle control could be found in the AON/OT, choroid plexus, subventricular zones, nor in the Nogo-A expressing cells in the hippocampus. Nevertheless, since the 11C7 scFv was detected via its penta His-Tag, the intensities of (A–O) should not be directly compared with (P–T). Representative images are shown. OM, olfactory mucosa; OB, olfactory bulb; AON, anterior olfactory nucleus; OT, olfactory tubercle. Scale bar: 100 μ m.

4. Discussion

Intranasal drug delivery is widely discussed as a promising approach to deliver drugs to the CNS. To use the great potential of intranasal N2B drug delivery, important aspects and challenges have to be tackled to advance it to clinical routine [54]. An impressive in-depth analysis of Koslovskaya and coworkers underlined the importance of quantitative

pharmacokinetic and bioactivity data [24]. Although many studies of intranasal delivery have been published until 2014, only a small minority of 3% presents quantitative, robust data that are suitable for a potential clinical development. While several important high-quality intranasal studies have been published since 2014, the individual studies differ from each other due to the heterogeneity of non-standardized application methods, which limits their interpretation. The most common described intranasal technique is the pipette-based conventional application method (Figure 2B) that was used in a multitude of intranasal *in vivo* studies [8,55,56]. This conventional method is usually performed with a minimum volume of 20 μ L per nostril in mice and a minimum volume of 40 μ L in rats, although many variations have been also published. A volume of 20 μ L substantially exceeds the volume of the murine nasal cavity. Even the stepwise application of said amount may not reduce the risk for much of the volume being swallowed. Notably, we have delivered conventionally an amount as little as 2.5 μ L per nostril (in mice with a body weight below 25 g) in Study 1, upon which appeared clear indications that the applied volume was swallowed (Figure 2F). To the authors' knowledge, this is the first time that the 'undesired fate' of intranasally applied substances is reported. Additionally, to the authors' knowledge there have been no reports published on the percentage of animals that were asphyxiated by intranasal delivery of high volumes using the conventional method. Rodents are obligate nose breathers [17] and therefore this is a highly relevant issue for both ethical reasons and biometric estimations. Since starting to use the refined technique in mice, no complications associated with the intranasal delivery have yet been experienced. All mice recovered well after catheter-based intranasal administration and displayed normal healthy behavior. To date, in all the authors' intranasal studies, no deaths have occurred prior to sacrificing the mice at the scheduled time.

Apart from the excessive volume, a further issue with the conventional method is that it is impossible to target the respiratory or the olfactory mucosa alone. Lochhead and Thorne have already suggested different N2B transport routes: the olfactory pathway and the trigeminal pathway [12]. They could demonstrate the distribution of insulin or insulin-like growth factor-I within the CNS of rats after conventional intranasal administration with the involvement of both pathways [55]. In a more recent study, the percentage of drugs that reached the olfactory nerve (presumably via the olfactory mucosa) and the trigeminal nerve (presumably via the respiratory mucosa) was analyzed after the use of the conventional method in rats with radiolabeled IgGs. Here, a far higher radioactivity was detected in the trigeminal nerve than in the olfactory nerve [44]. With a region-specific technique such as the one demonstrated in study 2, the in-depth mechanisms of N2B transport can now be addressed. In study 1, it was successfully demonstrated that the previously presented refined intranasal administration technique [25] was able to deliver 20% of the dose of a fluorescent tracer to the olfactory bulb, and was thus facilitated by the olfactory pathway.

Insulin has well-known peripheral metabolic effects and lowers the blood glucose concentration, but it also plays an important central role in cognition, learning and memory [56–59]. Furthermore, dysregulation of insulin is involved in the pathogenesis of Alzheimer's disease, where it is associated with lower levels of insulin in the CSF [60] and with amyloid-beta regulation [61–64]. The choice to use insulin for study 2 was influenced by the fact that a large number of animal and clinical intranasal studies have been performed with insulin (see [54] for review). For instance, radiolabeled insulin distributes widely throughout the mouse brain following conventional intranasal administration, with the highest levels detected in the trigeminal nerve and the olfactory bulbs [56]. Intranasal insulin delivered with a 'conventional' manual pump spray in a clinical study with healthy volunteers was rapidly delivered to the CSF [65]. In the context of the data from studies 1 and 2, this could be interpreted as no relevant traces of insulin reaching the olfactory region when using a manual pump spray in the human nostril. In fact, the use of an intranasal insulin spray developed as NasulinTM for the needle-free regimen of diabetes, was stopped after disappointing results in blood glucose control during a Phase 2a proof-

of-concept clinical trial [66]. It can be only speculated that the absorption of insulin was too heterogeneous due to high variations in the anatomy of the human nasal cavity and the non-standardized administration at different nasal epithelia.

Intranasal insulin also slowed the development of cognitive decline in different disease models [56] and improved learning and memory in wildtype mice [64]. Even clinical trials in Alzheimer's patients have been conducted with intranasal insulin detemir administered with an atomizer targeting predominantly the lower parts of the nasal cavity such as the respiratory mucosa [67–69]. Unfortunately, neither the animal nor the clinical studies present meaningful data of blood glucose levels [54]. It remains a matter of speculation if, with region-specific intranasal delivery, these clinical studies could have reached their endpoints.

With the results from study 3 it can now be concluded that the refined region-specific technique is highly suitable for the intranasal N2B delivery of complex proteins such as IgGs. Further, the importance of the antigen-specificity of the antibody as well as that of its Fc domain can be confirmed. In general, the understanding of mechanisms of IgG transport processes from the nasal olfactory mucosa to the brain are an important step along the way of developing a standardized delivery route for therapeutics. It is widely accepted that FcRn plays a pivotal role in antibody transport across mucosal tissues [42,70–73]. In the presented study, the involvement of FcRn in IgG transport through the olfactory mucosa *in vivo* in mice could be shown first. Earlier, the role of FcRn in *ex vivo* porcine mucosa models and in primary cells from porcine nasal mucosa [38,39] has been demonstrated. According to the literature, FcRn transcytosis of IgG in mucosal epithelial cells act as a mechanism for IgG delivery to the underlying tissue [74,75]. This may explain the intracellular pathways observed in Figure 5A–D with full IgGs binding to either FcRn or FCGRs while extracellular pathways were evident when applying a scFv (Figure 5E,F). It can be only assumed that the underlying mechanisms for this involve immune surveillance where antigens captured from mucosal IgGs are presented to immune cells. A clue for this possible function may be the earlier presented disappearance of IgGs in lymphoid follicles of the nasal mucosa [38]. Unpublished data of the present study indicated that IgGs may also be degraded in the endosomal system as previously shown in primary cells [39]. Thus, it can be speculated that low doses of intranasal IgGs were degraded for immunological reasons and entered the nasal mucosa via passive extracellular pathways after a saturation of the Fc receptor system. However, further experiments are necessary to investigate dose-effects relationships for region-specific intranasally delivered IgGs.

It is hoped that with the presented technique the field of intranasal delivery can be advanced, and can contribute to a better standardization of *in vivo* data.

5. Conclusions

This project successfully achieved the specific targeting of the olfactory, or the respiratory region, by using a catheter-based refined technique that was previously developed and validated with 3D-printed casts of the murine nasal cavity under 3R criteria [25]. It was further demonstrated that region-specific administration with a fluorophore (sodium fluorescein), small (insulin detemir) and large proteins (a CNS-specific murine IgG1 and scFv, and a non-CNS targeting isotope control mAb) resulted in different organ distributions as well as different peripheral and central bioactivities *in vivo*. For immunoglobulins, transport along the olfactory route to the CNS via neuronal connections and distribution within the CNS was observed. In summary, it was successfully demonstrated that region-specific intranasal administration via the olfactory region resulted in improved brain targeting and in reduced peripheral targeting in rodents.

Author Contributions: Conceptualization, K.S., C.P.; methodology, F.M., S.L., J.F., B.K.; validation, S.L., F.M., J.F.; investigation, S.G., B.K., S.K., R.V., C.H., S.H., S.S., A.S., K.E., R.H., L.K.; resources, K.S., C.P., L.K.; visualization, S.L., S.G., K.S.; writing—original draft preparation, F.M., K.S.; writing—review and editing, S.L., S.H., F.M., R.H.; supervision, K.S., C.P.; project administration, K.S.; funding acquisition, K.S. All authors have read and agreed to the published version of the manuscript.

Funding: The present research has been financially supported by the EU under the European Framework Program for Research and Innovation Horizon 2020 ('N2B-patch' Grant No. 721098); by the Baden-Württemberg State Ministry of Science, Research and Arts ('FcRn in N2B' and funds and a fellowship to A.S. by the Ulm and Biberach joint Graduate School in Pharmaceutical Biotechnology); by the German Federal Institute for Risk Assessment (BfR/ZEBET, '3D für 3R') from a grant "ALIVE" funded by the Federal Ministry for Economic Affairs and Energy (BMWi); and from fellowships from the Stiftung der Deutschen Wirtschaft (to S.L. and J.F.).

Institutional Review Board Statement: All procedures with animals were conducted in strict compliance with national and international guidelines for the Care and Use of Laboratory Animals. Animal experiments were approved by the local governing body (Regierungspräsidium Karlsruhe, Germany G-92/19) and were carried out in compliance with the ARRIVE guidelines. 3R (refine–reduce–replace) criteria were applied by training the staff intensively the intranasal delivery technique with 3D casts of the murine nasal cavity.

Informed Consent Statement: Not applicable.

Acknowledgments: Thanks to Martin Schwab from ETH Zürich/Switzerland for kindly providing the hydridoma cell line to produce 11C7. Special thanks to Rene Handrick from Biberach University for excellent advisory and technical support whenever needed.

Conflicts of Interest: The authors declare that the research was conducted in the absence of any commercial or financial relationships that could be construed as a potential conflict of interest.

References

- Wang, Z.; Xiong, G.; Tsang, W.C.; Schätzlein, A.G.; Uchegbu, I.F. Nose-to-brain delivery. *J. Pharmacol. Exp. Ther.* **2019**, *370*, 593–601. [\[CrossRef\]](#) [\[PubMed\]](#)
- Zhang, Y.; Chan, H.F.; Leong, K.W. Advanced materials and processing for drug delivery: The past and the future. *Adv. Drug Deliv. Rev.* **2013**, *65*, 104–120. [\[CrossRef\]](#) [\[PubMed\]](#)
- Neuwelt, E.; Abbott, N.J.; Abrey, L.; Banks, W.A.; Blakley, B.; Davis, T.; Engelhardt, B.; Grammas, P.; Nedergaard, M.; Nutt, J. Strategies to advance translational research into brain barriers. *Lancet Neurol.* **2008**, *7*, 84–96. [\[CrossRef\]](#)
- Dhuria, S.V.; Hanson, L.R.; Frey, W.H. Intranasal delivery to the central nervous system: Mechanisms and experimental considerations. *J. Pharm. Sci.* **2010**, *99*, 1654–1673. [\[CrossRef\]](#)
- Illum, L. Transport of drugs from the nasal cavity to the central nervous system. *Eur. J. Pharm. Sci.* **2000**, *11*, 1–18. [\[CrossRef\]](#)
- Gänger, S.; Schindowski, K. Tailoring Formulations for Intranasal Nose-to-Brain Delivery: A Review on Architecture, Physico-Chemical Characteristics and Mucociliary Clearance of the Nasal Olfactory Mucosa. *Pharmaceutics* **2018**, *10*, 116. [\[CrossRef\]](#)
- Keller, L.A.; Merkel, O.; Popp, A. Intranasal drug delivery: Opportunities and toxicologic challenges during drug development. *Drug Deliv. Transl. Res.* **2021**, 1–23. [\[CrossRef\]](#)
- Thorne, R.G.; Emory, C.R.; Ala, T.A.; Frey, W.H., II. Quantitative analysis of the olfactory pathway for drug delivery to the brain. *Brain Res.* **1995**, *692*, 278–282. [\[CrossRef\]](#)
- Doty, R.L. *Handbook of Olfaction and Gustation*, 3rd ed.; John Wiley & Sons Inc.: Hoboken, NJ, USA, 2015; ISBN 9781118139226.
- Pabst, R. Mucosal vaccination by the intranasal route. Nose-associated lymphoid tissue (NALT)—Structure, function and species differences. *Vaccine* **2015**, *33*, 4406–4413. [\[CrossRef\]](#)
- Costantino, H.R.; Illum, L.; Brandt, G.; Johnson, P.H.; Quay, S.C. Intranasal delivery: Physicochemical and therapeutic aspects. *Int. J. Pharm.* **2007**, *337*, 1–24. [\[CrossRef\]](#)
- Lochhead, J.J.; Thorne, R.G. Intranasal delivery of biologics to the central nervous system. *Adv. Drug Deliv. Rev.* **2012**, *64*, 614–628. [\[CrossRef\]](#) [\[PubMed\]](#)
- Schipper, N.G.M.; Verhoef, J.C.; Merkus, F.W.H.M. The Nasal Mucociliary Clearance: Relevance to Nasal Drug Delivery. *Pharm. Res. An Off. J. Am. Assoc. Pharm. Sci.* **1991**, *8*, 807–814.
- Hüttenbrink, K.-B.; Wrede, H.; Lagemann, S.; Schleicher, E.; Hummel, T. Endonasal measurement of mucociliary clearance at various locations in the nose: A new diagnostic tool for nasal function? *Laryngorhinootologie* **2006**, *85*, 24–31. [\[CrossRef\]](#) [\[PubMed\]](#)
- Doty, R.L. *Handbook of Olfaction and Gustation*, 2nd ed.; Marcel Dekker: New York, NY, USA, 2003; ISBN 0824707192.
- Mori, E.; Merkonidis, C.; Cuevas, M.; Gudziol, V.; Matsuwaki, Y.; Hummel, T. The administration of nasal drops in the 'Kaiteki' position allows for delivery of the drug to the olfactory cleft: A pilot study in healthy subjects. *Eur. Arch. Otorhinolaryngol.* **2015**, *273*, 939–943. [\[CrossRef\]](#)
- Harkema, J.R.; Carey, S.; Wagner, J.G. The nose revisited: A brief review of the comparative structure, function, and toxicologic pathology of the nasal epithelium. *Toxicol. Pathol.* **2006**, *34*, 252–269. [\[CrossRef\]](#)
- Nazareth, L.; Shelper, T.B.; Chacko, A.; Basu, S.; Delbaz, A.; Lee, J.Y.P.; Chen, M.; St John, J.A.; Ekberg, J.A.K. Key differences between olfactory ensheathing cells and Schwann cells regarding phagocytosis of necrotic cells: Implications for transplantation therapies. *Sci. Rep.* **2020**, *10*, 18936. [\[CrossRef\]](#) [\[PubMed\]](#)

19. Su, Z.; Chen, J.; Qiu, Y.; Yuan, Y.; Zhu, F.; Zhu, Y.; Liu, X.; Pu, Y.; He, C. Olfactory ensheathing cells: The primary innate immunocytes in the olfactory pathway to engulf apoptotic olfactory nerve debris. *Glia* **2013**, *61*. [\[CrossRef\]](#)
20. Carr, V.M.M.; Farbman, A.I. The dynamics of cell death in the olfactory epithelium? *Exp. Neurol.* **1993**, *124*. [\[CrossRef\]](#)
21. Crowe, T.P.; Greenlee, M.H.W.; Kanthasamy, A.G.; Hsu, W.H. Mechanism of intranasal drug delivery directly to the brain. *Life Sci.* **2018**, *195*, 44–52. [\[CrossRef\]](#)
22. Lochhead, J.J.; Wolak, D.J.; Pizzo, M.E.; Thorne, R.G. Rapid transport within cerebral perivascular spaces underlies widespread tracer distribution in the brain after intranasal administration. *J. Cereb. Blood Flow Metab.* **2015**, *35*, 371–381. [\[CrossRef\]](#)
23. Johnston, M.; Zakharov, A.; Papaiconomou, C.; Salmasi, G.; Armstrong, D. Evidence of connections between cerebrospinal fluid and nasal lymphatic vessels in humans, non-human primates and other mammalian species. *Cereb. Fluid. Res.* **2004**, *1*, 2. [\[CrossRef\]](#)
24. Kozlovskaya, L.; Abou-Kaoud, M.; Stepensky, D. Quantitative analysis of drug delivery to the brain via nasal route. *J. Control. Release* **2014**, *189*, 133–140. [\[CrossRef\]](#) [\[PubMed\]](#)
25. Flamm, J.; Boscher, M.; Maigler, F.; Akana, C.; Lindemann, J.; Kleiner, S.; Sommer, F.; Schindowski, K. Standardized refined intranasal administration for region-specific intranasal drug deposition in mice established with 3D rapid prototypes under 3R criteria. *Berl. Münch. Tierärztl. Wochenschr.* **2018**, *131*, 408–416. [\[CrossRef\]](#)
26. Lochhead, J.J.; Kellohen, K.L.; Ronaldson, P.T.; Davis, T.P. Distribution of insulin in trigeminal nerve and brain after intranasal administration. *Sci. Rep.* **2019**, *9*, 2621. [\[CrossRef\]](#) [\[PubMed\]](#)
27. Röhm, M.; Carle, S.; Maigler, F.; Flamm, J.; Kramer, V.; Mavoungou, C.; Schmid, O.; Schindowski, K. A comprehensive screening platform for aerosolizable protein formulations for intranasal and pulmonary drug delivery. *Int. J. Pharm.* **2017**, *532*, 537–546. [\[CrossRef\]](#)
28. Schindelin, J.; Arg, I.; Arganda-Carreras, I.; Frise, E.; Kaynig, V.; Longair, M.; Pietzsch, T.; Preibisch, S.; Rueden, C.; Saalfeld, S.; et al. Fiji: An open-source platform for biological-image analysis. *Nat. Methods* **2012**, *9*, 676–682. [\[CrossRef\]](#)
29. Kontermann, R.E. Half-life extended biotherapeutics. *Expert Opin. Biol. Ther.* **2016**, *16*, 903–915. [\[CrossRef\]](#)
30. Pardridge, W.M. Blood-Brain Barrier and Delivery of Protein and Gene Therapeutics to Brain. *Front. Aging Neurosci.* **2020**, *11*, 373. [\[CrossRef\]](#)
31. Richard, M.; Giannetti, N.; Saucier, D.; Sacquet, J.; Jourdan, F.; Pellier-Monnin, V. Neuronal expression of Nogo-A mRNA and protein during neurite outgrowth in the developing rat olfactory system. *Eur. J. Neurosci.* **2005**, *22*, 2145–2158. [\[CrossRef\]](#)
32. Iketani, M.; Yokoyama, T.; Kurihara, Y.; Strittmatter, S.M.; Goshima, Y.; Kawahara, N.; Takei, K. Axonal branching in lateral olfactory tract is promoted by Nogo signaling. *Sci. Rep.* **2016**, *6*, 39586. [\[CrossRef\]](#)
33. Wahl, A.S.; Correa, D.; Imobersteg, S.; Maurer, M.A.; Kaiser, J.; Augath, M.A.; Schwab, M.E. Targeting Therapeutic Antibodies to the CNS: A Comparative Study of Intrathecal, Intravenous, and Subcutaneous Anti-Nogo A Antibody Treatment after Stroke in Rats. *Neurotherapeutics* **2020**, *17*, 1153–1159. [\[CrossRef\]](#) [\[PubMed\]](#)
34. Sartori, A.M.; Hofer, A.S.; Schwab, M.E. Recovery after spinal cord injury is enhanced by anti-Nogo-A antibody therapy—From animal models to clinical trials. *Curr. Opin. Physiol.* **2020**, *14*, 1–6. [\[CrossRef\]](#)
35. Schwab, M.E. Functions of Nogo proteins and their receptors in the nervous system. *Nat. Rev. Neurosci.* **2010**, *11*, 799–811. [\[CrossRef\]](#)
36. Schwab, M.E.; Strittmatter, S.M. Nogo limits neural plasticity and recovery from injury. *Curr. Opin. Neurobiol.* **2014**, *27*, 53–60. [\[CrossRef\]](#)
37. Kempf, A.; Schwab, M.E. Nogo-A represses anatomical and synaptic plasticity in the central nervous system. *Physiology* **2013**, *28*, 151–163. [\[CrossRef\]](#)
38. Ladel, S.; Flamm, J.; Zadeh, A.S.; Filzwieser, D.; Walter, J.-C.; Schlossbauer, P.; Kinscherf, R.; Lischka, K.; Luksch, H.; Schindowski, K. Allogenic Fc Domain-Facilitated Uptake of IgG in Nasal Lamina Propria: Friend or Foe for Intranasal CNS Delivery? *Pharmaceutics* **2018**, *10*, 107. [\[CrossRef\]](#) [\[PubMed\]](#)
39. Ladel, S.; Maigler, F.; Flamm, J.; Schlossbauer, P.; Handl, A.; Hermann, R.; Herzog, H.; Hummel, T.; Mizaikoff, B.; Schindowski, K. Impact of glycosylation and species origin on the uptake and permeation of IgGs through the nasal airway mucosa. *Pharmaceutics* **2020**, *12*, 1014. [\[CrossRef\]](#) [\[PubMed\]](#)
40. Pyzik, M.; Sand, K.M.K.; Hubbard, J.J.; Andersen, J.T.; Sandlie, I.; Blumberg, R.S. The neonatal Fc Receptor (FcRn): A misnomer? *Front. Immunol.* **2019**, *10*, 1540. [\[CrossRef\]](#)
41. Ruano-Salguero, J.S.; Lee, K.H. Antibody transcytosis across brain endothelial-like cells occurs nonspecifically and independent of FcRn. *Sci. Rep.* **2020**, *10*, 3685. [\[CrossRef\]](#)
42. Schlachetzki, F.; Zhu, C.; Pardridge, W.M. Expression of the neonatal Fc receptor (FcRn) at the blood-brain barrier. *J. Neurochem.* **2002**, *81*, 203–206. [\[CrossRef\]](#)
43. Gil, V.; Nicolas, O.; Mingorance, A.; Ureña, J.M.; Tang, B.L.; Hirata, T.; Sáez-Valero, J.; Ferrer, I.; Soriano, E.; Del Rio, J.A. Nogo-A expression in the human hippocampus in normal aging and in Alzheimer disease. *J. Neuropathol. Exp. Neurol.* **2006**, *65*, 433–444. [\[CrossRef\]](#)
44. Kumar, N.N.; Lochhead, J.J.; Pizzo, M.E.; Nehra, G.; Boroumand, S.; Greene, G.; Thorne, R.G. Delivery of immunoglobulin G antibodies to the rat nervous system following intranasal administration: Distribution, dose-response, and mechanisms of delivery. *J. Control. Release* **2018**, *286*, 467–484. [\[CrossRef\]](#) [\[PubMed\]](#)

45. Cooper, P.R.; Ciambone, G.J.; Kliwinski, C.M.; Maze, E.; Johnson, L.; Li, Q.; Feng, Y.; Hornby, P.J. Efflux of monoclonal antibodies from rat brain by neonatal Fc receptor, FcRn. *Brain Res.* **2013**, *1534*, 13–21. [\[CrossRef\]](#)
46. Boroumand, S.; Kumar, N.; Lochhead, J.; Pizzo, M.; Nehra, G.; Thorne, R.G. Intranasal delivery of antibodies bypasses the blood-brain barrier and results in significantly higher central nervous system levels than systemic administration. *FASEB J.* **2018**, *32*, 1b617. [\[CrossRef\]](#)
47. McLean, B.N.; Miller, D.; Thompson, E.J. Oligoclonal banding of IgG in CSF, blood-brain barrier function, and MRI findings in patients with sarcoidosis, systemic lupus erythematosus, and Behcet's disease involving the nervous system. *J. Neurol. Neurosurg. Psychiatry* **1995**, *58*, 548–554. [\[CrossRef\]](#)
48. Link, H.; Tibbling, G. Principles of albumin and igh analyses in neurological disorders. III. Evaluation of igh synthesis within the central nervous system in multiple sclerosis. *Scand. J. Clin. Lab. Investig.* **1977**, *37*, 397–401. [\[CrossRef\]](#)
49. Lefvert, A.K.; Link, H. IgG production within the central nervous system: A critical review of proposed formulae. *Ann. Neurol.* **1985**, *17*, 13–20. [\[CrossRef\]](#) [\[PubMed\]](#)
50. Inoue, D.; Furubayashi, T.; Tanaka, A.; Sakane, T.; Sugano, K. Effect of Cerebrospinal Fluid Circulation on Nose-to-Brain Direct Delivery and Distribution of Caffeine in Rats. *Mol. Pharm.* **2020**, *17*, 4067–4076. [\[CrossRef\]](#)
51. Sun, B.L.; Wang, L.H.; Yang, T.; Sun, J.Y.; Mao, L.L.; Yang, M.F.; Yuan, H.; Colvin, R.A.; Yang, X.Y. Lymphatic drainage system of the brain: A novel target for intervention of neurological diseases. *Prog. Neurobiol.* **2018**, *163–164*, 118–143. [\[CrossRef\]](#)
52. Shetty, A.K.; Zanirati, G. The interstitial system of the brain in health and disease. *Aging Dis.* **2020**, *11*, 200. [\[CrossRef\]](#) [\[PubMed\]](#)
53. Krishnan, J.K.S.; Arun, P.; Chembukave, B.; Appu, A.P.; Vijayakumar, N.; Moffett, J.R.; Puthillathu, N.; Nambodiri, A.M.A. Effect of administration method, animal weight and age on the intranasal delivery of drugs to the brain. *J. Neurosci. Methods* **2017**, *286*, 16–21. [\[CrossRef\]](#) [\[PubMed\]](#)
54. Stützel, M.; Flamm, J.; Carle, S.; Schindowski, K. Nose-to-Brain delivery of insulin for Alzheimer's disease. *ADMET DMPK* **2015**, *3*, 190–202. [\[CrossRef\]](#)
55. Thorne, R.G.; Pronk, G.J.; Padmanabhan, V.; Frey, W.H. Delivery of insulin-like growth factor-I to the rat brain and spinal cord along olfactory and trigeminal pathways following intranasal administration. *Neuroscience* **2004**, *127*, 481–496. [\[CrossRef\]](#) [\[PubMed\]](#)
56. Francis, G.J.; Martinez, J.A.; Liu, W.Q.; Xu, K.; Ayer, A.; Fine, J.; Tuor, U.I.; Glazner, G.; Hanson, L.R.; Frey, W.H., 2nd; et al. Intranasal insulin prevents cognitive decline, cerebral atrophy and white matter changes in murine type I diabetic encephalopathy. *Brain* **2008**, *131*, 3311–3334. [\[CrossRef\]](#) [\[PubMed\]](#)
57. Benedict, C.; Hallschmid, M.; Hatke, A.; Schultes, B.; Fehm, H.L.; Born, J.; Kern, W. Intranasal insulin improves memory in humans. *Psychoneuroendocrinology* **2004**, *29*, 1326–1334. [\[CrossRef\]](#) [\[PubMed\]](#)
58. Shemesh, E.; Rudich, A.; Harman-Boehm, I.; Cukierman-Yaffe, T. Effect of intranasal insulin on cognitive function: A systematic review. *J. Clin. Endocrinol. Metab.* **2012**, *97*, 366–376. [\[CrossRef\]](#)
59. Plum, L.; Schubert, M.; Bruning, J.C. The role of insulin receptor signaling in the brain. *Trends Endocrinol. Metab.* **2005**, *16*, 59–65. [\[CrossRef\]](#)
60. Craft, S.; Watson, G.S. Insulin and neurodegenerative disease: Shared and specific mechanisms. *Lancet Neurol.* **2004**, *3*, 169–178. [\[CrossRef\]](#)
61. Freiherr, J.; Hallschmid, M.; Frey, W.H., 2nd; Brunner, Y.F.; Chapman, C.D.; Holscher, C.; Craft, S.; De Felice, F.G.; Benedict, C. Intranasal insulin as a treatment for Alzheimer's disease: A review of basic research and clinical evidence. *CNS Drugs* **2013**, *27*, 505–514. [\[CrossRef\]](#)
62. Craft, S. The role of metabolic disorders in Alzheimer disease and vascular dementia: Two roads converged. *Arch. Neurol.* **2009**, *66*, 300–305. [\[CrossRef\]](#)
63. Hong, M.; Lee, V.M. Insulin and insulin-like growth factor-1 regulate tau phosphorylation in cultured human neurons. *J. Biol. Chem.* **1997**, *272*, 19547–19553. [\[CrossRef\]](#) [\[PubMed\]](#)
64. Marks, D.R.; Tucker, K.; Cavallin, M.A.; Mast, T.G.; Fadool, D.A. Awake intranasal insulin delivery modifies protein complexes and alters memory, anxiety, and olfactory behaviors. *J. Neurosci.* **2009**, *29*, 6734–6751. [\[CrossRef\]](#) [\[PubMed\]](#)
65. Born, J.; Lange, T.; Kern, W.; McGregor, G.P.; Bickel, U.; Fehm, H.L. Sniffing neuropeptides: A transnasal approach to the human brain. *Nat. Neurosci.* **2002**, *5*, 514–516. [\[CrossRef\]](#)
66. Bloomberg CPEX Pharmaceuticals Announces Preliminary Results from Its Phase 2a Clinical Trial of Nasulin. Available online: <http://www.bloomberg.com/apps/news?pid=newsarchive&sid=aF8dtG4W0xT4> (accessed on 20 September 2021).
67. Claxton, A.; Baker, L.D.; Hanson, A.; Trittschuh, E.H.; Cholerton, B.; Morgan, A.; Callaghan, M.; Arbuckle, M.; Behl, C.; Craft, S. Long-acting intranasal insulin detemir improves cognition for adults with mild cognitive impairment or early-stage Alzheimer's disease dementia. *J. Alzheimers Dis.* **2015**, *44*, 897–906. [\[CrossRef\]](#)
68. Craft, S.; Claxton, A.; Baker, L.; Cholerton, B.; Hanson, A.; Callaghan, M.; Trittschuh, E.; Arbuckle, M. Therapeutic effects of long-acting intranasal insulin detemir for Alzheimer's dementia or mild cognitive impairment. *Alzheimer's Dement.* **2013**, *9*, 139–140. [\[CrossRef\]](#)
69. Craft, S.; Baker, L.D.; Montine, T.J.; Minoshima, S.; Watson, G.S.; Claxton, A.; Arbuckle, M.; Callaghan, M.; Tsai, E.; Plymate, S.R.; et al. Intranasal insulin therapy for Alzheimer disease and amnesic mild cognitive impairment: A pilot clinical trial. *Arch. Neurol.* **2012**, *69*, 29–38. [\[CrossRef\]](#) [\[PubMed\]](#)

70. Schneider, Z.; Jani, P.K.; Szikora, B.; Végh, A.; Kövesdi, D.; Iliás, A.; Cervenak, J.; Balogh, P.; Kurucz, I.; Kacs Kovics, I. Overexpression of bovine FcRn in mice enhances T-dependent immune responses by amplifying T helper cell frequency and germinal center enlargement in the spleen. *Front. Immunol.* **2015**, *6*, 357. [\[CrossRef\]](#)
71. Stapleton, N.M.; Brinkhaus, M.; Armour, K.L.; Bentlage, A.E.H.; de Taeye, S.W.; Temming, A.R.; Mok, J.Y.; Brasser, G.; Maas, M.; van Esch, W.J.E.; et al. Reduced FcRn-mediated transcytosis of IgG2 due to a missing Glycine in its lower hinge. *Sci. Rep.* **2019**, *9*, 7363. [\[CrossRef\]](#)
72. Tzaban, S.; Massol, R.H.; Yen, E.; Hamman, W.; Frank, S.R.; Lapierre, L.A.; Hansen, S.H.; Goldenring, J.R.; Blumberg, R.S.; Lencer, W.I. The recycling and transcytotic pathways for IgG transport by FcRn are distinct and display an inherent polarity. *J. Cell Biol.* **2009**, *185*, 673–684. [\[CrossRef\]](#) [\[PubMed\]](#)
73. Ye, L.; Zeng, R.; Bai, Y.; Roopenian, D.C.; Zhu, X. Efficient mucosal vaccination mediated by the neonatal Fc receptor. *Nat. Biotechnol.* **2011**, *29*, 158–163. [\[CrossRef\]](#)
74. Roopenian, D.C.; Akilesh, S. FcRn: The neonatal Fc receptor comes of age. *Nat. Rev. Immunol.* **2007**, *7*, 715–725. [\[CrossRef\]](#) [\[PubMed\]](#)
75. Dickinson, B.L.; Blumberg, R.S.; Wayne, I.; Invest, J.C.; Dickinson, B.L.; Badizadegan, K.; Wu, Z.; Ahouse, J.C.; Zhu, X.; Simister, N.E.; et al. Bidirectional FcRn-dependent IgG transport in a polarized human intestinal epithelial cell line. *J. Clin. Investig.* **1999**, *104*, 903–911. [\[CrossRef\]](#) [\[PubMed\]](#)

Curriculum Vitae

note: curriculum vitae not for public

-

-

Publications

Maigler, F.; Ladel, S.; Flamm, J.; Gänger, ...; K. Schindowski.; (2021). Selective CNS Targeting and Distribution with a Refined Region-Specific Intranasal Delivery Technique via the Olfactory Mucosa. *Pharmaceutics*, 13, 1904, doi:10.3390/pharmaceutics13111904.

Spindler, L. M., Feuerhake, A., Ladel, S., Günday, C., Flamm, J., Günday-Türel, N., ... Gruber-Traub, C. (2021). Nano-in-Micro-Particles Consisting of PLGA Nanoparticles Embedded in Chitosan Microparticles via Spray-Drying Enhances Their Uptake in the Olfactory Mucosa. *Frontiers in Pharmacology*, 12. <https://doi.org/10.3389/fphar.2021.732954>

Ladel, S., Maigler, F., Flamm, J., Schlossbauer, P., Handl, A., Hermann, R., ... Schindowski, K. (2020). Impact of Glycosylation and Species Origin on the Uptake and Permeation of IgGs through the Nasal Airway Mucosa. *Pharmaceutics*, 12(11), 1014. <https://doi.org/10.3390/pharmaceutics12111014>

Ladel, S., Schlossbauer, P., Flamm, J., Luksch, H., Mizaikoff, B., & Schindowski, K. (2019). Improved In Vitro Model for Intranasal Mucosal Drug Delivery: Primary Olfactory and Respiratory Epithelial Cells Compared with the Permanent Nasal Cell Line RPMI 2650. *Pharmaceutics*, 11(8), 367. <https://doi.org/10.3390/pharmaceutics11080367>

Ladel, S. *et al.* Improved In Vitro Model for Intranasal Mucosal Drug Delivery: Primary Olfactory and Respiratory Epithelial Cells Compared with the Permanent Nasal Cell Line RPMI 2650. *Pharmaceutics* **11**, 367 (2019).

Ladel, S. *et al.* Allogenic fc domain-facilitated uptake of IgG in nasal Lamina propria: Friend or foe for intranasal CNS delivery? *Pharmaceutics* **10**, 1–23 (2018).

7.2 Acknowledgements

Note: acknowledgements not for public.

7.3 Declaration

I hereby declare that I wrote the present dissertation with the topic:

“Development of models for intranasal drug delivery to identify IgG transport pathways”

independently and used no other aids than those cited. In each individual case, I have clearly identified the source of the passages that are taken word for word or paraphrased from other works.

I also hereby declare that I have carried out my scientific work according to the principles of good scientific practice in accordance with the current „Satzung der Universität Ulm zur Sicherung guter wissenschaftlicher Praxis“ (Rules of the University of Ulm for Assuring Good Scientific Practice).

Peine, 10/12/2021

Simone Ladel